

REVERSIBLE INHIBITION OF LYSINE-SPECIFIC
DEMETHYLASE 1 IS A NOVEL THERAPEUTIC
STRATEGY FOR SOLID TUMORS

by

Emily Rose Theisen

A dissertation submitted to the faculty of
The University of Utah
in partial fulfillment of the requirements for the degree of

Doctor of Philosophy

Department of Pharmaceutics and Pharmaceutical Chemistry

The University of Utah

May 2015

Copyright © Emily Rose Theisen 2015

All Rights Reserved

The University of Utah Graduate School

STATEMENT OF DISSERTATION APPROVAL

The dissertation of Emily Rose Theisen
has been approved by the following supervisory committee members:

Sunil Sharma, Chair 10/22/2014
Date Approved

Margit Janat-Amsbury, Member 10/23/2014
Date Approved

James Herron, Member 10/30/2014
Date Approved

David W. Grainger, Member 10/25/2014
Date Approved

Hamid Ghandehari, Member 10/23/2014
Date Approved

and by David W. Grainger, Chair/Dean of

the Department/College/School of Pharmaceutics and Pharmaceutical Chemistry

and by David B. Kieda, Dean of The Graduate School.

ABSTRACT

Cancer is a genomic disease driven by interplay between genetic and epigenetic factors. While genetic mutations are irreversible events, epigenetic regulation is dynamic and reversible, and small molecule blockade of the epigenetic machinery has shown clinical benefit in hematological malignancies. However, the promise of epigenetic therapy has yet to be realized in solid tumors due do limited efficacy and elevated risk of toxicity. Development of potent and specific inhibitors targeting the histone methylation machinery shows promise in tailoring epigenetic therapy for a specific malignancy and decreasing the risk of off-target effects.

One such target of interest is the histone lysine-specific demethylase 1 (LSD1). Several solid malignancies show upregulation of LSD1 associated with an aggressive clinical course. Validation of LSD1 as a target has been limited by poorly potent and non-specific tool compounds, hindering evaluation in *in vivo* models of disease. This work describes the discovery of a novel potent, specific, and reversible series of LSD1 inhibitors. The identified lead compound, HCI2509, is a noncompetitive inhibitor with nanomolar affinity for LSD1. HCI2509 impaired cell viability across several human cancer cell lines, with both Ewing sarcoma and endometrial cancers showing particularly potent responses.

Ewing sarcoma is a rare and aggressive pediatric malignancy characterized by by the chromosomal translocation-derived EWS/ETS fusion proteins. EWS/ETS fusions act

as oncogenic transcription factors and facilitate cellular reprogramming through the activation of oncogenes and repression of tumor suppressors. Treatment with HCI2509 reverses both EWS/ETS-mediated transcriptional activation and transcriptional repression, and leads to apoptotic cell death in Ewing sarcoma cells. Notably, HCI2509 shows single-agent efficacy in xenograft models of Ewing sarcoma and represents a new therapeutic strategy for this devastating disease.

HCI2509 also shows single-agent efficacy in a xenograft model of Type II endometrial carcinoma. Cases of Type II endometrial carcinoma comprise 11% of the incidence and 48% of the deaths due to endometrial cancer annually, such that new therapies are needed for this aggressive subtype. Reversible LSD1 inhibition was associated with tumor regression in an orthotopic model of this disease. These results demonstrate the promise of targeting the histone methylation machinery, specifically LSD1, as a therapeutic strategy for solid tumors.

This work is dedicated to my parents, Timothy O. Theisen and Barbara A. Filip,
my siblings, Jeffrey Martin and Frances Claire, and my grandparents,
Gertrude and Robert Theisen and Elaine and Lambert Lasecki,
for everything they have given and continue to give in love.

“Nothing in life is to be feared, it is only to be understood. Now is the time to understand more, so that we may fear less.”
Marie Curie as quoted in *Our Precarious Habitat*, Melvin A Bernarde, 1973

TABLE OF CONTENTS

ABSTRACT.....	iii
LIST OF FIGURES.....	ix
LIST OF TABLES.....	xii
LIST OF ABBREVIATIONS.....	xiv
ACKNOWLEDGEMENTS.....	xvii
Chapters	
1. INTRODUCTION AND BACKGROUND.....	1
1.1 Introduction.....	1
1.2 Summary of Dissertation.....	2
1.3 Background.....	4
1.4 Study Rationale and Objectives.....	29
1.5 References.....	32
2. HIGH THROUGHPUT VIRTUAL SCREENING IDENTIFIES NOVEL N ² - (1-PHENYLETHYLIDENE)-BENZOHYDRAZIDES AS POTENT, SPECIFIC, AND REVERSIBLE INHIBITORS OF LSD1	54
2.1 Abstract.....	55
2.2 Introduction.....	55
2.3 Results.....	56
2.4 Discussion.....	62
2.5 Conclusions.....	63
2.6 Experimental Section.....	63
2.7 References.....	66
2.8 Supplementary Materials.....	68
3. REVERSIBLE LSD1 INHIBITION INTERFERES WITH GLOBAL EWS/ETS TRANSCRIPTIONAL ACTIVITY AND IMPEDES EWING SARCOMA TUMOR GROWTH.....	88

3.1 Abstract.....	89
3.2 Introduction.....	89
3.3 Translational Relevance.....	90
3.4 Materials and Methods.....	90
3.5 Results.....	91
3.6 Discussion.....	98
3.7 References.....	101
4. REVERSIBLE INHIBITION OF LYSINE SPECIFIC DEMETHYLASE 1 IS A NOVEL ANTITUMOR STRATEGY FOR POORLY DIFFERENTIATED ENDOMETRIAL CARCINOMA.....	115
4.1 Abstract.....	116
4.2 Background.....	116
4.3 Methods.....	117
4.4 Results.....	118
4.5 Discussion.....	122
4.6 Conclusions.....	125
4.7 References.....	126
5. CONCLUSIONS AND OUTLOOK.....	136
5.1 Conclusions.....	136
5.2 Future Studies.....	142
5.3 Outlook.....	150
5.4 References.....	151
Appendices	
A. PURIFICATION OF LYSINE-SPECIFIC DEMETHYLASE 1.....	158
B. IN-HOUSE CELL LINE SCREEN AND XCELLIGENCE PROFILING.....	163
C. PHARMACOKINETIC MEASUREMENTS IN MICE AND RATS.....	169

LIST OF FIGURES

1.1	Histone methylation machinery	50
1.2	The crystal structure of lysine-specific demethylase 1.....	51
1.3	Catalytic oxidative demethylation of histone H3 lysine 4 by LSD1.....	52
1.4	Other proteins bind LSD1 through molecular mimicry	53
2.1	Mode of binding of compound 12 in complex with LSD1.....	58
2.2	MAO activity of select compounds.....	59
2.3	Compound 12 reversibly inhibits the activity of LSD1.....	59
2.4	Derivative melt curves of LSD1 in the presence of DMSO, compound 12, compound 13, and TCP.....	60
2.5	LSD1 kinetics with multiple concentrations of compound 12.....	60
2.6	Compounds with biochemical activity against LSD1 show <i>in vitro</i> EC50s clustered near 1 μ M.....	61
2.7	VCaP cells treated with compound 12 show a dose-dependent increase in H3K9 dimethylation.....	61
2.8	Scheme 1. General Procedure for the Synthesis.....	63
S2.1	Binding site model and definition of active site of LSD1 structure generated from PDB ID 2Z5U.....	85
S2.2	Flow diagram for the virtual ligand screening (VLS) using ICM-VLS, Schrodinger workflow GOLD programs.....	85
S2.3	Complete reaction schemes for compounds 11-22.....	86
S2.4	LC-MS data for compound 12 (96% purity).....	87
3.1	Global EWS/FLI transcriptional activity is disrupted by HCI2509.....	92

3.2	Morphological changes in A673 with HCI2509 treatment	94
3.3	Mechanism of action of HCI2509 <i>in vitro</i>	95
3.4	Regulation of HMOX1.....	97
3.5	HCI2509 activity <i>in vivo</i>	99
3.6	Model for HCI2509 mechanism of action in Ewing sarcoma.....	100
S3.1	Transcriptional profiling of HCI2509 in A673 and TTC-466.....	104
S3.2	Morphological changes with HCI2509 treatment.....	109
S3.3	Effects of HCI2509 on transformation, methylation, and apoptosis	111
S3.4	Regulation of HMOX1 in Ewing sarcoma.....	112
S3.5	Tumor volume, body weight and blood counts	114
4.1	HCI2509 impairs cell viability, proliferation and transformation in Type II EC cell lines.....	119
4.2	Treatment with HCI2509 causes changes in global histone methylation and induces LSD1 target genes	120
4.3	Dose-dependent cell cycle perturbation in Type II EC cell lines with HCI2509 treatment.....	121
4.4	HCI2509 induces apoptotic cell death.....	123
4.5	HCI2509 treatment causes tumor regression <i>in vivo</i>	124
S4.1	Time course evaluation of cell cycle perturbations caused by HCI2509 treatment.....	128
S4.2	TUNEL assay replicates and controls.....	131
S4.3	In depth xenograft model analysis.....	134
5.1	The effects of different classes of LSD1 inhibitors on EWS/FLI targets.....	153
5.2	HCI2509 decreases metastasis in nude rat model of Ewing sarcoma.....	155
5.3	Potential synergy between HCI2509 and temozolomide <i>in vivo</i>	156

5.4	HCI2509 does not sensitize cell to treatment with medroxyprogesterone 17-acetate (MPA).....	157
A.1	Chromatography tracking LSD1 purification.....	162
A.2	Purified protein is active.....	162
B.1	xCelligence screen of Ewing sarcoma cell lines	167
C.1	Typical standard curves to quantitate HCI2509 by LC-MS/MS.....	177
C.2	Plasma concentration-time curves for HCI2509 in mice as determined by LC-MS/MS.....	178
C.3	Plasma concentration-time curves for HCI2509 in mice as determined by LC-MS/MS – semilog.....	178
C.4	Plasma concentration-time curves for 40 mg/kg HCI2509 in mice as determined by LC-MS/MS.....	179
C.5	Plasma concentration-time curves for 40 mg/kg HCI2509 in mice as determined by LC-MS/MS – semilog.....	179

LIST OF TABLES

1.1	FDA-approved epigenetic therapies.....	48
1.2	Histone methylation is globally misregulated in cancer	48
1.3	Altered expression of KDMs in cancer.....	49
2.1	Commercially available highly-ranked hits from 121 screened compounds....	57
2.2	Synthesized compounds and their biochemical activity against LSD1.....	58
2.3	Off-target panel for compound 12.....	59
2.4	Melting temperatures as determined by DSF.....	60
2.5	Summary of Michaelis-Menten curve fits.....	61
2.6	Compound 12 inhibits proliferation in several cell lines <i>in vitro</i>	61
2.7	In vitro growth inhibition of compound panel in T-47D cells.....	61
S2.1	Docking scores of compounds 1-10.....	73
S2.2	Commercially available LSD1 hits (111) from the list of 121 compounds selected.....	74
S2.3	Tanimoto similarity coefficients comparing compound 12 and known LSD1 inhibitors from Chart 1.....	83
S2.4	Off-target inhibition assay results.....	84
S2.5	Different model fits for enzyme kinetics.....	84
S3.1	Primer sequences for qRT-PCR analysis.....	103
B.1	A 96-cell line panel.....	164
C.1	Pharmacokinetic parameters for 5 mg/kg HCl2509 dosed as solution IV.....	174

C.2	Pharmacokinetic parameters for 20 mg/kg HCl2509 dosed as solution PO....	175
C.3	Pharmacokinetic parameters for 50 mg/kg HCl2509 dosed as suspension PO.....	176

LIST OF ABBREVIATIONS

ALL	Acute lymphocytic leukemia
AML	Acute myeloid leukemia
AOD	Amine oxidase domain
BHC80	BRAF35-HDAC complex protein 80
CETSA	In-cell thermal shift assay
ChIP	Chromatin immunoprecipitation
CK2	Protein kinase 2
Co-REST	REST corepressor 1
CTCL	Cutaneous T-cell lymphoma
CYP	Cytochrome P450
DAPI	4',6-diamidino-2-phenylindole
DAVID	Database for Annotation, Visualization and Integrated Discovery
DNMT	DNA methyltransferase
DOT1L	DOT1-like histone H3K79 methyltransferase
DSF	Differential scanning fluorimetry
EC	Endometrial carcinoma
EC ₅₀	Concentration at 50% effect
EMT	Epithelial-to-mesenchymal transition
EZH2	Enhancer of zeste homolog 2

FAD	Flavin adenine dinucleotide
FAK	Focal adhesion kinase
Gfi-1	Growth factor independent 1
GSEA	Gene set enrichment analysis
H2a	Histone 2a
H2b	Histone 2b
H ₂ O ₂	Hydrogen peroxide
H3	Histone H3
H3K16	Histone H3 lysine 16
H3K27	Histone H3 lysine 27
H3K36	Histone H3 lysine 36
H3K4	Histone H3 lysine 4
H3K79	Histone H3 lysine 79
H3K9	Histone H3 lysine 9
H3T6	Histone H3 threonine 6
H4	Histone H4
H4K20	Histone H4 lysine 20
HAT	Histone acetyltransferase
HDAC	Histone deacetylase 1
hERG	Human ether-à-go-go
HMOX1	Heme oxygenase 1
HTVS	High throughput virtual screening
IGF-1	Insulin-like growth factor 1

JmjC	Jumonji-C-domain containing
KDM	Lysine demethylase
KMT	Lysine methyltransferase
LSD1	Lysine specific demethylase 1
MAO	Monoamine oxidase
MDS	Myelodysplastic syndrome
me1	Monomethyl
me2	Dimethyl
me3	Trimethyl
MSCV	Murine stem cell virus
MTA	Metastasis-associated 1
NuRD	Nucleosome remodeling and deacetylase complex
NURF	Nucleosome remodeling factor complex
PAO	Polyamine oxidase
PKC α	Protein kinase α
PRC2	Polycomb repressive complex 2
SAR	Structure-activity relationship
SNAG	Snail/Gfi
SWIRM	Swi3p, Rsc8p and Moira domain
TCP	Tranylcypromine
TGF β	Tumor growth factor β
VS	Virtual screen

ACKNOWLEDGEMENTS

I would also like to thank my dissertation committee: David Grainger, James Herron, Margit Janat-Amsbury, and Hamid Ghandehari. I have been honored to be mentored by Sunil Sharma in the laboratory he has established at the Huntsman Cancer Institute. To Sunil Sharma: Thank you for the opportunities and guidance that you have continued to provide me, and for seeing this project through to completion. I have been fortunate to work with Savita Sankar, Snehal Gajiwala, Jared Bearss, Raffaella Soldi, Barbara Graves, Stephen Lessnick, Michael Engel, and David Bearss, as well as other exceptional members of the CIT, Graves, and Lessnick Labs. I would like to express the deepest gratitude to my brother Jeffrey in the compilation of this manuscript. I must also acknowledge Charles Fehl, Jason Tanner, Holly Grainger, Phil Wilkes, Alana Jonat, Jessica McCombs, Abood Okal, Andrew Dixon, and Carol Lim for tending the light. Heartfelt thanks to all of my family and friends for their enduring support. I would also like to recognize Dr. You Han Bae for his enthusiasm for this area of research and his support in showcasing it to the department. This work was supported in part by the American Foundation for Pharmaceutical Education, Women in Cancer Research, and NCI/NIH Grants P30 CA042014 (to Huntsman Cancer Institute). We also acknowledge the use of the DNA sequencing and genomics core facilities at the Huntsman Cancer Institute.

CHAPTER 1

INTRODUCTION AND BACKGROUND

1.1 Introduction

While genetic information encoded in DNA contains the program for every cell, cell- and tissue-specific programming required for normal physiological function are regulated by a dynamic array of epigenetic and transcriptional machinery (1). This epigenomic level of regulation allows interaction between one's environment and one's genes and can result in heritable patterns of gene expression in the absence of genetic mutation. Cancer is a disease of the whole genome, characterized by both genetic aberrations and epigenomic misregulation driving the malignant phenotypes comprehensively described by Hanahan and Weinberg (2). Worldwide, the incidence of cancer is projected to double from 12.7 million new cases in 2008 to 21.4 million new cases, and 13.5 million deaths, by 2030 (3). Given that genomes and environments are singular for each patient, each individual malignancy is unique, such that universally efficacious treatment options are nonexistent. However, where genetic mutations are irreversible, the dynamic nature of the epigenetic machinery is susceptible to pharmacological intervention. Epigenetic enzymes which fuel oncogenic misregulation are emerging therapeutic targets.

The histone demethylase lysine specific demethylase 1 (LSD1) is one such target and is either upregulated in or critically important to the development and progression of various cancers, including neuroblastoma (4), acute myeloid leukemia (5), and prostate cancer (6). However, having only been discovered in 2004, the complicated biological mechanisms which regulate LSD1 function in healthy and diseased states are not yet fully elucidated. Moreover, the available tool compounds suffer from both poor potency and specificity, complicating interpretation of reported results. Hence, *we pursued a drug discovery program to identify potent, specific and reversible LSD1 inhibitors to use as tool compounds to preclinically screen the viability of LSD1 inhibition as a therapeutic strategy for solid tumors.* The discovery of such a series will further enable detailed investigation of the biological role of LSD1 in various cancers, and differentiate mechanisms that are common between malignancies and those that are more disease-specific. While this work focuses primarily on Ewing sarcoma and endometrial cancer, the compound series identified may provide therapeutic benefit in a diverse array of cancers for which LSD1 overexpression has been reported or LSD1 biology implicated.

1.2 Summary of this Dissertation

This chapter will provide an overview of the rapidly evolving field of cancer epigenetics, describing both the clinical challenges encountered to date by FDA-approved epigenetic therapies and the ways in which second generation epigenetic targeted therapies address these, focusing specifically on the challenges and promises of targeting LSD1. Additionally, this chapter will introduce the rationale for the studies described herein and identify the objectives met in Chapters 2-4. Chapter 2 describes the initial

discovery, hit-to-lead optimization, and biochemical characterization of the N¹-(1-phenylethylidene)-benzohydrazide series of LSD1 inhibitors that are the subject of the remainder of the dissertation.

Chapters 3 and 4 describe validation of the activity of LSD1 inhibition in two solid tumors of interest, Ewing sarcoma and Type II endometrial carcinoma. Chapter 3 investigates the unique activity of the lead compound, HCI2509, in Ewing sarcoma, focusing both on characterizing the effects of HCI2509 on the molecular drivers of Ewing sarcoma *in vitro* and validating single-agent efficacy in xenograft models *in vivo*. Ewing sarcoma is driven solely by the chromosomal translocation leading to expression of an EWS/ETS fusion oncoprotein and transcription factor, lacking additional genomic aberrations (7). Subsequent transcriptional reprogramming relies heavily on misregulation of the transcriptional and epigenetic machinery, presenting an ideal proof-of-concept system for *in vivo* studies. Chapter 4 moves beyond this to Type II endometrial cancer, which primarily occurs in adulthood, is clinically aggressive, and is driven by a more diverse and complex set of genetic, epigenetic, and environmental factors. In this chapter, studies describe both the *in vitro* anticancer effects of HCI2509 in multiple cell lines and the *in vivo* antitumor efficacy of HCI2509 in an orthotopic model of Type II endometrial cancer. Chapter 5 provides conclusions while also outlining future work suggested by the results described herein. Additionally, three appendices include data which were critical to the completion of these studies, but not published, including protein purification, cell-based screening results, and pharmacokinetic studies.

1.3 Background

1.3.1 Epigenetics and Cancer Pathogenesis

Epigenetics broadly refers to four layers of dynamic regulation within the nucleus: DNA methylation, histone posttranslational modifications, nucleosome positioning, and the expression of various noncoding RNAs. Mounting evidence implicates all four levels in the development and maintenance of oncogenic gene expression programs characteristic of cancer. However, the roles that nucleosome positioning and noncoding RNAs play in cancer are outside the scope of this work.

1.3.1.1 DNA Methylation

DNA methylation in mammals occurs only on cytosine bases that are 5' linked to guanosine (CpG) (8). Methylation is catalyzed by DNA methyltransferases (DNMT) DNMT1, DNMT3a, and DNMT3b. DNMT1 acts only on hemimethylated DNA and is responsible for the maintenance of DNA methylation patterns during replication, while both DNMT3a and 3b are capable of *de novo* DNA methylation (9,10). Cytosine is largely underrepresented in the genome with the exception of short regions (0.5-4 kb) called CpG islands, which are GC enriched (8,11). CpG islands are located at the proximal promoter region of roughly 50% of genes in the human genome (11). DNA methylation at the promoter functions to silence the downstream gene. As a cell progresses through normal development, increased promoter methylation at particular loci silences expression of genes which are lineage-inappropriate, reinforcing cellular differentiation (10). In cancer, global genomic demethylation is observed, with increased methylation occurring at the promoter regions of tumor suppressor genes (12,13). Many

of the silenced tumor suppressors are known to be frequently mutated, like *MGMT*, *CDKN2A*, *MLH1*, and *BRCA1*, suggesting both genetic and epigenetic routes can lead to the same oncogenic phenotype (14-18).

In addition to the promoter hypermethylation observed across human neoplasms, DNA methylation can itself promote C to T mutations through spontaneous hydrolytic deamination (19). This effect is not insignificant, up to 50% of the inactivating mutations of the tumor suppressor *TP53* occur at methylated cytosines (20). Additionally, cancer cells display genomic hypomethylation outside of the proximal promoter regions (21,22). This global loss of methylation is thought to contribute to genomic instability and structural alterations of chromosomes (23). Overall, changes in DNA methylation were the first characterized epigenetic phenomena observed in cancer, and inspired the development of pharmacological agents targeting the DNMTs, the first FDA-approved epigenetic therapies for cancer, discussed in section 1.3.2.

1.3.1.2 Histone Modifications

In order to fit the whole genome into the nucleus, eukaryotic cells utilize a packing scheme in which 147 bp of DNA is wrapped around an octameric complex containing two each of histone 2a (H2a), histone 2b (H2b), histone 3 (H3), and histone 4 (H4) (1). This DNA-histone complex comprises the nucleosome, which is further compacted into chromatin. Tightly compacted chromatin is termed heterochromatin, and genes located here are repressed or silenced, whereas euchromatin has an open conformation allowing the transcriptional machinery access to promote active gene expression (1). Conserved residues on histones, often found on the unstructured and

lysine-rich N-terminus, are subject to a variety of posttranslational modifications including methylation, acetylation, phosphorylation, SUMOylation, and ubiquitinylation, such that histone modification is more diverse and dynamic than DNA methylation (24). Particular modifications act combinatorially such that various patterns of modifications interact with DNA- and chromatin-binding proteins to define chromatin status and recruit transcriptional machinery. Using the N-terminal tail of H3 as an example, heterochromatin is marked by increased H3K9 and H3K27 trimethylation as well as DNA methylation, whereas euchromatin is characterized by acetylation at H3K9 and H3K16 (25). While acetylation of histone residues directly affects gene accessibility through increasing the strength of the DNA-histone electrostatic repulsion, histone methylation plays an important, but more complex, role in transcriptional regulation. Notably H3K9 and H3K27 methyl marks are repressive, where methylation at H3K4 is permissive and commonly found associated with the proximal promoter of actively transcribed genes (24,25).

The suite of histone modifications are written, erased, and read by a diverse complement of biomolecules, including proteins and nucleic acids. Often complexes possessing opposing functions are found co-localized in the nucleus, facilitating context-dependent dynamism (26-28). The existence of bivalent domains, containing both activating and repressive histone marks, further underscores the importance of epigenomic dynamism (29,30). Using histone acetylation as an example, acetyl marks are written by histone acetyltransferases (HATs), including the p300/CBP, GNAT, and MYST subfamilies, and erased by histone deacetylases (HDACs) (31). Acetylated histone lysines are recognized by proteins which contain a structural motif termed a bromodomain.

Bromodomain-containing proteins include chromatin remodelers, HATs, histone methyltransferases, and transcriptional co-activators and often possess another histone reader domain, such as the methyllysine-specific PHD finger, to facilitate combinatorial recognition of the chromatin state (32).

Aberrant global histone acetylation patterns are broadly observed in cancer (32), and many studies have implicated HATs, HDACs, and bromodomains in malignant epigenetic misregulation. For example, HATs are present in multiple oncogenic fusion proteins (33), the most well known being MOZ-TIF2 in aggressive leukemia (34,35). Somatic mutations are also documented in HATs, such as those documented in p300/CBP, in various solid tumors and hematological malignancies (36,37). While somatic mutations are not observed as commonly in HDACs, levels of HDAC expression are often altered in cancer, with overexpression correlating with aberrant silencing of tumor suppressor genes and impaired apoptosis (38,39). With respect to histone readers, mutations in bromodomain-containing proteins have also been documented in acute lymphocytic leukemia (ALL), midline carcinoma, renal carcinoma, and breast cancer (31).

1.3.2 Implications of Cancer Epigenetics for Therapy

These observations illustrate an emerging paradigm, whereby genetic mutations and epigenetic factors are two sides of the same coin. It should be noted that discoveries analogous to those described for HATs implicate mutations in DNMTs, the histone lysine methylation machinery, nucleosome remodelers, and noncoding RNAs in carcinogenesis. In fact, mutations in epigenetic regulators are now documented in almost all human malignancies (40-51). Alterations in the epigenetic regulatory machinery lead to genomic

instability, which further promotes mutations in other tumor suppressors and epigenetic proteins, further compounding epigenetic misregulation, and so on. However, unlike genetic drivers of cancer, epigenetic modifications are often reversible, presenting opportunities to pharmacologically disrupt and reverse malignant programming. Understanding the interplay and intersection between genetic and epigenetic factors is of critical importance to determine the most appropriate and efficacious way to therapeutically target genomic misregulation in cancer. Most importantly, better tools are needed to determine which epigenetic players represent oncogenic drivers in a given malignancy, such that small-molecule blockade disproportionately affects the cancer cell while leaving required epigenetic and genomic regulatory mechanisms intact in normal tissue. To date, DNMT inhibitors and HDAC inhibitors, are FDA-approved and their clinical use over the past decade has enhanced our knowledge about the promises and challenges of epigenetic therapy in the clinic (Table 1.1).

1.3.2.1 FDA-Approved Epigenetic Therapies

1.3.2.1.1 DNA Methyltransferase Inhibitors

The DNA demethylating agents, decitabine and 5-azacytidine, were first designed as cytotoxic chemotherapy in the 1960s (52,53), and their activity against DNMTs was only established 20 years later (54). 5-azacytidine gained FDA-approval in 2004 for the treatment of myelodysplastic syndrome (MDS), while decitabine was approved in 2006 for MDS and acute myeloid leukemia (AML) (55-58). Their approval was dependent upon drastic reductions in dose from the maximally tolerated dose, such that dose de-escalation improved both tolerability and shifted the mechanism of action from cytotoxic

activity to DNMT inhibition (59). At low doses, the nucleotide analogue is incorporated into DNA and acts as a suicide inhibitor for the DNMT, triggering its degradation (60-63). Pharmacokinetic studies of the doses used clinically shows nanomolar plasma concentrations, and at these exposures minimal cell death is observed *in vitro* (64). However, even after 1 exposure, increased expression of immunomodulatory and pro-apoptotic genes, as well as whole-genome demethylation were observed and coincided with decreased clonogenicity and tumorigenicity (64). Importantly, findings of durable cellular reprogramming seem to also apply to tumor stem-like cells (64). This suggests epigenetic therapies may be able to target this population of cells, which is typically resistant to multiple other treatment modalities and drives the metastases and disease recurrence that often prove fatal. These laboratory results are consistent with clinical observations of patients treated with DNMTs. A large proportion of the patient population treated with 5-azacytidine for AML or MDS need months before a response becomes apparent, perhaps due to long-term exhaustion of stem-like cells (65). Additionally, ~48% of high-risk MDS patients who prolonged DNMTi treatment duration beyond their initial response improved the magnitude of response with subsequent therapies (65). The clinical use of DNMT inhibitors has greatly improved therapeutic options for patient with both MDS and AML.

1.3.2.1.2 Histone Deacetylase Inhibitors

The second class of FDA-approved epigenetic therapies are the histone deacetylase inhibitors. Both vorinostat and romidepsin were approved for the treatment of cutaneous T-cell lymphoma (CTCL), with romidepsin also indicated for the treatment of

relapsed peripheral T-cell lymphoma (66-69). Multiple additional HDAC inhibitors are in development, but are outside the scope of this work and are reviewed comprehensively by Lane, *et al.* (70). Whereas HDAC inhibitors have shown striking responses in CTCL, their value remains largely unproven elsewhere in the clinic, likely due to analogous but less understood differences in dose-dependent mechanisms of action, the discussion of which is beyond the scope of this work.

1.3.2.2 Clinical Challenges Facing Epigenetics

In the indications where epigenetic therapy is approved significant clinical benefits have been observed. However, while epigenetic mechanisms play a central role in cancer pathogenesis across malignancies, clinical benefit in the most common solid tumor remains largely unachieved. The difficulty in translating epigenetic insights to clinical benefit stems from our limited understanding of the basic science through to the design and execution of clinical trials.

In the laboratory, prior to the advent of next generation sequencing and ensuing flood of genomic data, epigenetics research was heavily biased towards events occurring at the transcription start site. As these research programs were initiated the most obvious and observable phenomena was DNA methylation at silenced gene promoters and the downstream effects on transcription (51). However, cancer manifests at the level of the whole genome as is visible in the nuclei of cancer cells under a microscope. In the new era of “-omics,” our understanding of the global epigenomic events leading to cancer is certainly growing, however, the detailed mechanisms by which these events occur and how exactly they drive tumorigenesis remain largely undetermined and unexplored.

It is clear, however, that misregulation in the epigenome is far-reaching, representing a sort of software glitch that alters expression programs across hundreds of genes in diverse pathways and promotes tumorigenesis. Currently approved therapies clearly can rise to the challenge of targeting the cellular reprogramming. The Peter A. Jones group has largely demonstrated durable reprogramming of cancer cells following long-term low exposure to DNMT inhibitors in cell culture (64). Additionally, the process of “reprogramming” induced pluripotent stem cells from differentiated adult cells is enhanced by DNMT and HDAC inhibitors (71-73). These results buttress the potential for epigenetic therapy to show sweeping effects in solid tumors. However, the sort of “knockdown-rescue” experiments that are required to prove causality and achieve mechanistic insight in this realm are largely beyond our technical prowess.

While comprehensive understanding of the mechanisms by which approved therapies act remains elusive, several empirical observations have informed the current paradigm for dose de-escalation in their clinical use. At high doses, both DNMT and HDAC inhibitors show cytotoxic effects, with the more potent on-target effects dominant at low doses (51). HDAC inhibitors are limited in that HDACs are fairly promiscuous enzymes and show diverse function (74,75). In fact, some HDACs are localized to the cytoplasm, such that an analysis of whether the antitumor efficacy seen with HDAC treatment are on- or off-target is largely confounded (74). These types of observations continue to muddy the water.

Early trials of epigenetic therapy in solid tumors followed traditional clinical trial design, using dose-escalation to identify the maximally tolerated dose (MTD). In Phase II efficacy testing, the MTD for both HDAC and DNMT inhibitors showed pronounced off-

target cytotoxicity with little effect on the epigenetic pharmacodynamic endpoints. In order to evaluate the epigenetic activity of these classes of drugs, the doses needed to be reduced. This dose de-escalation was accompanied by the observation that cellular reprogramming was not apparent in the short-term, and required long-term pharmacodynamic monitoring (51). The high cytotoxic doses likely preclude the reprogramming required for true epigenetic therapy. Thus, clinical translation has been limited to date by suboptimal trial design which fails to account for the low-dose, long-term efficacy expected with epigenetic drugs.

As such, innovative trial designs are required to build on the early data in hematological malignancies and establish a new paradigm for epigenetic treatment in solid tumors. This really is early days, as several fundamental parameters remain undefined. For example, the therapeutic window for reprogramming in malignant versus normal tissues, or the length of time and criteria used to assess response, are unknown and yet unstudied. Clinical evaluation of new epigenetic therapeutic strategies may benefit from trial design used in other fields, like translational immunotherapy, to assess these sorts of parameters (76). Encouragingly, these lessons have been learned and dose de-escalation is being tested clinically in solid tumors, including nonsmall cell lung carcinoma, colorectal, and breast cancers and with promising early results (77).

1.3.2.3 Sensitizing Cancer to Other Treatments

Further optimization of DNMT and HDAC inhibitor dosing in solid tumors in the clinic will provide an opportunity to validate observations from the laboratory that cellular reprogramming induced by epigenetic targeted agents confers increased cellular

sensitivity to other modalities of treatment. This includes hormone therapy, chemotherapy, and immunotherapy either combined in parallel or implemented sequentially (51). Notably, Sharma, *et al.* (78) observed *in vitro* the existence of a drug-tolerant population of cells in multiple human tumor cell lines. The drug-tolerant phenotype was transient and reversible, and mediated by both IGF-1 receptor signaling as well as chromatin changes, suggesting a role for dynamic epigenetic regulation in the development of drug resistance (78). Inhibition of IGF-1 receptor signaling, HDACs, and the histone lysine demethylase JARID1A ablated this phenotype, suggesting a potential role for epigenetic therapies to augment sensitivity to other systemic anticancer therapies (78).

1.3.3 Emerging Epigenetic Targets

While DNMT and HDAC inhibitors provided proof-of-concept for epigenetic therapies in the clinic, insights from the last decade of cancer epigenetics research has uncovered mutations or aberrations in countless other classes of epigenetic regulators including histone mark readers, histone lysine methylation regulators, nucleosome remodelers, and the noncoding RNA machinery. This has resulted in a wave of target validation and drug discovery efforts across academia and industry. Several of these research tracks are now bearing fruit, with several novel classes of epigenetic targeted agents in Phase I and Phase II studies. For each program described herein, the Phase I studies have focused on or are studying a particular malignancy in which the target is an established driver of the disease, either through direct mutation or as a required player in epigenomic misregulation. This underscores the importance of picking the right patient

population with clear pharmacodynamic criteria for proof-of-concept studies.

Having optimized dosing and pharmacokinetic/pharmacodynamic relationships in these simpler populations, clinical research can move forward with the process of evaluating these agents in diverse patient populations with more complex disease states. This progress will lean heavily on continued insights from both basic and translational studies validating potential biomarkers to define the patient populations most likely to respond to different classes of epigenetic agents. The ultimate goal is to enable personalized epigenetic treatment for each individual malignancy. To date, the most advanced clinical programs are those targeting histone acetylation readers, or bromodomain inhibitors, and those targeting the histone lysine methylation machinery.

1.3.3.1 Targeting Bromodomains

Protein-protein interactions are notoriously difficult to target with small molecules, however, a class of inhibitors, exemplified by the molecules JQ-1 and iBET, have been shown to disrupt the interaction of the BET family (BRD2, BRD3, BRD4, and BRDt) of bromodomain proteins with acetylated histone lysine residues. Bromodomain inhibitors represent the first epigenetic agents to target histone posttranslational readers. The bromodomain of BET proteins is highly conserved, plays a critical role in cell cycle progression and transcriptional elongation, and is involved in translocations which drive the fatal NUT-midline carcinoma. *In vitro* and *in vivo* studies of the BET inhibitors consistently showed both downregulation of *MYC* transcript and disruption of the *MYC* transcriptional program across a wide variety of hematological and solid malignancies, as well as disruption of superenhancer motifs that reinforce *MYC* and *BLC2* expression (79-

88). At the time of writing three BET inhibitors programs had initiated clinical trials, with GSK525672 in two Phase I trials for NUT midline carcinoma and relapse or refractory hematological malignancies (89), TEN-010 for advanced solid malignancies or NUT midline carcinoma (90), and CPI-0610 in previously treated and aggressive lymphomas (91).

1.3.3.3 Targeting Histone Lysine Methylation

While histones can be methylated at lysine, arginine, and histidine side chains, lysine methylation is the best characterized and disproportionately represents the therapeutic development by targeting histone methylation, so it will be the focus of discussion. Unlike acetylation and phosphorylation, lysine methylation does not alter the charge of the residue. Of the posttranslational modifications, methylation shows the slowest turnover (92) and was originally thought to be irreversible, until the discovery of the first histone lysine demethylase in 2004 (93). Lysine residues can be either mono- (me1) (94), di- (me2) (95), or tri-methylated (me3) (96). Methylation at histone H3 lysine 4 (H3K4), lysine 9 (H3K9), lysine 27 (H3K27), lysine 36 (H3K36), lysine 79 (H3K79), and histone H4 lysine20 (H4K20) are the most studied, and a plethora of methyl mark writers, readers, and erasers have been identified which display diverse substrate specificities and allow for nuanced control of histone methylation status (Figure 1.1). Broadly speaking, methylation at H3K4, H3K36, and H3K79 typically correlates with euchromatin, while that at H3K9, H3K27, and H4K20 corresponds to repressive heterochromatin (31). Even more specifically, some methylation states may require stability through mitosis, such as established silencing within heterochromatin, while

others depend upon dynamism, so as to facilitate cell differentiation in response to external stimuli. Additionally, different modifications on the same residue may denote specific chromatin states. For example, H3K9me1 is typically associated with active chromatin, while H3K9me3 is associated with repressed genes (31). Moreover, these marks may distribute to different regions spatially, for example, H3K4me1 is found within enhancer regions of the genome, while H3K4me2/3 is enriched at the transcription start sites of actively-transcribed genes (31). This model of complexity between different marks and within methyl marks on the same lysine is supported by the observation that methyl marks at different lysine residues display different turnover rates (97).

The dynamics of histone methylation are regulated by histone lysine methyltransferases (KMTs) and histone lysine demethylases (KDMs). KMTs catalyze the addition of methyl marks to lysine from S-adenosylmethionine (94) and fall into one of two families, either the SET-domain containing proteins (98) or DOT1L-like proteins (99). KDMs likewise fall into two classes, either the amine oxidases (94) or jumonji C (JmjC)-domain containing, iron-dependent dioxygenases (100,101). In addition to the complexity by which histone methylation regulates chromatin, many KMTs and KDMs also act upon nonhistone substrates, challenging the interpretation of the biological role for these enzymes in the cell.

Like DNA methylation and histone acetylation, histone lysine methylation has been widely implicated in the development of various malignancies both through alterations in levels of expression as well as through mutation of KMTs and KDMs. The complete details of this are beyond the scope of this work, but are reviewed comprehensively by Albert and Helin (102) and Chi *et al.* (103). Broadly speaking,

various malignancies show aberrations in the global levels of histone lysine methyl marks, most commonly hypomethylation, that are associated with poorer survival, worse clinical outcomes, or higher disease recurrence (Table 1.2) (104). While causality remains unestablished, these observations may lead to the development of future biomarkers. At the interface between genetics and epigenetics, genomic studies have also identified several somatic mutations in the histone lysine methylation machinery or chromosomal translocations which involve KMTs or KDMs, further implicating misregulation of histone methylation in oncogenesis (102-104).

To date, two KMTs have proven to be tractable targets for the development of pharmacological inhibitors. The first is DOT1L, a KMT with specificity for H3K79 (99). Roughly 5-10% of acute leukemias, particularly infant and relapsed leukemias, present with a chromosomal translocation involving the KMT MLL at 11q23 (105). Loss of the C-terminus of *MLL* in rearrangements replaces the SET KMT domain with sequences derived from AF4, AF9, AF10, and ENL (105). These domains interact directly with DOT1L to maintain the *MLL-r* fusion-driven oncogenic transcriptional activity, such that DOT1L is necessary for transcription of key target genes driving leukemogenesis (105). Epizyme recently concluded the dose-escalation portion of their Phase I study of the DOT1L inhibitor, EPZ-5676, and began enrolling for the expansion phase of the trial in December 2013 (106). This was the first histone methyltransferase inhibitor to enter the clinic.

The second KMT with drug development programs entering early clinical studies is enhancer of zeste homolog 2 (EZH2). EZH2 is a KMT with substrate specificity for H3K27 and is the catalytic subunit of the polycomb repressive complex 2 (PRC2),

promoting gene silencing. EZH2 is a prime example of target complexity when considering histone methylation. EZH2 is observed in numerous cancers including breast (107), prostate (108), lung (109), skin (109), and colon cancer (109), as well as lymphomas (110). B-cell lymphomas have also been shown to contain somatic activating point mutations in EZH2, supporting its role as an oncogene (110). Further buttressing this model, the histone demethylase with substrate specificity for H3K27, UTX, contains inactivating point mutations in a variety of cancers (111). However, loss-of-function EZH2 mutations in MDS have been reported (112), highlighting the context-dependence of a single epigenetic target in a given disease. The second KMT inhibitor to enter the clinic was Epizyme's EPZ-6438, with the dose escalation study still active for patients with advanced solid tumors and relapsed or refractory B-cell lymphoma (113). GlaxoSmithKline has also initiated clinical trials with their EZH2 inhibitor, GSK2816126, in patients with relapsed or refractory diffuse large B cell and transformed follicular lymphoma (114).

In addition to KMTs, KDMs are attractive therapeutic targets in various cancers. Beyond genetic aberrations, expression levels of various KDMs are observed across many human malignancies (Table 1.3) (115). The first KDM inhibitor to reach the clinic is GSK2879552, an irreversible inhibitor of lysine specific demethylase 1 (LSD1/KDM1A) with Phase I studies initiated in early 2014 for patients with relapsed or refractory nonsmall cell lung carcinoma (116). LSD1 is the focus of the remainder of this work.

1.3.4 Lysine Specific Demethylase 1

Somatic mutations in *KDM1A* are not observed in cancer, but LSD1 overexpression has been documented in a number of both hematological and solid malignancies and is typically associated with de-differentiation, aggressive biology, and poorer outcomes. Increased levels of LSD1 are a biomarker for aggressive tumor biology and poor prognosis in breast (117) and prostate cancers (118-121). In prostate cancer, the overexpression of LSD1 promotes ligand-independent androgen-receptor-dependent transcription (119,120). LSD1 expression is inversely correlated with differentiation in neuroblastoma, suggesting a role in repressing differentiation (122). Interaction of the transcription factor TAL1 with LSD1 drives hematopoietic differentiation programs, with aberrant function of this axis observed in ~60% of T-cell acute lymphoblastic leukemia (123,124). In acute myeloid leukemia, LSD1 blocks differentiation and perpetuates the cancer stem-cell compartment (125,126). Upregulation of LSD1 has also been observed in bladder (127,128), lung (127), colorectal tumors (127), high grade sarcomas (129,130), and hepatocellular carcinoma (131,132).

1.3.4.1 Discovery, Structure, and Function

LSD1 is the main histone demethylase in the cell and comprises an 852 amino-acid flavin adenine dinucleotide (FAD)-dependent amine oxidase, depicted in Figure 1.2 (94). The discovery of this enzyme, conserved from yeast through humans, was the first concrete evidence for dynamic regulation of histone methylation. The first 171 N-terminal residues are unstructured, but appear to act as a tether for interactions with other proteins in chromatin-remodeling complexes (133,134). The majority of conserved

residues reside in close proximity to the amine oxidase domain (AOD) and appear to facilitate ligand packing and binding (133,134). The AOD is conserved and homologous to monoamine oxidases (MAO) A and B, as well as polyamine oxidase (PAO) (133,134). Like the MAOs, LSD1 binds FAD in a conserved Rossmann fold, however, unlike the MAOs, LSD1 binds FAD noncovalently (133,134). The FAD cofactor binding pocket is a narrow cavity through the center of the enzyme and within this pocket FAD interacts with LSD1 through salt bridges with Arg310 and Arg316. The isoalloxazine ring system is positioned for catalytic activity at the base of the substrate binding pocket near Lys661 (133). The FAD is reduced during the formation of the imine intermediate. Hydrolysis of the imine leaves the demethylated lysine and releases a molecule of formaldehyde, while the FADH⁻ is oxidized to FAD by oxygen, releasing a molecule of H₂O₂ (Figure 1.3) (135). Lys661 is critical for enzymatic activity by channeling molecular oxygen for FADH⁻ oxidation and recharging the redox potential at the catalytic site (136).

Other domains include a Swi3p, Rsc8p and Moira (SWIRM) domain and a tower domain. In most proteins, SWIRM domains interact directly with DNA, though this is not the case for LSD1. The tower domain, required for enzymatic activity (134), is a coiled-coil sequence inserted within the AOD which prominently protrudes as a docking site for additional protein-protein interactions, such as that with Co-REST, a common binding partner for LSD1. Co-REST contains two SANT domains, which confer DNA-binding in place of LSD1's odd SWIRM domain, and are required for functional demethylation of residues in the native nucleosome (133).

LSD1 demethylates both mono- and di-methyl marks on H3K4 and H3K9 (94,118). Methylation of H3K4 is associated with gene activation, while H3K9

methylation generally denotes gene repression. Due to the imine intermediate formed during demethylation, removal of the trimethyl mark is chemically inaccessible to LSD1 (134). The substrate N-terminal tail of H3 packs tightly into the asymmetric funnel-shaped binding pocket of LSD1. The amine terminus of H3Ala1 is bound in a highly electronegative pocket showing hydrogen bonding and electrostatic interactions with Asp555 of LSD1 (137). Lys4 is oriented toward the isoalloxazine ring system to facilitate oxidative attack on the N-CH₃ group by flavin (137,138). Residues 1-5 of histone H3 adopt a helical turn, 6-9 are sharply bent, and residue 10-16 are more extended and partially solvent exposed along the rim of the binding pocket (138).

Recent structural studies by Baron, *et al.* (136) show that multiple proteins contain conserved N-terminal sequences homologous to histone H3. These are often transcription factors that may function to hook LSD1 for recruitment to different genomic sites (136). Some examples include SNAI1 (related to morphogenetic events mediating tumor invasiveness), Ovo-like1 (epidermal proliferation and differentiation factor), SCRATCH1 (nervous system specific), gfi1 (a gene repressor involved in hematopoiesis whose expression is regulated by LSD1-containing complexes), and insm1 (insulinoma-associated 1; associated with differentiation of neural and pancreatic precursors; discovered in a neuroendocrine tumor) (136). The SNAI1-LSD1 interaction has been crystallized and shows a similar binding mode to histone H3 (Figure 1.4) (136). Other binding partners dock on the tower domain; for example, another SANT-domain-containing protein called MTA2 has also been shown to recruit LSD1 to chromatin as a member of the nuclear remodeling and deacetylase (NuRD) repressive complex, using a mechanism analogous to Co-REST (139). LSD1 has also been shown to be recruited by

the noncoding RNA HOTAIR into larger complexes containing PRC2 proteins (140).

Combinatorial regulation is commonly used to achieve the complex epigenetic functions that are required for differentiation and maintenance of cell- and tissue-specific gene expression programs. In addition to several interaction partners with H3-homologous N-terminal tails, additional posttranslational histone modifications alter binding affinity of LSD1 for the H3 substrate, such that the histone code can drastically help or hinder LSD1 activity. At least 16 amino acids are required for functional demethylation, though the 21 amino acid substrate shows higher binding affinity (141). Many of the H3 residues 10-21 bind along the SWIRM/AOD boundary. Modifications here will affect binding affinity of the histone tail and change enzymatic efficiency. Closer to the histone binding pocket, many residues have been studied in detail. Methylation of Lys9 shows no effect on LSD1 activity, while acetylation of this residue shows a 6-fold decrease in binding affinity (141). LSD1 activity is completely abolished by phosphorylation at Ser10 (141). Additionally, phosphorylation of H3T6 removes access to H3K4 and shifts the substrate specificity of LSD1 to H3K9 (142).

In addition to combinatorial regulation on the substrate histone tail, LSD1's function can be regulated by alternative splicing and posttranslational modifications. Two additional splice sites are observed in the *KDM1A* gene, one at exon 2 and exon 8 (143). The two additional splice sites may be incorporated either separately or together to result in three additional possibilities, either the 8a, 2a, or 8a/2a variants (143). The 2a variant results in a twenty amino acid insertion in the unstructured N-terminal region and may confer additional or altered specificity in recruiting other partners into chromatin-remodeling complexes (143). The 8a variant is found only in neuronal tissue and contains

a four amino acid insertion at the base of the tower domain. This insertion contains a phosphorylation site at Thr396b that, when phosphorylated, acts as a dominant negative form of LSD1 that cannot bind CoREST or HDACs and fails to repress neuronal differentiation genes (143,144). Levels of 8a accumulate as neuronal development progresses and the loss of this variant results in decreased development of neuronal morphological features *in vitro* (143). The combined 8a/2a variant is found in the brain and testis (143). LSD1 has also been reported as a substrate for phosphorylation by protein kinase C α (PKC α) (145) and protein kinase CK2 at Ser131, Ser137, and Ser166 (146), though the function of these posttranslational modifications remains undetermined.

1.3.4.2 An Epigenetic Effector with Context-Dependent Function

Based on the complexity of structural mechanisms which regulate LSD1 enzymatic activity and its protein-protein interactions, it is unsurprising that the physiological function of LSD1 depends largely on both the cellular context and protein-protein interaction partners. A few illustrative examples are described. At the most basic level, many LSD1/CoREST complexes contain BHC80, which recognizes and binds unmethylated H3K4 to prevent reactivation of target genes (147). Knockdown of BHC80 results in de-repression of LSD1-repressed genes, so BHC80 might function to keep LSD1-containing complexes at the unmodified site for continued repression (147). This also builds on data from Forneris, *et al.* (141) suggesting that LSD1 requires a histone substrate relatively free of other posttranslational modifications and is the last actor during events which effectively switch the local chromatin state. However, while the most commonly studied LSD1-containing complexes are repressive, involve interaction

with CoREST and HDACs, and are targeted at H3K4, in complex with the androgen and estrogen receptors LSD1 shows specificity for H3K9 and demethylation activates hormone-receptor-dependent transcription (118,148).

Members of the Snai1 family recruit LSD1, through their H3 homologous Snail/Gfi (SNAG) domain, to the promoters of epithelial genes, like E-cadherin (*CDH1*). This is particularly important during the epithelial-to-mesenchymal transition (EMT) in order to repress the epithelial gene expression program and cellular phenotype (149-151). In malignant cells, the resulting cellular program drives cells to display a more invasive phenotype, and may partially explain the observed association of increased LSD1 expression with aggressive tumor biology (149).

While it is relatively easy to envision the context-dependent function of LSD1 on a complex-to-complex basis, the most interesting data have demonstrated that LSD1 exists in opposing complexes that co-localize in the nucleus. These complexes often exist at the boundaries between heterochromatin and euchromatin and are important for normal development (152,153). In drosophila, the LSD1 homolog *dLsd1* and the histone demethylase *Lid* oppose each other at the boundaries of hetero- and euchromatin, with *dLsd1* promoting the expansion of heterochromatic regions. Interestingly, both play a pivotal role in modulating Notch-dependent gene expression (154). *dLsd1* is present at Notch target gene promoters and facilitates activation of transcription in antagonism of *Lid* when Notch signaling is on. However, when Notch signaling is off *dLsd1* and *Lid* cooperate to repress Notch target genes (154). Based on the complex structural and biochemical factors that affect LSD1's specificity, this dual role is not unexpected, but the regulatory mechanisms that mediate these phenotypes *in vivo* remain poorly understood.

In another interesting example, LSD1 is critical for pituitary development (155). However, early development requires LSD1-mediated gene activation, while terminal differentiation events require LSD1-mediated gene repression at the same target genes (155); again, the precise mechanisms which determine the spatiotemporal regulation of LSD1 remain undetermined.

As a final note on substrate specificity, it should be noted that LSD1 is known to demethylate nonhistone substrates, though how LSD1 is targeted to these substrates is not understood. Demethylation of the p53 protein at Lys370 by LSD1 prevents the binding of p53 with 53BP1 that is required for p53-mediated transcriptional activation (156). Thus, LSD1 can repress p53 tumor suppressive function through methylation status of a single lysine residue. LSD1 is also critical for the maintenance of global DNA methylation levels *in vivo* through regulation of DNMT1 (157). Demethylation by LSD1 is required for DNMT1 protein stability and comprises a functional link between the histone and DNA methylation apparatus (157). Another interesting nonhistone substrate for LSD1 is metastatic tumor antigen 1 (MTA1), a member of both the NuRD repressive and nucleosome remodeling factor (NURF) coactivator complexes. When methylated, MTA1 promotes formation of the NuRD complex, while demethylation by LSD1 induces a conformational change which promotes assembly of NURF complex components and switching function from transcriptionally repressive to transcriptionally activating (158); thereby neatly demonstrating the ways in which LSD1 can assemble in complexes with opposing function.

1.3.4.3 Challenges of Studying LSD1 Biology

The complexity of LSD1 biology presents obvious challenges to translate laboratory findings to the clinic. Whole-genome studies investigating TGF β -induced EMT have shown that LSD1 is the critical regulator of decreased genomic H3K9me₂ and increased H3K4me₃ and H3K36me₃ in a manner that may apply to malignant transformation (151). These types of findings speak to the potential power of specifically inhibiting LSD1 in cancer, but the biggest challenge remains understanding the underpinning of the biological mechanisms by which LSD1 acts. While the association of LSD1 with an aggressive clinical course has been established, LSD1 has also been reported to have some tumor suppressor function (139).

Target validation studies have traditionally used RNAi, MAO inhibitors, or polyamines to probe LSD1 biology in cancer. In various cancer models, inhibition of LSD1 or RNAi-mediated knockdown resulted in increased H3K4 methylation, reexpression of aberrantly silenced tumor suppressor genes (127,159), decrease in prosurvival gene expression (127,160), differentiation of dedifferentiated cancer cell (124,128), and decreased cancer cell proliferation and survival (117,121,122,124,125,127-129,160). However, none of these modes of LSD1 inhibition represent ideal positive controls for novel compound development. Knockdown-rescue experiments have shown rescue of complex phenotypes *in vivo* with an enzymatically dead mutant (*personal communication Michael Engel*), and no published studies that the author could find attempted knockdown and rescue with both the wild-type and enzymatically dead constructs. LSD1 is present in complexes at thousands of gene promoters throughout the nucleus, but only enzymatically active at a smaller subset

depending on external stimuli (161). Global knockdown removes LSD1 and may affect the stability of multiple nuclear complexes independent of LSD1 enzymatic activity, confounding extrapolation of results to enzymatic inhibitors. The monoamine oxidase inhibitor most commonly used for target validation has been tranylcypromine, which is not potent or specific for LSD1, nor are the polyamines. Thus, deconvoluting which effects are on- vs. off-target with these treatments is challenging and holding novel classes of LSD1 inhibitors to display the same biological output as MAOi and polyamines may falsely discredit bonafide LSD1 inhibitors. This is supported by recent molecular modeling work suggesting that LSD1 has multiple binding pockets on its surface (162) coupled with results described in Chapter 2 which show different classes of LSD1 inhibitor displaying different biophysical effects on LSD1 protein in solution. One could envision disrupting both enzymatic activity and potentially protein-protein interactions through direct or allosteric mechanisms, and depending on the interaction disrupted the biological readout could be different.

The complexity of LSD1 biology and the factors confounding its exploration also make predicting toxicity difficult. LSD1 knockout is embryonic lethal (163) and it is an important regulator for normal developmental transcriptional programs in hematopoiesis (123), adipogenesis (164), and neurogenesis (165,166). LSD1 expression is highest during early development and has roles in maintaining pluripotency (167,168) and the cell cycle in stem cells (169) and initiating differentiation during development (170). Conditional knockdown of LSD1 in adult mice led to alterations in hematopoiesis characterized by an expanded progenitor compartment and decreased terminal differentiation (171). This phenomenon was recapitulated to varying degrees with

tranylcypromine and its derivatives, though small molecules were not tested *in vivo* (171). It is unknown what the therapeutic window would be for a potent LSD1 inhibitor *in vivo*, and whether differences would be observed for reversible and irreversible inhibitors.

1.3.5 Pharmaceutics in Translational Science

In addressing the complexity of *in vivo* efficacy and toxicity of a novel epigenetic drug, translational scientists must exercise care in choosing an appropriate preclinical formulation. Primarily, the vehicle used for drug delivery and route of administration should not interfere in any way with evaluation of the biological system used for testing. Importantly, different stages of preclinical work place different constraints on the formulation used. For example, in proof-of-concept studies the formulation scientist should maximize exposure within the limits of tolerability. However, for pharmacokinetics studies, the formulation must provide detectable exposure without altering the properties of the test compound drastically. As a lead compound emerges and progresses toward the clinic, the formulations used must evolve to be more clinically relevant and acceptable to regulatory agencies.

While this may seem straightforward, the general solubility of new chemical entities evaluated is declining (172). Solubilizing agents which are acceptable in *in vitro* settings are poorly tolerated *in vivo*. Several alternative strategies can be used to overcome poor aqueous solubility and the appropriate solution is highly compound specific (173). For compounds which are weakly acidic or basic, pH adjustment using different buffering systems within the range of pH 2-9 can greatly improve aqueous

solubility. Another common strategy involves the use of cosolvents, though these have highly variable tolerability depending on the intended route of administration. Here organic molecules which are miscible with water provide nonpolar regions to interact with the solute. Commonly used cosolvents include polyethylene glycol 400 (PEG400), propylene glycol, dimethylacetamide, ethanol, and dimethyl sulfoxide (DMSO). Other strategies include co-complexation with cyclodextrins, which contain an interior non-polar region for solute binding, and inclusion of lipids or surfactants, which can lead to micelle formation of other macromolecular complexes. Use of surfactants can also stabilize drug suspensions and facilitate drug uptake. In the studies reported herein, cosolvent systems were the primary strategy for drug formulation, using guidelines previously reported to minimize confounding toxicities (173).

1.4 Study Rationale and Objectives

1.4.1 Rationale

Most studies of LSD1 biology to date have utilized either RNAi-mediated knockdown of LSD1, polyamine analogues, or tranylcypromine and its derivatives to investigate the biology of LSD1. These investigations suggest inhibition of LSD1 in cancer may provide benefit to some patients. However, these modes of LSD1 inhibition are neither potent nor specific, and even with well defined biological output, translation from mouse studies to the clinic remain difficult (174). More potent, specific, and reversible inhibitors of LSD1 are needed to carefully evaluate the biological impacts of LSD1 inhibition on global epigenomic regulation and tumorigenic phenotypes in *in vitro* and *in vivo* models of malignancy, identify biomarkers to guide clinical translation, and

assess the preclinical efficacy and toxicity of LSD1 inhibition.

- **Rationale:** Reversible inhibitors with improved specificity and potency profiles can be used to perform proof-of-concept studies to validate LSD1 inhibition as a prospective therapeutic strategy in solid tumors.

1.4.2 Hypothesis and Objectives

The primary objective of this work is to discover and evaluate a novel potent, specific, and reversible series of LSD1 inhibitors with physicochemical properties amenable for translation to the clinic. Our overarching hypothesis is that by targeting the key histone demethylase, potent and specific LSD1 inhibitors will exhibit single-agent efficacy in solid tumor models. In order to test this hypothesis, the first requirement is to discover and biochemically validate a series of novel LSD1 inhibitors, described in Chapter 2. The second requirement is to show that in malignancies sensitive to lead compound HCI2509, this efficacy translates to *in vivo* models of disease, described in Chapters 3 and 4. Critical aims and approaches are as follows:

1.4.2.1 Chapter 2, Hypothesis 1

A high-throughput virtual screening strategy can identify novel scaffolds which 1) show inhibitory activity in an enzymatic assay (goal IC₅₀ < 1 μM) and 2) can be optimized to low nanomolar potency leads.

- **Approach:** Identify a commercially available hit compound using high throughput virtual screening and followed by subsequent iterative biochemical testing and medicinal chemistry for hit-to-lead optimization.

1.4.2.2 Chapter 2, Hypothesis 2

The novel lead compound will 1) show specificity over homologous enzymes, 2) bind LSD1 reversibly, 3) not compete with the histone H3 N-terminal substrate for LSD1, and 4) show decreased cancer cell line viability.

- **Approach:** Biochemically characterize the lead compound HCI2509 in an array of biochemical assays and assess the effect of HCI2509 on cancer cell line viability *in vitro*.

1.4.2.3 Chapter 3, Hypothesis

LSD1 inhibition with HCI2509 impairs function of the NuRD complex, causes global derepression of EWS/FLI repressed target genes, and shows antitumor activity *in vivo* across Ewing sarcoma cell lines.

- **Approach 1:** Compare the global transcriptional profile of HCI2509 treatment against that of EWS/FLI- and EWS/ERG-knockdown and to validate selected findings across multiple cell lines.
- **Approach 2:** *In vitro* characterization of HCI2509 treatment against other EWS/FLI-knockdown associated phenotypes, including cell morphology and oncogenic transformation. Additionally characterize global methylation changes caused by HCI2509 treatment.
- **Approach 3:** Characterize LSD1 target engagement in cells through evaluation of the relationship between LSD1 inhibition, *HMOX1* induction, and EWS/FLI function.
- **Approach 4:** Evaluate the antitumor efficacy of HCI2509 in multiple Ewing

xenograft models.

1.4.2.4 Chapter 4, Hypothesis

LSD1 inhibition with HCI2509 is an effective therapeutic strategy for malignancies with a more complex etiology, specifically Type II endometrial carcinoma.

- **Approach 1:** Evaluate the effects of HCI2509 on proliferation, transformation, global histone methylation, and target gene derepression in hormone-resistant Type II endometrial carcinoma cell lines.
- **Approach 2:** Test HCI2509 for *in vivo* antitumor efficacy using an orthotopic xenograft model of Type II endometrial carcinoma tracking disease with bioluminescence.

These hypotheses and approaches, and the resulting data are discussed at length in their respective chapters. The results from Chapter 2 have been peer-reviewed and published in the *Journal of Medicinal Chemistry*. The studies described in Chapters 3 and 4 have been accepted at *Clinical Cancer Research* and submitted to *BMC Cancer*, respectively.

1.5 References

1. Alberts B, et al. *Molecular Biology of the Cell*, 5th ed. New York: Garland Science, 2008. Print.
2. Hanahan D, Weinberg RA. Hallmarks of cancer: the next generation. *Cell* 2011;144:646-74.
3. Global Health [Internet]. Atlanta: American Cancer Society; c2014 [cited 2014 May 3]. Available from: <http://www.cancer.org/aboutus/globalhealth/>.
4. Schulte JH, Lim S, Schramm A, Friedrichs N, Koster J, Versteeg R, et al. Lysine-specific demethylase 1 is strongly expressed in poorly differentiated neuroblastoma: implications for therapy. *Cancer Res* 2009;69:2065-71.

5. Harris WJ, Huang X, Lynch JT, Spencer GJ, Hitchin JR, Li Y, et al. The histone demethylase KDM1A sustains the oncogenic potential of MLL-AF9 leukemia stem cells. *Cancer Cell* 2012;21:473-87.
6. Lim S, Janzer A, Becker A, Zimmer A, Schüle R, Buettner R, et al. Lysine-specific demethylase 1 (LSD1) is highly expressed in ER-negative breast cancers and a biomarker predicting aggressive biology. *Carcinogenesis* 2010;31:512-520.
7. Crompton B, Stewart C, Taylor-Weiner A, Alexa G, Kurek K, Calicchio M, et al. The genomic landscape of pediatric Ewing sarcoma. [abstract]. In: Proceedings of the 105th Annual Meeting of the American Association for Cancer Research; 2014 Apr 5-9; San Diego, CA. Abstract nr 999.
8. Bird, A. DNA methylation patterns and epigenetic memory. *Genes Dev* 2002;16:6–21.
9. Kumar S, Cheng X, Klimasauskas S, Mi S, Posfai J, Roberts RJ, et al. The DNA (cytosine-5) methyltransferases. *Nucleic Acids Res* 1994;22:1-10.
10. Okano M, Bell DW, Haber DA, Li E. DNA methyltransferases DNMT3a and DNMT3b are essential for de novo methylation and mammalian development. *Cell* 1999;99:247-57.
11. Takai D, Jones PA. Comprehensive analysis of CpG islands in human chromosomes 21 and 22. *Proc Natl Acad Sci USA* 2002;99:3740–5.
12. Baylin SB, Herman JG. DNA hypermethylation in tumorigenesis: epigenetics joins genetics. *Trends Genet* 2000;16:168–174.
13. Jones PA, Laird PW. Cancer epigenetics comes of age. *Nature Genet* 1999;21:163–167.
14. Esteller M, Toyota M, Sanchez-Cespedes M, Capella G, Peinado MA, Watkins DN, et al. Inactivation of the DNA repair gene O⁶-methylguanine-DNA methyltransferase by promoter hypermethylation is associated with G to A mutations in K-ras in colorectal tumorigenesis. *Cancer Res* 2000;60:2368–71.
15. Herman JG, Civin CI, Issa JP, Collector MI, Sharkis SJ, Baylin SB. Distinct patterns of inactivation of p15INK4B and p16INK4A characterize the major types of hematological malignancies. *Cancer Res* 1997;57:837-41.
16. Esteller M, Silva JM, Dominguez G, Bonilla F, Matias-Guiu X, Lerma E. Promoter hypermethylation and *BRCA1* inactivation in sporadic breast and ovarian tumors. *J Natl Cancer Inst* 2000;92:564–569.

17. Kane MF, Loda M, Gaida GM, Lipman J, Mishra R, Goldman H, et al. Methylation of the hMLH1 promoter correlates with lack of expression of *hMLH1* in sporadic colon tumors and mismatch repair-defective human tumor cell lines. *Cancer Res* 1997;57:808–811.
18. Herman JG, Umar A, Polyak K, Graff JR, Ahuja N, Issa JP, et al. Incidence and functional consequences of hMLH1 promoter hypermethylation in colorectal carcinoma. *Proc Natl Acad Sci USA* 1998;95:6870–6875.
19. Coulondre C, Miller JH, Farabaugh PJ, Gilbert W. Molecular basis of base substitution hotspots in *Escherichia coli*. *Nature* 1978;274:775–780.
20. Rideout WM III, Coetzee GA, Olumi AF, Jones PA. 5-Methylcytosine as an endogenous mutagen in the human LDL receptor and p53 genes. *Science* 1990;249:1288–1290.
21. Feinberg AP, Vogelstein B. Hypomethylation distinguishes genes of some human cancers from their normal counterparts. *Nature* 1983;301:89–92.
22. Feinberg AP, Gehrke CW, Kuo KC, Ehrlich M. Reduced genomic 5-methylcytosine content in human colonic neoplasia. *Cancer Res* 1988;48:1159–1161.
23. Qu GZ, Grundy PE, Narayan A, Ehrlich M. Frequent hypomethylation in Wilms tumors of pericentromeric DNA in chromosomes 1 and 16. *Cancer Genet Cytogenet* 1999;109:34–39.
24. Fullgrabe J, Kavanaugh E, Joseph B. Histone onco-modifications. *Oncogene* 2011;30:3391-403.
25. Zinner R, Albiez H, Walter J, Peters A, Cremer T, Cremer M. Histone lysine methylation patterns in cell types are arranged in distinct three-dimensional nuclear zones. *Histochem Cell Biol* 2006;125:3-19
26. Asp P, Blum R, Vethantham V, Parisi F, Micsinai M, Cheng J, et al. Genome-wide remodeling of the epigenetic landscape during myogenic differentiation. *Proc Natl Acad Sci USA* 2011;108:E149-58
27. Wang J, Scully K, Zhu X, Cai L, Zhang J, Prefontaine GG, et al. Opposing LSD1 complexes function in developmental gene activation and repression programmes. *Nature* 2007;446:882-7.
28. Gao H, Lukin K, Ramírez J, Fields S, Lopez D, Hagman J. Opposing effects of SWI/SNF and Mi-2/NuRD chromatin remodeling complexes on epigenetic reprogramming by EBF and Pax5. *Proc Natl Acad Sci USA* 2009;106:11258-63.

29. Bernstein BE, Mikkelsen TS, Xie X, Kamal M, Huebert DJ, Cuff J, et al. A bivalent chromatin structure marks key developmental genes in embryonic stem cells. *Cell* 2006;125:315-26.
30. Ohm JE, McGarvey KM, Yu X, Cheng L, Schuebel KE, Cope L, et al. A stem cell-like chromatin pattern may predispose tumor suppressor genes to DNA hypermethylation and heritable silencing. *Nat Genet* 2007;39:237-42.
31. Dawson MA, Kouzarides T. Cancer epigenetics: from mechanism to therapy. *Cell* 2012;150:12-27.
32. Chung CW, Witherington J. Progress in the discovery of small-molecule inhibitors of bromodomain--histone interactions. *J Biomol Screen* 2011;16:1170-85.
33. Wang J, Iwasaki H, Krivtsov A, Febbo PG, Thorner AR, Ernst P, et al. Conditional MLL-CBP targets GMP and models therapy-related myeloproliferative disease. *EMBO J* 2005;24:368-81.
34. Deguchi K, Ayton PM, Carapeti M, Kutok JL, Snyder CS, Williams IR, et al. MOZ-TIF2-induced acute myeloid leukemia requires the MOZ nucleosome binding motif and TIF2-mediated recruitment of CBP. *Cancer Cell* 2003;3:259-7
35. Huntly BJ, Shigematsu H, Deguchi K, Lee BH, Mizuno S, Duclos N, et al. MOZ-TIF2, but not BCR-ABL, confers properties of leukemic stem cells to committed murine hematopoietic progenitors. *Cancer Cell* 2004;6:587-596.
36. Iyer NG, Ozdag H, Caldas C. p300/CBP and cancer. *Oncogene* 2004;23:4225-31.
37. Pasqualucci L, Dominguez-Sola D, Chiarenza A, Fabbri G, Grunn A, Trifonov V, et al. Inactivating mutations of acetyltransferase genes in B-lymphoma. *Nature* 2011;471:189-95.
38. Johnstone RW, Licht JD. Histone deacetylase inhibitors in cancer therapy: is transcription the primary target? *Cancer Cell* 2003;4:13-8
39. Bereshchenko OR, Gu W, Dalla-Favera R. Acetylation inactivates the transcriptional repressor BCL6. *Nat Genet* 2002;32:606-13.
40. Ley TJ, Ding L, Walter MJ, McLellan MD, Lamprecht T, Larson DE, et al. DNMT3A mutations in acute myeloid leukemia. *N Engl J Med*. 2010;363:2424–2433.
41. Thol F, Damm F, Lüdeking A, Winschel C, Wagner K, Morgan M, et al. Incidence and prognostic influence of DNMT3A mutations in acute myeloid leukemia. *J Clin Oncol*. 2011;29:2889–2896.

42. Metzeler KH, Maharry K, Radmacher MD, Mrózek K, Margeson D, Becker H, et al. TET2 mutations improve the new European LeukemiaNet risk classification of acute myeloid leukemia: a Cancer and Leukemia Group B study. *J Clin Oncol*. 2011;29:1373–1381.
43. Bejar R, Stevenson K, Abdel-Wahab O, Galili N, Nilsson B, Garcia-Manero G, et al. Clinical effect of point mutations in myelodysplastic syndromes. *N Engl J Med*. 2011;364:2496–2506.
44. Abdel-Wahab O, Pardanani A, Patel J, Wadleigh M, Lasho T, Heguy A, et al. Concomitant analysis of *EZH2* and *ASXL1* mutations in myelofibrosis, chronic myelomonocytic leukemia and blast-phase myeloproliferative neoplasms. *Leukemia*. 2011;25:1200–1202.
45. Metzeler KH, Becker H, Maharry K, Radmacher MD, Kohlschmidt J, Mrózek K, et al. *ASXL1* mutations identify a high-risk subgroup of older patients with primary cytogenetically normal AML within the ELN favorable genetic category. *Blood*. 2011;118:6920–6929.
46. Guglielmelli P, Biamonte F, Score J, Hidalgo-Curtis C, Cervantes F, Maffioli M, et al. *EZH2* mutational status predicts poor survival in myelofibrosis. *Blood*. 2011;118:5227–5234.
47. Tefferi A, Pardanani A, Lim KH, Abdel-Wahab O, Lasho TL, Patel J, et al. *TET2* mutations and their clinical correlates in polycythemia vera, essential thrombocythemia and myelofibrosis. *Leukemia*. 2009;23:905–911.
48. Tefferi A, Jimma T, Sulai NH, Lasho TL, Finke CM, Knudson RA, et al. *IDH* mutations in primary myelofibrosis predict leukemic transformation and shortened survival: clinical evidence for leukemogenic collaboration with *JAK2V617F*. *Leukemia*. 2012;26:475–480.
49. Tefferi A, Lasho TL, Abdel-Wahab O, Guglielmelli P, Patel J, Caramazza D, et al. *IDH1* and *IDH2* mutation studies in 1473 patients with chronic-, fibrotic- or blast-phase essential thrombocythemia, polycythemia vera or myelofibrosis. *Leukemia*. 2010;24:1302–1309.
50. De Carvalho DD, Sharma S, You JS, Su SF, Taberlay PC, Kelly TK, et al. DNA methylation screening identifies driver epigenetic events of cancer cell survival. *Cancer Cell*. 2012;21:655–667.
51. Baylin SB, Jones PA. A decade of exploring the cancer epigenome — biological and translational implications. *Nat Rev Cancer*. 2011;11:726–734.
52. Sorm F, Vesely J. Effect of 5-aza-2'-deoxycytidine against leukemic and hemopoietic tissues in AKR mice. *Neoplasma*. 1968;15:339–343.

53. Notari RE, DeYoung JL. Kinetics and mechanisms of degradation of the antileukemic agent 5-azacytidine in aqueous solutions. *J Pharm Sci.* 1975;64:1148–1157.
54. Jones PA, Taylor SM. Cellular differentiation, cytidine analogs and DNA methylation. *Cell.* 1980;20:85–93.
55. Kaminskas E, Farrell A, Abraham S, Baird A, Hsieh LS, Lee SL, et al. Approval summary: azacitidine for treatment of myelodysplastic syndrome subtypes. *Clin Cancer Res.* 2005;11:3604–3608.
56. Silverman LR, Demakos EP, Peterson BL, Kornblith AB, Holland JC, Odchimar-Reissig R, et al. Randomized controlled trial of azacitidine in patients with the myelodysplastic syndrome: a study of the cancer and leukemia group B. *J Clin Oncol.* 2002;20:2429–2440.
57. Kaminskas E, Farrell AT, Wang YC, Sridhara R, Pazdur R. FDA drug approval summary: azacitidine (5-azacytidine, Vidaza) for injectable suspension. *Oncologist.* 2005;10:176–182.
58. Kantarjian H, Issa JP, Rosenfeld CS, Bennett JM, Albitar M, DiPersio J, et al. Decitabine improves patient outcomes in myelodysplastic syndromes: results of a phase III randomized study. *Cancer.* 2006;106:1794–1803.
59. Azad N, Zahnow CA, Rudin CM, Baylin SB. The future of epigenetic therapy in solid tumours--lessons from the past. *Nat Rev Clin Oncol* 2013;10:256-66.
60. Gabbara S, Bhagwat AS. The mechanism of inhibition of DNA (cytosine-5)-methyltransferases by 5-azacytosine is likely to involve methyl transfer to the inhibitor. *Biochem J.* 1995;307:87–92.
61. Santi DV, Norment A, Garrett CE. Covalent bond formation between a DNA-cytosine methyltransferase and DNA containing 5-azacytosine. *Proc Natl Acad Sci USA.* 1984;81:6993–6997.
62. Ferguson AT, Vertino PM, Spitzner JR, Baylin SB, Muller MT, Davidson NE. Role of estrogen receptor gene demethylation and DNA methyltransferase. DNA adduct formation in 5-aza-2'-deoxycytidine-induced cytotoxicity in human breast cancer cells. *J Biol Chem.* 1997;272:32260–32266.
63. Ghoshal K, Datta J, Majumder S, Bai S, Kutay H, Motiwala T, et al. 5-Aza-deoxycytidine induces selective degradation of DNA methyltransferase 1 by a proteasomal pathway that requires the KEN box, bromo-adjacent homology domain, and nuclear localization signal. *Mol Cell Biol.* 2005;25:4727–4741.

64. Tsai HC, Li H, Van Neste L, Cai Y, Robert C, Rassool FV, et al. Transient low doses of DNAdemethylating agents exert durable antitumor effects on hematological and epithelial tumor cells. *Cancer Cell*. 2012;21:430–446.
65. Silverman LR, Fenaux P, Mufti GJ, Santini V, Hellström-Lindberg E, Gattermann N, et al. Continued azacitidine therapy beyond time of first response improves quality of response in patients with higher-risk myelodysplastic syndromes. *Cancer* 2011;117:2697-702.
66. Piekarz RL, Frye R, Turner M, Wright JJ, Allen SL, Kirschbaum MH, et al. Phase II multi-institutional trial of the histone deacetylase inhibitor romidepsin as monotherapy for patients with cutaneous T-cell lymphoma. *J Clin Oncol*. 2009;27:5410–5417.
67. Whittaker SJ, Demierre MF, Kim EJ, Rook AH, Lerner A, Duvic M, et al. Final results from a multicenter, international, pivotal study of romidepsin in refractory cutaneous T-cell lymphoma. *J Clin Oncol*. 2010;28:4485–4491.
68. O'Connor OA, Heaney ML, Schwartz L, Richardson S, Willim R, MacGregor-Cortelli B, et al. Clinical experience with intravenous and oral formulations of the novel histone deacetylase inhibitor suberoylanilide hydroxamic acid in patients with advanced hematologic malignancies. *J Clin Oncol*. 2006;24:166–173.
69. Duvic M, Talpur R, Ni X, Zhang C, Hazarika P, Kelly C, et al. Phase 2 trial of oral vorinostat (suberoylanilide hydroxamic acid, SAHA) for refractory cutaneous T-cell lymphoma (CTCL). *Blood*. 2007;109:31–39.
70. Lane AA, Chabner BA. Histone deacetylase inhibitors in cancer therapy. *J Clin Oncol* 2009;27:5459-68.
71. Hochedlinger K, Plath K. Epigenetic reprogramming and induced pluripotency. *Development* 2009;136:509-23.
72. Lister R, Pelizzola M, Kida YS, Hawkins RD, Nery JR, Hon G, et al. Hotspots of aberrant epigenomic reprogramming in human induced pluripotent stem cells. *Nature* 2011;471:68-73.
73. Feng B, Ng JH, Heng JC, Ng HH. Molecules that promote or enhance reprogramming of somatic cells to induced pluripotent stem cells. *Cell Stem Cell* 2009;4:301-12.
74. Gray SG, Ekström TJ. The human histone deacetylase family. *Exp Cell Res*. 2001;262:75-83.
75. Solomon JM, Pasupuleti R, Xu L, McDonagh T, Curtis R, DiStefano PS, et al. Inhibition of SIRT1 catalytic activity increases p53 acetylation but does not alter cell survival following DNA damage. *Mol Cell Biol*. 2006;26:28–38.

76. Brahmer JR, Tykodi SS, Chow LQ, Hwu WJ, Topalian SL, Hwu P, et al. Safety and activity of anti-PD-L1 antibody in patients with advanced cancer. *N Engl J Med.* 2012;366:2455-65.
77. Juergens RA, Wrangle J, Vendetti FP, Murphy SC, Zhao M, Coleman B, et al. Combination epigenetic therapy has efficacy in patients with refractory advanced non-small cell lung cancer. *Cancer Discov.* 2011;1:598-607.
78. Sharma SV, Lee DY, Li B, Quinlan MP, Takahashi F, Maheswaran S, et al. A chromatin-mediated reversible drug-tolerant state in cancer cell subpopulations. *Cell* 2010;141:69-80.
79. Delmore JE, Issa GC, Lemieux ME, Rahl PB, Shi J, Jacobs HM, et al. BET bromodomain inhibition as a therapeutic strategy to target c-Myc. *Cell* 2011;146:904-17. multiple myeloma
80. Mertz JA, Conery AR, Bryant BM, Sandy P, Balasubramanian S, Mele DA, et al. Targeting MYC dependence in cancer by inhibiting BET bromodomains. *Proc Natl Acad Sci U S A* 2011;108:16669-74.
81. Dawson MA, Prinjha RK, Dittmann A, Giotopoulos G, Bantscheff M, Chan WI, et al. Inhibition of BET recruitment to chromatin as an effective treatment for MLL-fusion leukaemia. *Nature* 2011;478:529-33.
82. Ott CJ, Kopp N, Bird L, Paranal RM, Qi J, Bowman T, et al. BET bromodomain inhibition targets both c-Myc and IL7R in high-risk acute lymphoblastic leukemia. *Blood* 2012;120:2843-52.
83. Puissant A, Frumm SM, Alexe G, Bassil CF, Qi J, Chanthery YH, et al. Targeting MYCN in neuroblastoma by BET bromodomain inhibition. *Cancer Discov.* 2013;3:308-23.
84. Wyce A, Ganji G, Smitheman KN, Chung CW, Korenchuk S, Bai Y, et al. BET inhibition silences expression of MYCN and BCL2 and induces cytotoxicity in neuroblastoma tumor models. *PLoS One* 2013;8:e72967.
85. Shimamura T, Chen Z, Soucheray M, Carretero J, Kikuchi E, Tchaicha JH, et al. Efficacy of BET bromodomain inhibition in Kras-mutant non-small cell lung cancer. *Clin Cancer Res* 2013;19:6183-92.
86. Bandopadhyay P, Bergthold G, Nguyen B, Schubert S, Gholamin S, Tang Y, et al. BET bromodomain inhibition of MYC-amplified medulloblastoma. *Clin Cancer Res* 2014;20:912-25.

87. Chapuy B, McKeown MR, Lin CY, Monti S, Roemer MG, Qi J, et al. Discovery and characterization of super-enhancer-associated dependencies in diffuse large B cell lymphoma. *Cancer Cell* 2013;24:777-90.
88. Asangani IA, Dommeti VL, Wang X, Malik R, Cieslik M, Yang R, et al. Therapeutic targeting of BET bromodomain proteins in castration-resistant prostate cancer. *Nature* 2014;doi: 10.1038/nature13229.
89. ClinicalTrials.gov [Internet]. Available from: <http://www.cancer.gov/clinicaltrials/search/results?protocolsearchid=10430216>
90. Tensha Therapeutics Announces First Clinical Trial of BET Bromodomain Inhibitor TEN-010 for Treatment of Cancer [Internet]. Cambridge: BusinessWire; c2013 [updated 2013 Nov 20; cited 2014 May 3]. Available from: <http://www.businesswire.com/news/home/20131120005823/en/Tensha-Therapeutics-Announces-Clinical-Trial-BET-Bromodomain>
91. Constellation Pharmaceuticals Initiates Clinical Development of CPI-0610, a Novel BET Protein Bromodomain Inhibitor, in Patients with Lymphoma [Internet]. Cambridge: Constellation Pharmacueitcal, Pure Communications, Inc.; c2014 [updated 2013 Sept 10; cited 2014 May 3]. Available from: <http://www.constellationpharma.com/2013/09/constellation-pharmaceuticals-initiates-clinical-development-of-cpi-0610-a-novel-bet-protein-bromodomain-inhibitor-in-patients-with-lymphoma/>.
92. Byvoet P, Shepherd GR, Hardin JM, Noland BJ. The distribution and turnover of labelled methyl groups in histone fractions of cultured mammalian cells. *Arch Biochem Biophys* 1972;148:558–567.
93. Shi Y, Lan F, Matson C, Mulligan P, Whetstine JR, Cole PA, et al. Histone demethylation mediated by the nuclear amine oxidase homolog LSD1. *Cell* 2004;119:941-53.
94. Murray K. The occurrence of ϵ -*N*-methyl lysine in histones. *Biochemistry* 1964;3:10–15.
95. Paik WK, Kim S. ϵ -*N*-dimethyllysine in histones. *Biochem Biophys Res Commun* 1967;27:479–483.
96. Haempel K, Lange HW, Birkofer L. ϵ -*N*-trimethyllysine, a new amino acid in histones. *Die Naturwissenschaften* 1968:55:37.
97. Zee BM, Levin RS, Xu B, LeRoy G, Wingreen NS, Garcia BA. In vivo residue-specific histone methylation dynamics. *J Biol Chem* 2010;285:3341-50.

98. Rea S, Eisenhaber F, O'Carroll D, Strahl BD, Sun ZW, Schmid M, et al. Regulation of chromatin structure by site-specific histone H3 methyltransferases. *Nature* 2000;406:593-9.
99. Feng Q, Wang H, Ng HH, Erdjument-Bromage H, Tempst P, Struhl K, et al. Methylation of H3 lysine 79 is mediated by a new family of HMTases without a SET domain. *Curr Biol* 2002;15:1052-8.
100. Tsukada Y, Fang J, Erdjument-Bromage H, Warren ME, Borchers CH, Tempst P, et al. Histone demethylation by a family of JmjC domain-containing proteins. *Nature* 2006;439:811-6.
101. Whetstine JR, Nottke A, Lan F, Huarte M, Smolikov S, Chen Z, et al. Reversal of histone lysine trimethylation by the JMJD2 family of histone demethylases. *Cell* 2006;125:467-81.
102. Albert M, Helin K. Histone methyltransferases in cancer. *Semin Cell Dev Biol* 2010;21:209-20.
103. Chi P, Allis CS, Wang GG. Covalent histone modifications—miswritten, misinterpreted and mis-erased in human cancers. *Nat Rev Cancer* 2010;10:457-69.
104. Greer EL, Shi Y. Histone methylation: a dynamic mark in health, disease, and inheritance. *Nat Rev Genet* 2012;13:343-57.
105. Daigle SR, Olhava EJ, Therkelsen CA, Basavapathruni A, Jin L, Boriack-Sjodin A, et al. Potent inhibition of DOT1L as a treatment of MLL-fusion leukemia. *Blood* 2013;122:1017-25.
106. DOT1L inhibitor [Internet]. Cambridge: Epizyme, Inc.; c2013 [updated 2013 Dec; cited 2014 May 3]. Available from: <http://www.epizyme.com/programs/dot1l-inhibitor/>.
107. Kleer CG, Cao Q, Varambally S, Shen R, Ota I, Tomlins SA, et al. EZH2 is a marker of aggressive breast cancer and promotes neoplastic transformation of breast epithelial cells. *Proc Natl Acad Sci USA* 2003;100:11606-11.
108. Varambally S, Dhanasekaran SM, Zhou M, Barrette TR, Kumar-Sinha C, Sanda MG, et al. The polycomb group protein EZH2 is involved in progression of prostate cancer. *Nature* 2002;419:624-9.
109. Bracken AP, Helin K. Polycomb group proteins: navigators of lineage pathways led astray in cancer. *Nat Rev Cancer* 2009;9:773-84.
110. Visser HP, Gunster MJ, Kluin-Nelemans HC, Manders EM, Raaphorst FM, Meijer CJ, et al. The Polycomb group protein EZH2 is upregulated in proliferating, cultured human mantle cell lymphoma. *Br J Haematol* 2001;112:950-958.

111. van Haaften G, Dalglish GL, Davies H, Chen L, Bignell G, Greenman C, et al. Somatic mutations of the histone H3K27 demethylase gene UTX in human cancer. *Nature Genet* 2009;41:521–3.
112. Ernst T, Chase AJ, Score J, Hidalgo-Curtis CE, Bryant C, Jones AV, et al. Inactivating mutations of the histone methyltransferase gene EZH2 in myeloid disorders. *Nature Genet* 2010;42:722–6.
113. EZH2 inhibitor [Internet]. Cambridge: Epizyme, Inc.; c2013 [updated 2013 Dec; cited 2014 May 3]. Available from: <http://www.epizyme.com/programs/ezh2-inhibitor/>.
114. GSK Clinical Study Register [Internet]. Brentford, Middlesex, UK: GlaxoSmith Kline plc.; c2001-2014 [updated 2014 Mar 13; cited 2014 May 3]. Available from: <http://www.gsk-clinicalstudyregister.com/study/117208#ps>
115. Suzuki T, Terashima M, Tange S, Ishimura A. Roles of histone methyl-modifying enzymes in development and progression of cancer. *Cancer Sci* 2013;104:795-800.
116. ClinicalTrials.gov [Internet]. Available from: <http://clinicaltrials.gov/ct2/show/NCT02034123>.
117. Lim S, Janzer A, Becker A, Zimmer A, Schüle R, Buettner R, et al. Lysine-specific demethylase 1 (LSD1) is highly expressed in ER-negative breast cancers and a biomarker predicting aggressive biology. *J Carcinogenesis* 2010;31:512-20.
118. Metzger E, Wissmann M, Yin N, Müller JM, Schneider R, Peters AHFM, et al. LSD1 demethylates repressive histone marks to promote androgen-receptor-dependent transcription. *Nature* 2005;437:436–9.
119. Wissmann M, Yin N, Müller JM, Greschik H, Fodor BD, Jenuwein T, et al. Cooperative demethylation by JMJD2C and LSD1 promotes androgen receptor-dependent gene expression. *Nat Cell Biol* 2007;9:347-53.
120. Cai C, He HH, Chen S, Coleman I, Wang H, Fang Z, et al. Androgen receptor gene expression in prostate cancer is directly suppressed by the androgen receptor through recruitment of lysine-specific demethylase 1. *Cancer Cell* 2011;20:457-71.
121. Kahl P, Gullotti L, Heukamp LC, Wolf S, Friedrichs N, Vorreuther R, et al. Androgen receptor coactivators lysine-specific histone demethylase 1 and four and a half LIM domain protein 2 predict risk of prostate cancer recurrence. *Cancer Res* 2006;66:11341-7.
122. Schulte JH, Lim S, Schramm A, Friedrichs N, Koster J, Versteeg R, et al. Lysine-specific demethylase 1 is strongly expressed in poorly differentiated neuroblastoma: implications for therapy. *Cancer Research* 2009;69:2065-71.

123. Hu X, Li X, Valverde K, Fu X, Noguchi C, Qiu Y, et al. LSD1-mediated epigenetic modification is required for TAL1 function and hematopoiesis. *Proc Natl Acad Sci USA* 2009;106:10141-6.
124. Li Y, Deng C, Hu X, Patel B, Fu X, Qiu Y, et al. Dynamic interaction between TAL1 oncoprotein and LSD1 regulates TAL1 function in hematopoiesis and leukemogenesis. *Oncogene* 2012;31:5007-18.
125. Schenk T, Chen WC, Göllner S, Howell L, Jin L, Hebestreit K, et al. Inhibition of the LSD1 (KDM1A) demethylase reactivates the all-trans-retinoic acid differentiation pathway in acute myeloid leukemia. *Nat Med* 2012;18:605-11.
126. Harris WJ, Huang X, Lynch JT, Spencer GJ, Hitchin JR, Li Y, et al. The histone demethylase KDM1A sustains the oncogenic potential of MLL-AF9 leukemia stem cells. *Cancer Cell* 2012;21:473-87.
127. Hayami S, Kelly JD, Cho HS, Yoshimatsu M, Unoki M, Tsunoda T, et al. Overexpression of LSD1 contributes to human carcinogenesis through chromatin regulation in various cancers. *Int J Cancer* 2011;128:574-86.
128. Kauffman EC, Robinson BD, Downes MJ, Powell LG, Lee MM, Scherr DS, et al. Role of androgen receptor and associated lysine-demethylase coregulators, LSD1 and JMJD2A, in localized and advanced human bladder cancer. *Mol Carcinog* 2011;50:931-44.
129. Bennani-Baiti IM, Machado I, Llombart-Bosch A, Kovar H. Lysine-specific demethylase 1 (LSD1/KDM1A/AOF2/BHC110) is expressed and is an epigenetic drug target in chondrosarcoma, Ewing's sarcoma, osteosarcoma, and rhabdomyosarcoma. *Hum Pathol* 2012;43:1300-7.
130. Schildhaus HU, Riegel R, Hartmann W, Steiner S, Wardelmann E, Merkelbach-Bruse S, et al. Lysine-specific demethylase 1 is highly expressed in solitary fibrous tumors, synovial sarcomas, rhabdomyosarcomas, desmoplastic small round cell tumors, and malignant peripheral nerve sheath tumors. *Hum Pathol* 2011;42:1667-75.
131. Magerl C, Ellinger J, Braunschweig T, Kremmer E, Koch LK, Höller T, et al. H3K4 dimethylation in hepatocellular carcinoma is rare compared with other hepatobiliary and gastrointestinal carcinomas and correlates with expression of the methylase Ash2 and the demethylase LSD1. *Hum Pathol* 2010;41:181-9.
132. Zhao ZK, Yu HF, Wang DR, Dong P, Chen L, Wu WG, et al. Overexpression of lysine specific demethylase 1 predicts worse prognosis in primary hepatocellular carcinoma patients. *World J Gastroenterol* 2012;18:6651-6.

133. Yang M, Gocke CB, Luo X, Borek D, Tomchick DR, Machius M, et al. Structural basis for CoREST-dependent demethylation of nucleosomes by the human LSD1 histone demethylase. *Molecular Cell* 2006, 23:377-387.
134. Stavropoulos P, Blobel G, Hoelz A. Crystal structure and mechanism of human lysine-demethylase 1. *Nat Struct Mol Biol* 2006;13:626-32.
135. Forneris F, Binda C, Vanoni MA, Mattevi A, Battaglioli E. Histone demethylation catalysed by LSD1 is a flavin-dependent oxidative process. *FEBS Lett* 2005;579:(2203-7).
136. Baron R, Binda C, Tortorici M, McCammon JA, Mattevi A. Molecular mimicry and ligand recongnition in binding and catalysis by the histone demethylase LSD1-CoREST complex. *Structure* 2011;19:212-220.
137. Yang M, Culhane JC, Szewczuk LM, Gocke CB, Brautigam CA, Tomchick DR, et al. Structural basis of histone demethylation by LSD1 revealed by suicide inactivation. *Nat Struct Mol Biol* 2007;14:535-9.
138. Forneris F, Binda C, Adamo A, Battaglioli E, Mattevi A. Structural basis of LSD1-CoREST selectivity in histone H3 recognition. *J Biol Chem* 2007;282:20070-4.
139. Wang Y, Zhang H, Chen Y, Sun Y, Yang F, Yu W, et al. LSD1 is a subunit of the NuRD complex and targets the metastasis programs in breast cancer. *Cell* 2009;138:660-672.
140. Tsai MC, Manor O, Wan Y, Mosammaparast N, Wang JK, Lan F, et al. Long noncoding RNA as modular scaffold of histone modification complexes. *Science* 2010;329:689–693.
141. Forneris F, Binda C, Vanoni MA, Battaglioli E, Mattevi A. Human histone demethylase LSD1 reads the histone code. *J Biol Chem* 2005;208:41360-5.
142. Metzger E, Imhof A, Patel D, Kahl P, Hoffmeyer K, Friedrichs N, et al. Phosphorylation of histone H3T6 by PKC β I controls demethylation at histone H3K4. *Nature* 2010;464:792-7.
143. Zibetti C, Adamo A, Binda C, Forneris F, Toffolo E, Verpelli C, et al. Alternative splicing of the histone demethylase LSD1/KDM1 contributes to the modulation of neurite morphogenesis in the mammalian nervous system. *J Neuroscience* 2010;30:2521-32.
144. Toffolo E, Rusconi F, Paganini L, Tortorici M, Pilotto S, Heise C, et al. Phosphorylation of neuronal lysine-specific demethylase 1 LSD1/KDM1A impairs transcriptional repression by regulating interaction with CoREST and histone deacetylases HDAC1/2. *J Neurochem* 2014;128:603-16.

145. Nam HJ, Boo K, Kim D, Han DH, Choe HK, Kim CR, et al. Phosphorylation of LSD1 by PKC α is crucial for circadian rhythmicity and phase resetting. *Mol Cell* 2014;53:791-805.
146. Costa R, Arrigoni G, Cozza G, Lolli G, Battistutta R, Izipisua Belmonte JC, et al. The lysine-specific demethylase 1 is a novel substrate of protein kinase CK2. *Biochim Biophys Acta* 2014;1844:722-9.
147. Lan F, Collins RE, De Cegil R, Alpatov R, Horton JR, Shi X, et al. Recognition of unmethylated histone H3 lysine 4 links BHC80 to LSD1-mediated gene repression. *Nature* 2007;448:718-722.
148. Garcia-Bassets I, Kwon Y-S, Telese F, Prefontaine GG, Hutt KR, Cheng CS, et al. Histone methylation-dependent mechanisms impose ligand dependency for gene activation by nuclear receptors. *Cell* 2007;128:505-518.
149. Lin T, Ponn A, Hu X, Law BK, Lu J. Requirement of the histone demethylase LSD1 in Snail1-mediate transcriptional repression during epithelial-mesenchymal transition. *Oncogene* 2010;29:4896-4904.
150. Lin Y, Wu Y, Li J, Dong C, Ye X, Chi YI, et al. The SNAG domain of Snail1 functions as a molecular hook for recruiting lysine-specific demethylase 1. *EMBO J* 2010;29:1803-16.
151. McDonald OG, Wu H, Timp W, Doi A, Feinberg AP. Genome-scale epigenetic reprogramming during epithelial-to-mesenchymal transition. *Nat Struct Mol Biol* 2011;18:867-74.
152. Rudolph T, Yonezawa M, Lein S, Heidrich K, Kubicek S, Schäfer C, et al. Heterochromatin formation in *Drosophila* is initiated through active removal of H3K4 methylation by the LSD1 homolog SU(VAR)3-3. *Mol Cell* 2007;26:103-15.
153. Lan F, Zaratiegui M, Villén J, Vaughn MW, Verdel A, Huarte M, et al. *S. pombe* LSD1 homologs regulate heterochromatin propagation and euchromatic gene transcription. *Mol Cell* 2007;26:89-101.
154. Stefano LD, Walker JA, Burgio G, Corona DFV, Mulligan P, Naar AM, et al. Functional antagonism between histon H3K4 demethylases in vivo. *Genes Dev* 2011;25:17-28.
155. Wang J, Scully K, Zhu X, Cai L, Zhang J, Prefontaine GG, et al. Opposing LSD1 complexes function in developmental gene activation and repression programmes. *Nature* 2007;446:882-7.
156. Huang J, Sengupta R, Espejo AB, Lee MG, Dorsey JA, Richter M, et al. p53 is regulated by the lysine demethylase LSD1. *Nature* 2007;449:105-8.

157. Wang J, Hevi S, Kurash JK, Lei H, Gay F, Bajko J, et al. The lysine demethylase LSD1 (KDM1) is required for maintenance of global DNA methylation. *Nat Genet* 2009;41:125-9.
158. Nair SS, Li DQ, Kumar R. A core chromatin remodeling factor instructs global chromatin signaling through multivalent reading of nucleosome codes. *Mol Cell* 2013;49:704-18.
159. Huang Y, Greene E, Stewart TM, Goodwin AC, Baylin SB, Woster PM, et al. Inhibition of lysine-specific demethylase 1 by polyamine analogues results in reexpression of aberrantly silenced genes. *Proc Natl Acad Sci* 2007;104:8023-8.
160. Willmann D, Lim S, Wetzel S, Metzger E, Jandausch A, Wilk W, et al. Impairment of prostate cancer cell growth by a selective and reversible LSD1 inhibitor. *Int J Cancer* 2012;131:2704-9.
161. Ram O, Goren A, Amit I, Shores N, Yosef N, Ernst J, et al. Combinatorial patterning of chromatin regulators uncovered by genome-wide location analysis in human cells. *Cell* 2011;147:1628-39.
162. Robertson JC, Hurley NC, Tortorici M, Ciossani G, Borrello MT, Vellore NA, et al. Expanding the druggable space of the LSD1/CoREST epigenetic target: new potential binding regions for drug-like molecules, peptides, protein partners, and chromatin. *PLoS Comput Biol* 2013;9:e1003158.
163. Foster CT, Dovey OM, Lezina L, Luo JL, Gant TW, Barlev N, et al. Lysine-specific demethylase 1 regulates the embryonic transcriptome and CoREST stability. *Mol Cell Biol* 2010;30:4851-63.
164. Musri MM, Carmona MC, Hanzu FA, Kaliman P, Gomis R, Párrizas M. Histone demethylase LSD1 regulates adipogenesis. *J Biol Chem* 2010;285:30034-41.
165. Fuentes P, Cánovas J, Berndt FA, Noctor SC, Kukuljan M. CoREST/LSD1 control the development of pyramidal cortical neurons. *Cereb Cortex* 2012;22:1431-41.
166. Sun G, Alzayady K, Stewart R, Ye P, Yang S, Li W, et al. Histone demethylase LSD1 regulates neural stem cell proliferation. *Mol Cell Biol* 2010;30:1997-2005.
167. Adamo A, Sesé B, Boue S, Castaño J, Paramonov I, Barrero MJ, et al. LSD1 regulates the balance between self-renewal and differentiation in human embryonic stem cells. *Nat Cell Biol* 2011;13:652-9.
168. Yin F, Lan R, Zhang X, Zhu L, Chen F, Xu Z, et al. LSD1 regulates pluripotency of embryonic stem/carcinoma cells through histone deacetylase 1-mediated deacetylation of histone H4 at lysine 16. *Mol Cell Biol* 2014;34:158-79.

169. Nair VD, Ge Y, Balasubramaniyan N, Kim J, Okawa Y, Chikina M, et al. Involvement of histone demethylase LSD1 in short-time-scale gene expression changes during cell cycle progression in embryonic stem cells. *Mol Cell Biol* 2012;32:4861-76.
170. Whyte WA, Bilodeau S, Orlando DA, Hoke HA, Frampton GM, Foster CT, et al. Enhancer decommissioning by LSD1 during embryonic stem cell differentiation. *Nature* 2012;482:221-5.
171. Sprüssel A, Schulte JH, Weber S, Necke M, Händschke K, Thor T, et al. Lysine-specific demethylase 1 restricts hematopoietic progenitor proliferation and is essential for terminal differentiation. *Leukemia* 2012;26:2039-51.
172. Takagi T, Ramachandran C, Bermejo M, Yamashita S, Yu LX, Amidon GL. A provisional biopharmaceutical classification of the top 200 oral drug products in the United States, Great Britain, Spain, and Japan. *Mol Pharmaceutics* 2006;3:631-643.
173. Li P, Zhao L. Developing early formulations: practice and perspective. *Int J Pharm* 2007;341:1-19.
174. Ledford H. Translational research: 4 ways to fix the clinical trial. *Nature* 2011;477:526-8.

Table 1.1 FDA-approved epigenetic therapies.

Agent Name (Trade Name)	Target	Indication	FDA-Approval Date
Azacitidine (Vidaza)	DNMT	Myelodysplastic syndrome	2004 May 19
Decitabine (Dacogen)	DNMT	Myelodysplastic syndrome	2006 May 2
Vorinostat (Zolinza)	HDAC	Cutaneous T-Cell Lymphoma	2006 Oct 6
Romidepsin (Istodax)	HDAC	Cutaneous T-Cell Lymphoma	2009 Nov 5

Table 1.2 Histone methylation is globally misregulated in cancer. (Adapted from (104))

Cancer Type	Methyl Mark	Consequence
Prostate Cancer	↓H3K4me2	High recurrence
Prostate Cancer	↓H4K2me2	High recurrence
Lung Cancer	↓H3K4me2	Poorer survival
Kidney Cancer	↓H3K4me2	Poorer survival
Breast Cancer	↓H3K4me2	Poorer survival
Breast Cancer	↓H3K27me3	Poorer survival
Breast Cancer	↓H4K20me3	Worse clinical outcomes
Pancreatic Cancer	↓H3K4me2	Poorer survival
Pancreatic Cancer	↓H3K9me2	Poorer survival
Pancreatic Cancer	↓H3K27me3	Poorer survival
Gastric Adenocarcinoma	↑H3K9me3	Poorer survival
Ovarian Cancer	↓H3K27me3	Poorer survival
Lymphomas	↓H4K20me3	Associated with
Colon Adenocarcinoma	↓H4K20me3	Associated with

Table 1.3 Altered expression of KDMs in cancer. (Adapted from (115))

Name	Synonym	Alteration	Associated Cancer
KDM1A	LSD1, AOF2	Overexpression	Prostate, neuroblastoma, lung, colorectal, bladder
KDM1A	LSD1, AOF2	Downregulation	Breast
KDM2B	FBXL10, JHDM1B	Overexpression	Pancreatic, leukemia
KDM2B	FBXL10, JHDM1B	Downregulation	Glioblastoma
KDM3A	JMJD1A, JHDM2A	Overexpression	Colorectal, renal cell carcinoma
KDM4A	JMJD2A	Overexpression	Lung, breast
KDM4B	JMJD2B	Overexpression	ER + breast, bladder, lung
KDM4C	JMJD2C, GASC1	Amplification	Esophageal, breast, medulloblastoma, primary mediastinal
KDM4C	JMJD2C, GASC1	Overexpression	Lymphoma
KDM5A	JARID1A, RBP2	Overexpression	Gastric, breast
KDM5A	JARID1A, RBP2	Translocation	Acute myeloid leukemia
KDM5B	JARID1B, PLU1	Overexpression	Breast, prostate, bladder, lung
KDM5B	JARID1B, PLU1	Downregulation	Melanoma
KDM6A	UTX	Mutation	Multiple myeloma, esophageal squamous cell, renal cell, chronic myelomonocytic leukemia
KDM6B	JMJD3	Downregulation	Lung, liver
PHF8	JHDM1F	Overexpression	Prostate

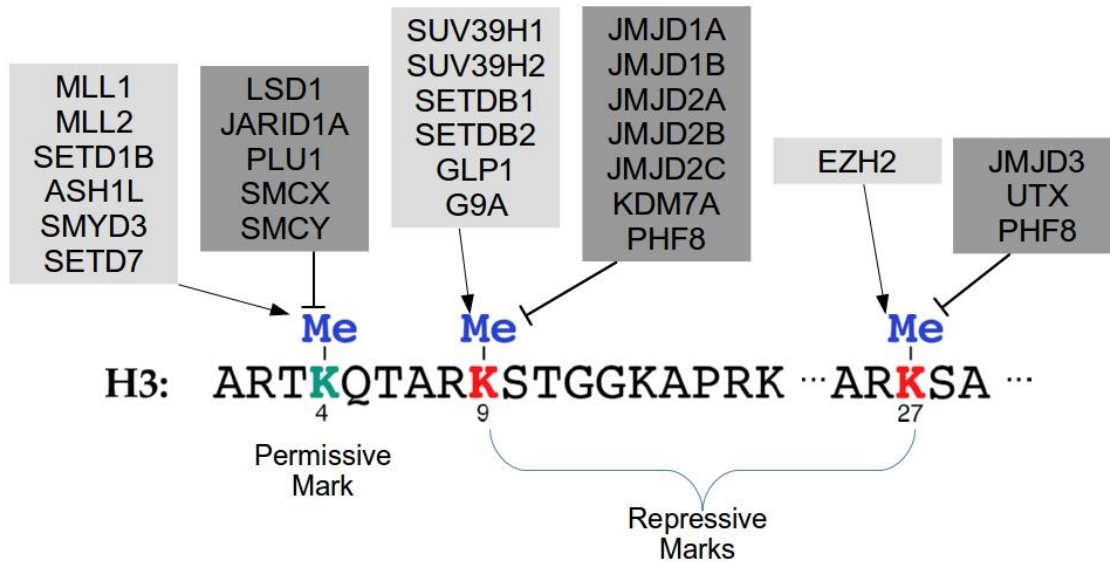


Figure 1.1 Histone methylation machinery. The histone methylation “writers” (methyltransferases; light gray) and “erasers” (demethylases; dark gray) for H3K4, H3K9, and H3K27.

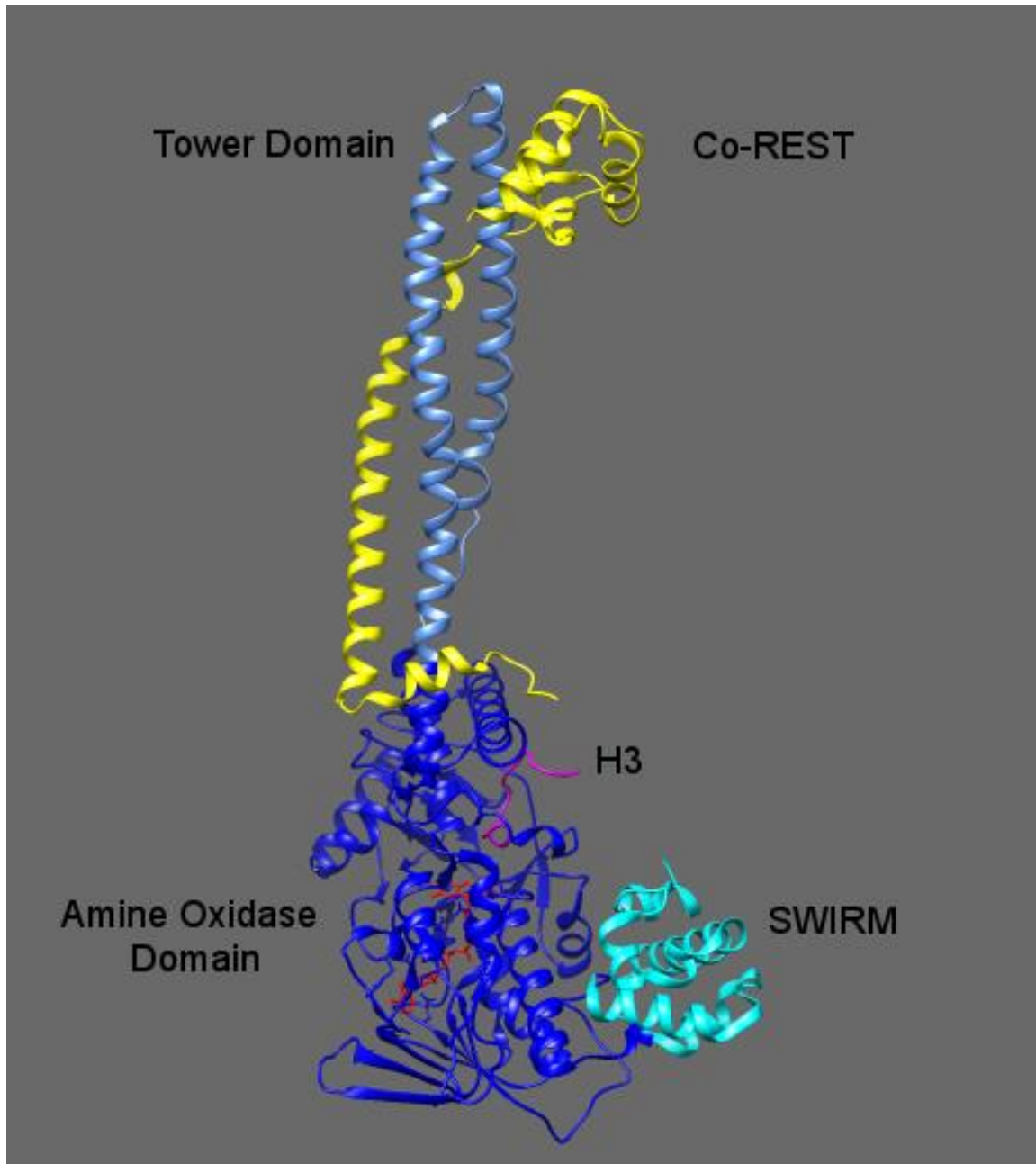


Figure 1.2 The crystal structure of lysine-specific demethylase 1. LSD1 (blue) in complex with both Co-REST (yellow) and an N-terminal H3 peptide (magenta). FAD is shown bound by the amine oxidase domain (red). PDB ID: 2V1D

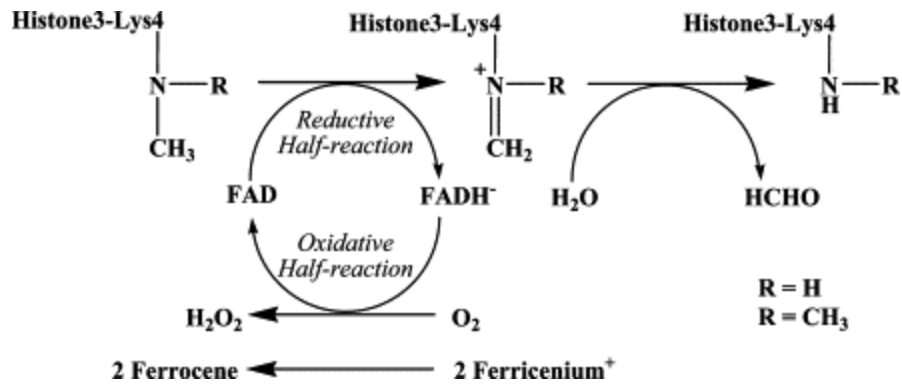


Figure 1.3 Catalytic oxidative demethylation of histone H3 lysine 4 by LSD1. Demethylation results in the generation of both H_2O_2 and formaldehyde. Adapted from Forneris, *et al.* (135).

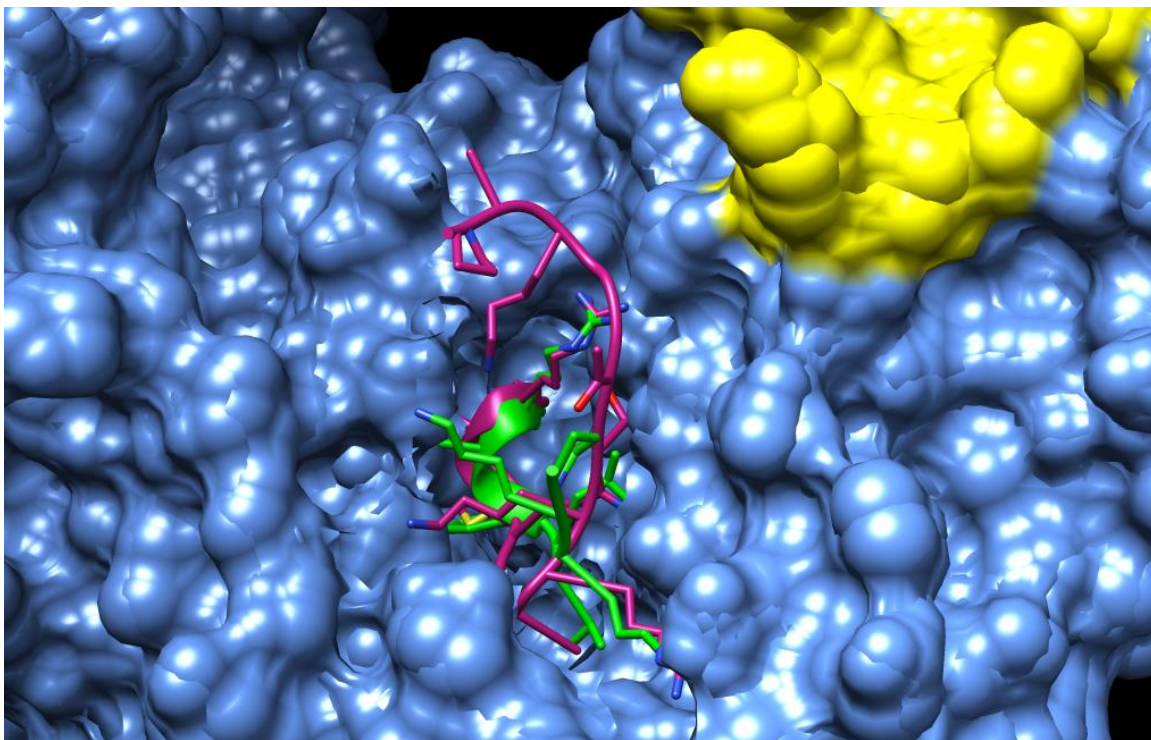


Figure 1.4 Other proteins bind LSD1 through molecular mimicry. Comparison of SNAG domain (green) and histone H3 (magenta) binding to the LSD1 (blue) and CoREST (yellow) complex. CoREST and LSD1 are visualized with a van der Waals surface.

CHAPTER 2

HIGH-THROUGHPUT VIRTUAL SCREENING IDENTIFIES NOVEL N²-(1-PHENYLETHYLIDENE)-BENZOHYDRAZIDES AS POTENT, SPECIFIC, AND REVERSIBLE INHIBITORS OF LSD1

Venkataswamy Sorna and Emily R. Theisen are co-first authors of this work. VS was responsible for the chemical synthesis and purification of the compound series. ERT wrote the manuscript and was responsible for biochemical assessment of HCI2509 as well as cell-based assays. Bret Stephens performed the initial compound screen of 121 compounds. ERT and BS screened compounds synthesized in-house.

Reproduced with permission from Venkataswamy Sorna, Emily R. Theisen, Bret Stephens, Steven L. Warner, David J. Bearss, Hariprasad Vankayalapati, and Sunil Sharma. *Journal of Medicinal Chemistry* **2013** 56 (23), 9496-9508.
Copyright 2013 American Chemical Society.

High-Throughput Virtual Screening Identifies Novel *N'*-(1-Phenylethylidene)-benzohydrazides as Potent, Specific, and Reversible LSD1 Inhibitors

Venkataswamy Sorna,^{†,⊥} Emily R. Theisen,^{†,‡,⊥} Bret Stephens,[†] Steven L. Warner,[†] David J. Bearss,[†] Hariprasad Vankayalapati,^{†,§} and Sunil Sharma^{*,†,§,||}

[†]Center for Investigational Therapeutics (CIT), Huntsman Cancer Institute, University of Utah, 2000 Circle of Hope, Salt Lake City, Utah 84112, United States

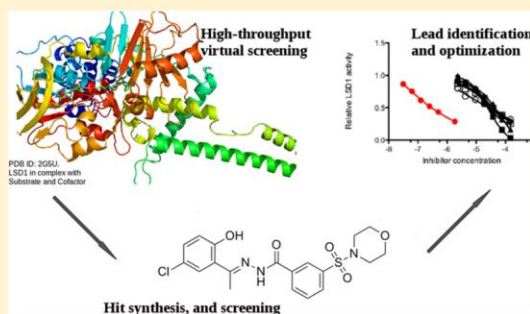
[‡]Department of Pharmaceutics and Pharmaceutical Chemistry, College of Pharmacy, University of Utah, 301 Skaggs Hall, Salt Lake City, Utah 84112, United States

[§]School of Medicine, University of Utah, 30 North 1900 East, Salt Lake City, Utah 84132, United States

^{||}Division of Medical Oncology, Huntsman Cancer Institute, University of Utah, 2000 Circle of Hope, Salt Lake City, Utah 84112, United States

Supporting Information

ABSTRACT: Lysine specific demethylase 1 (LSD1) plays an important role in regulating histone lysine methylation at residues K4 and K9 on histone H3 and is an attractive therapeutic target in multiple malignancies. Here we report a structure-based virtual screen of a compound library containing ~2 million small molecular entities. Computational docking and scoring followed by biochemical screening led to the identification of a novel *N'*-(1-phenylethylidene)-benzohydrazide series of LSD1 inhibitors with hits showing biochemical IC₅₀s in the 200–400 nM range. Hit-to-lead optimization and structure–activity relationship studies aided in the discovery of compound 12, with a K_i of 31 nM. Compound 12 is reversible and specific for LSD1 as compared to the monoamine oxidases shows minimal inhibition of CYPs and hERG and inhibits proliferation and survival in several cancer cell lines, including breast and colorectal cancer. Compound 12 may be used to probe LSD1's biological role in these cancers.



1. INTRODUCTION

Epigenetic dysregulation contributes to the aberrant gene expression programs characteristic of cancer.^{1,2} Transcriptional regulation through chromatin modification is reversible and dynamic such that enzymes implicated in the dysregulation of chromatin represent a new class of protein targets for drug development. Various chromatin modifications mediate changes in gene expression including DNA methylation, posttranslational histone modifications, and nucleosome remodeling. The N-terminal tails of histones are subject to a variety of posttranslational modifications such as phosphorylation, acetylation, methylation, and ubiquitination. Certain modifications, particularly lysine acetylation and methylation, are important for regulating the local chromatin state and are often dysregulated in cancer.²

Histone methylation was believed to be an irreversible mark until the discovery of lysine-specific demethylase 1 (LSD1) in 2004.³ LSD1 catalyzes the oxidative demethylation of mono- and dimethylated histone H3 at lysine 4 (H3K4me1 and H3K4me2) and lysine 9 (H3K9me1 and H3K9me2) through a

flavin adenine dinucleotide (FAD)-dependent amine oxidase reaction.^{3,4} While histone acetylation is associated with open chromatin and gene activation, the impact of histone methylation on the local chromatin state is more nuanced.⁵ Using the substrates for LSD1 as an example, H3K4 methylation is generally associated with gene activation, whereas methylation of H3K9 is associated with transcriptional repression.⁶ In this manner, LSD1 can act either as a corepressor or coactivator depending on its substrate.^{7,8} Thus, LSD1 is a component of both repressive and activating complexes and the substrate specificity of LSD1 depends on which complex LSD1 interacts with. Repressive complexes containing histone deacetylases (HDACs), CtBP, CoREST, and BHC80 target LSD1 toward H3K4.^{9–12} In these complexes, HDACs remove the H3K9 acetyl mark, allowing LSD1 access to H3K4 methylation.^{13,14} The unmethylated histone tail will then be bound by BHC80 to maintain the

Received: June 12, 2013

Published: November 17, 2013

repressive state.¹¹ However, in complex with the estrogen or androgen receptor, LSD1 is targeted toward H3K9 at the promoters of target genes.^{4,10,15} Subsequent demethylation of H3K9 results in the activation of estrogen and androgen receptor target genes.^{4,16}

LSD1 is a therapeutic target in cancer with overexpression observed in a variety of solid tumors, including neuroblastoma, breast, prostate, bladder, lung, liver, and colorectal tumors.^{16–20} In many of these cases, LSD1 is reported as a corepressor with specificity for H3K4. Increased methylation at the H3K4 mark through either LSD1 knockdown or inhibition was shown to reactivate expression of tumor suppressor genes in breast, bladder, lung, and colorectal cancers.^{18,21} In hormone-responsive cancer, association of LSD1 with the estrogen and androgen receptors led to increased proliferation.^{4,15} LSD1 inhibition decreased expression of target genes in these models. Thus, inhibition of LSD1 is an effective strategy to reexpress epigenetically silenced tumor suppressor genes as well as downregulate important proliferative pathways in multiple cancer types. However, because of the complexity of factors regulating LSD1 function, the precise role LSD1 plays in cancer and how that role differs between cancers is not fully understood.

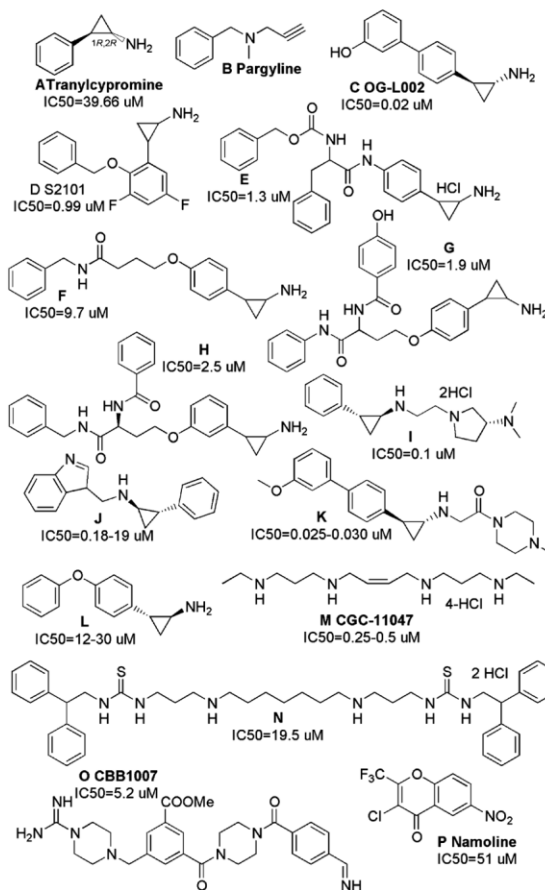
Several LSD1 inhibitors are reported (Chart 1), but they show poor selectivity and pharmacological properties making further exploration of LSD1 biology difficult. Monoamine oxidase (MAO) inhibitors such as tranylcypromine (TCP) and pargyline are known irreversible LSD1 inhibitors (A and B), and several reported inhibitors (C–L)^{22–29} are derivatives of these scaffolds with increased selectivity for LSD1. Peptide derivatives of pargyline have also been investigated, but delivery of peptide therapeutics to the nucleus remains an unsolved issue.^{30,31} Polyamine derivatives were also evaluated as LSD1 inhibitors (M and N), with compounds showing biochemical activity in the low micromolar range.^{21,32,33} Other reversible LSD1 inhibitors are reported to show selective activity against stem-like cancer cells (O)³⁴ and castration-resistant prostate cancer (P).³⁵ In vivo efficacy is reported for the reversible inhibitor, namoline (P), however this was accompanied by significant weight loss indicative of off-target toxicity.³⁵ In general, currently available small molecule LSD1 inhibitors display poor selectivity, low potency, or in vivo toxicity, limiting further interrogation of LSD1's contribution to cancer at the organismal level. Identification of novel potent, selective, and reversible LSD1 inhibitors is essential to further elucidate LSD1's role in cancer and identify whether or not reversible inhibition targeting LSD1 is a viable therapeutic strategy.

Here, we report a structure-based virtual screen (VS) of a diverse compound library utilizing docking with Glide, ICM, GOLD scoring, and GOLD consensus rescoring energy calculations, which led to the identification of a novel *N'*-(1-phenylethylidene)-benzohydrazide series of LSD1 inhibitors. On the basis of the initial hits, we rationally designed a series of small molecule LSD1 inhibitors which resulted in a selective and potent lead compound **12** which is a reversible and noncompetitive LSD1 inhibitor.

2. RESULTS

2.1. Docking Studies. The docking protocols used by both ICM and Glide SP were run with the adenosine phosphate fragment of FAD, riboflavin fragment of FAD, and known LSD1 ligands from Chart 1 as positive controls within the Glide dl-400 1000-compound decoy set to confirm the accuracy of

Chart 1. Representative Structures of Reported Classes of LSD1 Inhibitors^a



^aWhere appropriate compound IDs and IC₅₀ values are indicated.

the docking protocols. Specifically, known LSD1 ligands were identified in the top 2% of the total decoy set. The structure-based VS was performed using the Glide docking module within the Schrödinger Suite 2011. The small molecule ligand library of 13 million compounds was first docked using Glide High Throughput Virtual Screen (HTVS), a method specifically proven to discard noticeable nonbinders with minimal computational time and then filtered for standard rule-of-five (RO5) criteria, medchem tractability based on physicochemical parameters in predicted in QikProp, and undesirable chemical features. The top 15% of compounds (~2 million) from HTVS were then redocked with the more computationally expensive Glide standard precision (SP) scoring. This led to the selection of 0.5% (~10000) of the top-ranked compounds by SP for subsequent screening using Glide extra-precision (XP) and ICM docking and scoring methods. These methods from the Schrödinger and Molsoft suites, respectively, are more resource intensive and used in our workflow to minimize false positives.

While molecular docking has proven a useful tool to quickly identify bioactive compounds, there are still problems with the accuracy and consistency of scoring functions in VS methods.

Hence, we identified 121 compounds which scored either < -5.0 kcal/mol using Glide SP/XP or < -15.0 kcal/mol using ICM in addition to meeting certain physicochemical criteria, including solubility >50 $\mu\text{g/mL}$, permeability >50 nmol/s, and polar surface area (PSA) <120 \AA^2 as determined by QikProp. In addition to the algorithm rankings, redundant compounds were removed to improve chemical diversity of the final selections and visual inspection of the docking results was used to evaluate binding mode, position, and orientation. Taken together, this methodology identified a set of 121 hits for further analysis. GOLD was used to rescore these hits. The GOLD consensus scoring and fitness functions produced similar compound rankings within the 121 hits to that of ICM and Glide scores, further supporting our hit selection process. Interestingly, compounds with hydroxyl moieties, hydrophobic electron withdrawing groups, and heterocycloalkyl groups were well represented in the initial docking experiments from all VS programs used.

2.2. Initial Hits. On the basis of the selection criteria discussed above, 121 structurally distinct compounds were procured and screened in the LSD1 biochemical assay. This identified a series of *N'*-(1-phenylethylidene)-benzohydrazides, which showed potent activity against LSD1. Biochemical assay results and docking scores for the series are reported in Table 1, Supporting Information Tables S1 and S2. Out of the 121 in silico hits tested for LSD1 activity, compounds 1–5 showed biochemical activity in the 200–400 nM range. Compound 6 showed an IC_{50} of 19 nM against LSD1. The docking poses

determined from all three programs were predicted to be similar and show the protonated morpholin ring nitrogen of compound 6, forming a favorable ionic interaction. Interestingly, the 2-hydroxyphenyl moiety of compound 6 extended deeper into the pocket as compared to compounds 1–5. A representative binding mode is shown in Figure 1. These initial hits support the utility of our VS methodology. Compounds 7–10 had similar core structures to compounds 1–6 and represented some of the chemical diversity present in the 121 hits. These compounds included substitution of the critical 2-hydroxyphenyl groups with biaryl naphthalene (7), an electron donating methoxyl group (8), absence of the hydroxyl group (9), and the introduction of a small hydrophobic methyl group with a lack of 2-hydroxyl (10). The additional 111 negative hits are reported in Supporting Information Table S2.

The biochemical data showed compounds having 4-OH, 4-Br, or 3-Cl aryl substitutions on the benzohydrazides (compounds 1, 4, and 5, respectively) had similar activity against LSD1 with IC_{50} s of 218, 196 nM, and 333 nM, respectively. The 5-chloro-2-hydroxyl substituted derivative (2) and *N'*-(1-phenylethylidene)-benzohydrazide core (3) are well tolerated, with IC_{50} s of 275 and 291 nM, respectively. The 3-substituted sulfonyl functional group on the arylhydrazide moiety of compound 6 improved biochemical activity 10-fold with an IC_{50} of 19 nM. The exchange of the 2-hydroxyphenyl moiety with naphthalene in compound 7 impaired biochemical activity with an $\text{IC}_{50} > 10$ μM . Compounds 8–10 were representative examples of the remaining negative hits and showed no biochemical activity in the LSD1 assay. These biochemical results suggested further optimization of compounds 1–6 to explore the structure–activity relationship of the *N'*-(1-phenylethylidene)-benzohydrazide series and identified potential lead compounds shown in Table 2 for further screening against LSD1.

2.3. Structure–Activity Relationship of Initial Hits and Compound Optimization.

Compounds 11–22 were subsequently synthesized in-house, and their chemical structures and LSD1 inhibition are reported in Table 2. We utilized the *N'*-(1-phenylethylidene)benzohydrazide core scaffolds from hit compounds 3 and 6 for further optimization and SAR in order to increase metabolic stability over the benzylidenebenzohydrazide core of compounds 1, 2, 4, and 5. In compound 11, removing the sulfonyl moiety and retaining the 5-chloro-2-hydroxyphenyl group from compound 2 maintained a biochemically active compound ($\text{IC}_{50} = 128$ nM) with a 10-fold reduction in potency as compared to 6. In the case of 12, reintroduction of the sulfonyl functional group and inclusion of the 5-chloro-2-hydroxyphenyl moiety on the *N'*-(1-phenylethylidene)benzohydrazide inhibited LSD1 with an IC_{50} of 13 nM, which is comparable to compound 6. A representative binding mode of 12 generated from ICM is shown in Figure 1. Exchanging 2-hydroxyl with 2-chloro in compound 13 resulted in a complete loss of LSD1 activity, emphasizing the importance of the 2-hydroxyl group. As shown in Figure 1, the 2-hydroxyl moiety participates in hydrogen bonding and loss of this interaction likely impairs ligand binding. Replacement of the morpholin with an *N,N*-dimethyl sulfonamide (14) maintained LSD1 potency with an IC_{50} of 14 nM, highlighting the significance of the core sulfonamide. On the basis of Figure 1, we hypothesized both *N'*-(1-phenylethylidene)benzohydrazide and *N'*-(1-phenylpropylidene)benzohydrazide were likely accommodated, however the *N'*-(1-phenylpropylidene)benzohydrazide deriva-

Table 1. Commercially Available Highly-Ranked Hits from 121 Screened Compounds^a

S. No	Structure	IC_{50} (μM) LSD1
1		0.218
2		0.275
3		0.291
4		0.196
5		0.333
6		0.019
7		>10
8		>3
9		>3
10		>3

^aIncluded are biochemical IC_{50} s for compound 1–10.

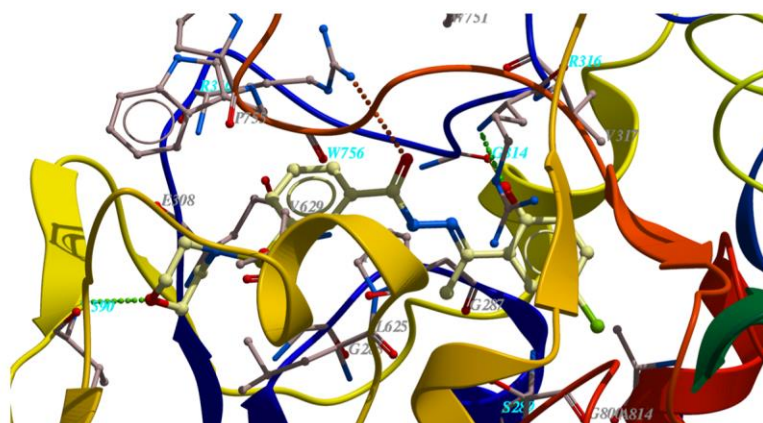


Figure 1. Mode of binding of compound 12 in complex with LSD1. The H-bonding interactions of compound 12 with LSD1 are depicted in dashed lines.

Table 2. Synthesized Compounds and Their Biochemical Activity against LSD1

S. No	Structure	IC ₅₀ (μM) LSD1
11		0.128
12		0.013
13		>3
14		0.014
15		>3
16		>3
17		>3
18		>3
19		>3
20		>3
21		>3
22		>3

tive (15) showed no LSD1 activity (IC₅₀ > 3 μM). Generally, compounds 15–22 showed no activity against LSD1 in the biochemical assay. An additional polar hydroxyl group did not

improve LSD1 activity nor did disubstitution of the aryl ring with strong electron withdrawing groups, like –F. Further, introduction of various heterorings were not tolerated. Because of the favorable biochemical activity of compound 12, we utilized it to further investigate the mechanism of inhibition of this series of LSD1 inhibitors.

2.4. Scaffold Novelty. Many different classes of LSD1 inhibitors are already reported (Chart 1), with some compounds showing nanomolar potency. We wanted to evaluate the similarity of the *N'*-(1-phenylethylidene)-benzohydrazide scaffold to previously reported inhibitors. The calculated Tanimoto similarity coefficients are reported in Supporting Information Table S3. Typically, 0.7 is used as a cutoff, with >0.7 indicating similar compounds. Generally, the similarity coefficients calculated are all <0.4, ranging from 0.11 to 0.39, demonstrating that compound 12 is structurally distinct from previously reported LSD1 inhibitors. The most dissimilar compounds were the polyamine derivatives (M and N) and the reversible inhibitor namoline (P), with similarity scores of 0.11. The most similar compounds were various derivatives of tranlycypromine (F, J, and K), with similarity scores of 0.35, 0.36, and 0.39, respectively. The similarity score for the other reversible inhibitor reported, O, was calculated to be 0.32. These results corroborated the novelty of the *N'*-(1-phenylethylidene)-benzohydrazide series, represented in Tables 1 and 2.³⁶

2.5. Lead Compound 12 Is Specific and Reversible.

The specificity of the compounds 1 and 12 were tested in MAO A and MAO B biochemical assays (Figure 2). In this assay, the MAO inhibitor TCP exhibited activity against both MAO A and B, with an IC₅₀ of 2.1 and 3.6 μM, respectively. Compound 1 was active against MAO B, with an IC₅₀ of 1.3 μM, but showed no activity against MAO A (IC₅₀ > 300 μM). In contrast, compound 12 did not exhibit activity against either MAO enzyme up to 300 μM. We further screened 12 against d-lactate dehydrogenase, glucose oxidase, a panel of cytochrome P450s (CYP), and human ether-à-go-go (hERG), with IC₅₀ values summarized in Table 3. Using an IC₅₀ of 3 μM as a cutoff, 12 showed low activity against CYP3A4, with an IC₅₀ of 2.96 μM. The inhibition data for the off-target assays are reported in the Supporting Information (Table S4).

We performed a jump dilution to assay the reversibility of compound 12 (Figure 3). In this assay, LSD1 was incubated

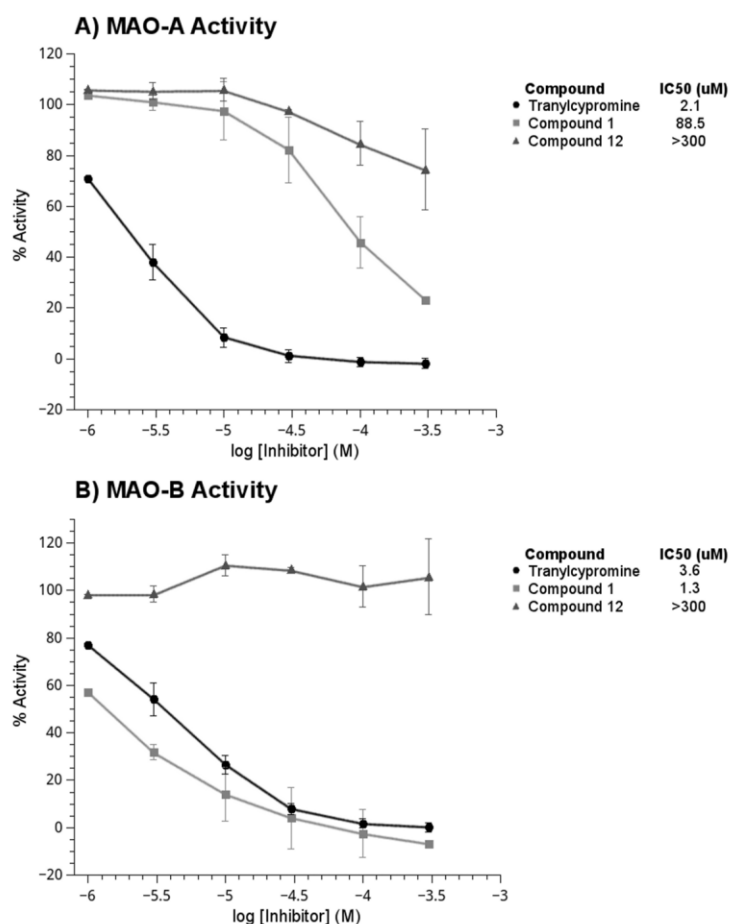


Figure 2. MAO activity of select compounds. (A) The MAO inhibitor TCP inhibited MAO A with an IC₅₀ of 2.1 μM, while compounds 1 and 12 inhibited MAO A with IC₅₀s of 88 and >300 μM, respectively. (B) Compound 12 did not inhibit MAO B at the concentrations tested (IC₅₀ > 300 μM). However, compound 1 exhibited significant activity against MAO B, with an IC₅₀ of 1.3 μM, similar 3.6 μM for TCP.

Table 3. Off-Target Panel for Compound 12

enzyme	IC ₅₀ (μM)
D-lactate dehydrogenase	>10
glucose oxidase	>10
CYP1A2	>10
CYP2C19	9.76
CYP2C9	8.04
CYP2D6	>10
CYP3A4	2.61
hERG	>10

with 10× the biochemical IC₅₀ of 12 for 1 h and then diluted 100-fold into the assay. The irreversible inhibitor TCP was used as a positive control, and the chemically similar but inactive compound 13 was used as a negative control. TCP incubation resulted in complete inactivation of the enzyme, which was not recovered once diluted into the assay buffer. When LSD1 was diluted into assay buffer after incubation with compound 12, its activity returned with only 14.4 ± 3% inhibition. When the drug concentration was held constant at 200 nM through the dilution, activity was inhibited 65.7 ± 5%, suggesting

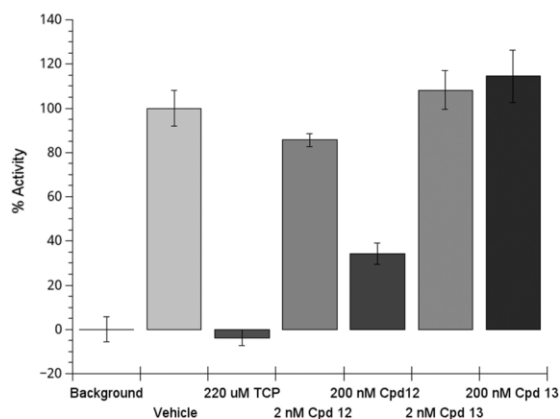


Figure 3. Compound 12 reversibly inhibits the activity of LSD1. Dilution of compound 12, but not of the covalently binding inhibitor TCP, results in recovery of LSD1 activity. Compound 13 is inactive.

compound **12** is a reversible inhibitor. Compound **13** showed no activity in this assay.

2.6. Compound 12 Is a Noncompetitive Inhibitor. We further performed differential scanning fluorimetry (DSF) to compare the melting profile of LSD1 bound by compound **12** with the LSD1-TCP complex. DSF uses SYPRO Orange, which preferentially fluoresces in the amphiphilic molten globule state of an unfolding protein. LSD1 was incubated either with compound **12**, **13**, or TCP for 30 min, and then DSF was performed. The raw melt curves were smoothed and fit to a Boltzmann curve for unfolding using Applied Biosystem's Protein Thermal Shift (PTS) software. Derivatives of the smoothed curves were plotted to generate the derivative plot shown in Figure 4. Both Boltzmann and derivative melting

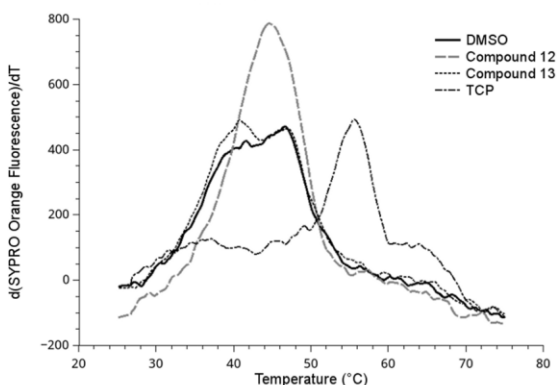


Figure 4. Derivative melt curves of LSD1 in the presence of DMSO, compound **12**, compound **13**, and TCP. LSD1 has a complex multiphase melt. Compound **12** and TCP induce changes in LSD1's melt profile in distinct manners. Compound **13** shows no difference from DMSO.

temperatures (T_m) were determined for each condition and are shown in Table 4. LSD1 alone showed a multiple-phase

Table 4. Melting Temperatures as Determined by DSF

treatment	Boltzmann $T_m \pm$ SD (°C)	first derivative $T_m \pm$ SD (°C)	second derivative T_m \pm SD (°C)
DMSO	43.28 \pm 0.45	40.49 \pm 0.81	46.31 \pm 1.08
15 μ M 12	44.60 \pm 0.47	45.35 \pm 1.27	N/A
15 μ M 13	43.29 \pm 0.67	40.76 \pm 0.58	46.69 \pm 0.76
220 μ M TCP	51.98 \pm 1.18	55.60 \pm 0.32	N/A

unfolding with a Boltzmann T_m of 43.28 \pm 0.45 °C and derivative T_m s at 40.49 \pm 0.81 °C and 46.31 \pm 1.1 °C. Compound **13** exhibited no effect on LSD1.

TCP stabilized LSD1 with a clear rightward shift of the derivative curve. Additional inspection of the data showed a long period of slow melting, followed by a sharp transition between 50 and 60 °C. The Boltzmann T_m was determined as 51.98 \pm 1.2 °C, and the derivative method placed the T_m during the rapid melt phase at 55.60 \pm 0.32 °C. Compound **12** shifted the T_m in a subtle but statistically significant fashion and constrained the melting dynamics of LSD1 to classical two-state unfolding. The Boltzmann T_m for compound **12** was 44.60 \pm 0.47 °C with a derivative T_m of 45.38 \pm 1.3 °C. This suggests

compound **12** binds LSD1, changes its solution dynamics in a manner distinct from TCP, and shows small change in T_m .

We used enzyme kinetics to investigate the mechanism of action of compound **12**. For each drug concentration, the initial velocity of the biochemical assay was plotted with respect to enzyme substrate in Figure 5. Our calculated K_m of 1.3 \pm 0.2

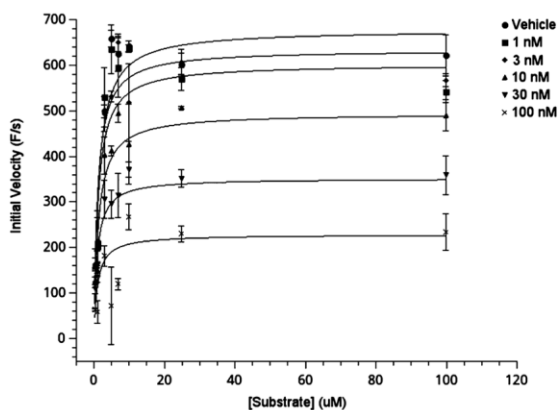


Figure 5. LSD1 kinetics with multiple concentrations of compound **12**. Compound **12** causes a decrease in v_{max} with no change in K_m , characteristic of noncompetitive inhibition.

μ M is similar to previous literature reports for the dimethylated K4 N-terminal H3 peptide.¹⁴ Curves were analyzed individually using the Michaelis–Menten suite or globally using the Enzyme Inhibition suite in GraphPad Prism 5, with the results of the analysis summarized in Table 5. The global fit to a mixed model inhibition gave a K_i of 31 \pm 12 nM and an α value of 1.3, which is most indicative of noncompetitive inhibition. This is consistent with the observed drop in v_{max} and little change in K_m with increasing concentration of **12**. (For a comparison of competitive, noncompetitive, and uncompetitive inhibition global curve fits, see Supporting Information Table S5.) Individually fitting each curve and using this data to determine a K_i for compound **12** produced a K_i of 34 \pm 1.9 nM, which correlated well with the global fit.

2.7. Compound 12 Activity in In Vitro Assays.

Compound **12** was used to evaluate sensitivity in a panel of cancer cell lines (Table 6). Cell line sensitivity to compound **12** varied by one log in a cell viability assay, with EC_{50} values ranging from 300 nM to 3 μ M. Nine of the 17 cell lines tested were sensitive to compound **12**, with an EC_{50} < 1 μ M. Endometrial, breast, colorectal, and pancreatic cancers were represented in the sensitive lines, consistent with a role for LSD1 in multiple cancers. EC_{50} values were determined in T-47D breast cancer cells to evaluate the correlation between cell sensitivity and biochemical activity against LSD1 (Table 7). With few exceptions, it was observed that T-47D cells were sensitive to test compounds that were active in the LSD1 biochemical assay. For compounds inactive in the biochemical assay, cellular sensitivity was more variable (Figure 6). Compounds with low EC_{50} s against T-47D cells but no biochemical activity may possess uncharacterized cytotoxic off-target activity. The only active biochemical compounds without T-47D activity were compounds **1** and **14**. These compounds may show decreased permeability or solubility in the cell-based assay format, although compound **14** still shows activity near

Table 5. Summary of Michaelis–Menten Curve Fits

fit	v_{\max} (F/s) \pm std error	K_m (μ M) \pm std error	k_i (nM) \pm std error	α \pm std error	R^2
global: mixed	687 \pm 11.43	1.284 \pm 0.1048	30.69 \pm 12.4	1.333 \pm 0.64	0.9241
Model Inhibition					
DMSO	697.5 \pm 26.32	1.405 \pm 0.2514	N/A	N/A	0.9275
1 nM	649.4 \pm 30.09	1.140 \pm 0.2662	13.50	N/A	0.8807
3 nM	642.9 \pm 27.07	1.393 \pm 0.2787	35.32	N/A	0.9082
10 nM	531.1 \pm 19.53	1.508 \pm 0.2573	31.92	N/A	0.9308
30 nM	376.4 \pm 12.25	1.108 \pm 0.1832	35.17	N/A	0.9326
100 nM	246.5 \pm 19.57	2.267 \pm 0.7461	54.66	N/A	0.7803
average k_i	N/A	N/A	34.11 \pm 6.54	N/A	N/A

Table 6. Compound 12 Inhibits Proliferation in Several Cell Lines in Vitro

cell line	IC ₅₀ (μ M)	cancer type
AN3 Ca	0.356	endometrial
BT-20	0.489	breast
BT-549	1.010	breast
HCT 116	0.614	colorectal
HER218	0.612	breast
Hs-578-T	1.700	breast
HT29	0.429	colorectal
MCF-7	0.637	breast
MDA-MB-231	1.040	breast
MDA-MB-435	1.440	melanoma
MDA-MB-468	2.730	breast
MIA PaCa-2	0.468	pancreatic
PANC-1	1.104	pancreatic
PC-3	2.160	prostate
SK-N-MC	0.329	sarcoma
T-47D	0.649	breast
U87	1.160	glioblastoma

Table 7. In Vitro Growth Inhibition of Compound Panel in T-47D Cells

compound	IC ₅₀ (μ M)
1	2.700
2	0.821
3	0.971
4	0.096
5	0.615
6	0.524
7	>10
8	>10
9	>10
10	>10
11	0.352
12	0.649
13	1.700
14	1.375
15	0.352
16	>10
17	>10
18	>10
19	0.565
20	0.270
21	0.616

1 μ M. Importantly, when the hydroxyl of compound 12 was substituted with a chlorine (compound 13), in vitro activity was

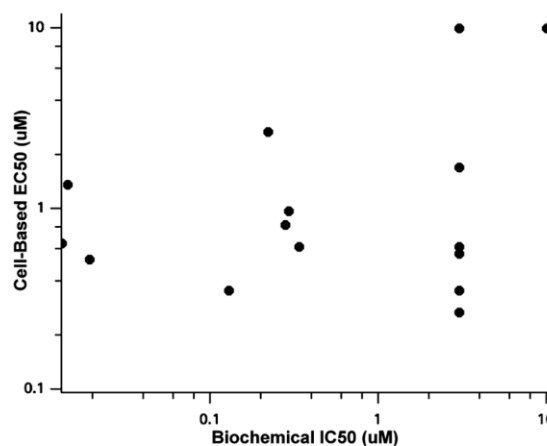


Figure 6. Compounds with biochemical activity against LSD1 show in vitro EC₅₀s clustered near 1 μ M. Compounds without LSD1 activity show a wide range of in vitro efficacy.

lost, confirming the importance of the hydroxyl group in that position for both biochemical and cellular activity.

In addition to cell viability, we assayed compound 12 for its effect on histone methylation in an androgen-sensitive prostate cancer cell line, VCaP. VCaP cells were treated for 24 h with vehicle or 0.1, 1, or 10 μ M of compound 12 for 24 h. We focused specifically on the H3K9me2 mark. H3K9me2 is a target for LSD1 in complex with the androgen receptor in prostate cancer.^{4,15} Demethylation of this mark activates transcription of androgen receptor target genes.^{4,15} An increase in H3K9me2 is observed at 24 h with both 1 and 10 μ M of treatment with 12 (Figure 7). This suggests the antiproliferative effects of compound 12 are on-target and related to changes in histone methylation mediated through reversible LSD1 inhibition.

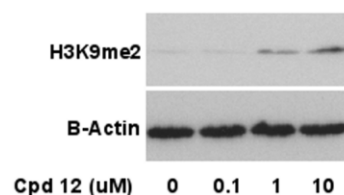


Figure 7. VCaP cells treated with compound 12 show a dose-dependent increase in H3K9 dimethylation.

3. DISCUSSION

We used a virtual screen (VS) methodology with a custom compound library to evaluate the chemical space outside of previously reported LSD1 inhibitors. All computational methods utilized the crystal structure of LSD1 in complex with an FAD-tranylcypromine adduct (PDB ID: 2ZSU).³⁷ The virtual small molecule screening library was curated from publicly available vendor libraries, totaling ~13 million compounds. We then performed structure-based VS using Glide in HTVS mode to weed out noticeable nonbinders along with custom filters to narrow the library to ~2 million compounds having drug-like properties and chemical diversity. Filters included medchem tractability, based on physicochemical parameters calculated in QikProp, and undesirable chemical features in addition to rule-of-five-based parameters (<5 H-bond donors, <8 H-bond acceptors, CLogP < 5, and molecular weight <500). This custom protocol increases the probability that hits from the top 0.5% of compounds from subsequent Glide SP docking will display favorable properties for later lead optimization and lead compound development. By cross-comparing results from three different docking algorithms (ICM, Glide XP, and GOLD), this study identified 121 initial hits that were procured and screened against LSD1 in a biochemical assay. Twelve novel compounds were subsequently synthesized in-house based on the SAR of the initial positive hits (1–6) to further elucidate the SAR, optimize drug-like properties, and increase potency. Biochemical activity for compounds 1–21 correlated well with in vitro activity in a breast cancer cell line, T-47D. Generally, compounds which were active in the biochemical assay showed an EC₅₀ in T-47Ds near or below 1 μM, suggesting a similar and consistent mechanism of action. Compounds with poor biochemical activity showed a range of activity in the cell viability assay, which indicates some of the compounds inactive against LSD1 may have uncharacterized off-target toxicities in vitro.

Ultimately, our lead optimization strategy successfully identified a series of compounds more potent and specific than other reported LSD1 inhibitors. Tanimoto similarity scores are reported (Supporting Information Table S3) comparing compound 12 against previously reported LSD1 inhibitors. The low range of similarity scores (0.11–0.39) supports these compounds as a novel class of LSD1 inhibitors. The in-house-synthesized compounds 11, 12, and 14 showed biochemical IC₅₀s between ~10 and 300 nM against LSD1 compared to 39.7 μM for TCP, which forms a noncovalent adduct with the FAD. The novelty of the scaffold may contribute to the improved specificity profile against the MAOs after lead optimization as compared to those reported for other compounds.²² FAD is bound in LSD1 by a Rossmann fold in a manner homologous to MAO A and B. Given the high structural homology of LSD1 to the monoamine oxidase family of enzymes (17.6% for both MAO A and B),³⁸ these are likely off-target hits for LSD1 inhibitors. TCP and pargyline derivatives targeting the H3-binding cavity of LSD1 often show some activity against either MAO A or MAO B, limiting their use in preclinical studies. Optimization from compound 1 to compound 12 improved the specificity profile where the initial hit compound 1 was more active against the MAO B and compound 12 displayed a favorable off-target profile with minimal activity against both MAO A and B. Compound 12 was also selective over other flavoenzymes D-LDH and GO as well as against cytochrome P450s and hERG.

We predicted that our lead optimization strategy would select reversible inhibitors of LSD1. Subsequent jump dilution experiments confirmed the reversibility of compound 12, inactivity of compound 13, and the irreversible mechanism of action of TCP. DSF analysis was performed to further probe the physical effect of compound 12 as compared to irreversible inhibition. In these experiments, LSD1 alone and in the presence of 13 shows a multiphase melting curve (Figure 4). This may indicate either two domains which melt at different temperatures or two populations of conformers with different thermal stability. The addition of compound 12 shows subtle changes in the *T_m*, with an effect on the melt profile evident in the derivative curve. Here, compound 12 appears to constrain LSD1's derivative profile to a Boltzmann distribution indicative of a classical two-state unfolding. Irreversible inhibition with TCP shows a long period of slow "melting" followed by a sharp melt between 50 and 60 °C. We conclude compound 12 alters the solution dynamics of LSD1 in a manner distinct from TCP.

Kinetic analysis was used to elucidate the reversible mechanism of action of our inhibitor series and to determine a *K_i* for compound 12. Michaelis–Menten plots were generated across five inhibitor concentrations and seven substrate concentrations. A global fit of the data showed that non-competitive inhibition best described compound 12's mechanism of action. This is corroborated by the decreased *v_{max}* and unchanged *K_m* observed when the individual curves for each inhibitor are fit independently. The *K_i* of 12 was near 30 nM. Compound 12 does not interfere with the binding of the N-terminal H3 peptide so transcription factors with N-terminal sequences homologous to histone H3 that have been shown to recruit LSD1, such as SNAI1 and Gfi-1, may still be able to recruit an inactive LSD1 via their SNAG domains.^{39–41} However, if the conformational dynamics of LSD1 are constrained by compound 12, other key protein–protein interactions which regulate LSD1's activity may be disrupted. Further studies are required to determine the effect of compound 12 on the protein–protein interactions which guide LSD1's biological function.

Compound 12 shows cellular activity against several cancer cell lines including endometrial, breast, colorectal, pancreatic, and prostate cancer. We further screened compound 12 for its effects on H3K9 dimethylation in the VCaP prostate cancer cell line. The H3K9me2 mark is a target for LSD1 in prostate cancer when in complex with the androgen receptor.^{4,15} Compound 12 showed a dose-dependent increase in the H3K9me2 mark after 24 h of treatment at both 1 and 10 μM. This result suggests compound 12 shows on-target activity in cell lines as well. The fact that significant changes in histone methylation are observed at 1 μM may be the reason for the EC₅₀ cluster around 1 μM in the cell viability assay for compounds with potent LSD1 biochemical activity. Further studies are needed to determine the exact mechanism of action of compound 12 in different cell lines.

Additional studies with compound 12 are currently underway to better characterize the binding mode, physicochemical attributes, and mechanism of action of these compounds including crystallographic, pharmacokinetic, and pharmacological studies. Importantly, as LSD1 activity often requires complexation with other proteins, like Co-REST, knowing the effects of inhibition on both enzymatic activity as well as complex stability is necessary to understand the pharmacology of reversible, noncompetitive inhibition with our compound series. The results presented so far lead us to conclude that

these compounds may be considered for future preclinical studies. Efforts are underway to develop additional analogues with ideal physicochemical properties for consideration in *in vivo* pharmacokinetic and pharmacodynamic studies.

4. CONCLUSIONS

In summary, we performed a structure-based VS of ~2 million diverse and preprocessed compounds from a library developed in-house with the goal of identifying a novel series of LSD1 inhibitors. A novel *N'*-(1-phenylethylidene)-benzohydrazide series was identified. Optimization and exploration of the SAR were performed using both virtual and biochemical techniques. Biochemical analysis shows a specific, potent, and reversible lead compound (**12**) to take into further crystallographic, mechanistic, and pharmacological studies. These results support structure-based approaches as valid starting points for lead optimization strategies.

5. EXPERIMENTAL SECTION

5.1. Computational Methods. **5.1.1. Structure-Based Virtual Screen.** All computational studies employed PDB ID 2Z5U for the structural coordinates of LSD1.³⁷ Virtual screening methods from Glide, ICM, and GOLD programs were used. The protein structure was prepared by 3D protonation, deletion of water molecules, and energy minimization using the ICM force field and distance-dependent dielectric potential with an RMS gradient of 0.1; heavy atoms in the protein were kept fixed, and histidine residues were considered as neutral. VS scoring calculations utilized default parameters unless explicitly specified otherwise. PocketFinder (ICM) and SiteMap (Schroedinger) were used to define the ligand-binding site for docking studies. In both cases, the PocketFinder and SiteMap predicted ligand site is located near both the substrate and FAD-binding pockets. Default parameters in ICM include a docking site as a rectangular box with a grid spacing of 0.5 Å centered at the ligand binding site as defined by PocketFinder. A threshold set to retain 2% of the ligands along with a threshold scores of -32, maximum ligand size of 500 molecular weight, H-bond donors of 5, H-bond acceptors of 10, and torsions of 10 were used. For Glide, the default parameters similarly included the docking site as a 12 Å box centered on the geometrical center of the SiteMap-defined ligand binding site, with the ligand internal energy offset option turned on with the top 10 ranked poses for each ligand retained for scoring. Energy grids representing the active site (van der Waals, H-bonding, electrostatics, and hydrophobic interaction) were calculated with a 0.5 Å grid spacing. Confirmation of the accuracy and efficiency of the applied docking protocol used a decoy set with the adenosine phosphate fragment of FAD, the riboflavin fragment of FAD, and known LSD1 inhibitors (Chart 1) as positive controls within the Glide dl-400 1000-compound decoy set provided in the Schroedinger Suite.⁴² We employed the structure-based VS to identify new small molecules which target this site on LSD1. Two separate docking runs were carried out with the ICM and Glide SP docking programs. The decoys with no valid poses after minimization were excluded from RMSD-score analysis but included in other evaluations as bad poses (GlideScore or Emodel = 10000).

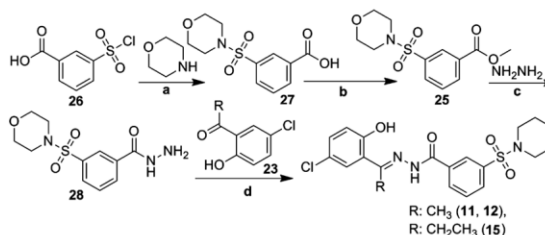
The compound database was prepared using Ligprep 2.1.23 of the Schroedinger Suite and ICM's inbuilt preparation of three-dimensional (3D) ligands such that physiologically relevant protonation states were used. Prepared ligands were then docked against LSD1. Two rounds of VS, including HTVS and standard precision (SP) docking, were adopted. The top 10000 compounds ranked by Glide HTVS followed by SP were stored and submitted for additional docking experiments using Glide XP and ICM. GOLD was used only for rescoring. Specifically, the final set of 121 hits was selected based on ICM and Glide SP/XP scores as well as pharmaceutical properties predicted in QikProp, and individual compounds were visually inspected to check the docking poses and interactions between ligands and LSD1. To filter out redundant compounds, we used ICM Molcart with search

criteria including compound ID, structure, and SMILES string to identify and discard the duplicates. Rescoring was performed on a minimized 121 top-ranked poses (selected from Glide SP and ICM) in Glide XP and GOLD using the "refine and do not dock" option. Finally, 121 compounds were purchased and screened in an LSD1 biochemical assay. The details of comparative docking and hit selection from ICM, Glide, and GOLD are available in the Supporting Information (Section S1).

5.1.2. Tanimoto Similarity Coefficient Calculation. Tanimoto similarity coefficients were calculated using the Molcart module of ICM.

5.2. Chemistry. All reagents and solvents were purchased from commercial sources and used without further purification. Solvents were of analytical or anhydrous grade (Sigma-Aldrich). Reactions were monitored by HPLC. Reverse phase preparative HPLC was performed using a preparative HPLC system. ¹H NMR spectra were recorded on a Varian Unity 400 instrument. Chemical shifts (δ) are reported in ppm downfield from solvent references. Mass spectra were obtained on a Finnegan LCQ Duo LCMS ion trap electrospray ionization (ESI) mass spectrometer. The general reaction scheme is depicted in Scheme 1, with specific reaction schemes for compounds **11**–**21** given in the

Scheme 1. General Procedure for the Synthesis of *N'*-(1-Phenylethylidene)-benzohydrazides^a



^aReagents and conditions: (a) THF, K₂CO₃, RT, 1 h; (b) conc H₂SO₄, CH₃OH, 65 °C, 12 h; (c) hydrazine, CH₃OH, reflux 12 h; (d) AcOH, CH₃OH, MW, 120 °C, 30 min.

Supporting Information (Figure S3). The purity of the synthesized compounds was determined by LC-MS analysis and was confirmed to be >95% purity for all biologically tested compounds.

5.2.1. (*E*)-*N'*-(1-(5-Chloro-2-hydroxyphenyl)ethylidene)-benzohydrazide (11**).** 1-(5-Chloro-2-hydroxyphenyl) ethanone **23** (100 mg, 0.586 mmol) and benzohydrazide (**24**) (80 mg, 0.586 mmol) was dissolved in methanol (4 mL) in the presence of acetic acid as a catalyst, and then the reaction mixture was heated via microwave irradiation to 120 °C for 30 min. Following cooling, the solvent was removed by vacuum and the resulting crude material was purified by Companion Rf (2% CH₃OH/CH₂Cl₂), affording the title compound **11** as a white solid (90 mg, 53%). ¹H NMR (400 MHz, DMSO): δ 7.95 (m, 2H), 7.67–7.62 (m, 2H), 7.56 (m, 2H), 7.35 (dd, 1H, *J* = 2.4 and 8.8 Hz), 6.95 (d, 1H, *J* = 8.4 Hz), 3.35 (s, 3H). ESI-MS: 289.0 [M + H]⁺. LC-MS purity of compound **11** was found to be >95%.

5.2.2. (*E*)-*N'*-(1-(5-Chloro-2-hydroxyphenyl) ethylidene)-3-(morpholinylsulfonyl) Benzohydrazide (12**).** The methyl 3-(morpholinylsulfonyl) benzoate **25** was prepared in two steps. The 3-(chlorosulfonyl) benzoic acid **26** (250 mg, 1.133 mmol) was added to morpholin (99 mg, 1.133 mmol) in THF (5 mL) in presence of K₂CO₃ (313 mg, 2.266 mmol), and the resulting reaction mixture was stirred at room temperature for 1 h. After completion of the reaction from TLC, the solvents were removed and the crude material was purified by Companion Rf (3% CH₃OH/CH₂Cl₂) to give compound **27** (160 mg, 0.590 mmol) in 52% yield as white solid. In a subsequent step, compound **27** (100 mg, 0.369 mmol) dissolved in methanol (4 mL) and was added the catalytic amount of conc H₂SO₄. The resulting reaction mixture was heated to 65 °C for overnight. The solvents were removed and the crude material after purification gave **25** in 54%

yields (60 mg, 0.200 mmol). ¹H NMR (400 MHz, CDCl₃): δ 8.38 (t, 1H, *J* = 1.6 Hz), 8.27 (m, 1H), 7.92 (m, 1H), 7.64 (t, 1H, *J* = 8.0 Hz), 3.95 (s, 3H), 3.73 (m, 4H), 3.00 (m, 4H). ESI-MS: 286.1 [M + H]⁺.

The methyl 3-(morpholinosulfonyl) benzoate **25** (120 mg, 0.421 mmol) was reacted with hydrazine hydrate (17.53 mg, 0.547 mmol) in methanol (5 mL) and was refluxed for 12 h at 65 °C. After completion of the reaction, solvents were removed by vacuum and the obtained crude material was purified by Companion Rf to give **28** (90 mg, 0.315 mmol, 75%). ¹H NMR (400 MHz, CDCl₃): δ 8.16 (m, 1H), 8.12 (m, 1H), 8.04 (m, 1H), 7.85 (m, 1H), 7.63 (t, 1H, *J* = 8.0 Hz), 4.19 (m, 2H), 3.71 (m, 4H), 2.97 (m, 4H). ESI-MS: 286.1 [M + H]⁺.

In the final step, either the ester compound **25** or 3-(morpholinosulfonyl) benzoic acid **27** was utilized for the preparation of series of benzohydrazide compounds. In one example starting with 1-(5-chloro-2-hydroxyphenyl) ethanone **23** (25.2 mg, 0.147 mmol) and hydrazine **28** (4.72 mg, 0.147 mmol) was refluxed in methanol (5 mL) in the presence of catalytic acetic acid for 1 h. In certain examples, the microwave heating to 120 °C for 30 min was performed. After completion of the reaction, the solvents was removed by vacuum and the resulting crude material was purified by Companion Rf with 2% CH₃OH/CH₂Cl₂ affording the title, in this case the compound **12** as a white solid (85%). ¹H NMR (400 MHz, DMSO-*d*₆): δ 13.31 (s, 1H), 11.69 (s, 1H), 8.27 (d, 1H, *J* = 7.6 Hz), 8.18 (s, 1H), 7.96 (d, 1H, *J* = 7.6 Hz), 7.83 (t, 1H, *J* = 7.6 Hz), 7.65 (d, 1H, *J* = 2.4 Hz), 7.33 (dd, 1H, *J* = 2.4 and 8.4 Hz), 6.94 (d, 1H, *J* = 9.2 Hz), 3.62 (m, 4H), 2.90 (m, 4H), 2.49 (s, 3H). ¹³C NMR (100 MHz, DMSO-*d*₆): δ 164.0, 158.4, 158.1, 135.5, 134.8, 133.7, 131.7, 131.5, 130.5, 128.6, 127.8, 122.8, 121.4, 119.8, 65.9, 46.6, 15.1. HRMS: expected 438.0885 [M + H], observed 438.0898 [M + H]. LC-MS purity of compound **12** was found to be >95%.

Similar experimental procedures were employed for the preparation of list of compounds given in Table 2, and their NMR and mass spectral data confirms the title compounds.

5.2.3. (E)-N'-(1-(2,5-Dichlorophenyl)ethylidene)-3-(morpholinosulfonyl)benzohydrazide (13). 1-(2,5-Dichlorophenyl)ethanone **29** (20 mg, 0.106 mmol) and 3-(morpholinosulfonyl) benzohydrazide **28** (30.2 mg, 0.106 mmol) was dissolved in methanol (volume: 4 mL) in the presence of acetic acid as a catalyst, and then the reaction mixture was heated via microwave irradiation to 120 °C for 30 min. Following cooling, the solvent was removed by vacuum and the resulting crude material was purified by Companion Rf with 1% CH₃OH/CH₂Cl₂, affording the title compound **13** as a solid (10 mg, 21%). ¹H NMR (400 MHz, CDCl₃): δ 8.29 (m, 1H), 8.09 (m, 1H), 7.81 (m, 1H), 7.57 (m, 1H), 7.40 (m, 1H), 7.26 (m, 2H), 3.52 (m, 4H), 2.91 (m, 4H), 2.28 (s, 3H). ESI-MS: 456.1 [M + H]⁺. LC-MS purity of compound **13** was found to be >95%.

5.2.4. (Z)-3-(2-(1-(5-Chloro-2-hydroxyphenyl)ethylidene)hydrazinecarbonyl)-N,N-dimethylbenzenesulfonamide (14). 3-(N,N-Dimethylsulfamoyl)benzoic acid (200 mg, 0.872 mmol) was refluxed in the presence of conc H₂SO₄ (5.64 mg, 0.044 mmol) in methanol at 70 °C for overnight, and after completion of the reaction, solvent was removed by vacuum and then compound was purified by Companion Rf with 1% CH₃OH/CH₂Cl₂, affording the methyl 3-(N,N-dimethylsulfamoyl)benzoate **30** as a solid (125 mg, 58.9%). ¹H NMR (400 MHz, CDCl₃): δ 8.42 (s, 1H), 8.27 (d, 1H, *J* = 8.0 Hz), 7.97 (d, 1H, *J* = 7.2 Hz), 7.65 (t, 1H, *J* = 8.0 Hz), 3.96 (s, 3H), 2.74 (s, 6H). ESI-MS: 244.0 [M + H]⁺.

Methyl 3-(N,N-dimethylsulfamoyl)-benzoate **30** (150 mg, 0.617 mmol) was added to the hydrazine (29.6 mg, 0.925 mmol) in methanol and refluxed for 8 h at 65 °C. Following cooling, reaction was monitored by TLC. After completion of the reaction, solvent was removed by vacuum and then compound was purified by Companion Rf with 1% CH₃OH/CH₂Cl₂, affording the 3-(hydrazinecarbonyl)-N,N-dimethylbenzenesulfonamide **31** as a solid (60 mg, 40%). ¹H NMR (400 MHz, CDCl₃): δ 8.11 (s, 1H), 8.01 (d, 1H, *J* = 8.4 Hz), 7.92 (d, 1H, *J* = 8.0 Hz), 7.65 (t, 1H, *J* = 8.0 Hz), 2.73 (s, 6H). ESI-MS: 244.0 [M + H]⁺.

3-(Hydrazinecarbonyl)-N,N-dimethylbenzenesulfonamide **31** (50 mg, 0.206 mmol) and 1-(5-chloro-2-hydroxyphenyl)ethanone **23** (35.1 mg, 0.206 mmol) was dissolved in methanol (volume: 4 mL)

in the presence of acetic acid as a catalyst, and then the reaction mixture was heated via microwave irradiation to 120 °C for 30 min. Reaction was monitored by TLC. After completion of the reaction, following cooling, the solvent was removed by vacuum and the resulting crude material was purified by Companion Rf with 1% CH₃OH/CH₂Cl₂, affording the title compound **14** as a solid (15 mg, 18%). ¹H NMR (400 MHz, acetone-*d*₆): δ 8.29 (m, 2H), 8.01 (d, 1H, *J* = 8.4 Hz), 7.83 (t, 1H, *J* = 8.4 Hz), 7.62 (d, 1H, *J* = 2.4 Hz), 7.32 (dd, 1H, *J* = 2.4 and 8.8 Hz), 6.96 (d, 1H, *J* = 8.8 Hz), 2.73 (s, 6H), 2.58 (s, 3H). ESI-MS: 396.0 [M + H]⁺. LC-MS purity of compound **14** was found to be >95%.

5.2.5. (Z)-N'-(1-(5-Chloro-2-hydroxyphenyl)propylidene)-3-(morpholinosulfonyl)benzohydrazide (15). 3-(Morpholinosulfonyl)benzohydrazide **28** (40 mg, 0.140 mmol) and 1-(5-chloro-2-hydroxyphenyl)propan-1-one **32** (25.9 mg, 0.140 mmol) was dissolved in methanol (volume: 4 mL) in the presence of acetic acid as a catalyst, and then the reaction mixture was heated via microwave irradiation to 120 °C for 30 min. Reaction was monitored by TLC. After completion of the reaction, following cooling, the solvent was removed by vacuum and the resulting crude material was purified by Companion Rf with 2% CH₃OH/CH₂Cl₂, affording the title compound **15** as a solid (20 mg, 31.6%). ¹H NMR (400 MHz, acetone-*d*₆): δ 8.26 (m, 2H), 8.00 (d, 1H, *J* = 7.6 Hz), 7.84 (t, 1H, *J* = 8.0 Hz), 7.64 (d, 1H, *J* = 2.4 Hz), 7.33 (m, 1H), 6.98 (d, 1H, *J* = 9.2 Hz), 3.69 (m, 4H), 3.10 (q, 2H, *J* = 7.6 Hz), 2.99 (m, 4H), 1.26 (t, 3H, *J* = 7.6 Hz). ESI-MS: 452.1 [M + H]⁺. LC-MS purity of compound **15** was found to be >95%.

5.2.6. (E)-N'-(1-(3-Chloro-2-fluorophenyl)ethylidene)-3-(morpholinosulfonyl)benzohydrazide (16). 1-(3-Chloro-2-fluorophenyl)ethanone **33** (20 mg, 0.116 mmol) and 3-(morpholinosulfonyl) benzohydrazide **28** (33.1 mg, 0.116 mmol) was dissolved in methanol (4 mL) in the presence of acetic acid as a catalyst, and then the reaction mixture was heated via microwave irradiation to 120 °C for 30 min. Following cooling, the solvent was removed by vacuum, and the resulting crude material was purified by Companion Rf with 2% CH₃OH/CH₂Cl₂, affording the title compound **16** as a white solid (22 mg, 43.2%). ¹H NMR (400 MHz, CDCl₃): δ 9.34 (s, 1H), 8.37 (m, 1H), 8.16 (m, 1H), 7.87 (d, 1H, *J* = 7.2 Hz), 7.65 (m, 1H), 7.41 (m, 1H), 7.10 (t, 1H, *J* = 8.0 Hz), 3.71 (m, 4H), 2.95 (m, 4H), 2.38 (s, 3H). ESI-MS: 440.1 [M + H]⁺. LC-MS purity of compound **16** was found to be >95%.

5.2.7. (E)-N'-(1-(2,6-Dihydroxyphenyl)ethylidene)benzohydrazide (17). 1-(2,6-Dihydroxyphenyl)ethanone (100 mg, 0.657 mmol) **34** and benzohydrazide **24** (89 mg, 0.657 mmol) was dissolved in methanol (4 mL) in the presence of acetic acid as a catalyst, and then the reaction mixture was heated via microwave irradiation to 120 °C for 30 min. Following cooling, the solvent was removed by vacuum and the resulting crude material was purified by Companion Rf with 2% CH₃OH/CH₂Cl₂, affording the title compound **17** as a white solid (100 mg, 56.3%). ¹H NMR (400 MHz, CD₃OD): δ 7.59 (m, 2H), 7.49 (m, 1H), 7.39 (m, 2H), 7.11 (t, 1H, *J* = 8.0 Hz), 6.45 (m, 2H), 2.35 (s, 3H). ESI-MS: 271.1 [M + H]⁺. LC-MS purity of compound **17** was found to be >95%.

5.2.8. (E)-N'-(1-(2-Chloropyridin-4-yl)ethylidene)-3-(morpholinosulfonyl)benzohydrazide (18). 1-(2-Chloropyridin-4-yl)ethanone **35** (20 mg, 0.129 mmol) and 3-(morpholinosulfonyl)benzohydrazide **28** (36.7 mg, 0.129 mmol) was dissolved in methanol (4 mL) in the presence of acetic acid as a catalyst, and then the reaction mixture was heated via microwave irradiation to 120 °C for 30 min. Following cooling, the solvent was removed by vacuum and the resulting crude material was purified by Companion Rf with 1% CH₃OH/CH₂Cl₂, affording the title compound **18** as a solid (32.6 mg, 60%). ¹H NMR (400 MHz, CDCl₃): δ 9.43 (m, 1H), 8.39 (m, 2H), 8.15 (d, 1H, *J* = 8.0 Hz), 7.93 (d, 1H, *J* = 7.6 Hz), 7.70 (t, 1H, *J* = 7.6 Hz), 7.52 (m, 1H), 3.73 (m, 4H), 3.02 (m, 4H), 2.35 (s, 3H). ESI-MS: 423.1 [M + H]⁺. LC-MS purity of compound **18** was found to be >95%.

5.2.9. (Z)-3-Bromo-4-chloro-N'-(1-(5-chloro-2-hydroxyphenyl)ethylidene)benzohydrazide (19). 3-Bromo-4-chlorobenzoic acid (200 mg, 0.849 mmol) was refluxed in the presence of conc H₂SO₄ (5.49 mg, 0.042 mmol) in methanol at 70 °C for overnight, and after

completion of the reaction, solvent was removed by vacuum and then compound was purified by Companion Rf with 1% CH₃OH/CH₂Cl₂, affording the methyl 3-bromo-4-chlorobenzoate **36** as a white solid (130 mg, 61.3%). ¹H NMR (400 MHz, CDCl₃): δ 8.29 (d, 1H, J = 2.0 Hz), 7.91 (dd, 1H, J = 2.0 and 8.4 Hz), 7.52 (d, 1H, J = 8.4 Hz), 3.92 (s, 3H). ESI-MS: 250.9 [M + H]⁺.

Compound **36** (120 mg, 0.481 mmol) was added to the hydrazine (23.12 mg, 0.721 mmol) in methanol at 70 °C for overnight. Reaction was monitored by TLC. After completion of the reaction, solvent was removed by vacuum and then compound was purified by Companion Rf with 2% CH₃OH/CH₂Cl₂, affording the intermediate 3-bromo-4-chlorobenzohydrazide **37** as a solid (30 mg, 25%). ¹H NMR (400 MHz, CDCl₃): δ 8.02 (d, 1H, J = 1.6 Hz), 7.60 (dd, 1H, J = 2.0 and 8.0 Hz), 7.52 (d, 1H, J = 8.0 Hz). ESI-MS: 250.9 [M + H]⁺.

The compound **37** (30 mg, 0.120 mmol) and 1-(5-chloro-2-hydroxyphenyl)ethanone **23** (20.51 mg, 0.120 mmol) was dissolved in methanol (volume: 4 mL) in the presence of acetic acid as a catalyst, and then the reaction mixture was heated via microwave irradiation to 120 °C for 30 min. Reaction was monitored by TLC. After completion of the reaction, following cooling, the solvent was removed by vacuum and the resulting crude material was purified by Companion Rf with 2% CH₃OH/CH₂Cl₂, affording the title compound **19** as a solid (15 mg, 31%). ¹H NMR (400 MHz, acetone-*d*₆): δ 8.30 (s, 1H), 7.98 (d, 1H, J = 8.4 Hz), 7.73 (d, 1H, J = 8.4 Hz), 7.61 (d, 1H, J = 2.4 Hz), 7.29 (dd, 1H, J = 2.4 and 8.4 Hz), 6.93 (d, 1H, J = 8.8 Hz), 2.55 (s, 3H). ESI-MS: 402.9 [M + H]⁺. LC-MS purity of compound **19** was found to be >95%.

5.2.10. (Z)-5-Bromo-6-chloro-N'-(1-(5-chloro-2-hydroxyphenyl)ethylidene)nicotinohydrazide (20). Methyl 5-bromo-6-chloronicotinate (100 mg, 0.399 mmol) was added to the hydrazine (19.19 mg, 0.599 mmol) in methanol at 70 °C for overnight. Reaction was monitored by TLC. After completion of the reaction, solvent was removed by vacuum and then compound was purified by Companion Rf with 1% CH₃OH/CH₂Cl₂, affording the 5-bromo-6-chloronicotinohydrazide **38** as a solid (20 mg, 20%). ¹H NMR (400 MHz, CD₃OD): δ 8.33 (d, 1H, J = 2.4 Hz), 8.01 (d, 1H, J = 2.4 Hz).

5-Bromo-6-chloronicotinohydrazide **38** (15 mg, 0.060 mmol) and 1-(5-chloro-2-hydroxyphenyl)ethanone **23** (10.22 mg, 0.060 mmol) was dissolved in methanol (volume: 4 mL) in the presence of acetic acid as a catalyst, and then the reaction mixture was heated via microwave irradiation to 120 °C for 30 min. Reaction was monitored by TLC. After completion of the reaction, following cooling, the solvent was removed by vacuum and the resulting crude material was purified by Companion Rf with 2% CH₃OH/CH₂Cl₂, affording the title compound **20** as a solid (8 mg, 33%). ¹H NMR (400 MHz, DMSO-*d*₆): δ 8.39 (d, 1H, J = 2.4 Hz), 8.28 (s, 1H), 7.63 (d, 1H, J = 2.4 Hz), 7.32 (dd, 1H, J = 2.4 and 8.8 Hz), 7.06 (d, 1H, J = 6.8 Hz), 6.92 (d, 1H, J = 9.2 Hz), 6.81 (d, 1H, J = 6.8 Hz), 2.47 (s, 3H). ESI-MS: 404.0 [M + H]⁺. LC-MS purity of compound **20** was found to be >95%.

5.2.11. (Z)-5-Chloro-N'-(1-(5-chloro-2-hydroxyphenyl)ethylidene)nicotinohydrazide (21). 5-Chloronicotinic acid (200 mg, 1.269 mmol) was refluxed in the presence of conv H₂SO₄ (8.20 mg, 0.063 mmol) in methanol at 70 °C for overnight, and after completion of the reaction, solvent was removed by vacuum and then compound was purified by Companion Rf with 1% CH₃OH/CH₂Cl₂, affording the methyl 5-chloronicotinate **39** as a solid (120 mg, 55%). ¹H NMR (400 MHz, CDCl₃): δ 9.07 (d, 1H, J = 1.6 Hz), 8.72 (d, 1H, J = 2.0 Hz), 8.26 (m, 1H), 3.95 (s, 1H).

Hydrazine (17.93 mg, 0.560 mmol) was added to the methyl 5-chloronicotinate **39** (80 mg, 0.466 mmol) in methanol at 70 °C overnight. Reaction was monitored by TLC. After completion of the reaction, solvent was removed by vacuum and then compound was purified by Companion Rf with 1% CH₃OH/CH₂Cl₂, affording the 5-chloronicotinohydrazide **40** as a solid (40 mg, 50%). ¹H NMR (400 MHz, CD₃OD): δ 8.85 (d, 1H, J = 2.0 Hz), 8.70 (d, 1H, J = 2.4 Hz), 8.22 (t, 1H, J = 2.0 Hz). ESI-MS: 172.0 [M + H]⁺.

5-chloronicotinohydrazide **40** (30 mg, 0.175 mmol) and 1-(5-chloro-2-hydroxyphenyl)ethanone **23** (29.8 mg, 0.175 mmol) was dissolved in methanol (volume: 4 mL) in the presence of acetic acid as

a catalyst, and then the reaction mixture was heated via microwave irradiation to 120 °C for 30 min. Reaction was monitored by TLC. After completion of the reaction, following cooling, the solvent was removed by vacuum and the resulting crude material was purified by Companion Rf with 2% CH₃OH/CH₂Cl₂, affording the title compound **21** as a solid (20 mg, 35.3%). ¹H NMR (400 MHz, acetone-*d*₆): δ 9.06 (s, 1H), 8.77 (s, 1H), 8.37 (s, 1H), 7.62 (d, 1H, J = 2.8 Hz), 7.31 (dd, 1H, J = 2.0 and 8.4 Hz), 6.95 (d, 1H, J = 8.8 Hz), 2.58 (s, 3H). ESI-MS: 324.0 [M + H]⁺. LC-MS purity of compound **21** was found to be >95%.

5.2.12. (Z)-3-(Morpholinofulfonyl)-N'-(1-(pyridin-3-yl)ethylidene)benzohydrazide (22). 3-(Morpholino sulfonyl)benzohydrazide **28** (40 mg, 0.140 mmol) and 1-(pyridin-3-yl)ethanone **41** (16.98 mg, 0.140 mmol) was dissolved in methanol (4 mL) in the presence of acetic acid as a catalyst, and then the reaction mixture was heated via microwave irradiation to 120 °C for 30 min. Reaction was monitored by TLC. After completion of the reaction, following cooling, the solvent was removed by vacuum and the resulting crude material was purified by Companion Rf with 2% CH₃OH/CH₂Cl₂, affording the title compound **22** as a solid (15 mg, 27.5%). ¹H NMR (400 MHz, CDCl₃): δ 9.53 (bs, 1H), 8.87 (s, 1H), 8.59 (m, 1H), 8.39 (m, 1H), 8.17 (m, 1H), 7.98 (m, 1H), 7.89 (d, 1H, J = 8.0 Hz), 7.67 (t, 1H, J = 8.0 Hz), 7.32 (m, 1H), 3.70 (m, 4H), 3.00 (m, 4H), 2.39 (s, 3H). ESI-MS: 389.0 [M + H]⁺. LC-MS purity of compound **22** was found to be >95%.

5.3. Biochemical Assays. **5.3.1. LSD1 Screening Assay.** The LSD1 screening biochemical assay kit was purchased from Cayman Chemical (Ann Arbor, MI). Test compounds were diluted to 20× the desired test concentration in 100% DMSO and 2.5 μL of the diluted drug sample was added to a black 384-well plate. The LSD1 enzyme stock was diluted 17-fold with assay buffer, and 40 μL of the diluted LSD1 enzyme was added to the appropriate wells. Substrate, consisting of horseradish peroxidase, dimethyl K4 peptide corresponding to the first 21 amino acids of the N-terminal tail of histone H3, and 10-acetyl-3,7-dihydroxyphenoxazine was then added to wells. Resorufin was analyzed on an Envision plate reader with an excitation wavelength of 530 nm and an emission wavelength of 595 nm.

5.3.2. Off-Target Assays. Monoamine oxidase A and B enzymes were purchased from Sigma (catalogue nos. m7316, and m7441, respectively). Biochemical kits were purchased as follows: MAO-Glo – Promega Corp. (Fitchburg, WI); D-lactate dehydrogenase, Cayman Chemical (Ann Arbor, MI); glucose oxidase, Life Technologies Corp. (Grand Island, NY). Inhibition assay were carried out according to the manufacturer's suggested protocol. CYP and hERG evaluation utilized the SelectScreen Biochemical P450 Profiling and hERG Screening Services provided by Invitrogen Corp. (Madison, WI).

5.3.3. Reversibility and Michaelis–Menten Analysis. Biochemical characterization of reversibility and K_i was performed using the biochemical screen from Cayman Chemical with purified recombinant full-length his₆-LSD1 substituted for the commercially provided protein mix. Reversibility was determined using jump dilution. LSD1 was incubated at 10× IC₅₀ of compound **12** or tranylcypromine for 1 h then diluted into the reaction 100-fold. The reaction buffer was either compound-free or contained 10× the IC₅₀. Compound **13** was used as a negative control. The K_i of compound **12** was determined using a Michaelis–Menten kinetic analysis across multiple concentrations of compound **12**. The data was plotted in GraphPad. K_i was determined using the following equation: K_i = [Inhibitor]/((v_{max}/v_{apparent-max}) – 1)

5.4. In Vitro Assays. **5.4.1. ATPite Cell Viability A.** ATPite was purchased from PerkinElmer (Waltham, MA). Cancer cell lines were obtained from ATCC. Cells were cultured according to the procedures provided. Cells were seeded in 96-well plates and then treated with different concentrations of inhibitor (0.1% final DMSO concentration). After 96 h of incubation, ATPite was added directly to the culture well. Luminescence was read 5 min later on an Envision plate reader.

5.4.2. Global H3K4 and H3K9 Methylation Analysis. VCaP cells were maintained in RPMI media containing 10% FBS and no phenol red. The day before the experiment was started, we plated 500000 cells per well of a 12-well plate. The following day, the culture medium was

replaced with fresh RPMI containing 10% FBS and compound 12. Individual compound 12 solutions were prepared using DMSO; the final concentration of the solvent in the culture medium was 1%. The cells then were incubated for 24 h at 37 °C. Individual wells were washed with PBS, and lysates were obtained as described previously.⁴³ We subjected 50 µg of total protein to electrophoresis and immunoblot analyses using anti-H3K9Me2 and anti-β-Actin antibodies, as described.³⁷ The extent of immunoreactivity then was assessed by chemiluminescence, following incubation with appropriate, horseradish peroxidase-labeled, secondary antibodies.

■ ASSOCIATED CONTENT

Supporting Information

Detailed virtual screening methods; purchased hits, analytical data; docking scores of compounds 1–10, commercially available LSD1 hits (111) from the list of 121 compounds selected, Tanimoto similarity coefficients comparing compound 12 and known LSD1 inhibitors from Chart 1; off-target inhibition; comparison of different model fits for enzyme kinetics; binding site model and definition of active site of LSD1 structure; flow diagram for the virtual ligand screening (VLS) using ICM-VLS; Schrodinger workflow GOLD programs; complete reaction schemes for compounds 11–22; LC-MS data for compound 12. This material is available free of charge via the Internet at <http://pubs.acs.org>.

■ AUTHOR INFORMATION

Corresponding Author

*Phone: +1-(801)587-5559. Fax: +1-(801)585-0101. E-mail: sunil.sharma@hci.utah.edu. Address: Huntsman Cancer Institute, Room 3360, 2000 Circle of Hope, Salt Lake City, Utah 84112, United States.

Author Contributions

[†]These authors contributed equally.

Notes

The authors declare the following competing financial interest(s): Drs. Sunil Sharma, David Bearss, Steve Warner, and Hariprasad Vankayalapati have equity interest in Salaris Pharmaceuticals.

■ ACKNOWLEDGMENTS

We gratefully acknowledge Dr. Yang Shi for the generous gift of the LSD1 expression construct, Dr. Diana Stafforini for her assistance with VCaP cell culture and blots, and Jediah Doane, Simon Currie, Dr. Niraja Bhachech, and Dr. Barbara Graves for their protein purification guidance. Research reported in this article utilized the Experimental Therapeutics program and was supported by the Huntsman Cancer Foundation and the National Cancer Institute of the National Institutes of Health under award number P30CA042014. The content is solely the responsibility of the authors and does not necessarily represent the official views of the NIH.

■ ABBREVIATIONS USED

BHC80, BRAF35-HDAC complex protein 80; Co-REST, REST corepressor 1; CYP, cytochrome P450; DSF, differential scanning fluorimetry; FAD, flavin adenine dinucleotide; Gfi-1, growth factor independent 1; H3, histone H3; H3K4, histone H3 at lysine 4; H3K4me1, monomethylation of histone H3 at lysine 4; H3K4me2, dimethylation of histone H3 at lysine 4; H3K4me3, trimethylation of histone H3 at lysine 4; H3K9, histone H3 at lysine 9; H3K9me1, monomethylation of histone H3 at lysine 9; H3K9me2, dimethylation of histone H3 at

lysine 9; HDAC, histone deacetylase; hERG, human ether-à-go-go; HTVS, high-throughput virtual screen; K4, lysine 4; K9, lysine 9; LSD1, lysine-specific demethylase; MAO, monoamine oxidase; NuRD, nucleosome remodeling and histone deacetylase; SAR, structure–activity relationship; SNAI1, snail homologue 1 (drosophila); TCP, tranlycypromine; VS, virtual screen

■ REFERENCES

- (1) Tsai, H.-C.; Baylin, S. B. Cancer epigenetics: linking basic biology to clinical medicine. *Cell Res.* **2011**, *21*, 502–517.
- (2) Füllgrabe, J.; Kavanagh, E.; Joseph, B. Histone onco-modifications. *Oncogene* **2011**, *30*, 3391–3403.
- (3) Shi, Y.; Lan, F.; Matson, C.; Mulligan, P.; Whetstone, J. R.; Cole, P. A.; Casero, R. A.; Shi, Y. Histone Demethylation Mediated by the Nuclear Amine Oxidase Homolog LSD1. *Cell* **2004**, *119*, 941–953.
- (4) Metzger, E.; Wissmann, M.; Yin, N.; Müller, J. M.; Schneider, R.; Peters, A. H. F. M.; Günther, T.; Buettner, R.; Schüle, R. LSD1 demethylates repressive histone marks to promote androgen-receptor-dependent transcription. *Nature* **2005**, *437*, 436–439.
- (5) Jenuwein, T.; Allis, C. D. Translating the Histone Code. *Science* **2001**, *293*, 1074–1080.
- (6) Lachner, M.; O'Sullivan, R. J.; Jenuwein, T. An epigenetic road map for histone lysine methylation. *J. Cell Sci.* **2003**, *116*, 2117–2124.
- (7) Forneris, F.; Binda, C.; Vanoni, M. A.; Mattevi, A.; Battaglioli, E. Histone demethylation catalysed by LSD1 is a flavin-dependent oxidative process. *FEBS Lett.* **2005**, *579*, 2203–2207.
- (8) Forneris, F.; Binda, C.; Battaglioli, E.; Mattevi, A. LSD1: oxidative chemistry for multifaceted functions in chromatin regulation. *Trends Biochem. Sci.* **2008**, *33*, 181–189.
- (9) Yang, M.; Gocke, C. B.; Luo, X.; Borek, D.; Tomchick, D. R.; Machius, M.; Otwinowski, Z.; Yu, H. Structural Basis for CoREST-Dependent Demethylation of Nucleosomes by the Human LSD1 Histone Demethylase. *Mol. Cell* **2006**, *23*, 377–387.
- (10) Shi, Y.-J.; Matson, C.; Lan, F.; Iwase, S.; Baba, T.; Shi, Y. Regulation of LSD1 Histone Demethylase Activity by Its Associated Factors. *Mol. Cell* **2005**, *19*, 857–864.
- (11) Lan, F.; Collins, R. E.; De Cegli, R.; Alpatov, R.; Horton, J. R.; Shi, X.; Gozani, O.; Cheng, X.; Shi, Y. Recognition of unmethylated histone H3 lysine 4 links BHC80 to LSD1-mediated gene repression. *Nature* **2007**, *448*, 718–722.
- (12) Lee, M. G.; Wynder, C.; Cooch, N.; Shiekhatar, R. An essential role for CoREST in nucleosomal histone 3 lysine 4 demethylation. *Nature* **2005**, *437*, 432–435.
- (13) Forneris, F.; Binda, C.; Dall'Aglio, A.; Fraaije, M. W.; Battaglioli, E.; Mattevi, A. A Highly Specific Mechanism of Histone H3-K4 Recognition by Histone Demethylase LSD1. *J. Biol. Chem.* **2006**, *281*, 35289–35295.
- (14) Forneris, F.; Binda, C.; Vanoni, M. A.; Battaglioli, E.; Mattevi, A. Human Histone Demethylase LSD1 Reads the Histone Code. *J. Biol. Chem.* **2005**, *280*, 41360–41365.
- (15) Garcia-Bassets, I.; Kwon, Y.-S.; Telese, F.; Prefontaine, G. G.; Hutt, K. R.; Cheng, C. S.; Ju, B.-G.; Ohgi, K. A.; Wang, J.; Escoubet-Lozach, L.; Rose, D. W.; Glass, C. K.; Fu, X.-D.; Rosenfeld, M. G. Histone Methylation-Dependent Mechanisms Impose Ligand Dependency for Gene Activation by Nuclear Receptors. *Cell* **2007**, *128*, 505–518.
- (16) Lim, S.; Janzer, A.; Becker, A.; Zimmer, A.; Schüle, R.; Buettner, R.; Kirfel, J. Lysine-specific demethylase 1 (LSD1) is highly expressed in ER-negative breast cancers and a biomarker predicting aggressive biology. *Carcinogenesis* **2010**, *31*, 512–520.
- (17) Schulte, J. H.; Lim, S.; Schramm, A.; Friedrichs, N.; Koster, J.; Versteeg, R.; Ora, I.; Pajtlar, K.; Klein-Hitpass, L.; Kuhfittig-Kulle, S.; Metzger, E.; Schüle, R.; Eggert, A.; Buettner, R.; Kirfel, J. Lysine-Specific Demethylase 1 Is Strongly Expressed in Poorly Differentiated Neuroblastoma: Implications for Therapy. *Cancer Res.* **2009**, *69*, 2065–2071.

- (18) Hayami, S.; Kelly, J. D.; Cho, H.-S.; Yoshimatsu, M.; Unoki, M.; Tsunoda, T.; Field, H. I.; Neal, D. E.; Yamaue, H.; Ponder, B. A. J.; Nakamura, Y.; Hamamoto, R. Overexpression of LSD1 contributes to human carcinogenesis through chromatin regulation in various cancers. *Int. J. Cancer* **2011**, *128*, 574–586.
- (19) Kahl, P.; Gullotti, L.; Heukamp, L. C.; Wolf, S.; Friedrichs, N.; Vorreuther, R.; Solleder, G.; Bastian, P. J.; Ellinger, J.; Metzger, E.; Schüle, R.; Buettner, R. Androgen Receptor Coactivators Lysine-Specific Histone Demethylase 1 and Four and a Half LIM Domain Protein 2 Predict Risk of Prostate Cancer Recurrence. *Cancer Res.* **2006**, *66*, 11341–11347.
- (20) Zhao, Z.-K.; Yu, H.-F.; Wang, D.-R.; Dong, P.; Chen, L.; Wu, W.-G.; Ding, W.-J.; Liu, Y.-B. Overexpression of lysine specific demethylase 1 predicts worse prognosis in primary hepatocellular carcinoma patients. *World J. Gastroenterol.* **2012**, *18*, 6651–6656.
- (21) Huang, Y.; Stewart, T. M.; Wu, Y.; Baylin, S. B.; Marton, L. J.; Perkins, B.; Jones, R. J.; Woster, P. M.; Casero, R. A. Novel oligoamine analogues inhibit lysine-specific demethylase 1 (LSD1) and induce re-expression of epigenetically silenced genes. *Clin. Cancer Res.* **2009**, *15*, 7217–7228.
- (22) Liang, Y.; Quenelle, D.; Vogel, J. L.; Mascaro, C.; Ortega, A.; Kristie, T. M. A Novel Selective LSD1/KDM1A Inhibitor Epigenetically Blocks Herpes Simplex Virus Lytic Replication and Reactivation from Latency. *mBio* **2013**, *4*, 00558-12.
- (23) Mimasu, S.; Umezawa, N.; Sato, S.; Higuchi, T.; Umehara, T.; Yokoyama, S. Structurally Designed *trans*-2-Phenylcyclopropylamine Derivatives Potently Inhibit Histone Demethylase LSD1/KDM1. *Biochemistry* **2010**, *49*, 6494–6503.
- (24) Binda, C.; Valente, S.; Romanenghi, M.; Pilotto, S.; Cirilli, R.; Karyinos, A.; Ciossani, G.; Botrugno, O. A.; Forneris, F.; Tardugno, M.; Edmondson, D. E.; Minucci, S.; Mattevi, A.; Mai, A. Biochemical, Structural, and Biological Evaluation of Tranylcypromine Derivatives as Inhibitors of Histone Demethylases LSD1 and LSD2. *J. Am. Chem. Soc.* **2010**, *132*, 6827–6833.
- (25) Ueda, R.; Suzuki, T.; Mino, K.; Tsumoto, H.; Nakagawa, H.; Hasegawa, M.; Sasaki, R.; Mizukami, T.; Miyata, N. Identification of Cell-Active Lysine Specific Demethylase 1-Selective Inhibitors. *J. Am. Chem. Soc.* **2009**, *131*, 17536–17537.
- (26) Ortega, A. M.; Castro-Palomino, L. J.; Fyfe, M. C. T. Lysine specific demethylase inhibitors and their use. *PCT Int. Appl. WO* 2011035941 A12011.
- (27) Guibourt, N.; Ortega, A. M.; Castro-Palomino, L. J. Phenylcyclopropylamine derivatives and their medical use. *PCT Int. Appl. , WO* 2010084160 A1, 2010.
- (28) Guibourt, N.; Ortega, A. M.; Castro-Palomino, L. J. Oxidase inhibitors and their use. *PCT Int. Appl. WO* 2010043721 A1, 2010.
- (29) McCafferty, D. G.; Pollock, J. Arylcyclopropylamines and methods of use. *PCT Int. Appl. US* 20100324147 A1, 2010.
- (30) Culhane, J. C.; Szewczuk, L. M.; Liu, X.; Da, G.; Marmorstein, R.; Cole, P. A. A Mechanism-Based Inactivator for Histone Demethylase LSD1. *J. Am. Chem. Soc.* **2006**, *128*, 4536–4537.
- (31) Culhane, J. C.; Wang, D.; Yen, P. M.; Cole, P. A. Comparative Analysis of Small Molecules and Histone Substrate Analogs as LSD1 Lysine Demethylase Inhibitors. *J. Am. Chem. Soc.* **2010**, *132*, 3164–3176.
- (32) Sharma, S. K.; Wu, Y.; Steinbergs, N.; Crowley, M. L.; Hanson, A. S.; Casero, R. A.; Woster, P. M. (Bis)urea and (Bis)thiourea Inhibitors of Lysine-Specific Demethylase 1 as Epigenetic Modulators. *J. Med. Chem.* **2010**, *53*, 5197–5212.
- (33) Huang, Y.; Greene, E.; Murray Stewart, T.; Goodwin, A. C.; Baylin, S. B.; Woster, P. M.; Casero, R. A. Inhibition of lysine-specific demethylase 1 by polyamine analogues results in reexpression of aberrantly silenced genes. *Proc. Natl. Acad. Sci. U. S. A.* **2007**, *104*, 8023–8028.
- (34) Wang, J.; Lu, F.; Ren, Q.; Sun, H.; Xu, Z.; Lan, R.; Liu, Y.; Ward, D.; Quan, J.; Ye, T.; Zhang, Hui. Novel Histone Demethylase LSD1 Inhibitors Selectively Target Cancer Cells with Pluripotent Stem Cell Properties. *Cancer Res.* **2011**, *71*, 7238–7249.
- (35) Willmann, D.; Lim, S.; Wetzel, S.; Metzger, E.; Jandausch, A.; Wilk, W.; Jung, M.; Forne, I.; Imhof, A.; Janzer, A.; Kirfel, J.; Waldmann, H.; Schüle, R.; Buettner, R. Impairment of prostate cancer cell growth by a selective and reversible lysine-specific demethylase 1 inhibitor. *Int. J. Cancer* **2012**, *131*, 2704–2709.
- (36) Vankayalapati, H.; Sorna, V.; Warner, S. L.; Bearss, D. J.; Sharma, S.; Stephens, B. Substituted (*E*)-*N'*-(1-phenylethylidene) benzohydrazide analogs as histone demethylase inhibitors. *PCT Int. Appl. WO* 2013025805 A1, 2013.
- (37) Mimasu, S.; Sengoku, T.; Fukuzawa, S.; Umehara, T.; Yokoyama, S. Crystal structure of histone demethylase LSD1 and tranylcypromine at 2.25 Å. *Biochem. Biophys. Res. Commun.* **2008**, *366*, 15–22.
- (38) Gooden, D. M.; Schmidt, D. M. Z.; Pollock, J. A.; Kabadi, A. M.; McCafferty, D. G. Facile synthesis of substituted *trans*-2-arylcyclopropylamine inhibitors of the human histone demethylase LSD1 and monoamine oxidases A and B. *Bioorg. Med. Chem. Lett.* **2008**, *18*, 3047–3051.
- (39) Lin, Y.; Wu, Y.; Li, J.; Dong, C.; Ye, X.; Chi, Y.-I.; Evers, B. M.; Zhou, B. P. The SNAG domain of Snail1 functions as a molecular hook for recruiting lysine-specific demethylase 1. *EMBO J.* **2010**, *29*, 1803–1816.
- (40) Laurent, B.; Randrianarison-Huetz, V.; Frisan, E.; Andrieu-Soler, C.; Soler, E.; Fontenay, M.; Dusanter-Fourt, I.; Duménil, D. A short Gfi-1B isoform controls erythroid differentiation by recruiting the LSD1–CoREST complex through the dimethylation of its SNAG domain. *J. Cell Sci.* **2012**, *125*, 993–1002.
- (41) Saleque, S.; Kim, J.; Rooke, H. M.; Orkin, S. H. Epigenetic Regulation of Hematopoietic Differentiation by Gfi-1 and Gfi-1b Is Mediated by the Cofactors CoREST and LSD1. *Mol. Cell* **2007**, *27*, 562–572.
- (42) Friesner, R. A.; Banks, J. L.; Murphy, R. B.; Halgren, T. A.; Klicic, J. J.; Mainz, D. T.; Repasky, M. P.; Knoll, E. H.; Shelley, M.; Perry, J. K.; Shaw, D. E.; Francis, P.; Shenkin, P. S. Glide: A new approach for rapid, accurate docking and scoring. 1. Method and assessment of docking accuracy. *J. Med. Chem.* **2004**, *47*, 1739–1749.
- (43) Xu, C.; Reichert, E. C.; Nakano, T.; Lohse, M.; Gardner, A. A.; Revelo, M. P.; Topham, M. K.; Stafforini, D. M. Deficiency of Phospholipase A2 Group 7 Decreases Intestinal Polyposis and Colon Tumorigenesis in ApcMin/+ Mice. *Cancer Res.* **2013**, *73*, 2806–2816.

2.8 Supplementary Materials

2.8.1 Supplementary Methods

2.8.1.1 Detailed Virtual Screening Methods

2.8.1.1.1 Preparation of the Binding Site Model

There were several X-ray crystal complex structures of LSD1 (PDB ID: 2Y48, 3BAT, 3BAU, 2XAF, 2XAG, 2XAH, 2XAJ, 2XAQ and 2XAS) at the beginning of our work, we used the LSD1 complex model with an X-ray crystal structure (PDB code 2Z5U) and protein coordinates used for fragment-based and structure-based virtual screening. Water molecules were then removed and the missing bond order and geometries were edited. Hydrogen atoms were added and the combined complex structure was submitted for protein preparation and energy minimization calculation using ICM and Schrodinger. The fully refined structure with bound ligand molecule was further submitted for grids calculation to define the active site as the collection of amino acids enclosed within a 12 Å radius sphere centered on the bound ligand (Figure 2.1). The target LSD1 was optimized using Monte Carlo simulation and energy optimizations.

2.8.1.1.2 Preprocessing of three-dimensional ligand databases

The external source database in the form of sdf format was processed using the ligand preparation tools. The final coordinates were stored in multi-sdf files. Custom filters included Lipinski's rule-of-five (Ro5) and manual filtering to remove very large molecules, dimers, polymers, molecules containing unusual heteroatoms, and highly reactive functional groups. Each of the databases were combined together with a final library of ~2 million molecules commercially available from 26 vendors were considered

for virtual screening using Glide SP/XP, ICM, and GOLD.

2.8.1.1.3 Virtual Screening Method

A flow scheme indicating the steps of the virtual screening (VS) process is shown in Figure 2.2. The database of 13 million library compounds was curated using Ligprep, the filters from Section 2.8.1.1.2, and Glide HTVS methods to attain the set of ~ 2 million compounds screened against the prepared target. Grid potentials were rapidly generated which accounted for shape of the binding pocket, hydrophobicity, electrostatic potentials, and hydrogen-bonding profile. The compounds were screened using our own workflow (Figure 2.2) for LSD1 binding properties using a rigid target and flexible ligands in the internal coordinate's space. The compounds experimentally confirmed as LSD1 inhibitors were used for regular docking into LSD1. Docking calculations of the LSD1 inhibitors were performed using the ICM and Glide docking module with default setup and rescoring with GOLD. The structures of the active compounds were energy minimized in the same environment and saved in PDB format. These energy-minimized inhibitors were then reposed into ICM and converted into ICM object, and MMFF charges were assigned for each of the ligand. Docking took an average of 3-4 min/molecule on a four AMD 64-bit processors RedHat linux server with 4 GB of RAM. The speed for each compound was dependent on the number of torsional degrees of freedom.

2.8.1.1.4 Postprocessing and Compound Selection Criteria

Compounds having desired scores, hydrogen bond formation and hydrophobic interactions were estimated by interatomic distances for further analysis. The conformational stability of each candidate was also estimated by force field energy difference between the complexes conformation and freely minimized conformation, and the top-scoring candidates from this category were selected for further analysis. Compounds in each of the three categories were visually inspected to eliminate candidates without ideal hydrogen bond geometry, hydrophobic molecular surfaces, or torsion angles. The resulting 121 focused screening structures were further analyzed using molecular property filters in QikProp, with calculated log S, permeability (Caco2 and MDCK) and Lipinski like criteria.

2.8.2 Analytical Data for Purchased Hits

The commercially available hit compounds given in **Table 1 (1-10)** were purchased from ChemBridge, <http://www.hit2lead.com>, and Enamine, <http://www.enamine.net>. Their characterizations were confirmed using ^1H NMR and Mass Spec and their purity was determined by HPLC.

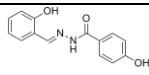
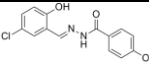
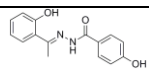
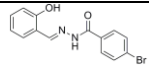
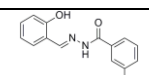
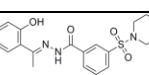
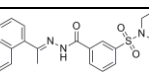
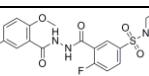
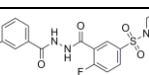
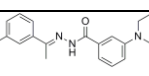
- (E)-4-hydroxy-N'-(2-hydroxybenzylidene)benzohydrazide (1): ^1H NMR (400 MHz, DMSO- d_6): δ 11.84 (s, 1H), 11.39 (s, 1H), 10.11 (s, 1H), 8.54 (s, 1H), 7.87 (m, 2H), 7.49 (d, 1H, J = 8.4 Hz), 7.28 (t, 1H, J = 8.4 Hz), 6.91 (m, 4H). ESI-MS: 256.2 $[\text{M}+\text{H}]^+$.
- (E)-N'-(5-chloro-2-hydroxybenzylidene)-4-hydroxybenzohydrazide (2): ^1H NMR (400 MHz, DMSO- d_6): δ 11.89 (s, 1H), 11.32 (bs, 1H), 10.04 (s, 1H), 8.57 (s,

- 1H), 7.82 (m, 2H), 7.61 (d, 1H, J = 2.4 Hz), 7.29 (dd, 1H, J = 2.4 & 8.8 Hz), 6.95 (d, 1H, J = 8.4 Hz), 6.88 (m, 2H). ESI-MS: 290.7 [M+H]⁺.
- (E)-4-hydroxy-N'-(1-(2-hydroxyphenyl)ethylidene)benzohydrazide (3): ¹H NMR (400 MHz, DMSO-d₆): δ 10.94 (s, 1H), 10.03 (bs, 1H), 7.84 (m, 2H), 7.62 (dd, 1H, J = 1.6 & 8.0 Hz), 7.29 (t, 1H, J = 8.4 Hz), 6.90 (m, 4H), 2.47 (s, 3H). ESI-MS: 270.28 [M+H]⁺.
 - (E)-4-bromo-N'-(2-hydroxybenzylidene)benzohydrazide (4): ¹H NMR (400 MHz, DMSO-d₆): δ 12.01 (s, 1H), 11.15 (s, 1H), 8.62 (s, 1H), 7.88 (m, 2H), 7.75 (m, 2H), 7.53 (d, 1H, J = 8.8 Hz), 7.31 (t, 1H, J = 8.8 Hz), 6.93 (m, 2H). ESI-MS: 319.16 [M+H]⁺.
 - (E)-3-chloro-N'-(2-hydroxybenzylidene)benzohydrazide (5): ¹H NMR (400 MHz, DMSO-d₆): δ 12.09 (s, 1H), 11.12 (s, 1H), 8.64 (s, 1H), 7.98 (s, 1H), 7.90 (m, 1H), 7.67 (m, 1H), 7.57 (m, 2H), 7.31 (t, 1H, J = 7.6 Hz), 6.93 (m, 2H). ESI-MS: 274.70 [M+H]⁺.
 - (E)-N'-(1-(2-hydroxyphenyl)ethylidene)-3-(morpholinosulfonyl)benzohydrazide (6): ESI-MS: 403.4 [M+H]⁺, purity by HPLC 97.25%.
 - (E)-3-(morpholinosulfonyl)-N'-(1-(naphthalen-1-yl)ethylidene)benzohydrazide (7): ESI-MS: 437.5 [M+H]⁺.
 - 5-chloro-N'-(2-fluoro-5-(morpholinosulfonyl)benzoyl)-2-methoxybenzohydrazide (8): ¹H NMR (400 MHz, DMSO-d₆): δ 7.90 (m, 3H), 7.51 (m, 2H), 7.22 (m, 1H), 4.02 (s, 3H), 3.71 (m, 4H), 2.97 (m, 4H). ESI-MS: 471.8 [M+H]⁺.
 - N'-(3-chlorobenzoyl)-2-fluoro-5-(morpholinosulfonyl)benzohydrazide (9): ¹H NMR (400 MHz, DMSO-d₆): δ 8.01 (m, 2H), 7.92 (m, 2H), 7.53 (m, 3H), 3.69

(m, 4H), 2.96 (m, 4H). ESI-MS: 441.8 [M+H]⁺.

- (E)-N,N-diethyl-3-(2-(1-(p-tolyl)ethylidene)hydrazinecarbonyl)benzenesulfonamide (10): ESI-MS: 387.5 [M+H]⁺, purity by HPLC 94%.

Supplementary Table S2.1. Docking scores of compounds 1-10

S. No	Structure	ICM score	Glide score	Gold fitness score
1		-42.25	-8.14	56.26
2		-42.25	-7.92	58.21
3		-21.91	-7.87	51.29
4		-37.77	-8.64	57.69
5		-36.3	-8.84	47.98
6		-24	-6.26	43.26
7		-20.97	-6.14	46.64
8		-18.39	-6.63	49.93
9		-8.16	-7.21	41.86
10		-8.5	-6.81	52.19

Supplementary Table S2.2. Commercially available LSD1 hits (111) from the list of 121 compounds selected.

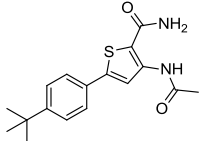
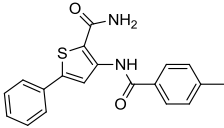
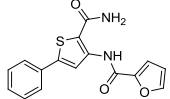
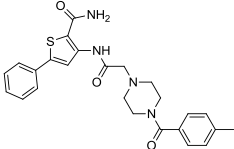
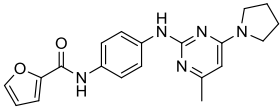
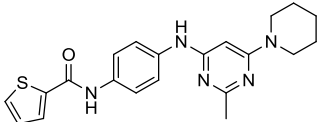
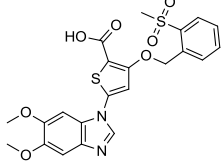
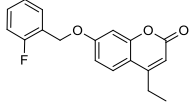
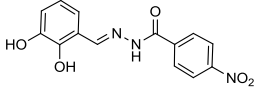
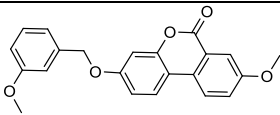
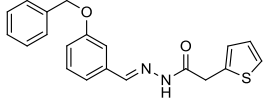
S. No	Structure	IC50 (μM) LSD1	ICM Score (kcal/mol)	GLIDE Score (kcal/mol)	GOLD Fitness Score (kcal/mol)
11		>100	-16.89	-4.87	27.21
12		>100	-16.34	-4.89	29.21
13		>100	-16.21	-4.76	24.21
14		>100	-21.21	-5.27	28.23
15		12.2	-17.22	-5.12	18.21
16		18.6	-26.81	-6.96	28.21
17		67.3	-27.28	-5.23	29.81
18		>100	-17.79	-7.43	22.74
19		>100	-14.34	-5.99	31.04
20		>100	-17.24	-4.76	20.17
21		>100	-28.21	-6.29	30.61

Table S2.2 Continued

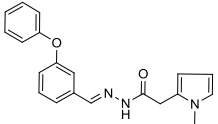
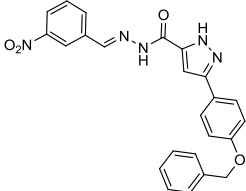
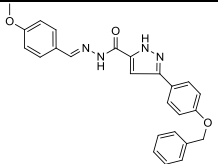
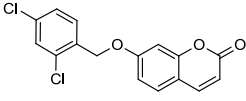
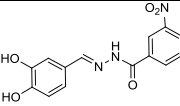
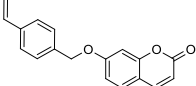
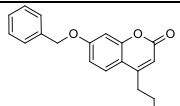
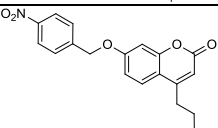
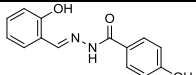
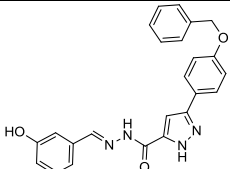
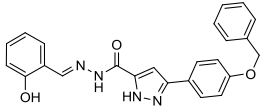
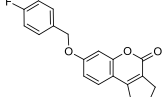
S. No	Structure	IC50 (μM) LSD1	ICM Score (kcal/mol)	GLIDE Score (kcal/mol)	GOLD Fitness Score (kcal/mol)
22		>100	-26.24	-7.14	34.82
23		>100	-23.23	-5.86	32.76
24		>100	-21.28	-6.13	32.52
25		>100	-14.93	-4.21	20.12
26		>100	-13.34	-7.24	32.61
27		>100	-11.21	-6.21	25.21
28		>100	-11.29	-5.34	23.78
29		>100	-16.25	-4.88	30.22
30		0.196	-42.25	-8.14	56.26
31		22	-27.29	-6.77	31.55
32		>100	-21.89	-6.69	32.31
33		>100	-13.29	-6.86	39.03

Table S2.2 Continued

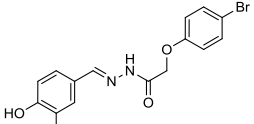
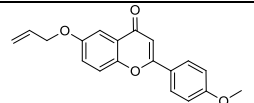
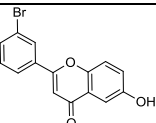
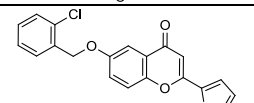
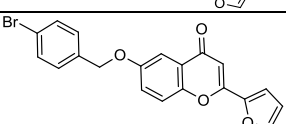
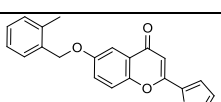
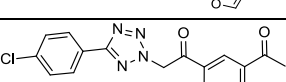
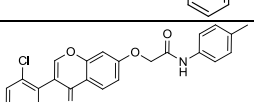
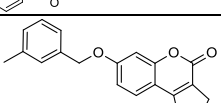
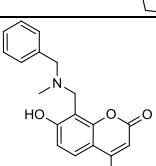
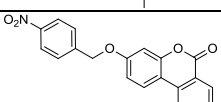
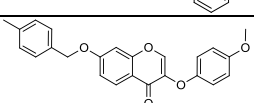
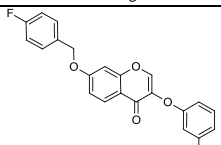
S. No	Structure	IC50 (μ M) LSD1	ICM Score (kcal/mol)	GLIDE Score (kcal/mol)	GOLD Fitness Score (kcal/mol)
34		>100	-22.95	-6.29	37.19
35		37	-21.38	-7.22	25.94
36		17	-19.29	-8.66	29.93
37		>100	-13.12	-5.13	22.14
38		>100	-17.37	-4.77	25.65
39		>100	-18.58	-4.86	25.92
40		>100	-16.43	-5.16	22.74
41		>100	-19.99	-6.16	21.04
42		>100	-16.19	-4.42	20.17
43		>100	-17.23	-5.66	20.61
44		>100	-13.87	-3.33	24.82
45		>100	-11.81	-5.77	22.76
46		>100	-17.99	-5.99	22.52

Table S2.2 Continued

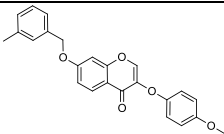
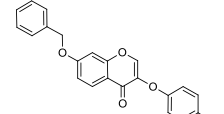
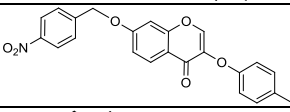
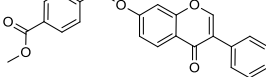
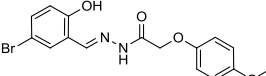
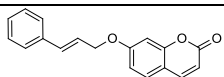
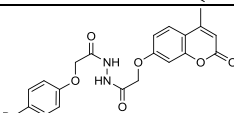
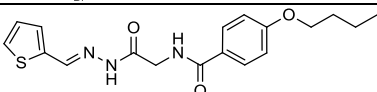
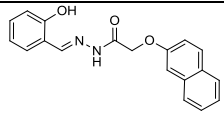
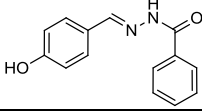
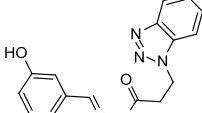
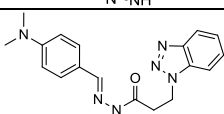
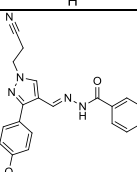
S. No	Structure	IC50 (μ M) LSD1	ICM Score (kcal/mol)	GLIDE Score (kcal/mol)	GOLD Fitness Score (kcal/mol)
47		>100	-14.39	-4.96	20.12
48		>100	-53.29	-4.77	22.61
49		>100	-17.64	-4.52	25.21
50		>100	-17.31	-4.86	23.78
51		>100	-21.28	-7.33	30.22
52		>100	-19.73	-4.97	31.55
53		>100	-17.34	-3.59	22.31
54		>100	-20.21	-6.76	39.03
55		>100	-26.29	-5.23	37.19
56		>100	-26.25	-6.22	35.94
57		67	-21.28	-6.66	39.93
58		>100	-19.33	-6.33	32.14
59		>100	-29.84	-5.67	25.65

Table S2.2 Continued

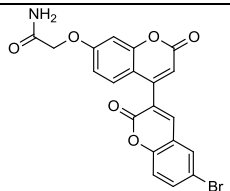
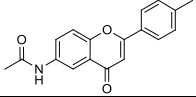
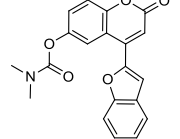
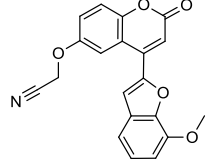
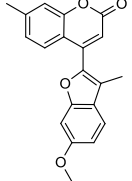
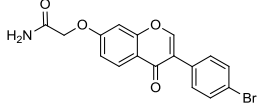
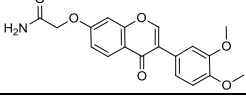
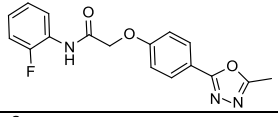
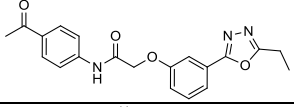
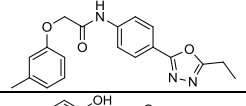
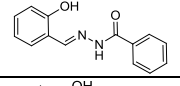
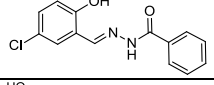
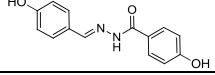
S. No	Structure	IC50 (μM) LSD1	ICM Score (kcal/mol)	GLIDE Score (kcal/mol)	GOLD Fitness Score (kcal/mol)
60		>100	-16.23	-4.19	25.92
61		>100	-11.97	-3.16	19.22
62		>100	-14.27	-3.17	20.71
63		18	-21.88	-4.42	22.23
64		>100	-17.13	-4.22	22.07
65		>100	-16.55	-5.13	26.62
66		>100	-17.11	-4.37	30.49
67		>100	-19.39	-2.79	33.71
68		>100	-16.87	-4.69	31.58
69		32	-21.88	-3.17	30.98
70		>1 uM	-24.43	-6.52	30.62
71		>1 uM	-23.94	-6.33	30.97
72		>1 uM	-21.41	-7.23	31.28

Table S2.2 Continued

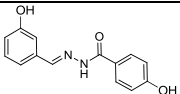
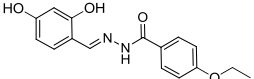
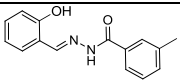
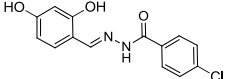
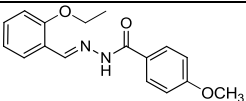
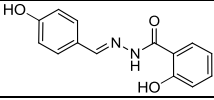
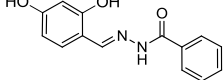
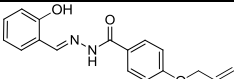
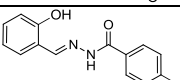
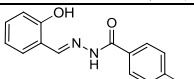
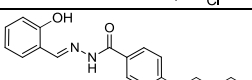
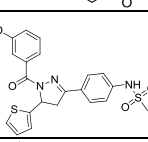
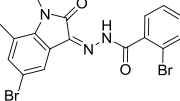
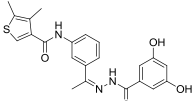
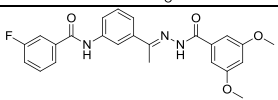
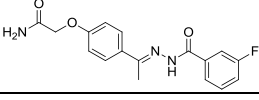
S. No	Structure	IC50 (μ M) LSD1	ICM Score (kcal/mol)	GLIDE Score (kcal/mol)	GOLD Fitness Score (kcal/mol)
73		>1 μ M	-21.99	-9.47	32.23
74		>1 μ M	-26.25	-8.99	35.26
75		>1 μ M	-29.18	-7.79	36.75
76		>1 μ M	-24.23	-7.17	30.42
77		>1 μ M	-23.37	-7.43	38.68
78		>1 μ M	-21.81	-7.46	30.59
79		>1 μ M	-26.54	-7.13	30.29
80		>1 μ M	-26.45	-8.17	35.82
81		>1 μ M	-27.31	-8.21	38.72
82		>1 μ M	-26.99	-7.06	31.62
83		>1 μ M	-26.35	-6.20	30.01
84		>10 μ M	-28.18	-6.42	31.67
84		>10 μ M	-22.33	-8.93	31.27
86		>10 μ M	-26.39	-8.13	34.82
87		>10 μ M	-31.96	-6.17	30.89
88		>10 μ M	-29.64	-6.86	31.04

Table S2.2 Continued

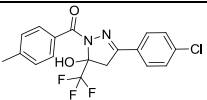
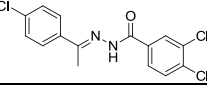
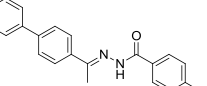
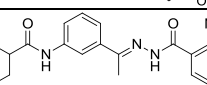
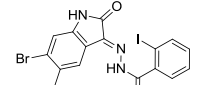
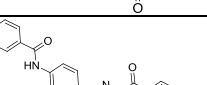
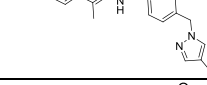
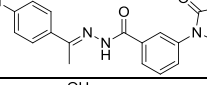
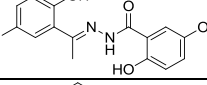
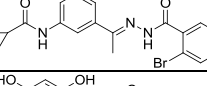
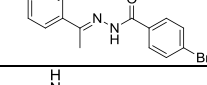
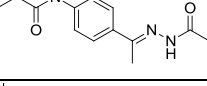
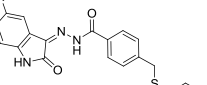
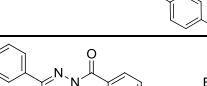
S. No	Structure	IC50 (μ M) LSD1	ICM Score (kcal/mol)	GLIDE Score (kcal/mol)	GOLD Fitness Score (kcal/mol)
89		>10 μ M	-21.75	-7.36	33.14
90		>10 μ M	-29.81	-7.77	32.02
91		>10 μ M	-26.79	-7.44	33.02
92		>10 μ M	-32.55	-8.16	33.69
93		>10 μ M	-19.28	-6.29	34.21
94		>10 μ M	-25.66	-7.67	31.48
95		>10 μ M	-21.77	-8.16	37.94
96		>10 μ M	-23.61	-7.16	33.75
97		>10 μ M	-29.59	-7.97	30.41
98		>10 μ M	-29.435	-8.89	32.92
99		>10 μ M	-31.41	-6.16	33.19
100		>10 μ M	-31.89	-9.23	32.41
101		>10 μ M	-36.29	-7.87	34.16
102		>10 μ M	-24.19	-7.22	33.67

Table S2.2 Continued

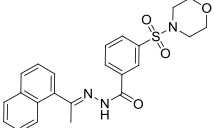
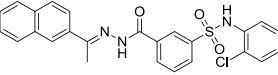
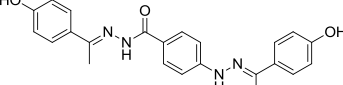
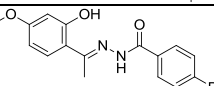
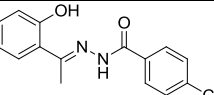
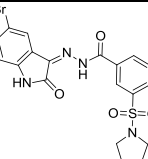
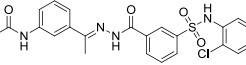
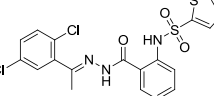
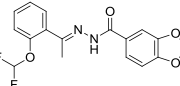
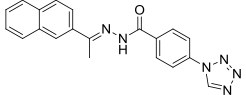
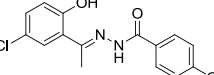
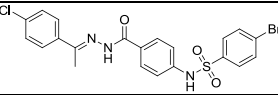
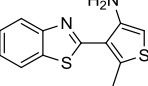
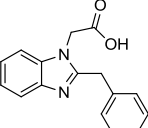
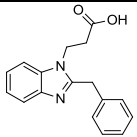
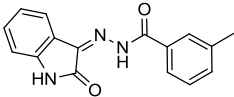
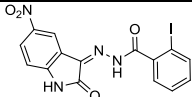
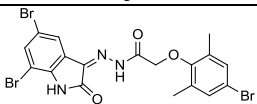
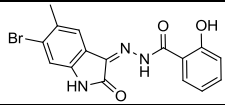
S. No	Structure	IC50 (μM) LSD1	ICM Score (kcal/mol)	GLIDE Score (kcal/mol)	GOLD Fitness Score (kcal/mol)
103		>10 uM	-27.11	-7.66	34.92
104		>10 uM	-22.17	-7.17	31.97
105		>10 uM	-32.77	-6.95	31.62
106		>10 uM	-36.74	-6.16	30.52
107		>10 uM	-36.75	-6.14	30.65
108		>10 uM	-31.56	-7.27	41.62
109		>10 uM	-21.87	-8.19	31.56
110		>10 uM	-34.21	-8.79	32.61
111		>10 uM	-39.88	-8.29	33.41
112		>10 uM	-34.13	-7.42	37.79
113		>10 uM	-33.39	-6.76	32.73
114		>10 uM	-31.21	-8.29	32.51
115		>100 uM	-16.44	-4.19	21.99
116		>10 uM	-24.21	-7.39	32.08

Table S2.2 Continued

S. No	Structure	IC50 (μ M) LSD1	ICM Score (kcal/mol)	GLIDE Score (kcal/mol)	GOLD Fitness Score (kcal/mol)
117		>10 μ M	-29.78	-6.49	35.05
118		>10 μ M	-24.43	-6.41	30.12
119		>10 μ M	-23.89	-7.99	32.45
120		>10 μ M	-21.29	-6.16	22.08
121		>10 μ M	-16.74	-5.19	25.05

Supplementary Table S2.3. Tanimoto similarity coefficients comparing compound **12** and known LSD1 inhibitors from **Chart 1**

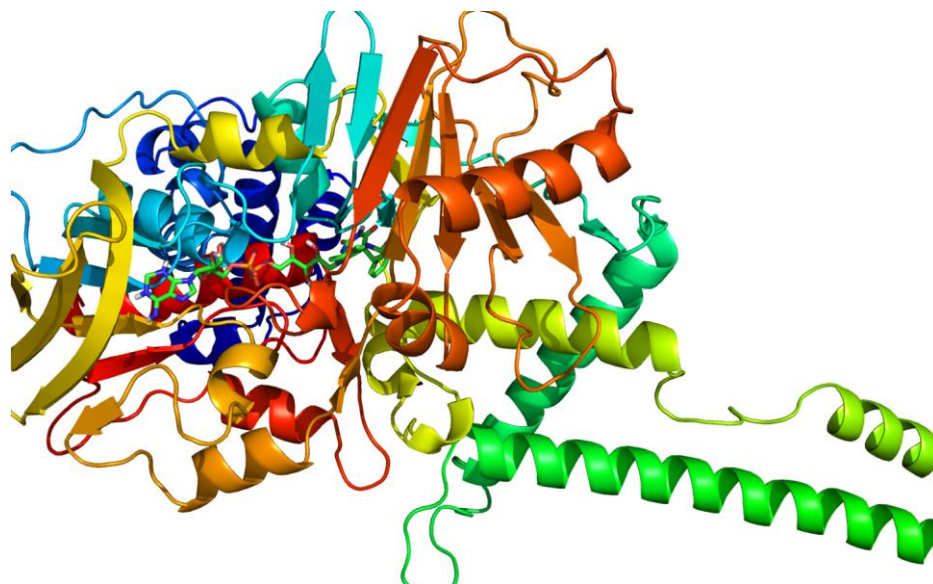
Compound	Tanimoto Similarity score
A	0.26
B	0.21
C	0.31
D	0.26
E	0.22
F	0.36
G	0.24
H	0.28
I	0.38
J	0.35
K	0.39
L	0.29
M	0.11
N	0.11
O	0.32
P	0.11

Supplementary Table S2.4. Off-target inhibition assay results.

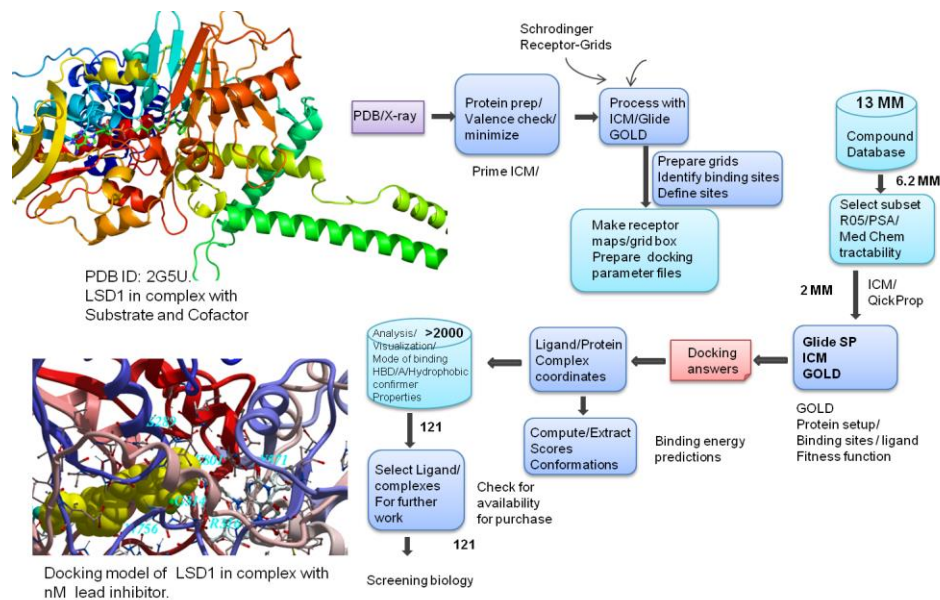
[12] (nM)	Activity % \pm SD					
	CYP1A2	CYP2C19	CYP2C9	CYP2D6	CYP3A4	hERG
30000						98 \pm 4
10000	60 \pm 3	53 \pm 1	46 \pm 2	94 \pm 2	21 \pm 2	104 \pm 2
3333	86 \pm 1	91 \pm 2	84 \pm 1	101 \pm 11	46 \pm 2	100 \pm 6
1111	87 \pm 2	105 \pm 0.4	98 \pm 3	102 \pm 10	71 \pm 4	102 \pm 7
370	96 \pm 1	111 \pm 3n/a	108 \pm 0.2	105 \pm 12	87 \pm 10	98 \pm 3
123	97 \pm 8	110 \pm 0.1	111 \pm 1	110 \pm 8	100 \pm 3	95 \pm 4
41.2	93 \pm 3	107 \pm 12	107 \pm 5	105 \pm 12	98 \pm 9	98 \pm 2
13.7	105 \pm 7	114 \pm 1	109 \pm 1	108 \pm 6	98 \pm 1	107 \pm 0.1
4.57	106 \pm 4	106 \pm 11	107 \pm 8	104 \pm 12	99 \pm 9	93 \pm 2
1.52	111 \pm 3	117 \pm 3	112 \pm 1	109 \pm 6	105 \pm 1	100 \pm 2
0.51	110 \pm 2	89 \pm 3	107 \pm 6	106 \pm 2	96 \pm 5	
	D-LDH	GO				
100000	103 \pm 7	105 \pm 3				
30000	103 \pm 6	106 \pm 3				
10000	106 \pm 5	108 \pm 6				
3000	112 \pm 5	92 \pm 3				
1000	121 \pm 6	97 \pm 0.3				
300	118 \pm 5	109 \pm 3				
100	119 \pm 5	102 \pm 1				

Supplementary Table S2.5. Different model fits for enzyme kinetics results.

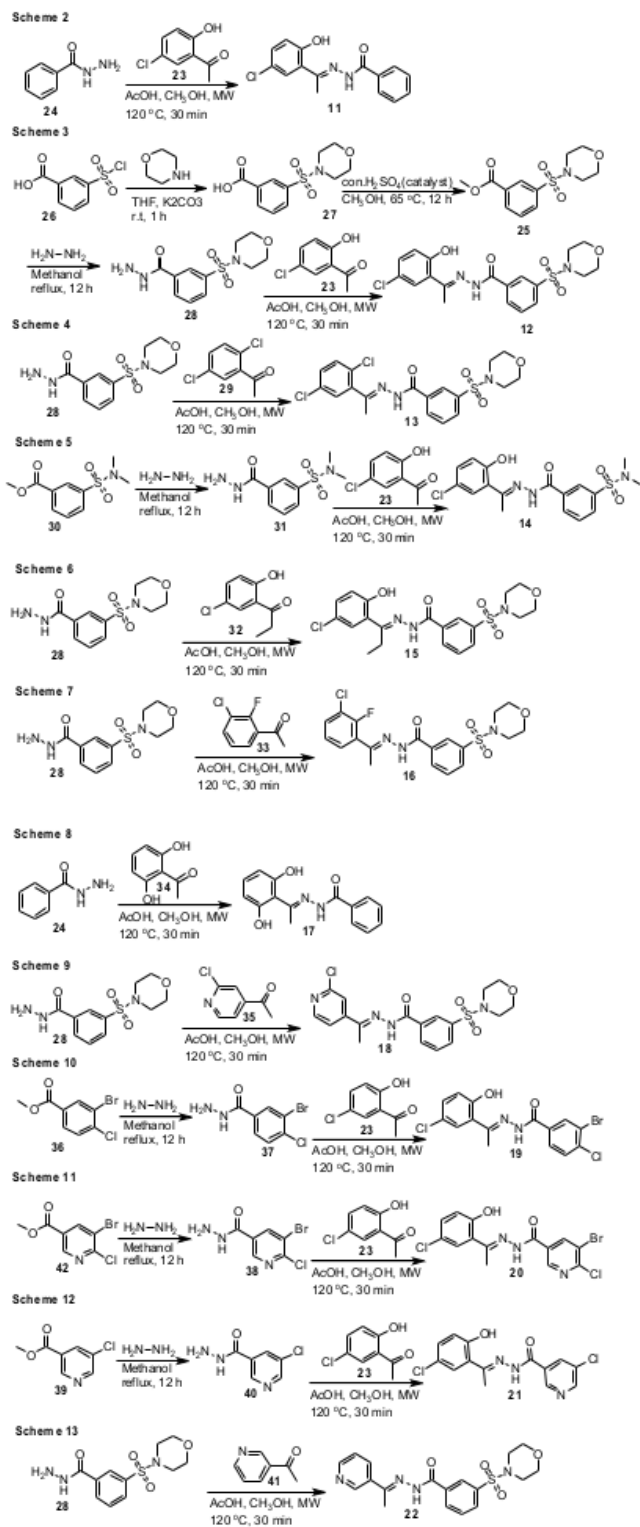
Model	Competitive	Noncompetitive	Uncompetitive
v_{\max} (F/s) \pm SE	635.8 \pm 12.83	688.9 \pm 10.80	695.8 \pm 11.67
K_m (μ M) \pm SE	0.919 \pm 0.1128	1.310 \pm 0.0928	1.411 \pm 0.1042
k_i (nM) \pm SE	4.136 \pm 0.7027	39.04 \pm 3.046	32.76 \pm 2.67
DMSO R^2	0.9033	0.9269	0.9275
1 nM R^2	0.8788	0.8774	0.8758
3 nM R^2	0.9022	0.9077	0.9076
10 nM R^2	0.8492	0.9154	0.9060
30 nM R^2	0.2257	0.9289	0.9146
100 nM R^2	-0.6184	0.6953	0.5652
Global R^2	0.8599	0.9239	0.9198



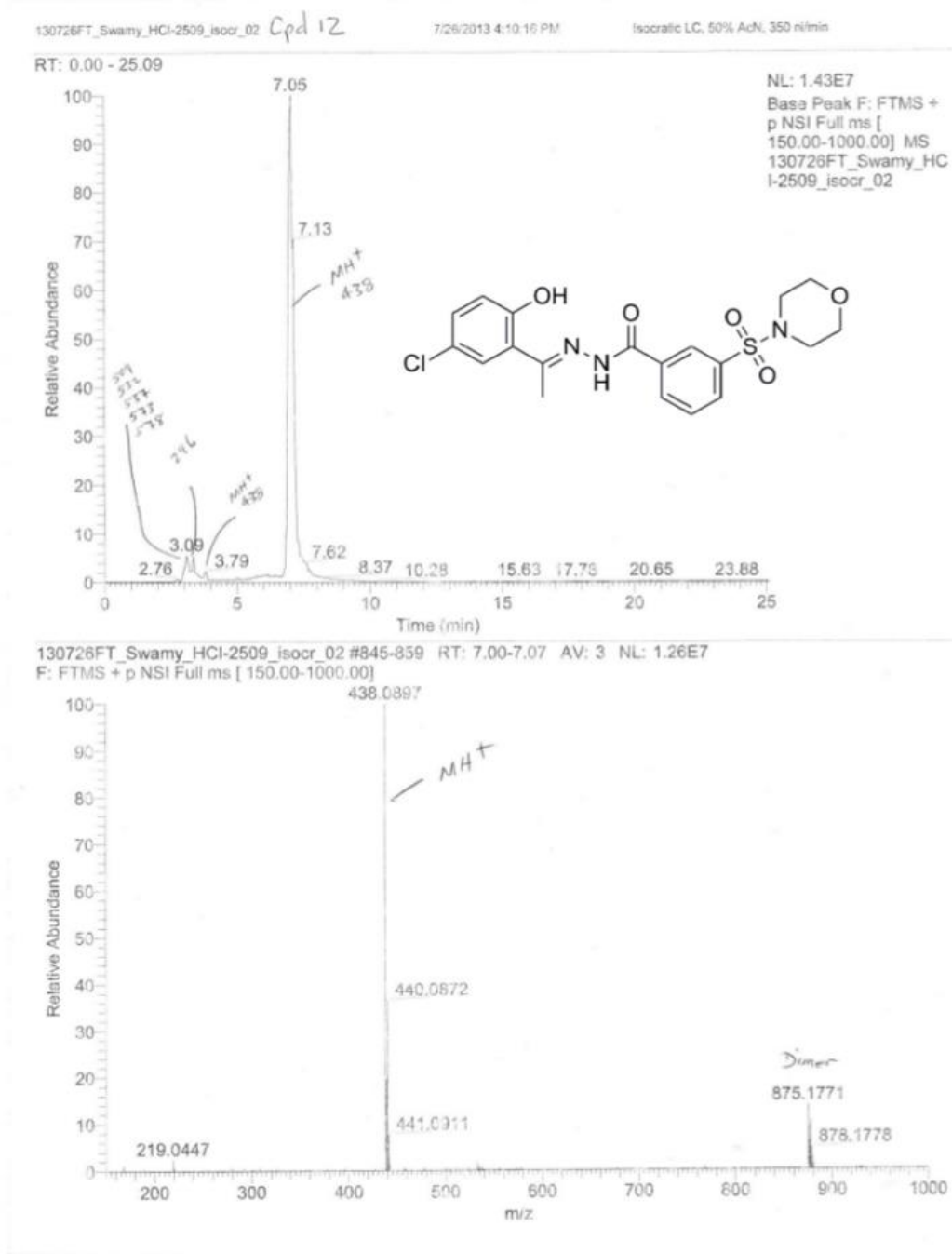
Supplementary Figure S2.1. Binding Site Model and definition of active site of LSD1 structure generated from PDB ID 2Z5U.



Supplementary Figure S2.2. Flow diagram for the Virtual Ligand Screening (VLS) using ICM-VLS, Schrodinger workflow GOLD programs.



Supplementary Figure S2.3. Complete reaction schemes for compounds 11-22



Supplementary Figure S2.4. LC-MS Data for Compound 12 (96% purity).

CHAPTER 3

REVERSIBLE LSD1 INHIBITION INTERFERES WITH GLOBAL EWS/ETS TRANSCRIPTIONAL ACTIVITY AND IMPEDES EWING SARCOMA TUMOR GROWTH

Savita Sankar and Emily R. Theisen are co-first authors of this work. SS and ERT executed RNA-seq studies with HCI2509. SS profiled EWS/ETS knockdown by RNA-seq. SS and ERT jointly analyzed sequencing data. SS and ERT generated EWS/ETS knockdown constructs to assay the cell viability shift. ERT performed viability experiments with EWS/FLI expressed in NIH3T3 cells. SS performed qPCR validation of target genes. Laura M. Hoffman stained, imaged, and analyzed cells by immunofluorescence microscopy. SS and ERT performed soft agars. ERT performed apoptosis assays. Timothy Mulvihill performed global methylation analysis. SS, ERT, and TM performed HMOX1 analysis. ERT and Jared Bearss were responsible for xenograft experiments. ERT and SS evaluated HMOX1 levels in tumors. ERT wrote the manuscript.

Reproduced with permission from Sankar S and Theisen ER, et al. *Clinical Cancer Research* **2014** 20 (17), 4584-4597.

Copyright 2014 American Association for Cancer Research.

Reversible LSD1 Inhibition Interferes with Global EWS/ETS Transcriptional Activity and Impedes Ewing Sarcoma Tumor Growth

Savita Sankar¹, Emily R. Theisen^{2,3}, Jared Bearss², Timothy Mulvihill⁴, Laura M. Hoffman⁵, Venkataswamy Sorna², Mary C. Beckerle^{1,5}, Sunil Sharma^{2,6}, and Stephen L. Lessnick^{1,7,8}

Abstract

Purpose: Ewing sarcoma is a pediatric bone tumor that absolutely relies on the transcriptional activity of the EWS/ETS family of fusion oncoproteins. While the most common fusion, EWS/FLI, utilizes lysine-specific demethylase 1 (LSD1) to repress critical tumor suppressors, small-molecule blockade of LSD1 has not yet been thoroughly explored as a therapeutic approach for Ewing sarcoma. We therefore evaluated the translational potential of potent and specific LSD1 inhibition with HCI2509 on the transcriptional program of both EWS/FLI and EWS/ERG as well as the downstream oncogenic phenotypes driven by EWS/ETS fusions in both *in vitro* and *in vivo* models of Ewing sarcoma.

Experimental Design: RNA-seq was used to compare the transcriptional profiles of EWS/FLI, EWS/ERG, and treatment with HCI2509 in both EWS/FLI- and EWS/ERG-containing cell lines. We then evaluated morphologic phenotypes of treated cells with immunofluorescence. The induction of apoptosis was evaluated using caspase-3/7 activation and TUNEL staining. Colony forming assays were used to test oncogenic transformation and xenograft studies with patient-derived cell lines were used to evaluate the effects of HCI2509 on tumorigenesis.

Results: HCI2509 caused a dramatic reversal of both the up- and downregulated transcriptional profiles of EWS/FLI and EWS/ERG accompanied by the induction of apoptosis and disruption of morphologic and oncogenic phenotypes modulated by EWS/FLI. Importantly, HCI2509 displayed single-agent efficacy in multiple xenograft models.

Conclusions: These data support epigenetic modulation with HCI2509 as a therapeutic strategy for Ewing sarcoma, and highlight a critical dual role for LSD1 in the oncogenic transcriptional activity of EWS/ETS proteins. *Clin Cancer Res*; 20(17); 4584–97. ©2014 AACR.

¹Department of Oncological Sciences, University of Utah School of Medicine, Salt Lake City, Utah. ²Center for Investigational Therapeutics at Huntsman Cancer Institute, University of Utah, Salt Lake City, Utah. ³Department of Pharmaceuticals and Pharmaceutical Chemistry, College of Pharmacy, University of Utah, Salt Lake City, Utah. ⁴University of Utah School of Medicine, Salt Lake City, Utah. ⁵Department of Biology, Huntsman Cancer Institute, University of Utah, Salt Lake City, Utah. ⁶Division of Medical Oncology, University of Utah School of Medicine, Salt Lake City, Utah. ⁷Center for Children's Cancer Research at Huntsman Cancer Institute, Salt Lake City, Utah. ⁸Division of Pediatric Hematology/Oncology, University of Utah School of Medicine, Salt Lake City, Utah.

Note: Supplementary data for this article are available at Clinical Cancer Research Online (<http://clincancerres.aacrjournals.org/>).

Savita Sankar and Emily R. Theisen contributed equally to this article.

Current address for S. Sankar: Massachusetts General Hospital Cancer Center and the Department of Medicine, Harvard Medical School, Boston, MA 02115.

Corresponding Author: Stephen L. Lessnick, Center for Children's Cancer Research, Huntsman Cancer Institute, 2000 Circle of Hope, Room 4242, Salt Lake City, UT 84112. Phone: 801-585-9268; Fax: 1-801-585-5357; E-mail: stephen.lessnick@hci.utah.edu

doi: 10.1158/1078-0432.CCR-14-0072

©2014 American Association for Cancer Research.

Introduction

Dynamic epigenetic regulation, including DNA methylation and posttranslational histone modification, is required for normal development and maintenance of tissue-specific transcriptional programs. Abnormal regulation can lead to altered gene expression and malignant transformation (1, 2). Indeed, enzymes which mediate epigenetic modifications are emerging as therapeutic targets in cancer (1, 2). Histone lysine methylation, specifically, can signify both activating and repressive chromatin, depending on the site of methylation (3). For example, methylation at histone H3K4 indicates active chromatin while methylation at H3K9 and H3K27 indicates repressive chromatin (3). While DNA methyltransferases (DNMT) and histone deacetylases (HDAC) are involved in global epigenetic processes, histone lysine methyltransferases (KMT) and demethylases (KDM) regulate histone methylation and gene expression in a manner that is often cell-type specific (4–8). Genetic mutations, chromosomal translocations, and translocation-derived fusion proteins affecting KMTs and KDMs contribute to impaired tumor suppression

Translational Relevance

Ewing sarcoma is an aggressive cancer, with bleak survival rates (10%–30%) for patients with metastatic or relapsed disease. Treatment with the LSD1 inhibitor HCI2509 disrupts the global transcriptional function of EWS/ETS fusions, impairs multiple EWS/ETS-associated oncogenic phenotypes, and shows single-agent efficacy in multiple xenograft models of Ewing sarcoma. With several targeted LSD1 inhibitors in preclinical development, these results highlight a new therapeutic strategy for this disease.

and altered developmental plasticity in several malignancies (8–14). Strategies targeting individual KMTs and KDMs critical for a particular malignancy may confer increased therapeutic specificity (15).

Lysine-specific demethylase 1 (LSD1) is a KDM implicated in neuroblastoma, acute myeloid leukemia, breast, prostate, bladder, lung, liver, and colorectal tumors (16–21). Recently, high LSD1 expression was reported in certain mesenchymal tumors, including Ewing sarcoma (22, 23). Ewing sarcoma is a highly aggressive pediatric malignancy characterized by the presence of a translocation-derived fusion oncoprotein and aberrant transcription factor, EWS/FLI (24). The majority of cases present with the EWS/FLI fusion, while several other related EWS/ETS fusions are occasionally observed as well (25). The most common of these is EWS/ERG, which presents in approximately 10% of cases (25). While the 5-year overall survival for patients with local disease is 70% to 80%, for those who present with metastases, or those who have relapsed, this drops to a bleak 10% to 30% (26, 27). In addition, treatment carries elevated risk for long-term side effects, including limb dysfunction, infertility, and secondary malignancies (28). Targeted therapies with increased efficacy and reduced toxicity are imperative. Though the role of LSD1 in Ewing sarcoma pathogenesis was still vague, the LSD1 inhibitor tranylcypromine impaired growth of Ewing sarcoma cell lines *in vitro* (23). Tranylcypromine is used clinically as a monoamine oxidase inhibitor, but has low potency as an LSD1 inhibitor, and has several documented off-target effects precluding widespread clinical use targeting this enzyme.

Further investigation showed LSD1 recruitment by EWS/FLI as a member of the nucleosome remodeling and histone deacetylase (NuRD) complex to repress the critical EWS/FLI targets *LOX* and *TGFBR2* (29). Treatment with the potent LSD1 inhibitor, HCI2509, caused derepression of these genes and impaired tissue culture cell viability in multiple Ewing sarcoma cell lines at physiologically relevant concentrations (29). The sensitivity of multiple cell lines to LSD1 inhibition suggests a pivotal role for LSD1 in Ewing sarcoma beyond repression of select EWS/FLI targets. The extent of the role that LSD1 plays in the global transcriptional program orchestrated by EWS/FLI, and other EWS/

ETS fusions, remains uncharacterized. The experiments herein describe the global transcriptional effects of HCI2509 treatment in Ewing sarcoma and the downstream antitumor effects that result.

Materials and Methods

Constructs and retroviruses

The Luciferase-RNAi (Luc-RNAi), EWS/FLI-RNAi (EF-2-RNAi), 3x-FLAG EWS/FLI, 3x-FLAG Δ 22, and 1x-FLAG R2L2 cDNA are previously described (30–32). The 1x-HA HMOX1 cDNA was generated and subcloned into the Murine Stem Cell Virus (MSCV) retroviral vector (Clontech). siRNA controls targeted toward LSD1, CHD4, REST, RCoR1, NCoR, and Sin3A are described previously (29).

Antibodies and reagents

The following antibodies were used for immunodetection: M2-anti-FLAG (HRP; Sigma A8592), anti-FLI-1 (Santa-Cruz sc-356X), anti- α -Tubulin (Calbiochem CP06), anti-HA (Abcam ab91110), anti-H3 total (Abcam ab1791), anti-H3K4 me1 (Abcam ab8895), anti-H3K4 me2 (Millipore, 07-030), anti-H3K4 me3 (Active Motif, 39159), anti-H3K9 me1 (Abcam ab9045), anti-H3K9 me2 (Abcam ab1220), anti-H3K9 me3 (Abcam ab8898), anti-HMOX1 (Sigma SAB1410641), anti-Paxillin (BD Transduction Labs 610619), anti-LSD1 (Cell Signaling Technology 2184) AlexaFluor secondary (Molecular Probes), AlexaFluor Phalloidin (Molecular Probes). HCI2509 is previously described (33).

Cell culture

Ewing sarcoma cell lines harboring the EWS/FLI (A673, TC-71, SK-N-MC, SKES1, and EWS502) or EWS/ERG fusion (TTC-466) were grown in appropriate selection media, as previously described (34, 35). NIH 3T3 cells with and without EWS/FLI expression were previously reported (36). Growth assays (3T5) were previously described (35).

Colony formation assays

Soft agar assays were described previously (35). Methylcellulose assays were performed by plating 1×10^5 cells in a 1:1 mix of 2% methylcellulose and growth media as described previously (29).

Quantitative reverse-transcriptase PCR

Total RNA was extracted using an RNeasy kit (Qiagen). Total RNA was then amplified and detected using SYBR green fluorescence for quantitation. Normalized fold enrichment was calculated by determining the fold-change of each condition relative to the control. The data in each condition was normalized to internal housekeeping control genes, *GAPDH* and *RPL19*. Primer sequences are provided in Supplementary Data (Supplementary Table S3).

Chromatin immunoprecipitation

Chromatin immunoprecipitation (ChIP) was performed as previously described (37) using anti-LSD1 antibody (Abcam ab17721). Quantitative PCR was performed with *HMOX1* gene primers amplifying a region ~29 base pairs

upstream of the transcription start site (TSS). *BCL2L1* was used as a normalization control (38). Primer sequences are provided in the Supplementary Data (Supplementary Table S3).

In vivo studies

Xenografts: A673, SK-N-MC, or SKES1 cells were injected into the right hindflanks of nude mice at 1×10^6 cells or 1×10^6 cells or 2.5×10^6 cells per flank, respectively. For all xenograft studies, 10 mice per condition were injected subcutaneously; therefore, 10 tumors were measured per group. In the SK-N-MC study, one animal perished due to an unrelated rash and was censored from analysis. Tumors were measured using digital calipers and volumes were calculated as follows: $(L \times W \times D)/2$. Treatment was initiated on day 7 after bioluminescent imaging confirmed tumor engraftment in the A673 study, whereas SK-N-MC and SKES1 studies were initiated once tumors reached a volume of $>100 \text{ mm}^3$. Mice in each group were sacrificed once tumors reached a size limit of 2 cm^3 . Kaplan–Meier survival curves were plotted using GraphPad Prism. Tumor volume and body weight were recorded for all three models. Harvested tumors were flash frozen, homogenized by mortar and pestle in liquid nitrogen, and analyzed for RNA or protein. All xenograft experiments were performed in accordance with protocol 11–11003 approved by the University of Utah Institutional Animal Care and Use Committee.

Blood Counts: The facial vein was identified and pierced with a lancet, blood was collected in a heparin capillary tube, and analyzed using a HemaTrue hematology analyzer (Heska).

Immunofluorescence assays

A total of 5×10^4 – 1.5×10^5 A673 and TTC-466 cells were seeded onto fibronectin-coated coverslips, allowed to adhere for ≥ 24 hours, treated with vehicle or HCI2509 at 0.5, 1, and $2 \mu\text{mol/L}$ for 3 days in DMEMc + 10% FBS, and fixed, stained, and imaged as previously described (39). Briefly, cells were immunostained with paxillin antibody (1:100) or LSD1 antibody (1:400) and then with secondary antibody (1:100) and DAPI ($0.3 \mu\text{mol/L}$). Fluorescent cell images were collected on a Zeiss Axioskop2 mot plus microscope with a $40 \times$ dry objective (NA 0.75 NeoFluor), AxioCam MR camera, and Axiovision v4.8.1 software (Carl Zeiss MicroImaging, Inc.). Cell area analysis was performed with ImageJ (NIH freeware) and MetaMorph software (Molecular Devices); ≥ 50 cells were analyzed from ≥ 10 microscope fields, conversion factor $1 \mu\text{m} = 6.2$ pixels. Image datasets were analyzed in GraphPad Prism 5 using unpaired *t*-tests and graphed as mean and SD.

RNA sequencing analysis, GSEA, and Venn overlaps

See Supplementary Methods for a description of RNA-seq data collection. Overlaps between the different gene sets were performed using VennMaster (<http://www.informatik.uni-ulm.de/ni/mitarbeiter/HKestler/vennm/doc.html>). Statistical significance of the overlaps was determined using χ^2 analysis. Gene set enrichment analysis (GSEA) was

performed using GSEA v2.0.10 (<http://www.broad.mit.edu/gsea/>). Functional annotation analysis was performed by DAVID (david.abcc.ncifcrf.gov). Heatmaps were generated by converting read counts to fragments per kilobase gene model per million reads (FPKM). Genes were included in the heatmap if their differential abundance was more than 3-fold in both experiments and the Benjamini–Hochberg false discovery rate was <0.05 . The data were normalized per gene across both experiments and \log_{10} transformed. Heatmaps were created using the R gplots package. Ranks were based on averages of treatment and control.

Cell viability determination and EC₅₀ shift analysis

A673 cells were stably infected and selected for expression of control Luc-RNAi or EF-2-RNAi. A total of 2×10^4 cells per well were seeded in a 96-well plate, allowed 24 hours to adhere, and treated with either vehicle or HCI2509 for 96 hours. Viability was assayed using CellTiter-Glo (Promega).

In vitro apoptosis assays

Caspase/viability. 2×10^4 cells per well were seeded in a 96-well plate, treated with either vehicle or two times their respective EC₅₀ for HCI2509. Caspase activation and cell viability were assayed using Caspase-Glo 3/7 (Promega) and CellTiter-Glo (Promega), respectively, at 0, 24, and 48 hours.

TUNEL staining. A673 cells were treated with either vehicle or $2 \mu\text{mol/L}$ HCI2509 for 48 hours and then assayed using the DeadEnd Colorimetric TUNEL (Promega). Images were collected on an Olympus 1×70 inverted microscope, Olympus EOS Rebel XSi camera, and EOS Utility software (Canon U.S.A., Inc.).

Data availability

Raw sequence reads can be found in the NCBI SRA under numbers SRA096343, SRA096347, SRA096354. Differentially expressed genes from each RNA-seq dataset are in Supplementary Table S1.

Results

LSD1 inhibition reverses the EWS/ETS-driven transcriptional program in Ewing sarcoma

HCI2509 is a specific and reversible noncompetitive inhibitor of LSD1 previously shown to derepress the critical EWS/FLI target genes *LOX* and *TGFBR2* and to kill multiple Ewing sarcoma cell lines *in vitro* (29, 30). Interestingly, HCI2509-mediated derepression of *LOX* and *TGFBR2* was dependent on the expression of EWS/FLI. To determine whether the Ewing sarcoma cell death observed with HCI2509 treatment was also dependent on EWS/FLI, we knocked down the fusion protein using retroviral-mediated shRNA, and assessed viability after treatment with HCI2509. Cells expressing EWS/FLI were approximately 10-fold more susceptible to treatment with HCI2509 compared to cells with EWS/FLI knockdown (Fig. 1A), which confirmed the efficacy of HCI2509 is dependent upon the presence of EWS/FLI. On the basis of previous results showing that HCI2509 decreased viability in multiple

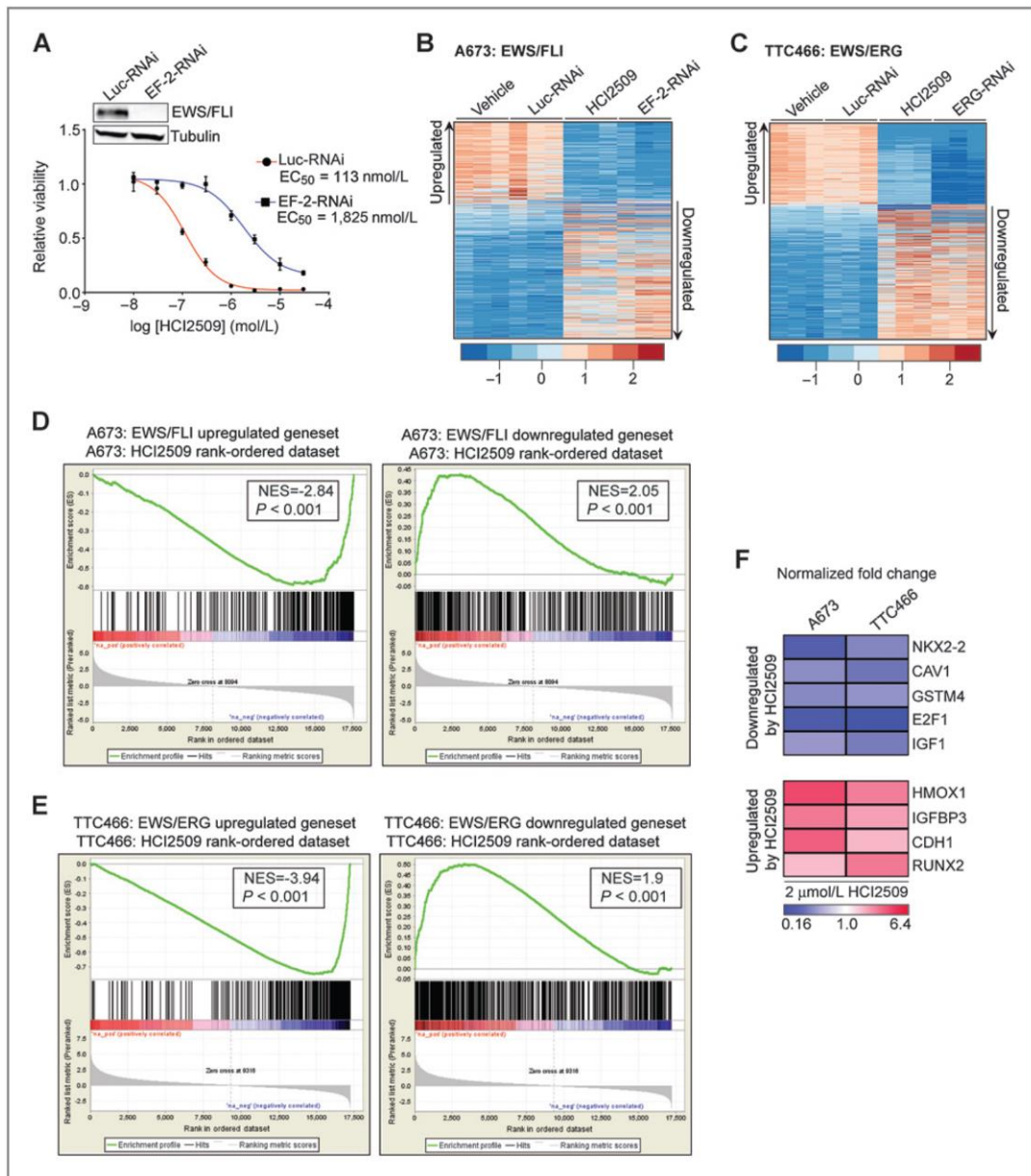


Figure 1. Global EWS/FLI transcriptional activity is disrupted by HCI2509. A, cell viability assay showing the difference in HCI2509 sensitivity between A673 cells with control [EC₅₀ = 113 nmol/L; 95% confidence interval (CI), 81.9–158 nmol/L] and EWS/FLI knockdown (EC₅₀ = 1,825 nmol/L; 95% CI, 1,111–2,999 nmol/L). The dose-response curves were determined after 96 hours of treatment and normalized to the vehicle controls. Mean and SD are shown ($n = 3$). Stable EWS/FLI knockdown was analyzed by Western Blot analysis as shown in the inset. B and C, heatmap representation of the HCI2509 expression profile matched to the rank-ordered EWS/FLI- (B) and EWS/ERG knockdown (C) profiles. Genes were ranked by mean deviation of the log-transformed FPKM (Fragments Per Kilobase per Million mapped reads). The columns for each condition represent one independent biologic replicate. Each row represents a different gene. D and E, GSEA from RNA-seq experiments using the EWS/FLI-regulated genes (D) in A673 cells as the rank-ordered dataset and the 281 HCI2509 upregulated and 376 HCI2509 downregulated genes as the gene sets and EWS/ERG-regulated genes (E) in TTC-466 cells as the rank-ordered dataset and the 216 HCI2509 upregulated and 357 HCI2509 downregulated genes as the gene sets. Normalized enrichment scores (NES) and P values are shown. F, qRT-PCR validation of *NKX2.2*, *CAV1*, *GSTM4*, *E2F1*, *IGF-1*, *RUNX2*, *IGFBP3*, *HMOX1*, and *CDH1* as HCI2509 targets in A673 and TTC-466 cells treated for 48 hours with vehicle or HCI2509 at $2 \times$ EC₅₀. Normalized fold change is indicated as a heatmap. The P value for each fold change is < 0.05 ($n = 3$). Individual P values are reported in Supplementary Table S2.

patient-derived Ewing sarcoma cell lines containing EWS/FLI, we next asked whether the effects were restricted to EWS/FLI-containing lines, or whether they can be generalized to other Ewing sarcoma-associated fusions. As was seen for EWS/FLI-containing cell lines, the Ewing sarcoma cell line TTC-466 containing the alternative EWS/ETS fusion, EWS/ERG, was also sensitive to HCI2509 treatment (Supplementary Fig. S1A). Like A673 cells, TTC-466 cells with EWS/ERG knockdown showed decreased sensitivity to HCI2509. We further tested whether introducing EWS/FLI into a heterologous cell line induced sensitization to HCI2509 treatment in NIH 3T3 fibroblasts (Supplementary Fig. S1B). No sensitization was observed, suggesting EWS/ETS-dependent sensitization is unique to Ewing sarcoma cells.

To assess changes in gene expression caused by LSD1 inhibition in the context of EWS/ETS fusion transcriptional activity, we first generated transcriptional signatures for EWS/FLI and EWS/ERG. A673 and TTC-466 cell lines were subjected to retroviral-mediated shRNA knockdown of EWS/FLI and EWS/ERG, respectively, and the differentially expressed genes were assessed using RNA-seq (A673 data is previously reported; ref. 40). We first analyzed the similarity between EWS/FLI and EWS/ERG transcriptional regulation, and found the overlap between these transcriptional profiles was significant by both χ^2 and GSEA (Supplementary Fig. S1C and S1D).

Having established similarity between the EWS/FLI and EWS/ERG transcriptional profiles, we next determined the global transcriptional signature of HCI2509 using RNA-seq in both A673 and TTC-466 cells. The comparison of the HCI2509 signature with both fusion proteins showed treatment with HCI2509 comprehensively reversed the transcriptional profiles driven by both EWS/FLI (Fig. 1B) and EWS/ERG (Fig. 1C). Thus, genes normally upregulated by EWS/FLI and EWS/ERG were downregulated by LSD1 inhibition with HCI2509, and vice versa. χ^2 analysis showed a statistically significant overlap between EWS/FLI-activated and HCI2509-downregulated genes and vice versa (Supplementary Fig. S1E). This was also true for the TTC-466 cell line (Supplementary Fig. S1F). Importantly, when either EWS/FLI- or EWS/ERG-upregulated target genes were analyzed with HCI2509-upregulated genes, and vice versa, no significant overlap was observed (data not shown). These results suggest substantial reversal of global transcriptional activity of both EWS/ETS fusions and highlights the importance of LSD1 in EWS/ETS-mediated transcriptional dysregulation, for both EWS/ETS-repressed and EWS/ETS-activated genes.

We alternatively compared HCI2509 and EWS/ETS transcriptional profiles using GSEA with a more stringent cutoff of a 4-fold change and FDR of 1×10^{-15} for the EWS/FLI gene set and a 3-fold change and FDR of 1×10^{-10} for the EWS/ERG gene set. The HCI2509 downregulated genes clustered significantly with upregulated EWS/ETS target genes and vice versa (Fig. 1D and E). This confirmed the mechanism of HCI2509 action specifically correlated to the EWS/ETS transcriptional function.

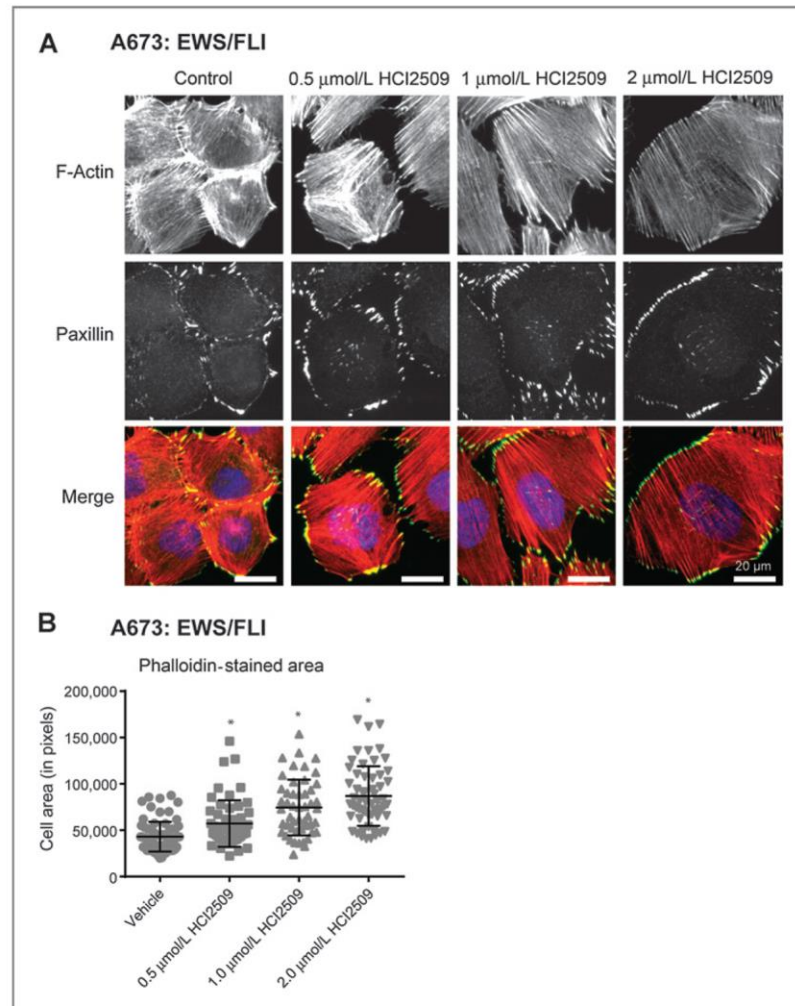
Because EWS/FLI interacts directly with the NuRD/LSD1 complex, we hypothesized the effects of LSD1 inhibition would be observed at genes regulated by direct binding of EWS/FLI. To test this, we compared the HCI2509 regulated gene list to a set of previously identified EWS/FLI direct target genes (38). GSEA showed significant correlation for genes both up- and downregulated directly by EWS/FLI in the HCI2509-regulated gene list (Supplementary Fig. S1G), suggesting that LSD1 is critical to the transcriptional function of EWS/FLI at its direct targets. Since HDAC2 and HDAC3 were previously shown to be directly recruited by EWS/FLI to mediate transcriptional repression (29), we also compared changes in gene expression mediated by the HDAC inhibitor vorinostat (30) to the EWS/FLI direct targets (38). As expected, genes that are directly repressed by EWS/FLI became derepressed with vorinostat treatment (Supplementary Fig. S1H). However, vorinostat had no effect on genes directly activated by EWS/FLI (Supplementary Fig. S1H). Together, these data illustrate that LSD1 inhibition has a unique dual effect in both transcriptional activation and repression mediated by EWS/FLI, whereas targeted inhibition of HDACs only blocks EWS/FLI-mediated transcriptional repression.

We next assessed the functional significance of the HCI2509 and EWS/ETS overlapping gene sets with the Database for Annotation, Visualization, and Integrated Discovery (DAVID). The most significant classes of genes downregulated by HCI2509 are related to DNA replication and cell cycle while the classes of genes upregulated by HCI2509 are related to regulation of cell death and extracellular matrix (Supplementary Fig. S1I and S1J). These are consistent with previously described molecular functions dependent upon EWS/FLI (41). We then used both A673 and TTC-466 cell lines to validate target genes from the HCI2509 RNA-seq profiles which have been identified as EWS/FLI targets critical for oncogenic transformation, survival, and differentiation (31, 42–48). Using quantitative reverse transcriptase PCR (qRT-PCR), genes activated by EWS/FLI, including *NKX2.2*, *CAV1*, *GSTM4*, *E2F1*, and *IGF1*, were all significantly downregulated in both cell lines with HCI2509 treatment. Conversely, genes repressed by EWS/FLI, including *RUNX2*, *IGFBP3*, *CDH1*, and *HMOX1*, were significantly upregulated in both cell lines after treatment (Fig. 1F). Using this 9 gene panel we tested other patient-derived Ewing sarcoma cell lines (EWS-502, SK-N-MC, SKES1, TC-71) to confirm the transcriptional effects of HCI2509 treatment were not cell line specific. Each cell line showed results congruent with A673 and TTC-466 cells (Supplementary Fig. S1K) indicating the disruption of EWS/ETS transcriptional activity by HCI2509 occurs in all tested Ewing sarcoma cell lines.

HCI2509 recapitulates morphologic phenotypes associated with EWS/FLI knockdown

The disruption of EWS/ETS transcriptional activity by HCI2509 should manifest in changes to cellular phenotypes associated with the presence of EWS/ETS. To test this, we first asked whether HCI2509 mimics the morphologic

Figure 2. Morphologic changes in A673 with HCl2509 treatment. A, immunofluorescence images of A673 cells treated with increasing doses of HCl2509 for 3 days. Staining was performed for F-actin stress fibers (red–phalloidin) and for focal adhesions (green–paxillin), and nuclei (blue). HCl2509 induced a dose-dependent increase in the cell spreading and morphology. B, cell area in pixels shows a dose-dependent increase in cell spreading with increasing doses of HCl2509. A673 cells were fixed and stained with phalloidin. Cell area was quantified as previously described (39). Data is plotted as Mean with SD and *P* values were calculated using a Student's *t*-test (*, *P* < 0.0001).



phenotypes associated with EWS/ETS knockdown. Ewing sarcoma is characterized histologically by small round blue-staining cells. In the context of EWS/FLI knockdown, cells display morphologic phenotypes typical of the putative mesenchymal stem cell cell-of-origin (39). EWS/FLI knockdown induces a robust actin cytoarchitecture with striking actin stress fibers anchored to integrin-based focal adhesions, increased cell adhesion, and spreading, that correlated with increased migration (39). To assess the effect of HCl2509 on cellular architecture, we performed immunofluorescence microscopy. Control A673 cells showed the characteristic small round cell phenotype of Ewing sarcoma with short, thin actin fibers (Fig. 2A and Supplementary Fig. S2A). Treatment with HCl2509 induced organizing of actin stress fibers throughout a well-spread cell, with robust

paxillin-containing focal adhesions (Fig. 2A and Supplementary Fig. S2A). Cell area of the phalloidin-stained cells was measured to quantify the effect. HCl2509-treated A673 cells showed a dose-dependent increase in cell area (Fig. 2B). To show observed morphologic changes were on target, we knocked down LSD1 using siRNA and assessed both cytoskeletal architecture and cell area. Consistent with the increased cell spreading phenotypes we observed with HCl2509 treatment, decreased LSD1 protein levels correlated with increased cell spreading (Supplementary Fig. S2B and S2C). TTC-466 likewise showed dose-dependent changes in actin staining, focal adhesions, and cell spreading (Supplementary Fig. S2D–S2F), suggesting treatment with HCl2509 generated the morphology associated with the loss of EWS/FLI.

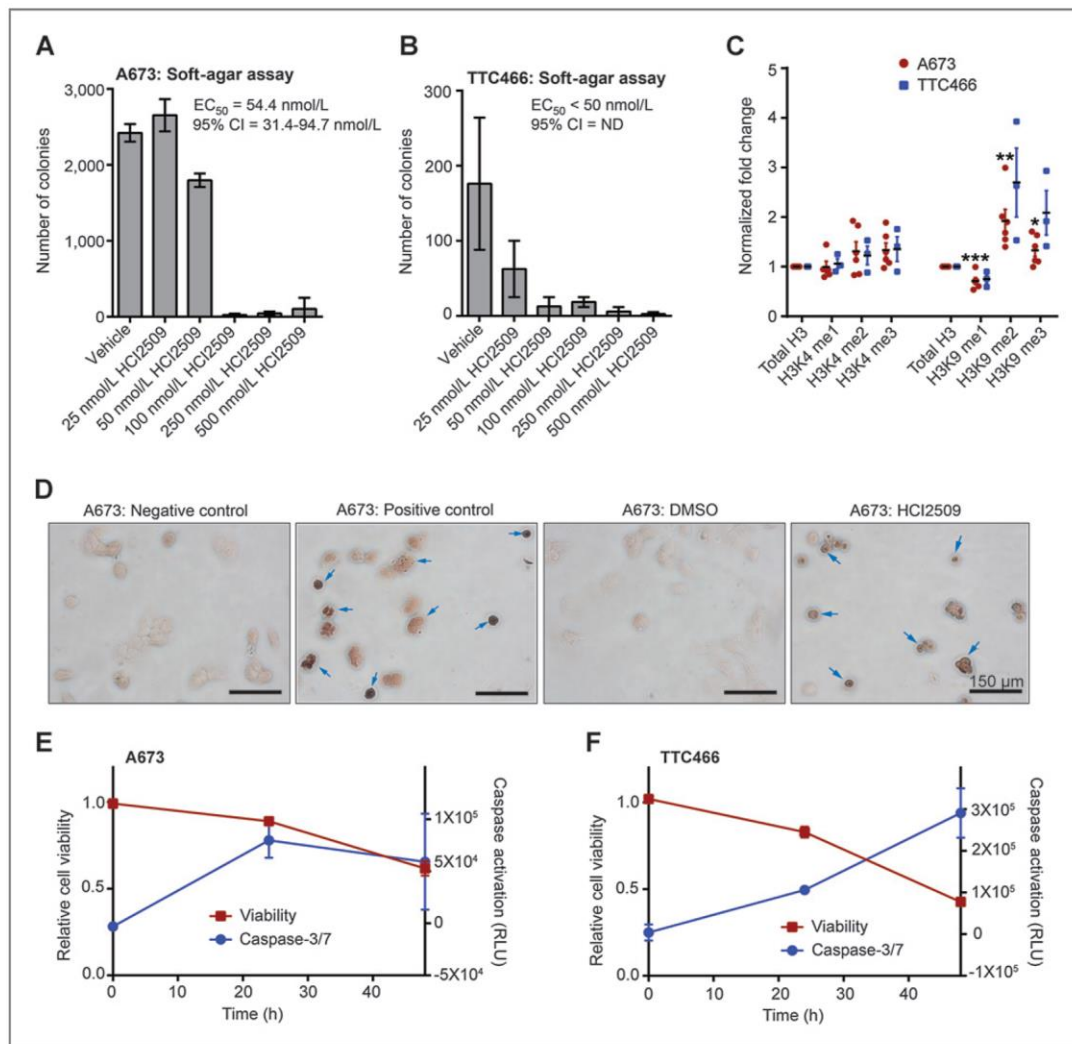


Figure 3. Mechanism of action of HCI2509 *in vitro*. A and B, quantification of colonies formed by (A) A673 cells and (B) TTC-466 cells treated with either vehicle (0.3% DMSO) or increasing doses of HCI2509. Error bars indicate SD of duplicate assays. EC_{50} values were determined using GraphPad Prism 6. C, quantification of global methylation changes at histone H3K4 and H3K9 in A673 (red, $n = 5$) and TTC-466 (blue, $n = 3$) following 48-hour treatment with 2 $\mu\text{mol/L}$ HCI2509. Methyl marks were assayed by Western blot analysis and the relative band intensities were quantified using ImageQuant (GE Healthcare Biosciences). Each sample was normalized to total H3 and fold change was determined in comparison with a vehicle control. Error bars indicate SEM and P values were calculated using a Student's t -test (*, $P = 4.25\text{E}-2$; **, $P = 1.07\text{E}-2$; ***, $P = 6.36\text{E}-3$). D, TUNEL staining of A673 cells treated with either vehicle (0.3% DMSO) or 2 $\mu\text{mol/L}$ HCI2509. Negative control indicates lack of labeling and positive control indicates DNase treatment with labeling. Arrows indicated TUNEL-positive cells. E and F, cell viability and caspase activation at 0, 24, and 48 hours in A673 (E) and TTC-466 cells (F) treated with 2 $\mu\text{mol/L}$ HCI2509. Measurements were normalized to their respective vehicle (0.3% DMSO) sample at the appropriate time point.

HCI2509 affects oncogenic transformation, histone methylation, and causes apoptosis

We next tested whether HCI2509 would impair EWS-ETS-driven oncogenic transformation using colony formation assays as a measure of anchorage-independent growth (Fig. 3A and B and Supplementary Fig. S3A–S3C). Interestingly, both the A673 and TTC-466 showed a shift in

sensitivity (Fig. 3A and B) to the low nanomolar range in three-dimensional cultures. Thus, the EC_{50} observed was significantly lower than those seen in viability assays (29).

Given the role of LSD1 in H3K4 and H3K9 demethylation, we also characterized changes in global histone methylation at these residues (Fig. 3C). Immunodetection of methylation status was quantified using densitometry for

statistical analysis. Due to the subtlety of the observed changes, several biologic replicates were performed. Interestingly, A673 cells showed no change in H3K4 monomethylation, and while H3K4 dimethylation (H3K4me2) and trimethylation (H3K4me3) trended higher, the effect was not statistically significant (Fig. 3C). However, H3K9 monomethylation (H3K9me1) significantly decreased, with a complementary increase in H3K9 dimethylation (H3K9me2) and trimethylation (H3K9me3; Fig. 3C). TTC-466 cells generally recapitulated the effects seen in A673 (Fig. 3C), but the results showed more variability.

We used DAVID analysis to examine the functional relevance of HCl2509 differentially expressed genes apart from the overlap with the EWS/FLI transcriptional profile (Supplementary Fig. S1E). Notably, genes upregulated by HCl2509 related to cell-cycle arrest and programmed cell death, while downregulated genes associated with S-phase, cell cycle, and proliferation (data not shown). Thus, HCl2509 likely reduces Ewing sarcoma cell viability (29) through induction of apoptosis. We therefore used TUNEL staining and caspase activation to assay whether HCl2509 triggered apoptosis. TUNEL-stained cells treated with HCl2509 for 48 hours showed increased staining as compared with vehicle (Fig. 3D). Similarly, treatment with HCl2509 showed increased activation of caspase-3/7 over 48 hours, which corresponded with decreased viability in multiple Ewing sarcoma cell lines (Fig. 3E and F and Supplementary Fig. S3D–S3F). Collectively, these data show HCl2509 not only reversed EWS/FLI-associated oncogenic phenotypes, but also altered H3K9 methylation status and induced apoptosis.

HMOX1 is an on-target response biomarker for HCl2509 treatment *in vitro*

Screening efforts to identify HCl2509 (33) suggested induction of *HMOX1* was an effect proportional to the biochemical potency of the inhibitor (Supplementary Fig. S4A). We evaluated whether *HMOX1* constituted biologic output to demonstrate target engagement. *HMOX1* was significantly upregulated by HCl2509 in both EWS/ETS transcriptional profiles. We assessed the regulation of *HMOX1* by alternative EWS/ETS fusions and found *HMOX1* was repressed across EWS/ETS fusions (Fig. 4A). Moreover, Venn Master analysis revealed *HMOX1* was one of 81 genes present in the overlap between EWS/FLI targets upregulated by HCl2509 and genes downregulated by EWS/FLI in primary Ewing sarcoma samples (ref. 41; Fig. 4B). On the basis of the repression of *HMOX1* in primary tumors and robust HCl2509-induced derepression across tested cell lines, we asked whether *HMOX1* protein also increased. We found *HMOX1* protein levels elevated with EWS/FLI knockdown returned to baseline levels with EWS/FLI re-expression (Fig. 4C) and likewise increased in response to HCl2509 (Fig. 4D).

We next asked whether *HMOX1* induction was dependent upon both LSD1 and EWS/FLI function. Targeted LSD1 ChIP showed enrichment at the *HMOX1* promoter (Fig. 4E). Both siRNA-mediated knockdown of LSD1 and

LSD1 inhibition with HCl2509 derepressed *HMOX1* in a dose-dependent manner (Fig. 4F and G). Moreover, this dose-dependent increase was validated at the protein level using ELISA (Fig. 4H). EWS/FLI knockdown resulted in similar *HMOX1* induction as 100 nmol/L LSD1 siRNA (Fig. 4I). *HMOX1* repression was restored with full-length EWS/FLI rescue; however, rescue with either the $\Delta 22$ mutant (49) lacking most of the EWS domain or the DNA-binding mutant R2L2 (50) failed to repress *HMOX1* (Fig. 4I and Supplementary Fig. S4B). This is consistent with other EWS/FLI-repressed targets (29), and jointly implicates the repressive function of the EWS domain together with the DNA-binding domain of FLI in suppressing *HMOX1* expression.

The necessity of the EWS domain raised the question about which corepressor complex EWS/FLI recruits to repress *HMOX1*. EWS/FLI is known to recruit the NuRD complex to enact repressive transcriptional activity at some target genes (29) so we first probed whether NuRD was responsible for *HMOX1* repression. Knockdown of the NuRD complex with CHD4-RNAi induced a 4.5-fold increase in *HMOX1* (Fig. 4J). RNAi-mediated knockdown of the REST, Co-REST, NcoR/SMRT, and Sin3A complexes were also evaluated. Only REST knockdown showed a significant, though lower magnitude, increase in *HMOX1* mRNA (Supplementary Fig. S4C). These results are consistent with recruitment of LSD1 by REST (51), but highlight the central role of the NuRD complex in repressing *HMOX1*.

Because *HMOX1* protein was strongly induced in cells treated with HCl2509 in addition to those with EWS/FLI knockdown, we investigated whether *HMOX1* affects cellular transformation. A673 cells overexpressing *HMOX1* (Supplementary Fig. S4D) showed little difference in doubling times compared with control (Supplementary Fig. S4E). In addition, oncogenic transformation was not affected in cells overexpressing *HMOX1* (Supplementary Fig. S4F). These findings support a model in which *HMOX1* is directly repressed by EWS/FLI-mediated recruitment of the NuRD complex with its associated LSD1 subunit, but does not play a role in proliferation or the oncogenic phenotype. Thus, in Ewing sarcoma *HMOX1* is a useful biologic readout of LSD1 inhibition and associated disruption of EWS/ETS transcriptional activity.

HCl2509 as a single agent significantly reduces tumor growth *in vivo*

Having observed HCl2509-mediated disruption of global EWS/ETS transcriptional function, reversal of EWS/ETS-associated morphologic and oncogenic phenotypes, and induction of apoptosis, we next investigated whether HCl2509 would impair tumorigenesis *in vivo*. In A673, SK-N-MC, and SKES1 xenograft models, daily intraperitoneal treatment with 30 mg/kg HCl2509 delayed tumor growth as a single agent (Fig. 5A and B and Supplementary Fig. S5A). Animal weights were recorded to monitor non-specific toxicity with none observed (Supplementary Fig. S5B–S5D). Blood counts were also examined due to

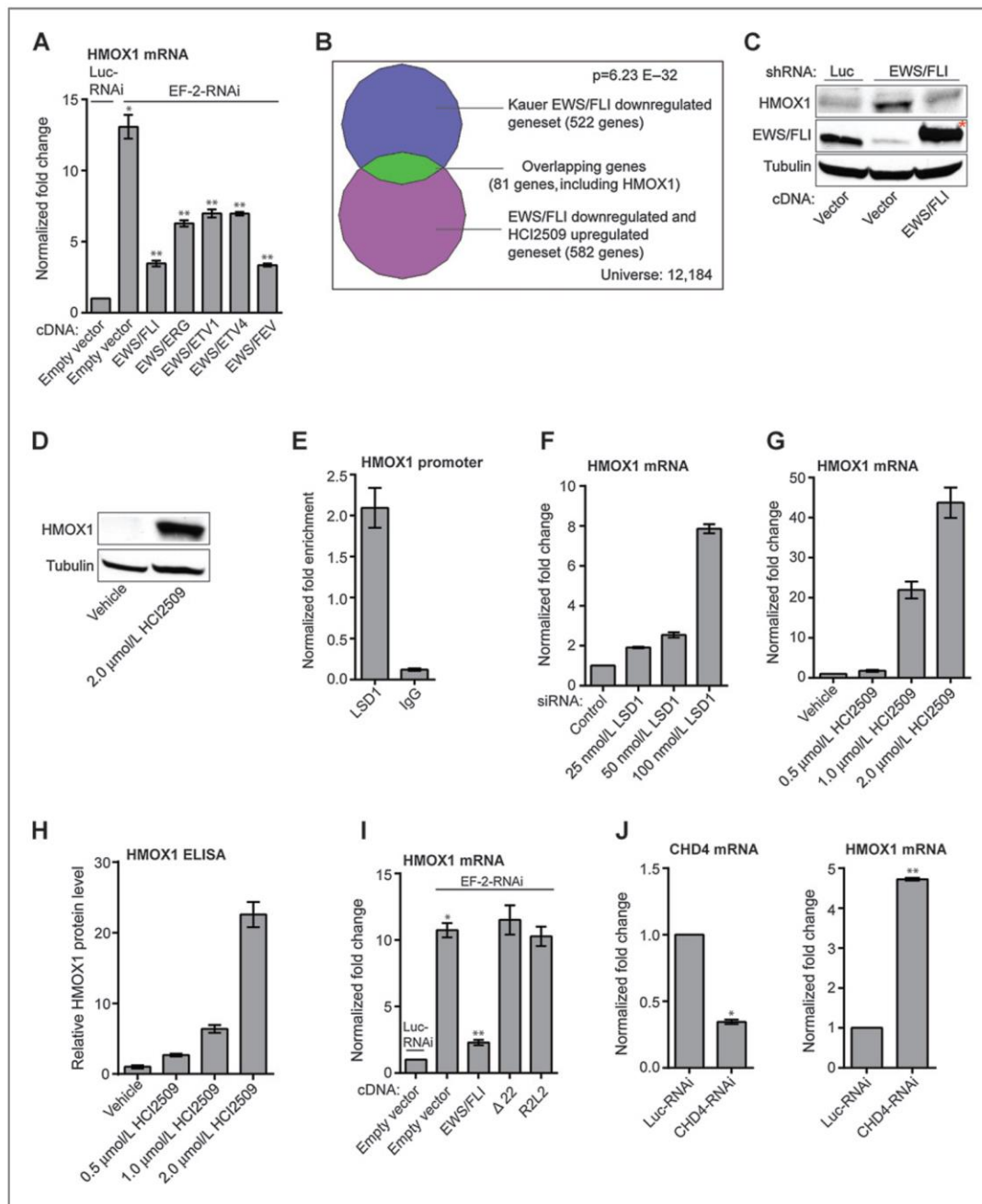


Figure 4. Regulation of HMOX1. A, validation of HMOX1 as a target gene of multiple EWS/ETS fusion. qRT-PCR analysis of HMOX1 in A673 cells infected with a control shRNA (Luc) or an EWS/FLI shRNA followed by rescue with an empty vector, an RNAi-resistant EWS/FLI, EWS/ETV1, EWS/ERG, EWS/ETV4, or EWS/FEV cDNA. Error bars indicate SD ($n = 3$). P values were calculated using Student's t -test. *, P value determined against Luc-RNAi/Empty vector ($P = 1.51E-5$). **, P values determined against EF-2-RNAi/Empty vector ($P \leq 2.79E-4$). B, Venn diagram representation of the HCl2509-upregulated and EWS/FLI-downregulated gene set (from Supplementary Fig. S1E) overlapped with EWS/FLI-downregulated targets in primary tissue samples. The χ^2 determined P value is indicated. (Continued on the following page.)

hematopoietic toxicity associated with LSD1 knockdown (52). During 4 weeks of treatment, no significant difference was observed between vehicle and treated groups (Supplementary Fig. S5E). Importantly, animals treated with HCI2509 showed improved survival over 60 days (Fig. 5C and D) as compared with vehicle in both A673 and SK-N-MC xenograft models.

We also evaluated HMOX1 in tumors from the A673 study using 6 tumors from the vehicle group and 6 tumors from the treatment group. HMOX1 RNA was elevated in three treatment tumors as compared with the control tumors (Fig. 5E). Moreover, this result was validated at the protein level with HMOX protein nearly undetectable in three representative control tumors and expressed in all three HCI2509-treated tumors with elevated HMOX1 mRNA (Fig. 5F). This suggested HCI2509 both engages LSD1 and disrupts EWS/FLI transcriptional activity *in vivo*. When considered with the impaired tumorigenesis and increased survival, these data substantiate LSD1 inhibition with HCI2509 as a potential therapeutic strategy for Ewing sarcoma.

Discussion

Our findings reveal a novel dual role for LSD1 in mediating both the transcriptional activating and repressive function of EWS/ETS fusions in Ewing sarcoma and modulating the oncogenic phenotypes resulting from the presence of EWS/ETS fusion proteins. Small-molecule blockade of LSD1 with the potent and reversible inhibitor, HCI2509, comprehensively disrupted the transcriptional signature of EWS/FLI and EWS/ERG as well as the subsequent downstream malignant characteristics of Ewing sarcoma cells as depicted in Fig. 6. Transcription factors are notoriously difficult targets for drug discovery and development programs and identification of small molecules which disrupt EWS/FLI has been an elusive goal (53). Recently, disruption of the c-Myc oncogenic transcription factor was achieved through targeted inhibition of the epigenetic reader BRD4 with the small-molecule inhibitor JQ1, which downregulated MYC transcription, decreased c-Myc protein, and disrupted c-Myc transcriptional function (54, 55). Our results likewise support an approach undermining oncogenic transcription factors by targeting their associated epigenetic machinery. The observed difference in transcriptional outcomes between LSD1 inhibition and HDAC inhibition with vorinostat (30) highlights the importance of selecting the correct target and demonstrates

the potential to tailor epigenetic therapy based on the context of the disease.

The A673 cell line has been used to investigate the transcriptional effects of EWS/FLI because it is relatively tolerant of EWS/FLI knockdown (31). While A673 cells expressing EWS/FLI shRNA lose transformation (31) and show morphologic characteristics similar to the putative cell-of-origin for Ewing sarcoma (39), cell growth and viability are not impaired. HCI2509 treatment largely reproduced the loss of transformation consistent with downregulation of EWS/ETS-activated targets and upregulation of EWS/ETS-repressed targets. However, unlike EWS/FLI knockdown, treatment with HCI2509 triggered caspase-dependent apoptosis in A673 cells. This effect was consistent across cell lines, suggesting additional mechanisms of action for HCI2509. Upon analysis of the genes regulated by HCI2509, but not overlapping with the EWS/FLI transcriptional profile we noted that in this context, HCI2509 upregulated genes associated with cell-cycle arrest and programmed cell death, while genes associated with S-phase, cell cycle, and proliferation were downregulated. This is consistent with both the observed apoptotic phenotype and the reported role for LSD1 in the maintenance of dedifferentiation in cancer (16–19, 56) and regulation of the cell cycle in stem-like cells (57–60). In addition, LSD1 is known to regulate non-histone proteins, including p53 (61). LSD1-mediated demethylation of p53 disrupts association of its cofactor 53BP1 and prevents induction of apoptosis (61). Thus, the sensitivity of Ewing sarcoma cell lines to LSD1 inhibition with HCI2509 may be the result of two tiers of LSD1-specific effects and this is reflected in the different EC₅₀s of the phenotypes described with treatment. Sankar and colleagues previously reported the EC₅₀ for HCI2509 in cell viability assays for multiple Ewing sarcoma cell lines ranging from 0.19 to 1.4 μmol/L (29). In this report, both A673 and TTC-466 cell lines show a loss of transformation in colony forming assays below 100 and 50 nmol/L of HCI2509 treatment, respectively. This suggests a model for HCI2509 mechanism of action in Ewing sarcoma where the first tier of effects disrupt the transforming function of EWS/ETS at concentrations much lower than the second tier of effects, which result in induction of apoptosis. Nonetheless, the proapoptotic effects of HCI2509 may be due to as yet undescribed off-target effects. However, we feel this is unlikely, as the only off-target for HCI2509 known to us is mild inhibition of CYP3A4 with a biochemical IC₅₀ of 2.61 μmol/L (33).

(Continued.) C and D, Western blot analysis of HMOX1 protein levels with EWS/FLI knockdown/rescue (B) and HCI2509 treatment (C). HMOX1 and EWS/FLI levels were assessed in A673 cells using anti-HMOX1 and anti-FLI antibodies. Tubulin was used as a loading control. (*) indicates the 3x-FLAG-tagged EWS/FLI cDNA that runs slightly higher than endogenous EWS/FLI. E, ChIP of LSD1 with the level of enrichment for LSD1 at the HMOX1 transcription start site plotted as normalized fold enrichment compared with the enrichment at BCL2L1 as a negative control. IgG was used as a negative antibody control. The error bars indicate SEM ($n = 3$). The Student's *t*-test determined *P* value is $1.10E-3$. F–J, validation of HMOX1 repression as on target. *P* values were calculated using a Student's *t*-test. qRT-PCR analysis of HMOX1 in A673 cells treated with: vehicle (F), 25 nmol/L ($P = 1.43E-5$), 50 nmol/L ($P = 3.05E-4$), and 100 nmol/L LSD1 siRNA ($P = 7.39E-6$) and vehicle (G), 0.5 μmol/L ($P = 3.65E-2$), 1 μmol/L (5.82E-4), and 2 μmol/L HCI2509 (3.48E-4). H, quantification of protein levels by ELISA for A673 cells treated with vehicle, 0.5 μmol/L ($P = 6E-4$), 1 μmol/L ($P = 1E-4$), and 2 μmol/L HCI2509 ($P = 1E-4$). I, qRT-PCR analysis of HMOX1 in A673 cells treated with (I) knockdown of EWS/FLI and rescue with full-length, Δ22, and R2L2 mutants. *, *P* value determined against Luc-RNAi/Empty vector ($P = 1.32E-6$). **, *P* value determined against EF-2-RNAi/Empty vector ($P = 3.99E-6$). J, qRT-PCR analysis of both CHD4 and HMOX1 mRNA in the presence of control or CHD4 RNAi. *, $P = 2.95E-7$; **, $P = 3.98E-9$. Error bars indicate SD ($n = 3$).

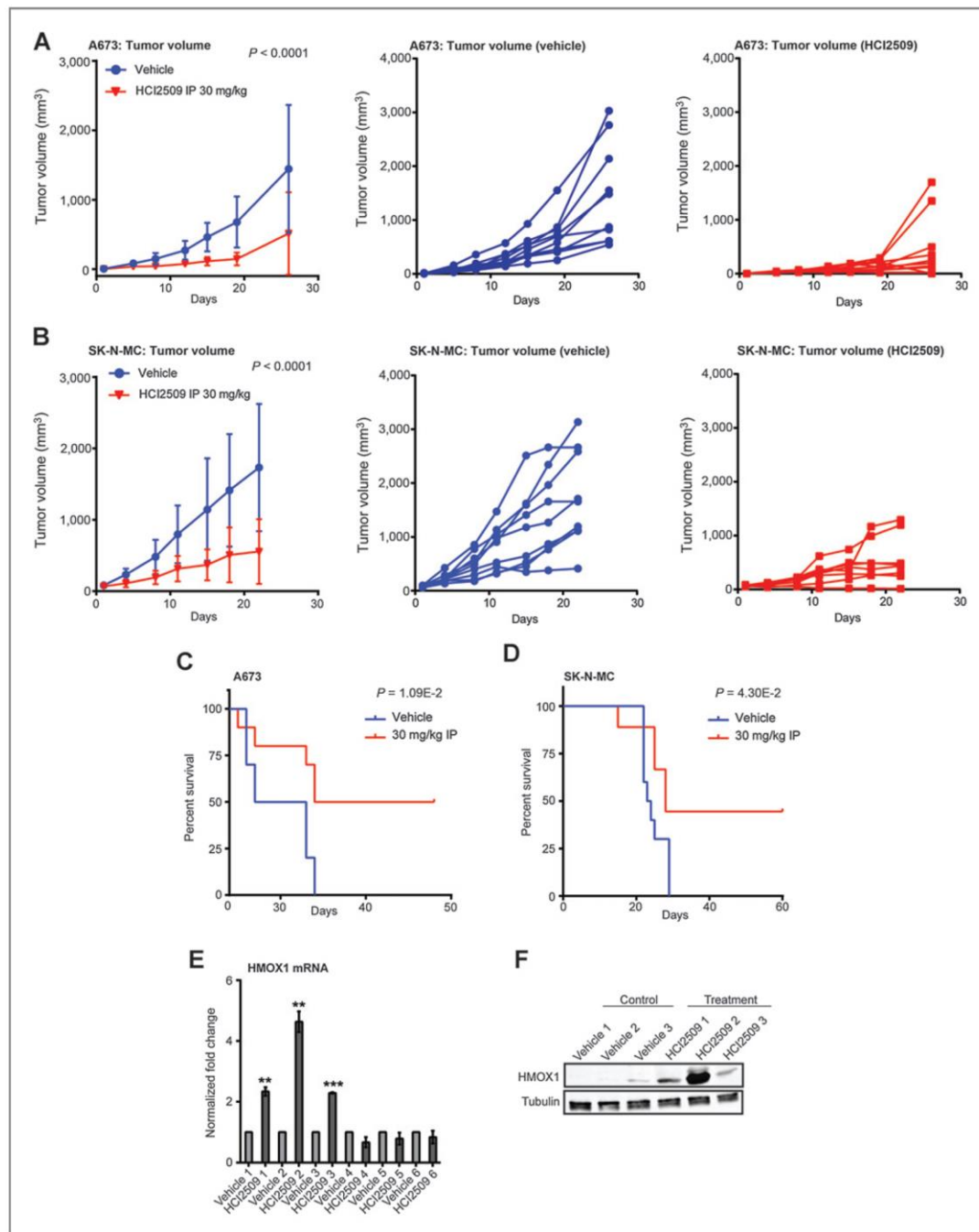
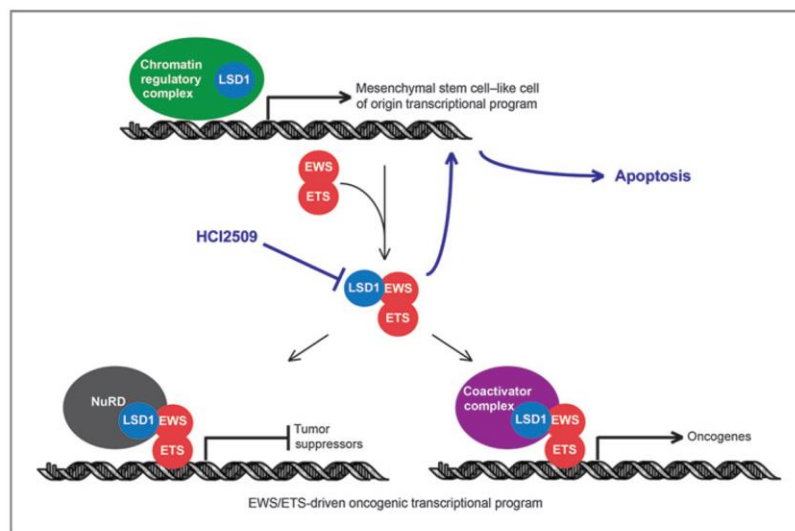


Figure 5. HCl2509 activity *in vivo*. A and B, *in vivo* subcutaneous hind-flank xenograft studies measuring tumor volume for animals bearing tumors grown from (A) A673 cells and (B) SK-N-MC cells. N = 10 for all groups, with the exception of SK-N-MC HCl2509-treated group as noted. For tumor volumes, P values were determined by two-way ANOVA comparing the treatment curve to the vehicle curve. Individual tumor growth curves are shown for the vehicle-treated (blue) and HCl2509-treated (red) groups. (Continued on the following page.)

Figure 6. Model for HCI2509 mechanism of action in Ewing sarcoma. HCI2509 treatment inhibits LSD1, which impairs the ability of EWS/ETS fusion proteins to globally alter gene expression. This leads, in part, to a reversion to the transcriptional program of the putative cell-of-origin and causes apoptosis.



Given its known capability to demethylate both H3K4 and H3K9 mono- and dimethyl marks, and its dual role in modulating activated and repressed genes, we were surprised to observe the only significant changes in global histone methylation occurring at the H3K9 residue. Methylation at H3K9 is typically associated with gene repression so this may be linked to the apparent role of LSD1 in EWS/ETS-mediated gene activation. LSD1-mediated demethylation of MTA1 causes a switch in the associated complex from the repressive NuRD complex to the activated NURF complex (62). In turn, NURF directs the demethylase activity of LSD1 toward H3K9 (62). This presents a plausible mechanism by which EWS/FLI recruits LSD1 as a member of the NuRD complex and is then able to enact both transcriptional activation and repression. Alternatively, LSD1 was recently described to mediate a global reduction in H3K9me2 during the epithelial-to-mesenchymal transition (EMT; ref. 63). Inhibition of LSD1 in this model impaired the cellular migration and chemoresistance resulting from EMT. It is possible that the observed increase in H3K9me2 in Ewing sarcoma cells may be due to a similar phenomenon. Additional studies are required to elucidate the molecular mechanisms choreographing whether LSD1 facilitates EWS/FLI-mediated transcriptional activation or repression and the genome-wide positioning of LSD1 histone substrates in the presence and absence of both EWS/FLI and HCI2509. The absence of significant changes at the

H3K4 mark may be due to limitations of our study design to assay global histone marks at the same time point as the transcriptional profiling. In embryonic stem cells, LSD1 was shown to mediate short-term changes at H3K4 important for cell-cycle progression and these changes may not have been observed in global methylation analyses at 48 hours (58).

Ewing sarcoma is an aggressive cancer for which few agents show single-agent efficacy *in vivo*. We assessed *HMOX1* induction in the A673 study and while most animals in the treatment group had delayed tumorigenesis, the endpoint study design did not allow us to assay *HMOX1* levels during earlier time points of treatment. Importantly, we were able to observe induction of *HMOX1* in a subset of tumors from the treated group as compared with the vehicle group. On the basis of our *in vitro* results we expected to see a more robust *HMOX1* induction in the context of antitumor efficacy. While the presence of an EWS/ETS fusion may predict a favorable response to an LSD1 inhibitor, these results underscore the difficulty in identifying of appropriate treatment response biomarkers in Ewing sarcoma.

On the basis of the dramatic transcriptional effects of HCI2509 described *in vitro*, we predict improved dosing will result in enhanced tumor regression in future studies with this class of LSD1 inhibitors. This is a critical hurdle for translation of this strategy to the clinic for Ewing sarcoma. Even with a preliminary preclinical formulation we were

(Continued.) C and D, survival curves for mice bearing subcutaneous hind-flank xenografts of A673 cells (C) or SK-N-MC cells (D). N = 10 for the A673 group. In the SK-N-MC treatment group, one mouse died due to a treatment-unrelated rash and was censored from further analysis. Therefore, in the SK-N-MC study, 10 and 9 mice were used for the vehicle and HCI2509 treatment groups, respectively. The mice were sacrificed once their tumors reached a size limit of 2 cm³. Percent survival was plotted as Kaplan-Meier survival curves using GraphPad Prism. The log-rank (Mantel-Cox Test) determined P values using GraphPad Prism are indicated. E and F, analysis of *HMOX1* expression by qRT-PCR (E) and Western blot analysis (F) in tumors from both vehicle and treatment A673 groups. Only the three tumors which showed an increase in *HMOX1* RNA (E) were used for Western blotting with three random vehicle tumors (F). *HMOX1* levels were assessed using an anti-*HMOX1* antibody. Tubulin was used as a loading control. Error bars indicate SD (*, P < 0.01; **, P < 0.001).

able to observe significant delay in tumor growth and improved survival out to 60 days. Optimization of formulation, salt forms, and synthesis of more soluble derivatives will allow fine tuning of drug exposure. Future studies are required to optimize dosing and determine whether or not LSD1 inhibition with HCI2509 is safe, tolerated, and synergistic with other clinically relevant treatment strategies for Ewing sarcoma, like irinotecan and temozolomide. Taken together, the dramatic effects of HCI2509 on the transcriptional activity of EWS/ETS fusions and its observed single-agent efficacy *in vivo* validate this class of LSD1 inhibitors as a potential targeted strategy to treat Ewing sarcoma.

Disclosure of Potential Conflicts of Interest

S. Sharma is an employee of and holds ownership interest (including patents) in Salaris Pharmaceuticals. S.L. Lessnick is a consultant/advisory board member for Salaris Pharmaceuticals. No potential conflicts of interest were disclosed by the other authors.

Authors' Contributions

Conception and design: S. Sankar, E.R. Theisen, M. Beckerle, S. Sharma, S.L. Lessnick

Development of methodology: S. Sankar, E.R. Theisen, S. Sharma, S.L. Lessnick

Acquisition of data (provided animals, acquired and managed patients, provided facilities, etc.): S. Sankar, E.R. Theisen, J. Bearss, T. Mulvihill, L.M. Hoffman

Analysis and interpretation of data (e.g., statistical analysis, biostatistics, computational analysis): S. Sankar, E.R. Theisen, S.L. Lessnick
Writing, review, and/or revision of the manuscript: S. Sankar, E.R. Theisen, L.M. Hoffman, V. Sorna, M. Beckerle, S. Sharma, S.L. Lessnick
Administrative, technical, or material support (i.e., reporting or organizing data, constructing databases): S. Sankar
Study supervision: M. Beckerle, S.L. Lessnick
Other (design and synthesis of the novel molecule used for this manuscript): V. Sorna

Grant Support

S.L. Lessnick was supported by NIH/NCI grant R01 CA140394. S.L. Lessnick and S. Sharma were supported by a Developmental Research Program subaward from the SARC Sarcoma SPORE (U54 CA168512). The Sunshine Project from the Pediatric Cancer Foundation, the Make Some Noise: Cure Kids Cancer Foundation, and the Alan B. Slika Foundation. S. Sankar was supported by the HHMI Med into Grad program at the University of Utah (U2M2G). E.R. Theisen was supported by the American Foundation for Pharmaceutical Education 2013 Pre-Doctoral Fellowship (AFPE), and T. Mulvihill was supported by the University of Utah MD/PhD Program. L.M. Hoffman and M. Beckerle were supported by NIH grant R01 GM50877. The authors also acknowledge support of funds in conjunction with NCI grant P30 CA042014 awarded to the Huntsman Cancer Institute, as well as funds from the Experimental Therapeutics Program at Huntsman Cancer Institute.

The costs of publication of this article were defrayed in part by the payment of page charges. This article must therefore be hereby marked *advertisement* in accordance with 18 U.S.C. Section 1734 solely to indicate this fact.

Received January 10, 2014; revised May 15, 2014; accepted June 10, 2014; published OnlineFirst June 24, 2014.

References

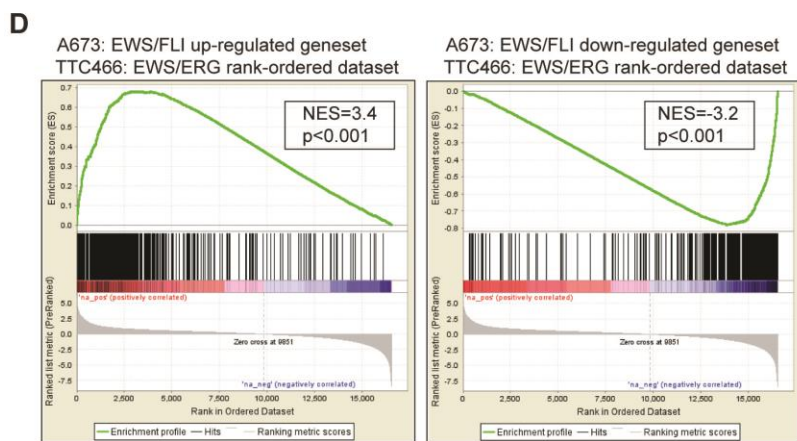
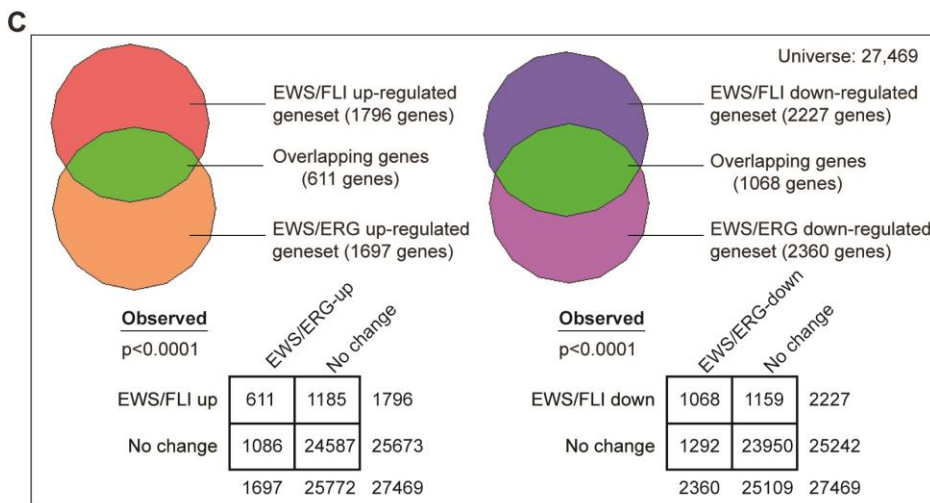
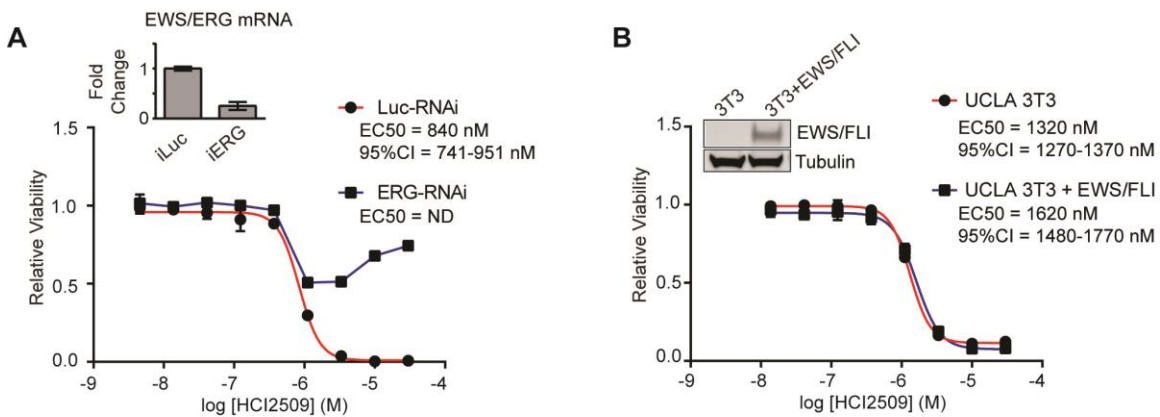
- Dawson MA, Kouzarides T. Cancer epigenetics: from mechanism to therapy. *Cell* 2012;150:12–27.
- Sharma S, Kelly TK, Jones PA. Epigenetics in cancer. *Carcinogenesis* 2010;31:27–36.
- Lachner M, O'Sullivan RJ, Jenuwein T. An epigenetic road map for histone lysine methylation. *J Cell Sci* 2003;116:2117–24.
- Stresemann C, Lyko F. Modes of action of the DNA methyltransferase inhibitors azacytidine and decitabine. *Int J Cancer* 2008;123:8–13.
- Choudhary C, Kumar C, Gnani F, Nielsen ML, Rehman M, Walther TC, et al. Lysine acetylation targets protein complexes and co-regulates major cellular functions. *Science* 2009;325:834–40.
- Kubicek S, Gilbert JC, Fomina-Yadlin D, Gitlin AD, Yuan Y, Wagner FF, et al. Chromatin-targeting small molecules cause class-specific transcriptional changes in pancreatic endocrine cells. *Proc Natl Acad Sci USA* 2012;109:5364–69.
- Islam AB, Richter WF, Lopez-Bigas N, Benevolenskaya EV. Selective targeting of histone methylation. *Cell Cycle* 2011;10:413–24.
- Popovic R, Licht JD. Emerging epigenetic targets and therapies in cancer medicine. *Cancer Discov* 2012;2:405–13.
- McCabe MT, Ott HM, Ganji G, Korenchuk S, Thompson C, Van Aller GS, et al. EZH2 inhibition as a therapeutic strategy for lymphoma with EZH2-activating mutations. *Nature* 2012;492:108–12.
- Popovic R, Zeleznik-Le NJ. MLL: How complex does it get? *J Cell Biochem* 2005;95:234–42.
- Hormaeche I, Licht JD. Chromatin modulation by oncogenic transcription factors: new complexity, new therapeutic targets. *Cancer Cell* 2007;11:475–78.
- Yoshimi A, Kurokawa M. Key roles of histone methyltransferase and demethylase in leukemogenesis. *J Cell Biochem* 2011;112:415–24.
- Hudlebusch HR, Santoni-Rugiu S, Simon R, Ralfkiaer E, Rossing HH, Johansen JV, et al. The histone methyltransferase and putative oncoprotein MMSET is overexpressed in a large variety of human tumors. *Clin Cancer Res* 2011;17:2919–33.
- Bernt KM, Zhu N, Sinha AU, Vempati S, Faber J, Krivtsov AV, et al. MLL-rearranged leukemia is dependent on aberrant H3K79 methylation by DOT1L. *Cancer Cell* 2011;20:66–78.
- Tian X, Zhang S, Liu H-M, Zhang Y-B, Blair CA, Mercola D, et al. Histone lysine-specific methyltransferases and demethylases in carcinogenesis: new targets for cancer therapy and prevention. *Curr Cancer Drug Targets* 2013;13:558–79.
- Schulte JH, Lim S, Schramm A, Friedrichs N, Koster J, Versteeg R, et al. Lysine-specific demethylase 1 is strongly expressed in poorly differentiated neuroblastoma: implications for therapy. *Cancer Res* 2009;69:2065–71.
- Harris WJ, Huang X, Lynch JT, Spencer GJ, Hitchin JR, Li Y, et al. The histone demethylase KDM1A sustains the oncogenic potential of MLL-AF9 leukemia stem cells. *Cancer Cell* 2012;21:473–87.
- Lim S, Janzer A, Becker A, Zimmer A, Schüle R, Buettner R, et al. Lysine-specific demethylase 1 (LSD1) is highly expressed in ER-negative breast cancers and a biomarker predicting aggressive biology. *Carcinogenesis* 2010;31:512–520.
- Kahl P, Gullotti L, Heukamp LC, Wolf S, Friedrichs N, Vorreuther R, et al. Androgen receptor coactivators lysine-specific histone demethylase 1 and four and a half LIM domain protein 2 predict risk of prostate cancer recurrence. *Cancer Res* 2006;66:11341–7.
- Hayami S, Kelly JD, Cho H-S, Yoshimatsu M, Unoki M, Tsunoda T, et al. Overexpression of LSD1 contributes to human carcinogenesis through chromatin regulation in various cancers. *Int J Cancer* 2011;128:574–86.
- Zhao Z-K, Yu H-F, Wang DR, Dong P, Chen L, Wu W-G, et al. Overexpression of lysine specific demethylase 1 predicts worse prognosis in primary hepatocellular carcinoma patients. *World J Gastroenterol* 2012;18:6651–6.
- Schildhaus H-U, Riegel R, Hartmann W, Steiner S, Wardelmann E, Merkelbach-Bruse S, et al. Lysine-specific demethylase 1 is highly expressed in solitary fibrous tumors, synovial sarcomas, rhabdomyosarcomas, desmoplastic small round cell tumors, and malignant peripheral nerve sheath tumors. *Hum Pathol* 2011;42:1667–75.
- Bennani-Baiti I-M, Machado I, Llombart-Bosch A, Kovar H. Lysine-specific demethylase 1 (LSD1/KDM1A/AOF2/BHC110) is expressed and is an epigenetic drug target in chondrosarcoma, Ewing's

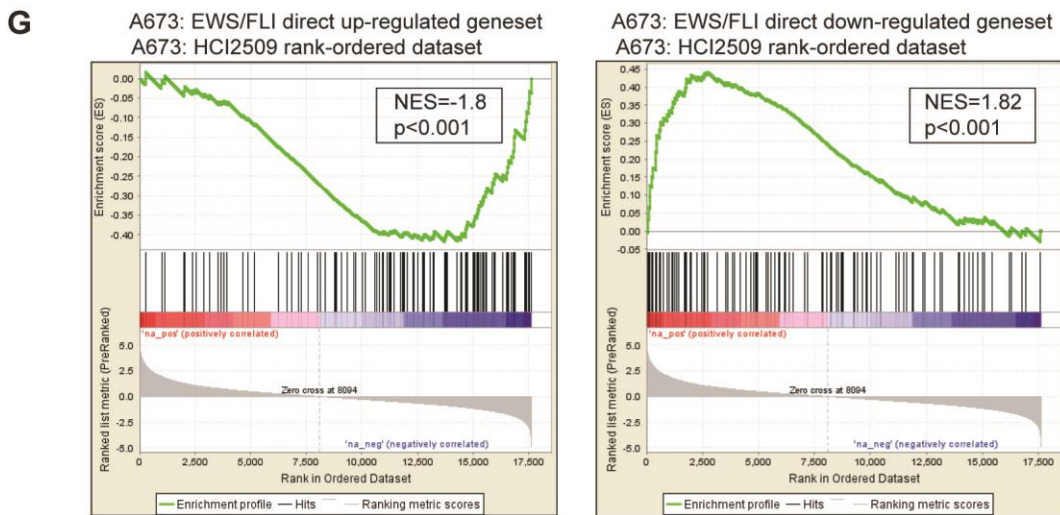
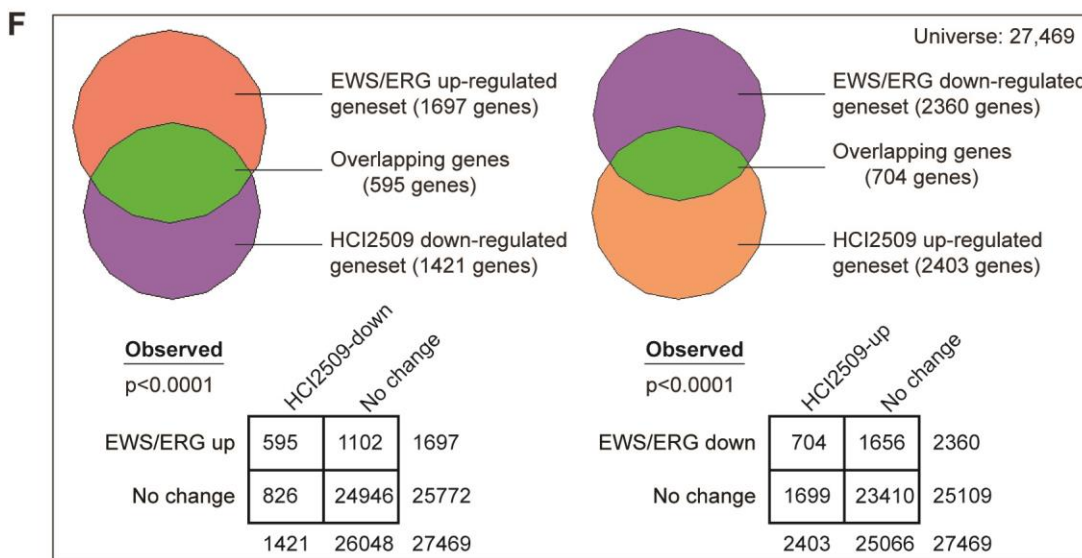
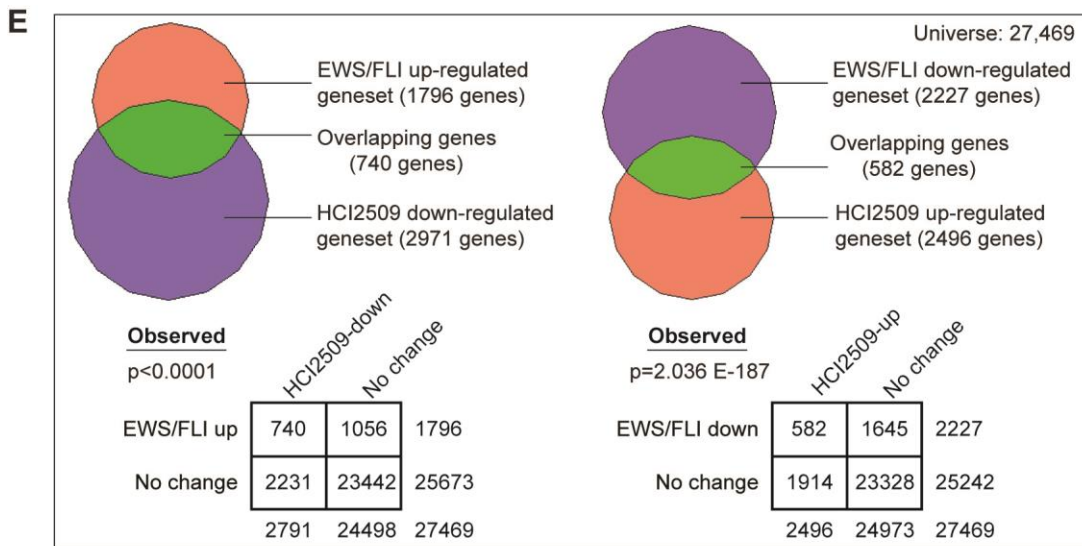
- sarcoma, osteosarcoma, and rhabdomyosarcoma. *Hum Pathol* 2012;43:1300–7.
24. Delattre O, Zucman J, Plougastel B, Desmaziere C, Melot T, Peter M, et al. Gene fusion with an ETS DNA-binding domain caused by chromosome translocation in human tumours. *Nature* 1992;359:162–5.
 25. Sankar S, Lessnick SL. Promiscuous partnerships in Ewing's sarcoma. *Cancer Genet* 2011;204:351–65.
 26. Linabery AM, Ross JA. Childhood and adolescent cancer survival in the U.S. by race and ethnicity (diagnostic period 1975–1999). *Cancer* 2008;113:2575–96.
 27. Randall RL, Lessnick SL, Jones KB, Gouw LG, Cummings JE, Cannon-Albright L, et al. Is there a predisposition gene for Ewing's sarcoma? *J Oncol* 2010;20:397632.
 28. D'Adamo DR. Appraising the current role of chemotherapy for the treatment of sarcoma. *Semin Oncol* 2011;38 Suppl 3:S19–29.
 29. Sankar S, Bell R, Stephens B, Zhuo R, Sharma S, Bearss DJ, et al. Mechanism and relevance of EWS/FLI-mediated transcriptional repression in Ewing sarcoma. *Oncogene* 2012;32:5089–100.
 30. Owen LA, Kowalewski AA, Lessnick SL. EWS/FLI mediates transcriptional repression via NKX2.2 during oncogenic transformation in Ewing's sarcoma. *PLoS ONE* 2008;3:e1965.
 31. Smith R, Owen LA, Trem DJ, Wong JS, Whangbo JS, Golub TR, et al. Expression profiling of EWS/FLI identifies NKX2.2 as a critical target gene in Ewing's sarcoma. *Cancer Cell* 2006;9:405–16.
 32. Braunreiter CL, Hancock JD, Coffin CM, Boucher KM, Lessnick SL. Expression of EWS-ETS fusions in NIH3T3 cells reveals significant differences to Ewing's sarcoma. *Cell Cycle* 2006;5:2753–9.
 33. Soma V, Theisen ER, Stephens B, Warner SL, Bearss DJ, Vankayalapati H, et al. High-throughput virtual screening identifies novel N¹-(1-phenylethylidene)-benzohydrazides as potent, specific, and reversible inhibitors of LSD1. *J Med Chem* 2013;56:9496–508.
 34. Kinsey M, Smith R, Lessnick SL. NR0B1 is required for the oncogenic phenotype mediated by EWS/FLI in Ewing's sarcoma. *Mol Cancer Res* 2006;4:851–9.
 35. Lessnick SL, Dacwag CS, Golub TR. The Ewing's sarcoma oncoprotein EWS/FLI induces a p53-dependent growth arrest in primary human fibroblasts. *Cancer Cell* 2002;1:393–401.
 36. May WA, Lessnick SL, Braun BS, Kiemsz M, Lewis BC, Lunsford LB, et al. The Ewing's sarcoma EWS/FLI-1 fusion gene encodes a more potent transcriptional activator and is a more powerful transforming gene than FLI-1. *Mol Cell Biol* 1993;13:7393–8.
 37. Hollenhorst PC, Shah AA, Hopkins C, Graves BJ. Genome-wide analyses reveal properties of redundant and specific promoter occupancy within the ETS gene family. *Genes Dev* 2007;21:1882–94.
 38. Gangwal K, Sankar S, Hollenhorst PC, Kinsey M, Haroldsen SC, Shah AA, et al. Microsatellites as EWS/FLI response elements in Ewing's sarcoma. *Proc Natl Acad Sci USA* 2008;105:10149–54.
 39. Chaturvedi A, Hoffman LM, Welm AL, Lessnick SL, Beckerle MC. The EWS/FLI oncogene drives changes in cellular morphology, adhesion, and migration in Ewing sarcoma. *Genes Cancer* 2012;3:102–16.
 40. Sankar S, Gomez NC, Bell R, Patel M, Davis IJ, Lessnick SL, et al. EWS and RE1-silencing transcription factor inhibit neuronal phenotype development and oncogenic transformation in Ewing sarcoma. *Genes Cancer* 2013;4:213–23.
 41. Kauer M, Ban J, Kofler R, Walker B, Davis S, Meltzer P, et al. A molecular function map of Ewing's sarcoma. *PLoS One* 2009;4:e5415.
 42. Tirado OM, Mateo-Lozano S, Villar J, Dettin LE, Llorca A, Gallego S, et al. Caveolin-1 (CAV1) is a target of EWS/FLI-1 and a key determinant of the oncogenic phenotype and tumorigenicity of Ewing's sarcoma cells. *Cancer Res* 2006;66:9937–47.
 43. Luo W, Gangwal K, Sankar S, Boucher KM, Thomas D, Lessnick SL. GSTM4 is a microsatellite-containing EWS/FLI target involved in Ewing's sarcoma oncogenesis and therapeutic resistance. *Oncogene* 2009;28:4126–32.
 44. Dauphinot L, De Oliveira C, Melot T, Sevenet N, Thomas V, Weissman BE, et al. Analysis of the expression of cell cycle regulators in Ewing cell lines: EWS-FLI-1 modulates p57KIP2 and c-Myc expression. *Oncogene* 2001;20:3258–65.
 45. Prieur A, Tirode F, Cohen P, Delattre O. EWS/FLI-1 silencing and gene profiling of Ewing cells reveal downstream oncogenic pathways and a crucial role for repression of insulin-like growth factor binding protein 3. *Mol Cell Biol* 2004;24:7275–83.
 46. Cironi L, Riggi N, Provero P, Wolf N, Suvà ML, Suvà D, et al. IGF1 is a common target gene of Ewing's sarcoma fusion proteins in mesenchymal progenitor cells. *PLoS One* 2008;3:e2634.
 47. Li X, McGee-Lawrence ME, Decker M, Westendorf JJ. The Ewing's sarcoma fusion protein, EWS-FLI, binds Runx2 and blocks osteoblast differentiation. *J Cell Biochem* 2010;111:933–43.
 48. Kang H-G, Jenabi JM, Zhang J, Keshelava N, Shimada H, May WA, et al. E-Cadherin cell-cell adhesion in Ewing tumor cells mediates suppression of anoikis through activation of the ErbB4 tyrosine kinase. *Cancer Res* 2007;67:3094–105.
 49. May WA, Gishizky ML, Lessnick SL, Lunsford LB, Lewis BC, Delattre O, et al. Ewing sarcoma 11;22 translocation produces a chimeric transcription factor that requires the DNA-binding domain encoded by FLI1 for transformation. *Proc Natl Acad Sci USA* 1993;90:5752–6.
 50. Bailly RA, Bosselut R, Zucman J, Cormier F, Delattre O, Roussel M, et al. DNA-binding and transcriptional activation properties of the EWS-FLI-1 fusion protein resulting from the t(11;22) translocation in Ewing sarcoma. *Mol Cell Biol* 1994;14:3230–41.
 51. Zheng D, Zhao K, Mehler MF. Profiling RE1/REST-mediated histone modifications in the human genome. *Genome Biol* 2009;10:R9.
 52. Sprüssel A, Schulte JH, Weber S, Necke M, Händschke K, Thor T, et al. Lysine-specific demethylase 1 restricts hematopoietic progenitor proliferation and is essential for terminal differentiation. *Leukemia* 2012;26:2039–51.
 53. Stegmaier K, Wong JS, Ross KN, Chow KT, Peck D, Wright RD, et al. Signature-based small molecule screening identifies cytosine arabinoside as an EWS/FLI modulator in Ewing sarcoma. *PLoS Med* 2007;4:e122.
 54. Mertz JA, Conery AR, Bryant BM, Sandy P, Balasubramanian S, Mele DA, et al. Targeting MYC dependence in cancer by inhibiting BET bromodomains. *Proc Natl Acad Sci USA* 2011;108:16669–74.
 55. Delmore JE, Issa GC, Lemieux ME, Rahl PB, Shi J, Jacobs HM, et al. BET bromodomain inhibition as a therapeutic strategy to target c-Myc. *Cell* 2011;146:904–17.
 56. Wang J, Lu F, Ren Q, Sun H, Xu Z, Lan R, et al. Novel histone demethylase LSD1 inhibitors selectively target cancer cells with pluripotent stem cell properties. *Cancer Res* 2011;71:7238–49.
 57. Chau CM, Deng Z, Kang H, Lieberman PM. Cell cycle association of the retinoblastoma protein Rb and the histone demethylase LSD1 with the Epstein-Barr virus latency promoter Cp. *J Virol* 2008;82:3428–37.
 58. Nair VD, Ge Y, Balasubramanian N, Kim J, Okawa Y, Chikina M, et al. Involvement of histone demethylase LSD1 in short-time-scale gene expression changes during cell cycle progression in embryonic stem cells. *Mol Cell Biol* 2012;32:4861–76.
 59. Scoumanne A, Chen X. The lysine-specific demethylase 1 is required for cell proliferation in both p53-dependent and -independent manners. *J Biol Chem* 2007;282:15471–5.
 60. Cho H-S, Suzuki T, Dohmae N, Hayami S, Unoki M, Yoshimatsu M, et al. Demethylation of RB regulator MYPT1 by histone demethylase LSD1 promotes cell cycle progression in cancer cells. *Cancer Res* 2011;71:655–60.
 61. Huang J, Sengupta R, Espejo AB, Lee MG, Dorsey JA, Richter M, et al. p53 is regulated by the lysine demethylase LSD1. *Nature* 2007;449:105–8.
 62. Nair SS, Li D-Q, Kumar R. A core chromatin remodeling factor instructs global chromatin signaling through multivalent reading of nucleosome codes. *Mol Cell* 2013;49:704–18.
 63. McDonald OG, Wu H, Timp W, Doi A, Feinberg AP. Genome-scale epigenetic reprogramming during epithelial to mesenchymal transition. *Nat Struct Mol Biol* 2011;18:867–74.

Supplementary Table S3.1. Primer Sequences for qRT-PCR analysis from RNA.

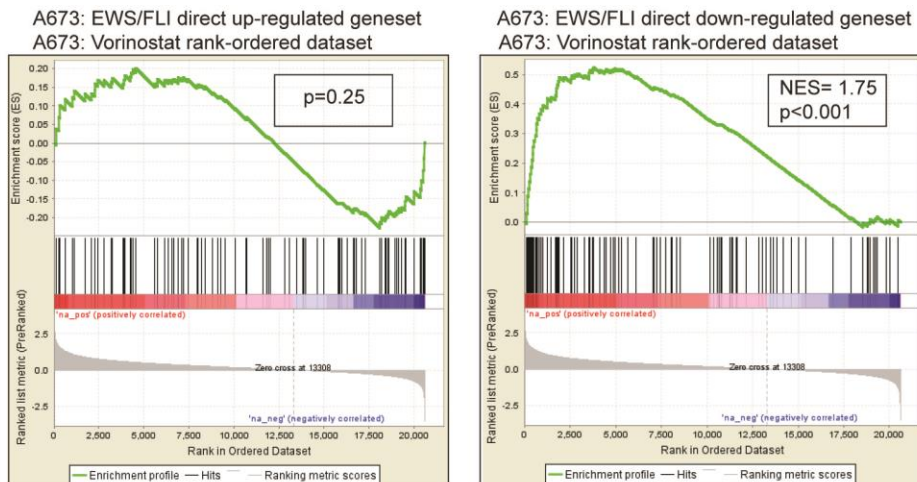
Gene	Forward	Reverse
NKX2-2	5' CTACGACAGCAGCGACAACC 3'	5' GCCTTGGAGAAAAGCACTCG 3'
CAV1	5' ATCGACCTGGTCAACCGCGAC 3'	5' CGAAGTAAATGCCCCAGATGA 3'
E2F1	5' GCCACTGACTCTGCCACCATA 3'	5' GGTGGGGAAAAGGCTGATGAAC 3'
IGF1	5' GAAGATGCACACCATGTCCTC 3'	5' CTCCAGCCTCCTTAGATCACA 3'
GSTM4	5' GCTGCCCTACTTGATTGATGG 3'	5' TGATTGGAGACGTCCATAGCC 3'
HMOX1	5' AACTTTCAGAAGGGCCAGGT 3'	5' GTAGACAGGGGCGAAGACTG 3'
IGFBP3	5' CATCAAGAAAGGGCATGCTAA 3'	5' CTACGGCAGGGACCATATTCT 3'
CDH1	5' TGCCCAGAAAATGAAAAAGG 3'	5' GTGTATGTGGCAATGCGTTC 3'
RUNX2	5' CCTCGGAGAGGTACCAGATG 3'	5' AACTCCTGCCTCGTCCACT 3'

Supplementary Figure S3.1. Transcriptional Profiling of HCI2509 in A673 and TTC-466. (A,B) Cell viability assay showing the difference in HCI2509 sensitivity between (A) TTC-466 cells with control and EWS/ERG knockdown or (B) NIH 3T3 cells with control and EWS/FLI expression. The dose-response curves were determined after 96 hours of treatment and normalized to the vehicle controls. $n=3$ for each point. Error bars denote standard deviation. EC_{50} and 95% CI were determined using GraphPad Prism 6. Note the line for ERG-RNAi data in (A) is a connecting line, not a curve fit. (C) Venn diagram representations of the overlap between the EWS/FLI and EWS/ERG transcription profiles, both generated by RNA-seq. Chi-square determined p-values are indicated with the observed contingency tables shown. (D) Gene set enrichment analysis (GSEA) using genes regulated by EWS/FLI in A673 cells (RNA-seq) as the rank-ordered dataset and the EWS/ERG-upregulated or the EWS/ERG-downregulated genesets (RNA-seq). Normalized enrichment scores (NES) and p-values are shown. (E,F) Venn diagram representations generated from respective RNA-seq data sets using default cutoffs (2-fold change, FDR=10%). (E) represents the overlap between the HCI2509 and the EWS/FLI-knockdown transcription profiles, both generated in A673 cells; (F) the overlap between the HCI2509 and the EWS/ERG-knockdown transcription profiles, both generated in TTC-466 cells. Chi-square determined p-values are indicated with the observed contingency tables shown. (G,H) GSEA using genes directly regulated by EWS/FLI in A673 cells (ChIP-chip and RNA-seq overlap) as the geneset and HCI2509 regulated genes in A673 cells (RNA-seq) as the rank-ordered dataset in (G) or the vorinostat regulated genes in A673 cells (microarray) as the rank-ordered dataset in (H). Normalized enrichment scores (NES) and p-values are shown. (I,J) Top ten categories from DAVID functional analysis of the (I) EWS/FLI up-/HCI2509 down- and EWS/FLI down-/HCI2509 upregulated genesets and (J) EWS/ERG up-/HCI2509 down- and EWS/ERG down-/HCI2509 upregulated genesets. The log transformed enrichment scores for each category are indicated on the x-axis. (K) Validation of *NKX2.2*, *CAVI*, *GSTM4*, *E2F1*, *IGF-1*, *RUNX2*, *IGFBP3*, *HMOX1* and *CDH1* as HCI2509 targets by qRT-PCR analysis using EWS-502, SK-ES-1, SK-N-MC, and TC-71 cells treated for 48 hours with vehicle or HCI2509 at $2 \times EC_{50}$. The p-value for each fold change is < 0.05 ($n=3$). Individual p-values are reported in Supplementary Table S2.

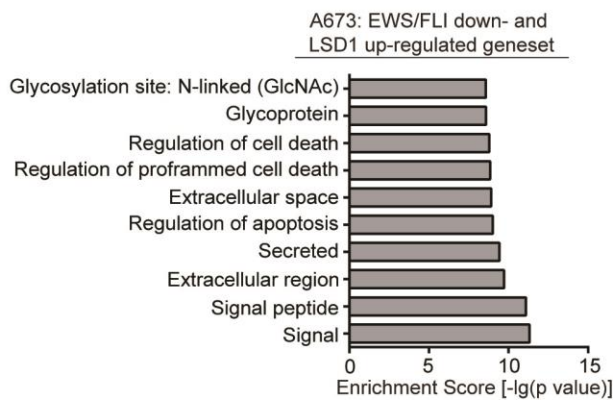
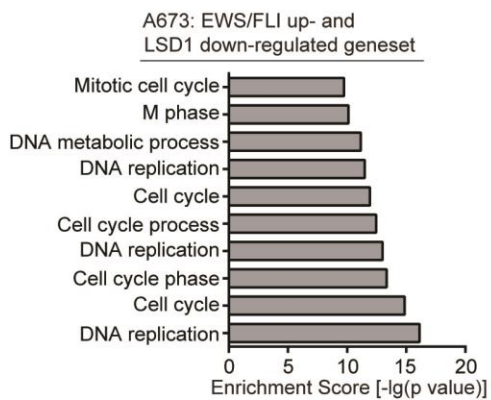




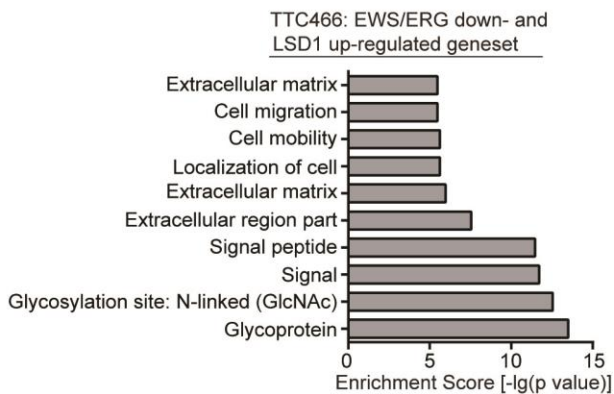
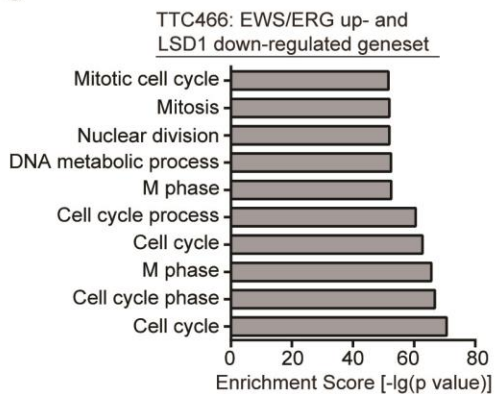
H

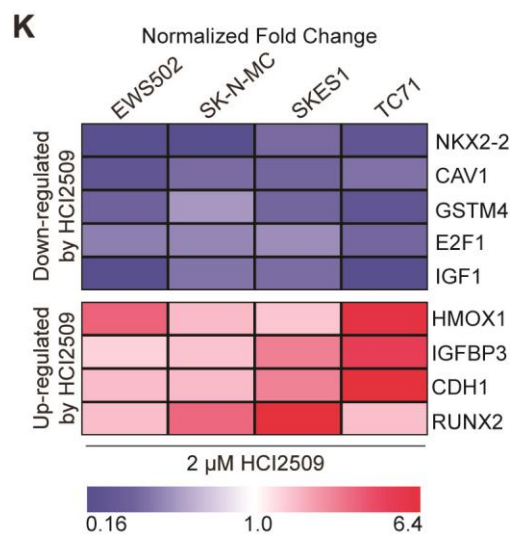


I



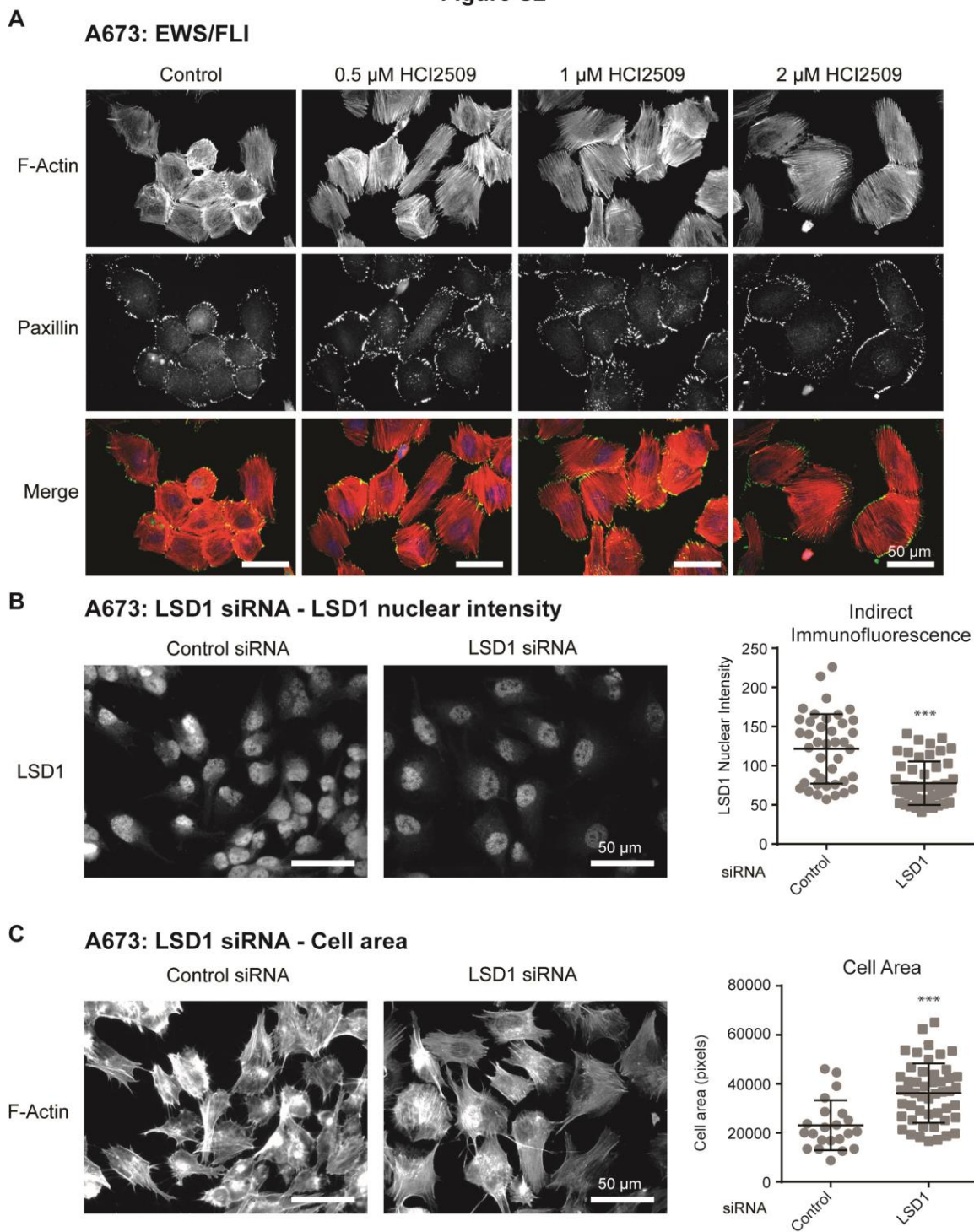
J

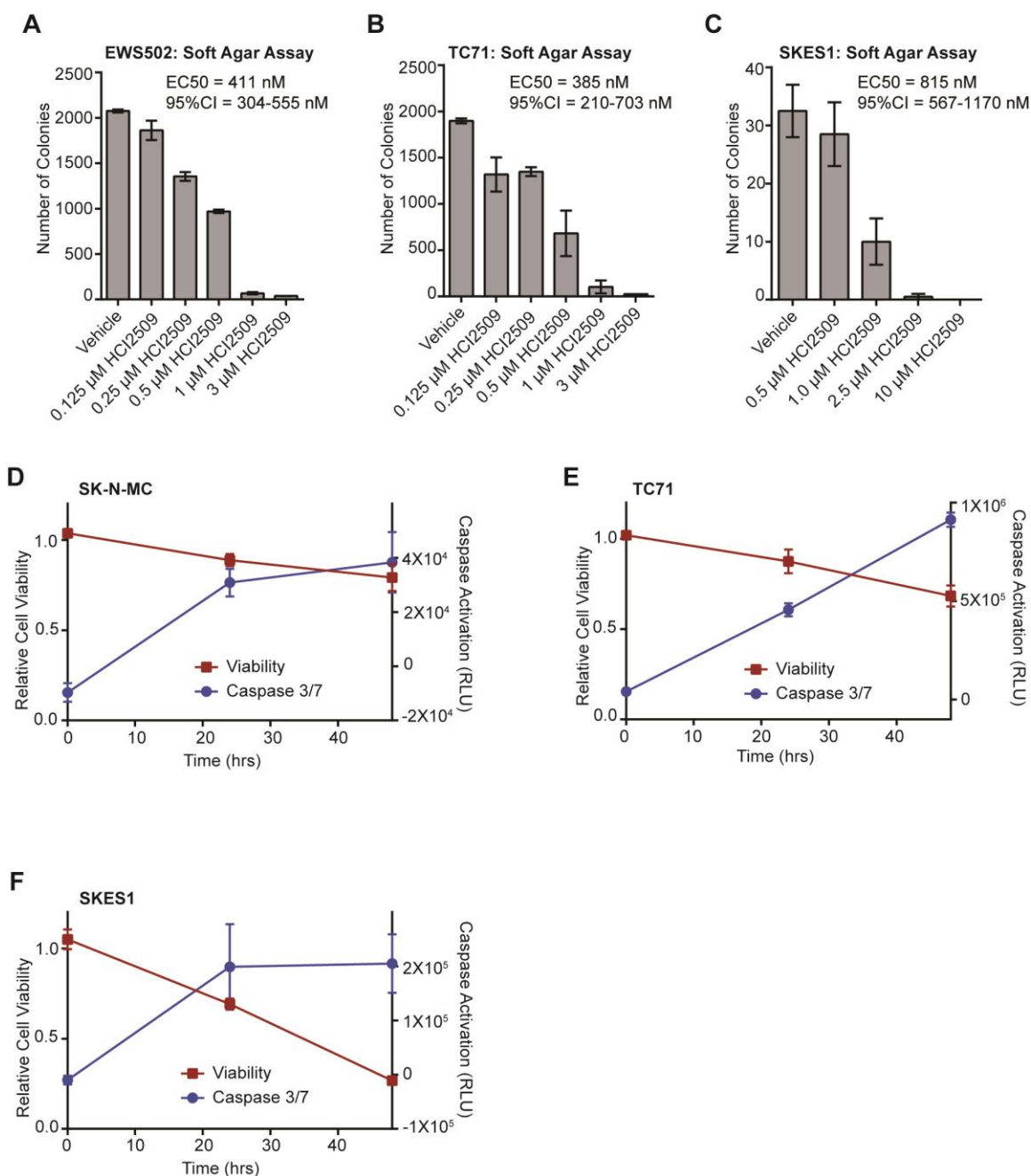




Supplementary Figure S3.2. Morphological changes with HCl2509 treatment (A) Whole-field immunofluorescence images of A673 cells treated with increasing doses of HCl2509 for 72 hours. Staining was performed for F-actin stress fibers (red – phalloidin) and for focal adhesions (green – paxillin), and nuclei (blue). HCl2509 induced a dose-dependent increase in the cell spreading and morphology. (B,C) Immunofluorescence images of A673 cells treated with either control siRNA or LSD1 siRNA 50 nM for 48 hours. Staining was performed for (B) LSD1 and (C) F-actin stress fibers. Measurements of LSD1 nuclear signal and cell area were performed on at least 6 fields for each transfection. Decrease in LSD1 nuclear signal correlated with more organized actin fibers and cell spreading. (D) Whole-field and (E) close up immunofluorescence images of TTC-466 cells treated with increasing doses of HCl2509 for 3 days. Staining was performed for F-actin stress fibers (red – phalloidin) and for focal adhesions (green – paxillin), and nuclei (blue). HCl2509 induced a dose-dependent increase in the cell spreading and morphology. (F) Measurement of cell area in pixels in phalloidin images shows a dose-dependent increase in cell spreading with of HCl2509. TTC-466 cells were fixed and stained with phalloidin. Cell area was quantified as previously described (39). Data is shown as scatter plot with mean plus standard deviation, and unpaired parametric t-test was used to determine p-values (* $p < 0.05$, *** $p < 0.0001$).

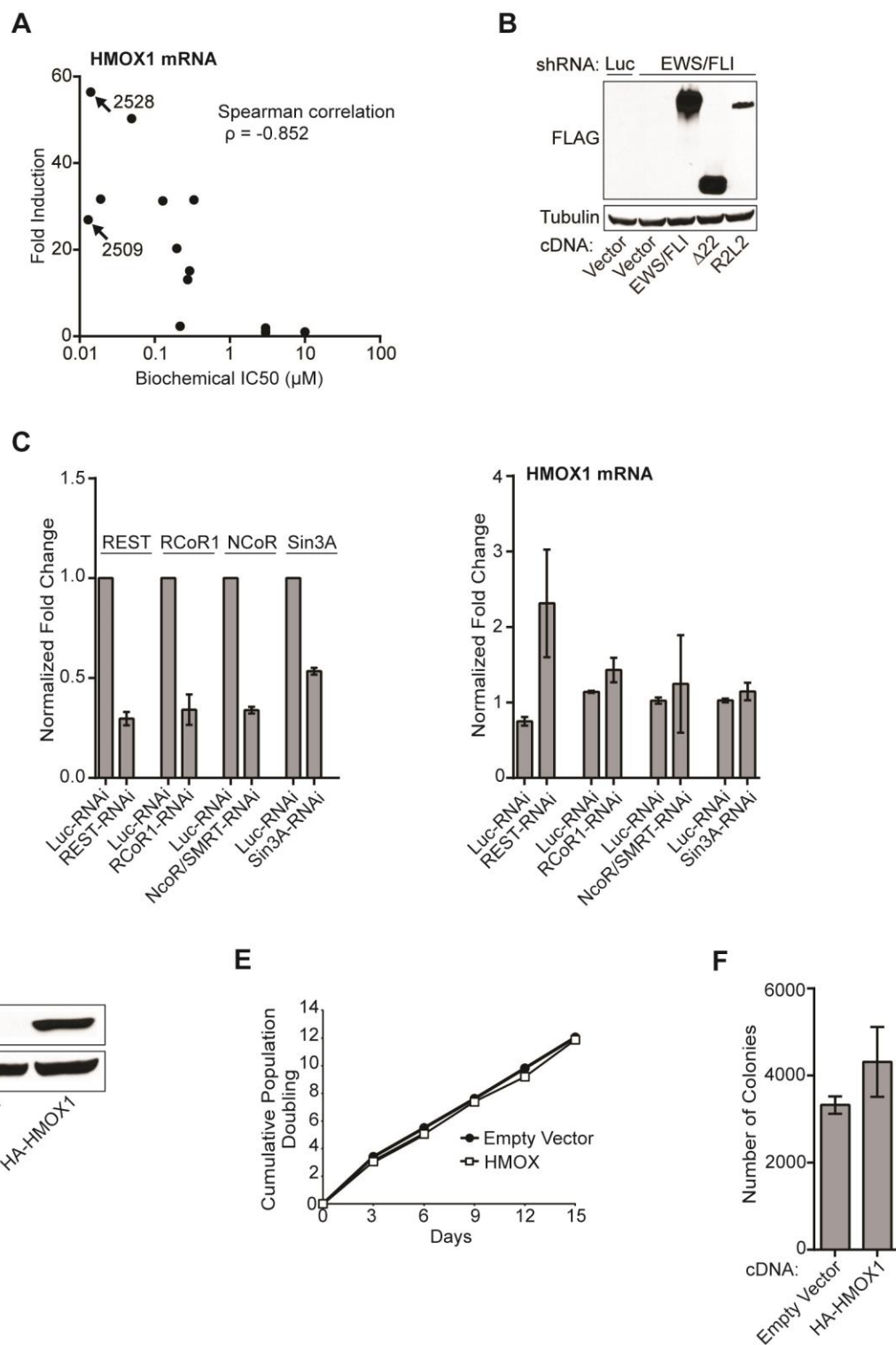
Figure S2

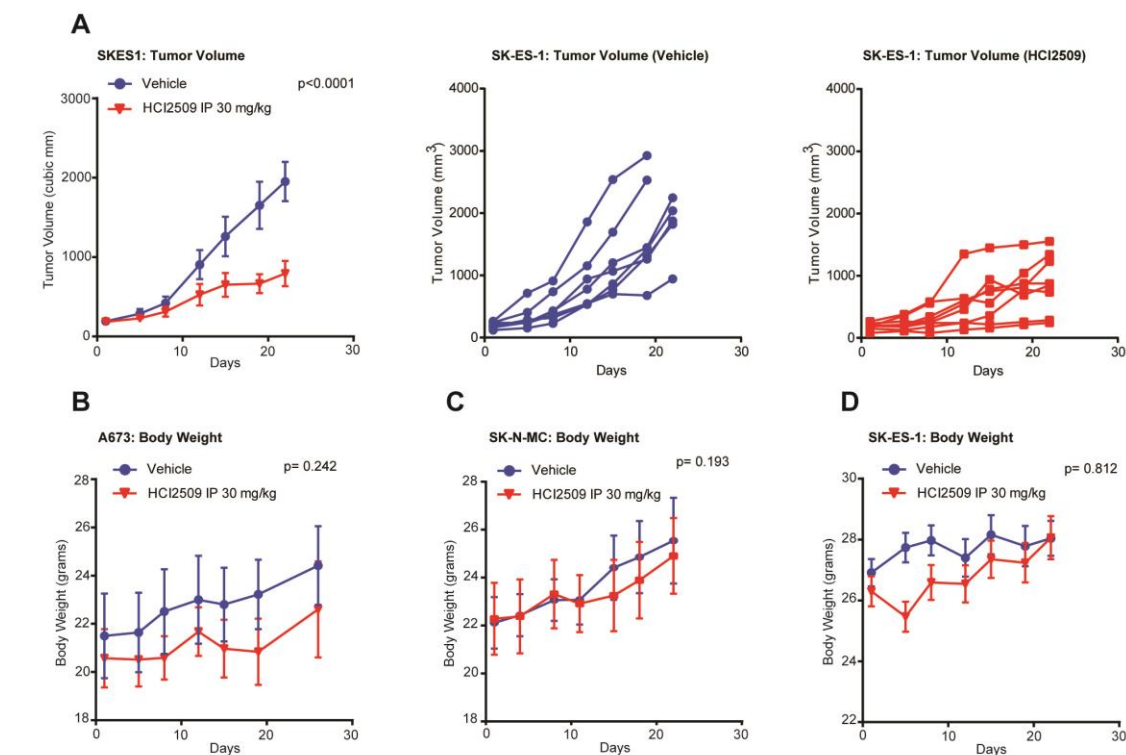




Supplementary Figure S3.3. Effects of HCl2509 on Transformation, Methylation, and Apoptosis. (A,B,C) Quantification of colonies formed by (A) EWS-502, (B) TC71, and (C) SK-ES-1 cells treated with either vehicle (0.3% DMSO) or varying doses of HCl2509. Error bars indicate SD of duplicate assays. EC₅₀ values were determined using GraphPad Prism 6. (D,E,F) Cell viability and caspase activation at 0, 24, and 48 hours in (D) SK-N-MC, (E) TC71, and (F) SK-ES-1 cells treated with 2xEC₅₀ HCl2509. Measurements were normalized to their respective vehicle (0.3% DMSO) sample at the appropriate time point. Error bars indicate SD (n=3).

Supplementary Figure S3.4. Regulation of HMOX1 in Ewing sarcoma. (A) qRT-PCR for HMOX1 induction following treatment with candidate LSD1 inhibitors with respect to inhibitor biochemical potency against LSD1 in a biochemical assay (Cayman Chemical). (B) Western blot analysis to demonstrate expression of the RNAi-resistant 3x-FLAG tagged EWS/FLI, $\Delta 22$, or R2L2 cDNA constructs using an anti-FLAG antibody in A673 cells expressing a control shRNA (Luc) or an EWS/FLI shRNA. Tubulin was used as the loading control. (C) qRT-PCR analysis to assess level of knockdown of various corepressors or *HMOX1* induction in A673 cells treated with either Luc-RNAi or RNAi for REST (REST $p=3.53E-6$, *HMOX1* $p=1.92E-2$), RCoR1 (RCoR1 $p=1.18E-4$, *HMOX1* $p=3.67E-2$), NCoR/SMRT (NCoR/SMRT $p=2.60E-7$, *HMOX1* $p=5.85E-1$), or Sin3A (Sin3A $p=1.27E-6$, *HMOX1* $p=1.57E-1$). Error bars indicate SD and p-values were determined using students t-test ($n=3$). (D) Western blot analysis for HMOX1 expression in A673 cells infected either with empty vector or an HA-tagged HMOX1 cDNA using an anti-HMOX1 antibody. Tubulin was used as a loading control. (E) Growth assays (3T5) for A673 cells described in (D). Student's t-test showed no significant difference in growth curves. (F) Quantification of colonies formed by A673 cells described in (D). Error bars indicate SD of duplicate assays.





E

Measurement	Vehicle Day 0	Vehicle Day 24	2509 Day 0	2509 Day 24	Normal Range
WBC ($\times 10^3/\mu\text{L}$)	6.53 ± 1.06	7.75 ± 4.13	9.15 ± 0.92	9.64 ± 3.25	2.6-10.1
HCT (%)	39.60 ± 6.76	42.75 ± 11.27	42.90 ± 12.44	44.20 ± 11.86	32.8-48.0
PLT ($\times 10^3/\mu\text{L}$)	230.75 ± 55.09	214.00 ± 61.97	177.75 ± 45.02	195.00 ± 45.02	250-1540

Supplementary Figure S3.5. Tumor volume, body weight and blood counts. (A) *In vivo* subcutaneous hind-flank xenograft studies measuring tumor volume for animals bearing tumors grown from (A) SK-ES-1 cells. The p-value was determined by 2-way ANOVA comparing the treatment curve to the vehicle curve. Individual tumor growth curves are shown for the vehicle-treated (blue) and HCl2509-treated (red) groups. (B,C,D) Body weight measurements for animals bearing tumors grown from (B) A673 cells, (C) SK-N-MC cells, and (D) SK-ES-1 cells. N=10 for all groups, with the exception of SK-N-MC HCl2509 treated group as noted. For body weights, the change in body weight normalized to day 0 was considered and a student's t-test was used to determine the p-value. (E) Blood counts for white blood cells (WBC), hematocrit (HCT), and platelets (PLT) from immunodeficient mice treated intraperitoneally either with vehicle or 40 mg/kg HCl2509 MWF for 24 days \pm SD. Blood was drawn using a cheek draw and assayed at both day 0 and day 24. The normal range is reported.

CHAPTER 4

REVERSIBLE INHIBITION OF LYSINE SPECIFIC DEMETHYLASE 1 IS A NOVEL ANTITUMOR STRATEGY FOR POORLY DIFFERENTIATED ENDOMETRIAL CARCINOMA

Emily Rose Theisen and Snehal Gajiwala performed the experiments and wrote the manuscript. Jared Bearss provided insight in experimental design. Sunil Sharma and Margit Janat-Amsbury designed and supervised the experiments and wrote the manuscript. Venkataswamy Sorna and Margit Janat-Amsbury contributed reagents, facilities, and personnel. All authors read and approved the final manuscript.

RESEARCH ARTICLE

Open Access

Reversible inhibition of lysine specific demethylase 1 is a novel anti-tumor strategy for poorly differentiated endometrial carcinoma

Emily R Theisen^{1,2}, Snehal Gajiwala¹, Jared Bearss¹, Venkataswamy Sorna¹, Sunil Sharma^{1,3} and Margit Janat-Amsbury^{2,4,5*}

Abstract

Background: Endometrial cancer is the most common gynecologic malignancy. Type II endometrial carcinoma is often poorly differentiated and patients diagnosed with Type II disease (~11%) are disproportionately represented in annual endometrial cancer deaths (48%). Recent genomic studies highlight mutations in chromatin regulators as drivers in Type II endometrial carcinoma tumorigenesis, suggesting the use of epigenetic targeted therapies could provide clinical benefit to these patients. We investigated the anti-tumor efficacy of the LSD1 inhibitor HCI2509 in two poorly differentiated Type II endometrial cancer cell lines AN3CA and KLE.

Methods: The effects of HCI2509 on viability, proliferation, anchorage-independent growth, global histone methylation, LSD1 target gene induction, cell cycle, caspase activation and TUNEL were assayed. KLE cells were used in an orthotopic xenograft model to assess the anti-tumor activity of HCI2509.

Results: Both AN3CA and KLE cells were sensitive to HCI2509 treatment with IC_{50} s near 500 nM for cell viability. Inhibition of LSD1 with HCI2509 caused decreased proliferation and anchorage independent growth in soft agar, elevated global histone methylation, and perturbed the cell cycle in both cell lines. These effects were largely dose-dependent. HCI2509 treatment also caused apoptotic cell death. Orthotopic implantation of KLE cells resulted in slow-growing and diffuse tumors throughout the abdomen. Tumor burden was distributed log-normally. Treatment with HCI2509 resulted 5/9 tumor regressions such that treatment and regressions were significantly associated ($p = 0.034$).

Conclusions: Our findings demonstrate the anti-cancer properties of the LSD1 inhibitor HCI2509 on poorly differentiated endometrial carcinoma cell lines, AN3CA and KLE. HCI2509 showed single-agent efficacy in orthotopic xenograft studies. Continued studies are needed to preclinically validate LSD1 inhibition as a therapeutic strategy for endometrial carcinoma.

Background

Endometrial carcinoma (EC) arises from the lining of the uterus and is the most commonly diagnosed invasive gynecologic malignancy, exceeding the incidence of cervical, ovarian, vaginal, and vulvar cancers combined [1,2]. With 50,230 new cases and 8,590 deaths estimated in the U.S. for 2014 it is the fourth most prevalent

cancer among women in developed countries, and the sixth worldwide [1,3,4]. Most patients present with low-grade early-stage disease, but patients diagnosed with more aggressive, high-grade, advanced disease that has spread beyond the uterus will progress within 1 year [5]. EC has been broadly classified into two subtypes based on differing clinico-pathologic characteristics. Over 80% of ECs are categorized as Type I endometrioid adenocarcinomas [6,7], while the remaining are Type II serous, clear-cell, poorly differentiated, and grade 3 endometrioid carcinomas [6,7]. Type I malignancies are associated with extended periods of elevated estrogen exposure, obesity, and estrogen and progesterone receptor positivity. These

* Correspondence: margit.janat-amsbury@hsc.utah.edu

²Department of Pharmaceutics and Pharmaceutical Chemistry, College of Pharmacy, University of Utah, Salt Lake City, UT, USA

⁴Department of Obstetrics and Gynecology, Division of Gynecologic Oncology, University of Utah, Salt Lake City, UT 84132, USA

Full list of author information is available at the end of the article



cancers present and are diagnosed in earlier stages and are typically more differentiated, responsive to progesterone treatment, and consequently have a more favorable prognosis [6,7]. Type I tumors are more common than Type II tumors in pre- and perimenopausal women [6]. On the other hand, Type II EC more frequently occurs in postmenopausal women and tumors are typically poorly differentiated [7]. Unlike Type I, Type II disease is unrelated to hyperestrogenic risk factors, diagnosed in later stages of the disease, and is clinically more aggressive. While representing only ~15% of all clinical cases Type II disease is responsible for around ~48% of endometrial cancer-related deaths, despite adjuvant chemotherapy and radiation, mainly due to metastasis and recurrent disease [7]. Better therapeutic strategies are needed for these patients.

No single hereditary risk factor plays a dominant role in endometrial cancer, which is driven by an interplay of genetic, environmental, and epigenetic factors. Several instances of epigenetic misregulation have been described in endometrial cancer. Specifically, alterations in DNA methylation have been broadly observed, with promoter hypermethylation leading to silencing of the progesterone receptor and other tumor suppressors like *MLH1*, *APC*, *MGMT*, and *PTEN* [8,9]. Hypomethylation at the *CD133* promoter has been observed in tumor initiating cells, suggesting epigenetic regulation does affect the mechanisms driving tumorigenicity and disease recurrence [10]. Additionally, the expression of various histone modifying enzymes are altered in endometrial cancer, including histone deacetylases as well as the histone methyltransferase *EZH2*. Their inhibition decreases proliferation and invasiveness in endometrial cancer cell lines [11-14]. Importantly, the advent of next generation sequencing has allowed further characterization of the molecular etiology of Type II EC, shedding more light on possible epigenetic targets and allowing for novel treatment options to be developed. Analysis of the genomic landscape of Type II EC identified somatic mutations in members of the nucleosome remodeling and deacetylase complex (NuRD), *CHD4* and *MBD3*, as well as mutations in the chromatin and transcriptional regulators *EP300*, *ARID1A*, and *TAF1* as candidate driver events [15-17]. While the functional significance of these mutations in Type II EC remains to be elucidated, these data underscore the significance of the interplay between genetic and epigenetic factors in the development, progression and prognosis of Type II EC.

Unlike genetic mutations, epigenetic changes, including DNA methylation and posttranslational modifications of histones, are dynamic and reversible through pharmacological intervention, such that the readers, writers, and erasers of epigenetic marks are emerging therapeutic targets [18,19]. Patterns of histone lysine methylation are maintained in a more cell-type specific manner than DNA methylation or histone acetylation, and it is thought that

pharmacologically modulating offending histone lysine methyltransferases or demethylases can confer increased therapeutic specificity and decreased dose-limiting off-target toxicities [20-23]. Lysine-specific demethylase 1 (LSD1) is a histone lysine demethylase with specificity for mono- and dimethylated histone H3 lysine 4 (H3K4) and lysine 9 (H3K9) [24,25]. Methylation at H3K4 is generally considered to be permissive, while H3K9 methylation is repressive [26]. LSD1 is upregulated in several malignancies and associated with decreased differentiation, aggressive tumor biology, and poor prognosis [27-34]. HCI2509 is a small molecule inhibitor of LSD1 that has shown *in vitro* anti-tumor efficacy in triple negative breast cancer, and single-agent *in vivo* efficacy in both Ewing sarcoma and castration-resistant prostate cancer [35-38]. A cell line panel showed one Type II EC cell line, AN3CA, to be sensitive to treatment with HCI2509 [35]. In this investigation, we validate this result in another Type II cell line, KLE, and further evaluate the mechanism of action by testing whether HCI2509 causes global changes in histone methylation, modulates the LSD1 target gene *HMOX1* and *CDH1*, and disrupts oncogenic transformation. More importantly, we also assess whether HCI2509 displays any anti-tumor efficacy *in vivo*. In order to most accurately represent disease spread mimicking human EC as well as more predictable therapeutic efficacy, we utilize an orthotopic xenograft mouse model to demonstrate the *in vivo* activity of HCI2509 against poorly differentiated Type II EC.

Methods

Antibodies and reagents

Immunodetection was performed with the following antibodies: anti- α -Tubulin (Calbiochem CP06), anti-LSD1 (Cell Signaling C69G12), anti-H3 (Cell Signaling Technology D2B12), anti-H3K4me3 (Cell Signaling Technology C42D8), anti-H3K9me2 (Cell Signaling Technology 9753), anti-H3K27me3 (Cell Signaling Technology C36B11). Propidium iodide (Sigma P4864), medroxyprogesterone 17-acetate (MPA; Sigma M1629). HCI2509 is previously described [35].

Cell culture, proliferation, colony formation assays, cell viability, and caspase 3/7 activation

Endometrial carcinoma cell lines AN3CA and KLE were obtained from ATCC and maintained in the DMEM/F12 supplemented with 10% FBS, 100 units/ml penicillin, and 100 μ g/ml streptomycin. All experiments were performed prior to passage 10. Proliferation assays (3T5) and colony formation assays were performed as previously described [39,40]. Cell viability and caspase activation were performed using Cell Titer-Glo and Caspase 3/7-Glo (Promega). The same vehicle (0.3% DMSO) was

used for both HCI2509 and MPA in all *in vitro* treatments.

Western blots and quantitative reverse-transcriptase polymerase chain reaction (qRT-PCR)

AN3CA and KLE cells were seeded in triplicate in 6-well dishes at a density of 3.5×10^5 cells/well or 2×10^5 cells/well, respectively. Cells were treated with varying concentrations of HCI2509 for 48 hours, harvested, and flash frozen for protein or RNA extraction. Total RNA was extracted from treated cells using an RNeasy Plus kit (Qiagen). cDNA was generated using qScript cDNA Super-Mix (Quanta Bioscience). Template was then amplified, detected, and quantified using SYBR green fluorescence. Each replicate was normalized to the internal house-keeping gene (RPL19) and induction was calculated relative to the vehicle control. The following primers were used: RPL19_fwd 5'-ATGTATCACAGCCTGTACCTG-3', RPL19_rev 5'-TTCTTGGTCTCTTCCTCCTTG-3'; HM OX1_fwd 5'-AACTTTCAGAAGGGCCAGGT-3', HMO X1_rev 5'-GTAGACAGGGGCGAAGACTG-3'; CDH1_fwd 5'-TGCCCAGAAAATGAAAAAGG-3', CDH1_rev 5'-GTGTATGTGGCAATGCGTTC-3'.

Cell cycle analysis

1×10^6 cells (KLE, AN3CA) were seeded in 10 cm dishes and treated with either vehicle alone or HCI2509 for the appropriate duration, trypsinized, centrifuged at 1000 rcf for 5 min, and fixed in ice cold 70% ethanol. Staining was performed by centrifuging 1.5×10^6 fixed cells at 770 rcf for 5 minutes, aspirating ethanol, and resuspending in 350 μ L of staining buffer (4 mM citrate, 3% PEG8000, 50 μ g/mL propidium iodide (PI), 180 units/mL RNase, 0.1% Triton X-100) incubating at 37°C for 20 minutes, and adding 350 μ L of salting buffer (400 mM NaCl, 3% PEG8000, 50 μ g/mL PI, 0.1% Triton X-100). Cells were analyzed on a BD FACSCanto with Software Diva vs6.1.3 (BD Biosciences San Jose CA).

TUNEL and fluorescence microscopy

9×10^4 AN3CA cells or 3×10^4 KLE cells were seeded onto glass coverslips in a 12-well dish. Cells were treated with either vehicle or 3 X EC50 HCI2509 for 72 hours to correlate with the caspase activation assay. Cells were fixed in formalin and stained with the DeadEnd Fluorescent TUNEL system (Promega). DNase treatment and no labeling reaction were used as positive and negative internal controls, respectively. Cells were then stained with AlexaFluor Phalloidin (1:100) (Molecular Probes) and DAPI (0.3 μ M) (Molecular Probes). Fluorescent cell images were collected on a Zeiss Axioskop2 mot plus microscope with a 40X dry objective (NA 0.75 NeoFluor), AxioCam MR camera, and Axiovision v4.8.1 software (Carl Zeiss MicroImaging, Inc.).

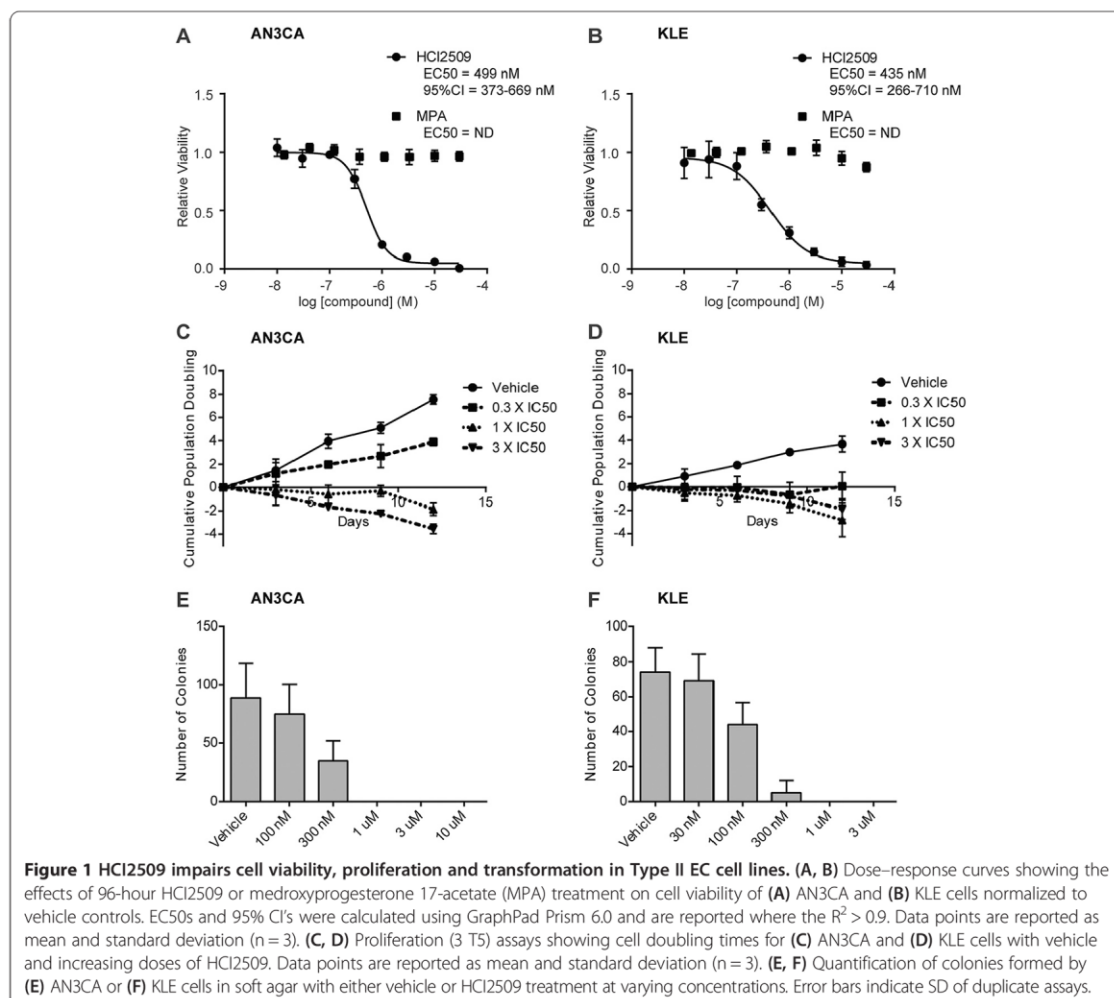
In vivo xenograft studies

All xenograft experiments were performed in accordance with protocol 11-12001 approved by the University of Utah IACUC. Female nude mice (strain J:Nu) were purchased from Jackson Laboratory (Bar Harbor, ME) and housed under appropriate conditions. Mice were anesthetized with 100 mg/kg ketamine and 10 mg/kg xylazine and surgical procedures were carried out in a clean room on a circulating water warming pad set to 38°C. A frontal midline incision was made to enter the peritoneal cavity and 2×10^6 KLE cells expressing luciferase were implanted into the bifurcation of the uterus in 50 μ L of 1:1 DMEM/F12:Matrigel (Corning). Following tumor cell implantation, the peritoneum and skin were each sutured separately and recovery was assessed daily for 7 days by weight measurements and visual inspection. VivoGlo Luciferin (Promega) was resuspended in PBS at a concentration of 30 mg/ml and passed through a 0.22 μ M filter. Mice were imaged on day 7 using an IVIS Spectrum (PerkinElmer). Images were acquired 10 minutes after intraperitoneal (IP) administration of 100 μ L luciferin. Mice with detectable tumor on day 7 were randomized into three groups: Vehicle only (n = 7; 100 μ L 1:1 PBS:PEG400 IP daily), HCI2509 30 mg/kg (n = 9; 100 μ L suspension IP daily), or untreated (n = 3). Body weight was tracked three times per week and luminescence was tracked weekly for the entire treatment period of 35 days. At day 42 of the study, mice were sacrificed, organs including uteri harvested and weighed, and fixed in formalin prior to paraffin embedding.

Results

HCI2509 impairs viability, proliferation, and transformation in Type II endometrial cancer cell lines

We first validated previous data suggesting that Type II endometrial carcinoma cells were sensitive to LSD1 inhibition with HCI2509 [35]. Both AN3CA and KLE cell lines exhibited a dose-dependent decrease in cell viability after 96 hours of treatment with HCI2509 (Figure 1A, B) with EC₅₀ values determined at 499 nM and 435 nM, respectively (Figure 1A, B). In separate experiments, treatment with medroxyprogesterone 17-acetate (MPA) showed no effect on cell viability, confirming that both cell lines exhibit resistance to hormone treatment (Figure 1A, B). Having determined the EC₅₀ we next tested the effect of HCI2509 on population doubling times using a 3T5 proliferation assay in treatment conditions below and above the EC₅₀ (Figure 1C, D). HCI2509 decreased proliferation rates in a dose dependent manner in both AN3CA and KLE cell lines. Interestingly, even the lowest tested treatment concentration (0.3 X IC₅₀) resulted in cytostasis in KLE cells. At and above the IC₅₀, both cell lines exhibited negative growth, suggesting cell death.



In addition to the anti-proliferative effects seen in the 2-dimensional viability and proliferation assays, we also tested the ability of HCl2509 to impair anchorage-independent growth in soft agar. Cells were tested for colony formation at a range of concentrations spanning 30 nM to 10 μ M. Based on the increased sensitivity of the KLE cells in the proliferation assay, the dose range tested in agars was shifted one half-log lower than that for AN3CA cells. HCl2509 impaired colony formation in both cell lines in a dose-dependent manner (Figure 1E, F). Above the viability EC₅₀ for both cell lines, anchorage-independent growth was ablated, and at concentrations below the EC₅₀ for KLE cells, colony formation was reduced, suggesting that HCl2509 impaired transformation at concentrations lower than those for which it induces cell death in KLE cells. AN3CA cells showed reduced colony formation near the viability EC₅₀.

LSD1 inhibition results in global histone methylation changes and induction of LSD1 target genes

LSD1 is the primary histone demethylase for the cell and having demonstrated dose-dependent effects on viability, proliferation, and transformation, we next investigated whether HCl2509 treatment also caused dose-dependent increases in histone methylation marks. We evaluated both LSD1 histone substrates, H3K4 and H3K9. Analysis of H3K4me1 and H3K4me2 showed no effect of HCl2509 treatment on the monomethyl mark and accumulation of H3K4me2 in only AN3CA cells (Additional file 1: Figure S2A, B). We next asked whether at 48 hours impaired demethylation of H3K4 may result in accumulation of the H3K4 trimethyl mark. While trimethyllysine is not chemically accessible to LSD1, the effect of demethylation at promoter H3K4 is gene repression, and impaired demethylation at that

mark may result in increased levels of the transcriptionally activating H3K4me3 chromatin. Additionally, H3K4me3 is depleted in an LSD1-dependent fashion during the epithelial-to-mesenchymal transition (EMT) [41]. HCI2509 treatment resulted in a dose-dependent increase in H3K4me3 in both cell lines (Figure 2A, B).

In complex with the estrogen and androgen hormone receptors, LSD1 is shown to activate target gene expression through removal of repressive H3K9 methylation. H3K9me2 is also shown to be largely depleted during EMT through an LSD1-dependent mechanism and this loss of H3K9me2 is associated with transformation [41]. Thus, we evaluated the effects of HCI2509 on H3K9me2 and observed an increase in H3K9me2 in AN3CA cells (Figure 2A). Interestingly, treatment with HCI2509 showed no effect on H3K9me2 in KLE cells (Figure 2B). We also predicted that changes in global methylation status in either H3K4 or H3K9 would occur in synchrony with additional global changes to chromatin state, so we also blotted for H3K27me3, a mark typically associated with gene repression and heterochromatin [26].

HCI2509 treatment induced a dose-dependent increase in H3K27me3 in both cell lines. The observed elevation of histone methylation by HCI2509 occurred with no change observed for LSD1 protein levels (Figure 2A, B).

We also asked whether HCI2509 modulated expression of LSD1 target genes. Induction of *HMOX1* has been shown to be a biological readout for LSD1 engagement by HCI2509 [35,38]. We additionally evaluated the expression of *CDH1* (E-cadherin). E-cadherin is a cell-surface adhesion molecule that is repressed during SNAIL-LSD1-mediated EMT and is often misregulated in Type II endometrial cancer [42,43]. HCI2509 treatment induced increased transcription of both *HMOX1* and *CDH1* in both AN3CA and KLE cell lines (Figure 2C, D), suggesting LSD1 target engagement by HCI2509.

LSD1 inhibition disrupts normal cell cycle progression in human endometrial cancer cell lines

The observation of decreased proliferative rates prompted us to test the effect of HCI2509 treatment on cell cycle progression in both AN3CA and KLE cells. Cell

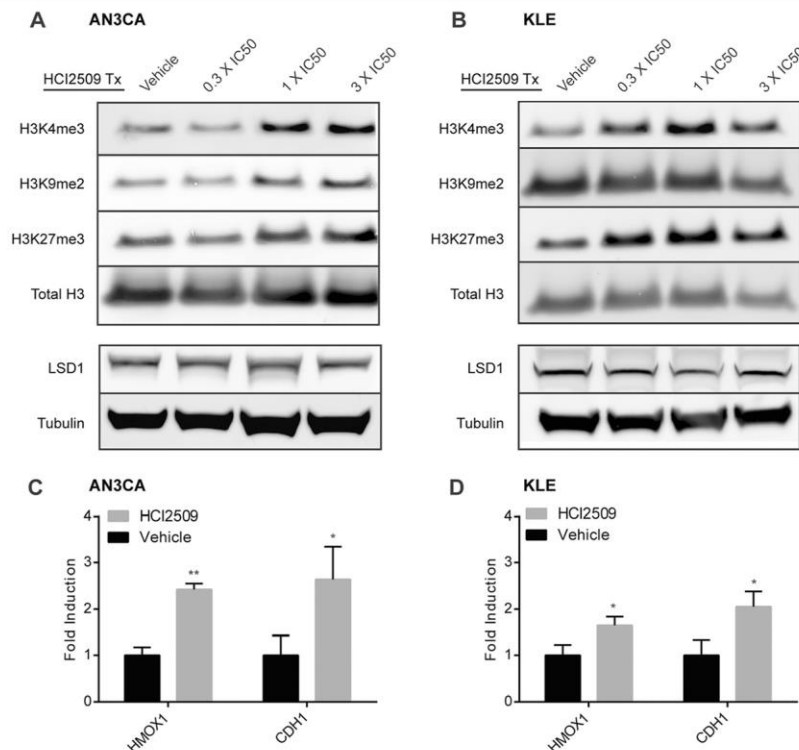
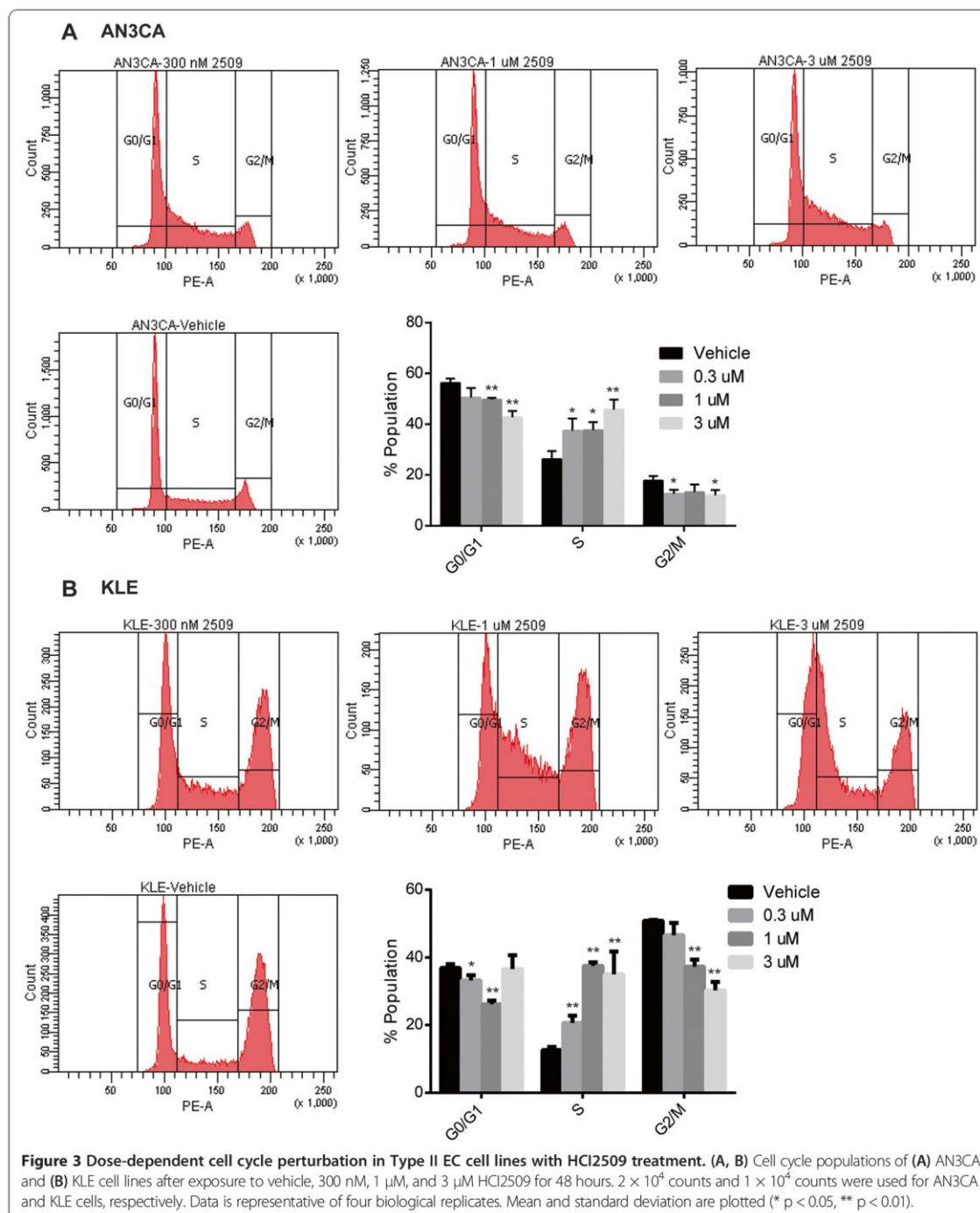


Figure 2 Treatment with HCI2509 causes changes in global histone methylation and induces LSD1 target genes. (A, B) Western blot analysis of H3K4me3, H3K9me2, H3K27me3 and LSD1 after 48 hours of vehicle or HCI2509 treatment at varying concentrations in **(A)** AN3CA and **(B)** KLE cells. Images are representative of two repeat experiments performed in triplicate. **(C, D)** qRT-PCR analysis of LSD1 target genes, *HMOX1* and *CDH1*, after treatment with 3X EC50 for **(C)** AN3CA and **(D)** KLE cells. Data represents the mean and standard deviation (n = 3) and all replicates were normalized to internal housekeeping gene *RPL19*.

cycle analysis was performed with either vehicle or HCl2509 exposure at 300 nM, 1 μ M, or 3 μ M for 48 hours. AN3CA cells showed a dose-dependent increase in the percentage of cells in S-phase (Figure 3A). This was accompanied by a decrease in the G0/G1 population. In a time-course experiment 3 μ M HCl2509 shows an



accumulation of cells in the G0/G1 population from 6–12 hours before developing the increased S-phase fraction at 24 and 48 hours (Additional file 2: Figure S3A). KLE cells show a similar accumulation in early S-phase with increasing concentrations of HCI2509 (Figure 3B). Unlike the AN3CA data, the increase in the S-phase fraction occurs at the expense of the G2/M population of cells. The time-course experiment with KLE cells in 3 μ M HCI2509 interestingly never passed through the same distribution as observed for 1 μ M HCI2509 at 48 hours, and failed to show any obvious change until 48 hours (Additional file 2: Figure S3B). These data suggest that LSD1 inhibition with HCI2509 perturbs cell cycle progression in both Type II endometrial carcinoma cell lines, most likely through an accumulation in early S-phase.

HCI2509 induces apoptosis in AN3CA and KLE cells

In addition to cell cycle disruption, we investigated the mechanism causing negative cell doubling in both AN3CA and KLE cells. We hypothesized that HCI2509 treatment may cause apoptotic cell death and therefore tested both cell lines for caspase 3/7 activation. Caspase activity was assayed in parallel with cell viability using 3X the EC_{50} and comparing to vehicle control. Viability and caspase activation were assessed over a time-course of 72 hours in both cell lines. Interestingly, in the context of HCI2509 treatment AN3CA showed decreased cell viability and caspase activity over the course of 48 hours with increased caspase activation occurring at 72 hours (Figure 4A). The decrease in caspase activation during the first 48 hours of treatment is likely due to a decreased number of cells/well due to cytostasis relative to vehicle. HCI2509-treated KLE cells showed a concomitant increase in caspase activity and decrease in cell viability over 72 hours (Figure 4B). These data suggest an initial cytostasis which is followed by apoptotic cell death induced after 48 hours. We next confirmed apoptotic cell death using fluorescent TUNEL staining. AN3CA and KLE cells were treated with either vehicle or 3X EC_{50} HCI2509 for 72 hours and then assayed for TUNEL staining. Both cell lines showed decreased cell density and the presence of apoptotic cells with HCI2509 treatment, while vehicle treated cells appeared healthy and well spread on the coverslip (Figure 4C, D, Additional file 3: Figure S4A, S4B). Internal controls for the TUNEL assay are reported in Additional file 3: Figure S4C. These results confirmed apoptotic cell death induced by HCI2509 treatment.

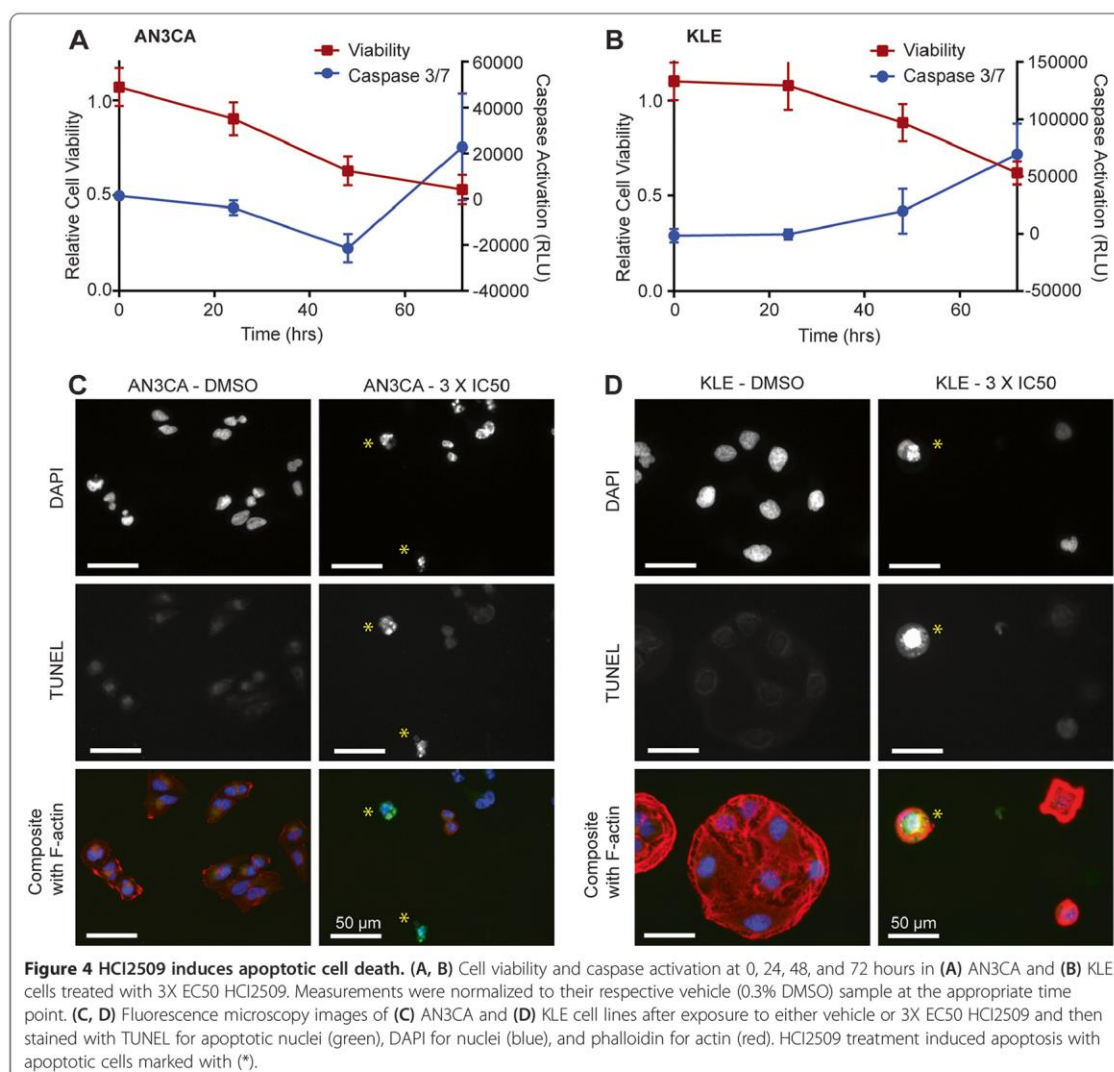
HCI2509 leads to tumor regression in an orthotopic endometrial carcinoma mouse xenograft model

We further evaluated the efficacy of HCI2509 in an orthotopic xenograft model of endometrial carcinoma utilizing the KLE cell line stably transfected with luciferase to facilitate bioluminescence imaging. After implantation (day 0)

and recovery, bioluminescence was measured weekly for the duration of the study (42 d). Total body weight was measured 3 times weekly, and weekly points were plotted (Figure 5A). At day 7, animals with detectable tumor were randomized into vehicle only and HCI2509 treatment groups (Additional file 4: Figure S5A). We observed the tumor luminescence values were better fit to a log-normal distribution than a normal distribution, which is common for various biological phenomena such as latency times for infections or survival times after a diagnosis of cancer (Additional file 4: Figure S5B) [44]. For this reason, the geometric mean of the tumor volumes for both conditions are plotted (Figure 5B). Values observed at day 7 were higher than those observed for the remainder of the study and therefore excluded from the graph. This initial burst of proliferation, and associated luminescence, followed by a drop off before later hitting exponential growth is commonly observed in xenograft studies. After 35 days of treatment (day 42 of the study) proliferating disease was observed in all of the vehicle treated animals, while 5 of the 9 drug treated animals showed no detectable luminescence (Figure 5C). Lack of luminescence is incorporated as the background reading of the instrument for each day of the experiment, as determined by an unimplanted, non-tumor bearing, healthy control. We used a Fisher's exact test to evaluate the effect of treatment vs. vehicle on either tumor or regression and found HCI2509 significantly associated with tumor regression ($p = 0.034$). No difference in body weight was seen between the vehicle and treatment groups indicating tolerability of HCI2509. The luminescence readout for the untreated control group are plotted together with data from the vehicle and treatment groups in Additional file 4: Figure S5D as are the body weight measurements including the non-tumor bearing control. When considered with the *in vitro* data suggesting decreased proliferation, transformation and induced apoptosis in concert with increased global histone methylation and LSD1 engagement, these data support LSD1 inhibition with HCI2509 as a potential therapeutic strategy for Type II endometrial carcinoma.

Discussion

LSD1 is an emerging target for poorly differentiated and aggressive solid malignancies. Our findings suggest that LSD1 inhibition holds potential as a new therapeutic strategy for Type II endometrial cancer, which may accompany current state of the art treatment of EC in the future. Targeted LSD1 inhibition with HCI2509 showed potent anti-cancer activity both *in vitro* and *in vivo* with multiple tumor regressions observed in our orthotopic EC model. Type II EC constitutes an unmet medical need, with disproportionately high number of annual EC deaths relative to the proportion of Type II EC diagnoses as compared to Type I disease. While it is known that



epigenetics, genetics, and the environment all contribute to the development of EC, recent studies demonstrating mutations in chromatin remodeling complexes as driver events in Type II EC [15-17] underscore the need for research to evaluate more effective and new therapeutic strategies targeting these mechanisms.

Chromatin modifiers or ubiquitin ligase complexes were recently implicated in 35% of clear cell endometrial and 50% of serous endometrial tumors [15]. One of the most commonly altered genes was *CHD4*, a member of the NuRD complex, along with the observation of frequent mutations in *MBD3*, another NuRD component

[15]. *CHD4* mutations were all predicted to disrupt normal function of the protein, suggesting a functional role in the development of EC [15]. LSD1 is bound by NuRD and has been shown to repress both tumor suppressor genes [45] and genes associated with metastasis and invasion [46] in complex with NuRD. It is possible that the role of LSD1 is altered in endometrial cancer through functional mutations in NuRD members, and this results in sensitivity to LSD1 inhibition. However, the role of NuRD mutations in endometrial cancer remain unstudied. Detailed studies addressing the role of NuRD and whether LSD1 and NuRD work in concert in

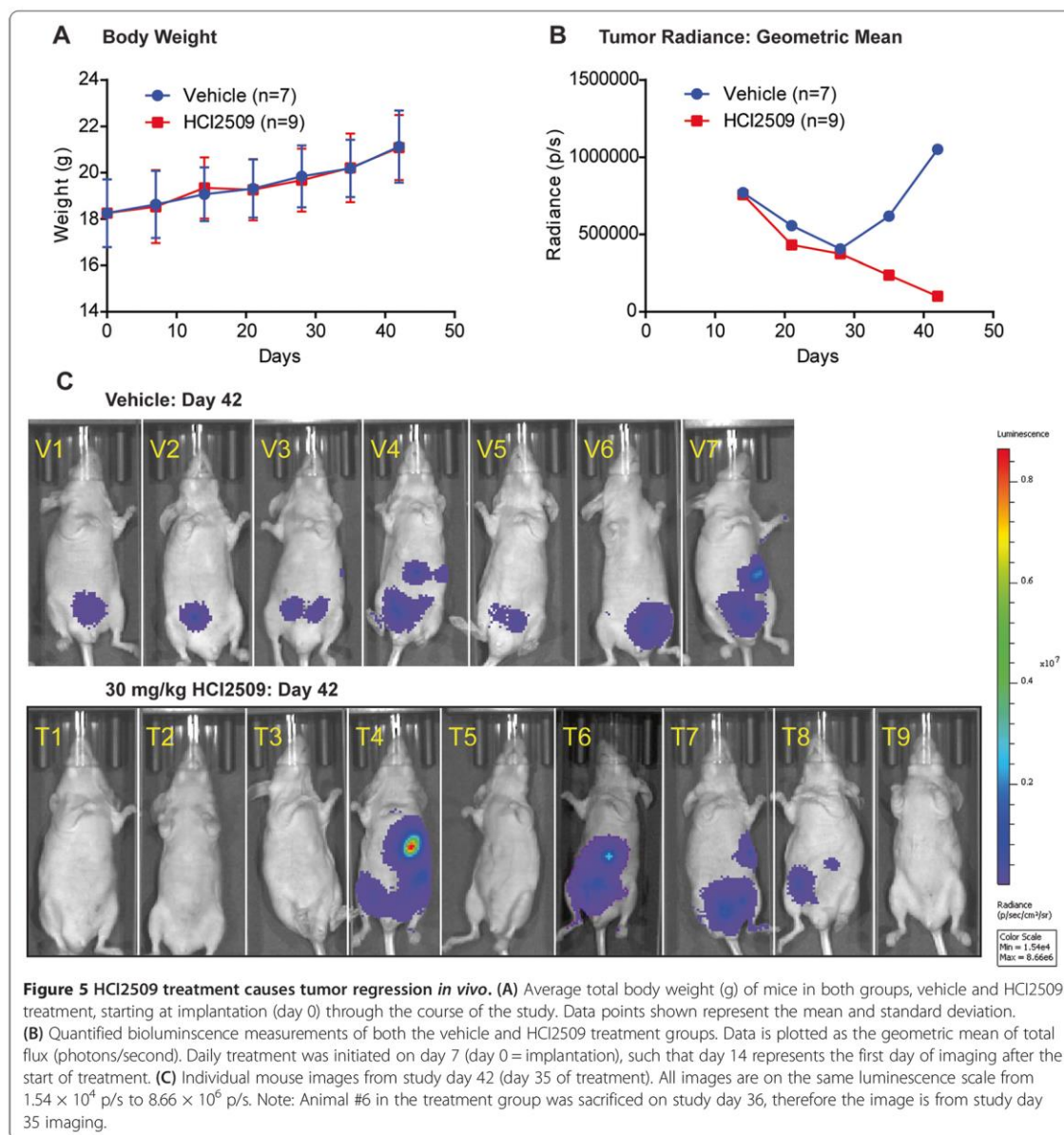


Figure 5 HCl2509 treatment causes tumor regression *in vivo*. (A) Average total body weight (g) of mice in both groups, vehicle and HCl2509 treatment, starting at implantation (day 0) through the course of the study. Data points shown represent the mean and standard deviation. (B) Quantified bioluminescence measurements of both the vehicle and HCl2509 treatment groups. Data is plotted as the geometric mean of total flux (photons/second). Daily treatment was initiated on day 7 (day 0 = implantation), such that day 14 represents the first day of imaging after the start of treatment. (C) Individual mouse images from study day 42 (day 35 of treatment). All images are on the same luminescence scale from 1.54×10^4 p/s to 8.66×10^6 p/s. Note: Animal #6 in the treatment group was sacrificed on study day 36, therefore the image is from study day 35 imaging.

endometrial cancer could lead to insight regarding which patients may benefit from LSD1 inhibition or other epigenetic intervention.

This is especially true in light of the results showing that not only are LSD1 substrates affected by HCl2509, H3K27me3 was elevated in both cell lines, suggesting LSD1 inhibition exhibited downstream epigenetic regulatory effects. Interestingly, decreased H3K27me3 is

associated with poorer survival in both breast and ovarian cancers [47], though this has not been studied in Type II EC. The H3K27 methyltransferase EZH2 is over-expressed in ~60% of Type II EC and has been linked to focal adhesion kinase (FAK) and deregulation of E-cadherin [13]. This presents another possible avenue to define the functional linkage of epigenetic misregulation with Type II EC biology. The differences observed

between cell lines with respect to H3K9me2 are consistent with the highly contextual dependence of LSD1 function. In summary, the histone methylation data presented here contrasts with that shown for HCI2509 in Ewing sarcoma [38], and emphasizes the importance of additional mechanistic studies to be conducted in the future to better define LSD1 biology.

Corroborating other *in vitro* findings, results observed for the effects of HCI2509 on the cell cycle showed a dose-dependent increase in S-phase and decrease in the G2/M for both AN3CA and KLE cells. Time course analysis revealed what appeared to be a moderate G1/G0 arrest at 12 hours in AN3CA cells, though not in the KLE cells. The primary effect seen was an accumulation in early S-phase in both cell lines. LSD1 has been shown to play a critical role in maintaining the cell cycle in embryonic stem cells [48,49], as well as promoting proliferation and cell cycle progression in cancer cells [50,51], and the data here is consistent with this observation.

One of the biggest limitations in studying new epigenetic therapies in a given disease is the lack of mechanistic understanding to distinguish which molecular events are drivers and passengers in tumorigenesis. In the meantime, translational progress requires potent and specific tool compounds and to validate new therapeutic strategies. Because epigenetics represents the intersection between genes and the environment, it is likely that the phenomena observed in tissue culture will not represent the disease state in a mouse, and further, the difficulties translating from mouse studies to humans is well documented [52]. To mitigate these issues, we placed emphasis on early testing of whether epigenetic modulation with an LSD1 inhibitor would work *in vivo* in Type II EC. Further, we also wanted to recapitulate the tumor environment as reliably as possible in an orthotopic setting using relevant human cancer cells. In our KLE model, the generated tumors showed a dip in luminescent signal after the first week as is common and in the vehicle group signal rebounded in an exponential growth pattern by day 42. The doubling time for KLE cells in tissue culture is fairly slow, around 72 hours, indicating *in vivo* disease progression rate being consistent with the character of the cell line. We were encouraged to see signal present throughout the abdominal cavity in several mice throughout the study, as this suggested an invasive and disseminated disease. Based on the limited number of animals in this pilot *in vivo* study, we favored endpoints over additional tissue evaluation of responsive tumors to better understand molecular effects caused by HCI2509 treatment, rendering responsive tumors unavailable for additional experiments. Further dose finding, frequency, and survival studies are planned.

Ultimately, this is the first data including histone methylation changes, target gene elevation, and induced

apoptosis in EC and is very encouraging. Additional studies should evaluate LSD1 inhibition in more translational and patient-derived models, both *in vitro* and *in vivo*. To do so will require expanding the mechanistic insight based on the recent implication of chromatin remodelers in Type II EC using more potent and specific tool compounds. Additional investigation of epigenetics, as well as the relationship between specific pharmacodynamic and pharmacokinetic markers of response, will be needed to gain an in depth understanding of these mechanisms in the development of EC. Furthermore, LSD1 inhibition with HCI2509 should be evaluated for synergistic effects with other targeted inhibitors of other pathways implicated in Type II EC, such as FAK [13] signaling, as well as conventional treatment modalities including hormone therapy currently applied in the treatment of EC.

Conclusions

In conclusion, we have demonstrated that the treatment of Type II endometrial carcinoma cell lines with the LSD1 inhibitor HCI2509 decreased proliferation and transformation, induced histone methylation and LSD1 target gene expression, perturbed cell cycle progression, and induced apoptotic cell death *in vitro*. Moreover, in an orthotopic endometrial carcinoma animal model with human KLE cells, HCI2509 treatment resulted in 5/9 tumor regressions over the course of 42 days. Taken together these findings support further investigation of the role of LSD1 in Type II endometrial carcinoma biology as well as LSD1 inhibition as a novel therapeutic strategy for this aggressive gynecologic malignancy.

Additional files

Additional file 1: Figure S2. Changes to histone H3 lysine 4 monomethyl and dimethyl marks with HCI2509 treatment. (A, B) Western blot analysis of H3K4me1 and H3K4me2 after 48 hours of vehicle or HCI2509 treatment at varying concentrations in (A) AN3CA and (B) KLE cells. Images are representative of two repeat experiments performed in triplicate.

Additional file 2: Figure S3. Time course evaluation of cell cycle perturbations caused by HCI2509 treatment. (A, B) Cell cycle populations of (A) AN3CA and (B) KLE cell lines after exposure to vehicle (0 and 48 hours) or 3 μ M HCI2509 (6, 12, 24, and 48 hours). 2×10^4 counts and 1×10^4 counts were used for AN3CA and KLE cells, respectively. Data is representative of four biological replicates.

Additional file 3: Figure S4. TUNEL assay replicates and controls. (A, B) Fluorescence microscopy images of (A) AN3CA and (B) KLE cell lines after exposure to either vehicle or 3X EC50 HCI2509 and then stained with TUNEL for apoptotic nuclei (green), DAPI for nuclei (blue), and phalloidin for actin (red). HCI2509 treatment induced apoptosis with apoptotic cells marked with (*). (C) Fluorescence microscopy images of TUNEL negative and positive controls with untreated AN3CA and KLE cells. Negative controls were generated by adding labeled nucleotide with no enzyme and positive controls were generated by pretreating DNase before TUNEL labeling. Cells are stained with TUNEL (green), DAPI (blue), and phalloidin for actin (red).

Additional file 4: Figure S5. HCl2509 treatment causes tumor regression *in vivo*. (A) Individual mouse images from study day 7 (day 0 of treatment). All images are on the same luminescence scale from 1.54×10^4 p/s to 8.66×10^6 p/s. (B) Quantified bioluminescence measurements of both the vehicle and HCl2509 treatment groups pooled. Total flux (photons/second) was rank ordered and plotted on a semi-log plot. The linearity of the log-transformed data supports a log-normal distribution. (C) Fisher's exact test shows significant association of HCl2509 treatment with tumor regression. Both the observed and expected contingency tables are shown with the reported p-value. (D) Tumor volume and body weight measurements including both the untreated and unimplanted control. Tumor volumes are plotted as the geometric mean of the observed luminescent signal and body weight is plotted as the average and SD.

Abbreviations

APC: Adenomatous polyposis coli; ARID1A: AT rich interactive domain 1A; CD133: Cluster of differentiation 133; CDH1: E-cadherin; EC: Endometrial carcinoma; EC50: Effective concentration at 50%; EMT: Epithelial-to-mesenchymal transition; EP300: E1A binding protein p300; EZH2: Enhancer of zeste homolog 2; FAK: Focal adhesion kinase; FGFR: Fibroblast growth factor receptor; H3: Histone H3; H3K4 (me3): Histone H3 lysine 4 (dimethylated); H3K9 (me2): Histone H3 lysine 9 (trimethylated); H3K27 (me3): Histone H3 lysine 27 (trimethylated); HMOX1: Heme oxygenase 1; LSD1: Lysine-specific demethylase 1; MGMT: O-6-methylguanine-DNA methyltransferase; MLH1: mutL homolog 1; MPA: Medroxyprogesterone 17-acetate; NuRD: Nucleosome remodeling and deacetylase; PTEN: Phosphatase and tensin homolog; TAF1: TATA box binding protein (TBP)-associated factor; TUNEL: Terminal deoxynucleotidyl transferase dUTP nick end labeling.

Competing interests

SS is a founder and Chief Medical Officer of Salaris Pharmaceuticals, a company focused on epigenetic therapies for cancer.

Authors' contributions

ERT, SG and JB performed the experiments and wrote the manuscript. SS and MJA (corresponding author) designed and supervised the experiments and wrote the manuscript. VS and MJA contributed reagents, facilities and personnel. All authors read and approved the final manuscript.

Authors' information

Sunil Sharma and Margit Janat-Amsbury are co-senior authors.

Acknowledgments

We thank Jason Tanner and Jeffrey Theisen for their support, discussion, and thoughtful feedback. This work was supported by the American Foundation for Pharmaceutical Education 2013 Pre-Doctoral Fellowship (AFPE), NCI grant P30 CA042014 awarded to the Huntsman Cancer Institute, and the Department of Obstetrics and Gynecology.

Author details

¹Center for Investigational Therapeutics (CIT) at Huntsman Cancer Institute, University of Utah, Salt Lake City, UT, USA. ²Department of Pharmaceutics and Pharmaceutical Chemistry, College of Pharmacy, University of Utah, Salt Lake City, UT, USA. ³Division of Medical Oncology, University of Utah School of Medicine, Salt Lake City, UT, USA. ⁴Department of Obstetrics and Gynecology, Division of Gynecologic Oncology, University of Utah, Salt Lake City, UT 84132, USA. ⁵Center for Nanomedicine, Nano Institute of Utah, Salt Lake City, UT, USA.

Received: 6 June 2014 Accepted: 30 September 2014

Published: 9 October 2014

References

1. Siegel R, Naishadham D, Jemal A: **Cancer Statistics, 2012.** *CA Cancer J Clin* 2012, **62**:10–29.
2. Jemal A, Siegel R, Ward E, Hao Y, Xu J, Thun MJ: **Cancer statistics, 2009.** *CA Cancer J Clin* 2009, **59**:225–249.
3. National Cancer Institute: **Endometrial Cancer Home Page.** <http://www.cancer.gov/cancertopics/types/endometrial>.

4. Ferlay J, Shin H-R, Bray F, Forman D, Mathers C, Parkin DM: **Estimates of worldwide burden of cancer in 2008: GLOBOCAN 2008.** *Int J Cancer* 2008, **127**:2893–2917.
5. Sutton G, Axelrod JH, Bundy BN, Roy T, Homesley HD, Malfetano JH, Mychalczak BR, King ME: **Whole abdominal radiotherapy in the adjuvant treatment of patients with stage III and IV endometrial cancer: a gynecologic oncology group study.** *Gynecol Oncol* 2005, **97**:755–763.
6. Bokhman JV: **Two pathogenic types of endometrial carcinoma.** *Gynecol Oncol* 1983, **15**:10–17.
7. Mendivil A, Schulder KM, Gehrig PA: **Non-endometrioid adenocarcinoma of the uterine corpus: a review of selected histological subtypes.** *Cancer Control* 2009, **16**:46–52.
8. Xiong Y, Dowdy SC, Bosquet JG, Zhao Y, Eberhardt NL, Podratz KC, Jiang S-W: **Epigenetic-mediated upregulation of progesterone receptor B gene in endometrial cancer cell lines.** *Gynecol Oncol* 2005, **99**:135–141.
9. Tao MH, Freudenheim JL: **DNA methylation in endometrial cancer.** *Epigenetics* 2010, **5**:491–498.
10. Friel AM, Zhang L, Curley MD, Therrien VA, Sergent PA, Belden SE, Borger DR, Mohapatra G, Zukerberg LR, Foster R, Rueda BR: **Epigenetic regulation of CD133 and tumorigenicity of CD133 positive and negative endometrial cancer cells.** *Reprod Biol Endocrinol* 2010, **8**:147.
11. Fakhry H, Miyamoto T, Kashima H, Suzuki A, Ke H, Konishi I, Shiozawa T: **Immunohistochemical detection of histone deacetylases in endometrial carcinoma: involvement of histone deacetylase 2 in the proliferation of endometrial carcinoma cells.** *Hum Pathol* 2010, **41**:848–858.
12. Jiang S, Dowdy SC, Meng XW, Wang Z, Jones MB, Podratz, Jiang S-W: **Histone deacetylase inhibitors induce apoptosis in both Type I and Type II endometrial cancer cells.** *Gynecol Oncol* 2007, **105**:493–500.
13. Zhou J, Roh J-W, Bandyopadhyay S, Chen Z, Munkarah AR, Hussein Y, Alosch B, Jazaerly T, Hayek K, Semaan A, Sood AK, Ali-Fehmi R: **Overexpression of enhancer of zeste homolog 2 (EZH2) and focal adhesion kinase (FAK) in high grade endometrial carcinoma.** *Gynecol Oncol* 2013, **128**:344–348.
14. Eskander RN, Ji T, Huynh B, Wardeh R, Randall LM, Hoang B: **Inhibitor of enhancer of zeste homolog 2 (EZH2) expression is associated with decreased tumor cell proliferation, migration, and invasion in endometrial cancer cell lines.** *Int J Gynecol Cancer* 2013, **23**:997–1005.
15. Le Gallo M, O'Hara AJ, Rudd ML, Urlick ME, Hansen NF, O'Neil NJ, Price JC, Zhang S, England BM, Godwin AK, Sgroi DC, NISC Comparative Sequencing Program, Hieter P, Mullikin JC, Merino MJ, Bell DW: **Exome sequencing of serous endometrial tumors identifies recurrent somatic mutations in chromatin-remodeling and ubiquitin ligase complex genes.** *Nat Genet* 2012, **44**:1310–1315.
16. Zhao S, Choi M, Overton JD, Bellone S, Roque DM, Cocco E, Guzzo F, English DP, Varughese J, Gasparini S, Bortolomai I, Buza N, Hui P, Abu-Khalaf M, Ravaggi A, Bignotti E, Bandiera E, Romani C, Todeschini P, Tassi R, Zanotti L, Carrara L, Pecorelli S, Silasi DA, Ratner E, Azodi M, Schwartz PE, Rutherford TJ, Stiegler AL, Mane S, et al: **Landscape of somatic single-nucleotide and copy-number mutations in uterine serous carcinoma.** *Proc Natl Acad Sci U S A* 2013, **110**:2916–2921.
17. Le Gallo M, Bell DW: **The emerging genomic landscape of endometrial cancer.** *Clin Chem* 2014, **60**:98–110.
18. Dawson MA, Kouzarides T: **Cancer epigenetics: from mechanism to therapy.** *Cell* 2012, **150**:12–27.
19. Sharma S, Kelly TK, Jones PA: **Epigenetics in cancer.** *Carcinogenesis* 2010, **31**:27–36.
20. Stresmann C, Lyko F: **Modes of action of the DNA methyltransferase inhibitors azacitidine and decitabine.** *Int J Cancer* 2008, **123**:8–13.
21. Choudhary C, Kumar C, Gnad F, Nielsen ML, Rehman M, Walther TC, Olsen JV, Mann M: **Lysine acetylation targets protein complexes and co-regulates major cellular functions.** *Science* 2009, **325**:834–840.
22. Islam AB, Richter WF, Lopez-Bigas N, Benevolenskaya EV: **Selective targeting of histone methylation.** *Cell Cycle* 2011, **10**:413–424.
23. Popovic R, Licht JD: **Emerging epigenetic targets and therapies in cancer medicine.** *Cancer Discov* 2012, **2**:405–413.
24. Shi Y, Lan F, Matson C, Mulligan P, Whetstone JR, Cole PA, Casero RA: **Histone demethylation mediated by the nuclear amine oxidase homolog LSD1.** *Cell* 2004, **119**:941–953. Ref 19.
25. Metzger E, Wissmann M, Yin N, Mueller JM, Schneider R, Peters AHFM, Guenther T, Buettner R, Schuele R: **LSD1 demethylates repressive histone marks to promote androgen-receptor-dependent transcription.** *Nature* 2005, **437**:436–439.

26. Lachner M, O'Sullivan RJ, Jenuwein T: An epigenetic road map for histone lysine methylation. *J Cell Sci* 2003, **116**:2117–2124.
27. Schulte JH, Lim S, Schramm A, Friedrichs N, Koster J, Versteeg R, Ora I, Pajtler K, Klein-Hitpass L, Kuhfittig-Kulle S, Metzger E, Schüle R, Eggert A, Buettner R, Kirfel J: Lysine-specific demethylase 1 is strongly expressed in poorly differentiated neuroblastoma: implications for therapy. *Cancer Res* 2009, **69**:2065–2071.
28. Harris WJ, Huang X, Lynch JT, Spencer GJ, Hitchin JR, Li Y, Ciceri F, Blaser JG, Greystoke BF, Jordan AM, Miller CJ, Ogilvie DJ, Somerville TC: The histone demethylase KDM1A sustains the oncogenic potential of MLL-AF9 leukemia stem cells. *Cancer Cell* 2012, **21**:473–487.
29. Lim S, Janzer A, Becker A, Zimmer A, Schüle R, Buettner R, Kirfel J: Lysine-specific demethylase 1 (LSD1) is highly expressed in ER-negative breast cancers and a biomarker predicting aggressive biology. *Carcinogenesis* 2010, **31**:512–520.
30. Kahl P, Gullotti L, Heukamp LC, Wolf S, Friedrichs N, Vorreuther R, Solleder G, Bastian PJ, Ellinger J, Metzger E, Schüle R, Buettner R: Androgen receptor coactivators lysine-specific histone demethylase 1 and four and a half LIM domain protein 2 predict risk of prostate cancer recurrence. *Cancer Res* 2006, **66**:11341–11347.
31. Hayami S, Kelly JD, Cho HS, Yoshimatsu M, Unoki M, Tsunoda T, Field HI, Neal DE, Yamaue H, Ponder BA, Nakamura Y, Hamamoto R: Overexpression of LSD1 contributes to human carcinogenesis through chromatin regulation in various cancers. *Int J Cancer* 2011, **128**:574–586.
32. Zhao ZK, Yu HF, Wang DR, Dong P, Chen L, Wu WG, Ding WJ, Liu YB: Overexpression of lysine specific demethylase 1 predicts worse prognosis in primary hepatocellular carcinoma patients. *World J Gastroenterol* 2012, **18**:6651–6656.
33. Schildhaus HU, Riegel R, Hartmann W, Steiner S, Wardelmann E, Merkelbach-Bruse S, Tanaka S, Sonobe H, Schüle R, Buettner R, Kirfel J: Lysine-specific demethylase 1 is highly expressed in solitary fibrous tumors, synovial sarcomas, rhabdomyosarcomas, desmoplastic small round cell tumors, and malignant peripheral nerve sheath tumors. *Hum Pathol* 2011, **42**:1667–1675.
34. Bennani-Baiti I-M, Machado I, Llombart-Bosch A, Kovar H: Lysine-specific demethylase 1 (LSD1/KDM1A/AOF2/BHC110) is expressed and is an epigenetic drug target in chondrosarcoma, Ewing's sarcoma, osteosarcoma, and rhabdomyosarcoma. *Hum Pathol* 2012, **43**:1300–1307.
35. Sorna V, Theisen ER, Stephens B, Warner SL, Bearss DJ, Vankayalapati H, Sharma S: High-throughput virtual screening identifies novel N'-(1-phenylethylidene)-benzohydrazides as potent, specific, and reversible inhibitors of LSD1. *J Med Chem* 2013, **56**:9496–9508.
36. Stephens BJ, Theisen ER, Warner SL, Sharma S, Bearss DJ: Abstract 1045: Activity of the LSD1 inhibitor HCl-2509 in ER-negative breast cancer cells. In *Proceedings of the American Association for Cancer Research 103rd Annual Meeting 2012: 31 March –4 April 2012*. Chicago, IL: 2012.
37. Theisen ER, Bearss J, Sorna V, Bearss DJ, Sharma S: Abstract 3: Targeted inhibition of LSD1 in castration-resistant prostate cancer. In *Proceedings of the American Association for Cancer Research 104th Annual Meeting 2013*. Washington, DC: 2013. 6-10 April 2013.
38. Sankar S, Theisen ER, Bearss J, Mulvihill T, Hoffman LM, Sorna V, Beckerle MC, Sharma S, Lessnick SL: LSD1 inhibition interferes with global EWS/ETS transcriptional activity and impedes Ewing sarcoma tumor growth. *Clin Cancer Res* 2014, **20**:4584–4597.
39. Lessnick SL, Dacwag CS, Golub TR: The Ewing's sarcoma oncoprotein EWS/FLI induces a p53-dependent growth arrest in primary human fibroblasts. *Cancer Cell* 2002, **1**:393–401.
40. Nakamura M, Kyo S, Zhang B, Zhang X, Mizumoto Y, Takakura M, Maida Y, Mori N, Hashimoto M, Ohno S, Inoue M: Prognostic impact of CD133 expression as a tumor-initiating cell marker in endometrial cancer. *Hum Pathol* 2010, **41**:1516–1529.
41. McDonald OG, Wu H, Timp W, Doi A, Feinberg AP: Genome-scale epigenetic reprogramming during epithelial-mesenchymal transition. *Nat Struct Mol Biol* 2011, **18**:867–874.
42. Lin T, Ponn A, Hu X, Law BK, Lu J: Requirement of the histone demethylase LSD1 in Snai1-mediated transcriptional repression during epithelial-mesenchymal transition. *Oncogene* 2010, **29**:4896–4904.
43. Llobet D, Pallares J, Yeremian A, Santacana M, Eritja N, Velasco A, Dolcet X, Matias-Guiu X: Molecular pathology of endometrial carcinoma: practical aspects from the diagnostic and therapeutic viewpoints. *J Clin Pathol* 2009, **62**:777–785.
44. Limpert E, Stahel WA, Abbt M: Log-normal distributions across the sciences: keys and clues. *Bioscience* 2001, **51**:341–352.
45. Sankar S, Bell R, Stephens B, Zhuo R, Sharma S, Bearss DJ, Lessnick SL: Mechanism and relevance of EWS/FLI-mediated transcriptional repression in Ewing sarcoma. *Oncogene* 2013, **32**:5089–5100.
46. Wang Y, Zhang H, Chen Y, Sun Y, Yang F, Yu W, Liang J, Sun L, Yang X, Shi L, Li R, Li Y, Zhang Y, Li Q, Yi X, Shang Y: LSD1 is a subunit of the NuRD complex and targets the metastasis programs in breast cancer. *Cell* 2009, **138**:660–672.
47. Wei Y, Xia W, Zhang Z, Liu J, Wang H, Adsay NV, Albarracín C, Yu D, Abbruzzese JL, Mills GB, Bast RC Jr, Hortobagyi GN, Hung MC: Loss of trimethylation at lysine 27 of histone H3 is a predictor of poor outcome in breast, ovarian, and pancreatic cancers. *Mol Carcinog* 2008, **47**:701–706.
48. Nair VD, Ge Y, Balasubramanian N, Kim J, Okawa Y, Chikina M, Troyanskaya O, Sealfon SC: Involvement of histone demethylase LSD1 in short-time-scale gene expression changes during cell cycle progression in embryonic stem cells. *Mol Cell Biol* 2012, **32**:4861–4876.
49. Yin F, Lan R, Zhang X, Zhu L, Chen F, Xu Z, Liu Y, Ye T, Sun H, Lu F, Zhang H: LSD1 regulates pluripotency of embryonic stem/carcinoma cells through histone deacetylase 1-mediated deacetylation of histone H4 at lysine 16. *Mol Cell Biol* 2014, **34**:158–179.
50. Scourmanne A, Chen X: The lysine-specific demethylase 1 is required for cell proliferation in both p53-dependent and -independent manners. *J Biol Chem* 2007, **282**:15471–15475.
51. Cho HS, Suzuki T, Dohmae N, Hayami S, Unoki M, Yoshimatsu M, Toyokawa G, Takawa M, Chen T, Kurash JK, Field HI, Ponder BA, Nakamura Y, Hamamoto R: Demethylation of RB regulator MYPT1 by histone demethylase LSD1 promotes cell cycle progression in cancer cells. *Cancer Res* 2011, **71**:655–660.
52. Lum DH, Matsen C, Welm AL, Welm BE: Overview of human primary tumorgraft models: comparisons with traditional oncology preclinical models and the clinical relevance and utility of primary tumorgrafts in basic and translational oncology research. *Curr Protoc Pharmacol* 2012, Chapter 14:Unit 14.22.

doi:10.1186/1471-2407-14-752

Cite this article as: Theisen et al.: Reversible inhibition of lysine specific demethylase 1 is a novel anti-tumor strategy for poorly differentiated endometrial carcinoma. *BMC Cancer* 2014 **14**:752.

Submit your next manuscript to BioMed Central and take full advantage of:

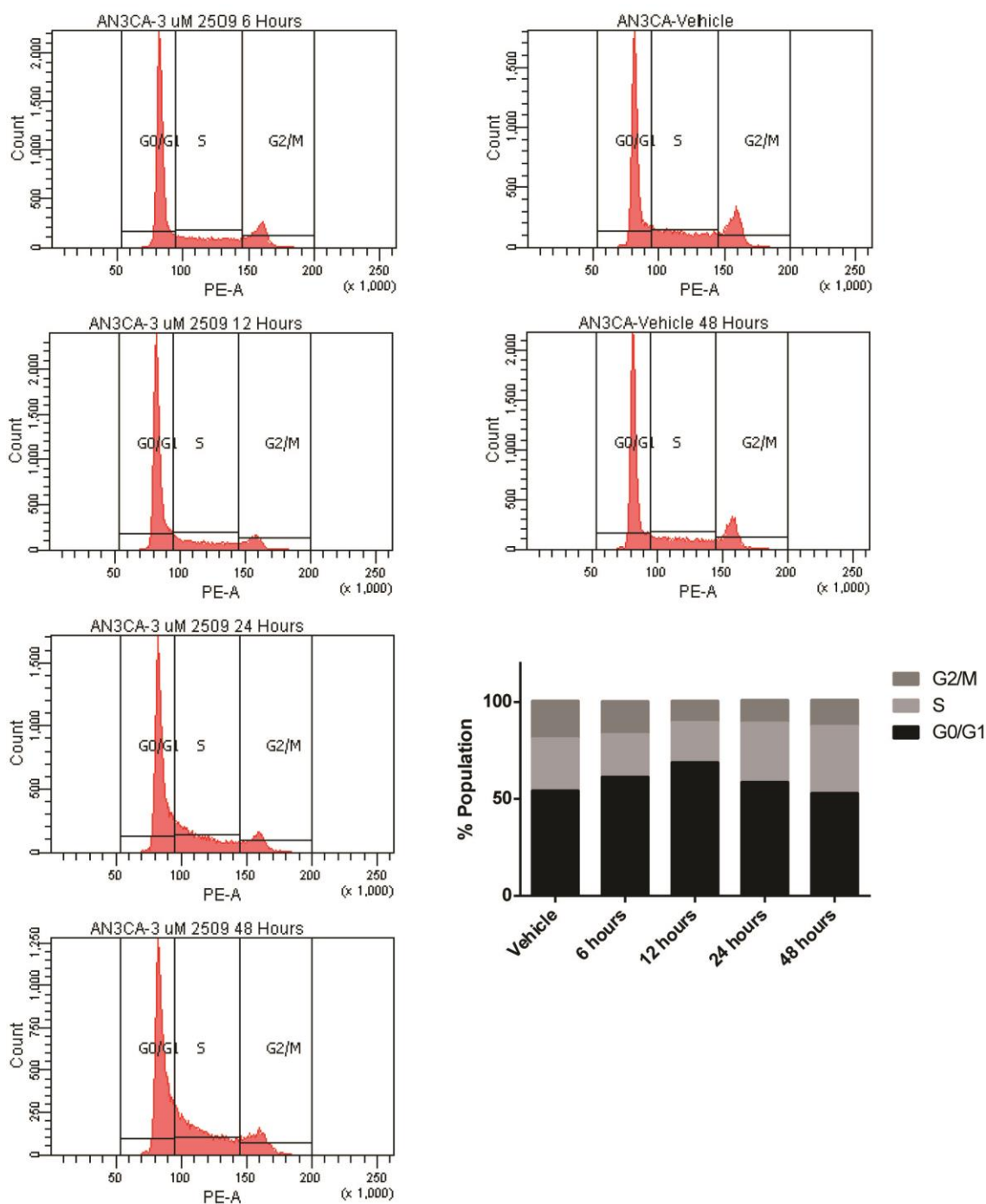
- Convenient online submission
- Thorough peer review
- No space constraints or color figure charges
- Immediate publication on acceptance
- Inclusion in PubMed, CAS, Scopus and Google Scholar
- Research which is freely available for redistribution

Submit your manuscript at
www.biomedcentral.com/submit

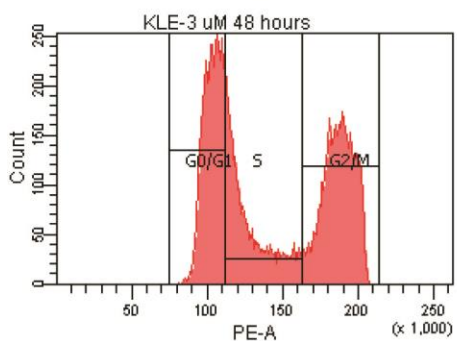
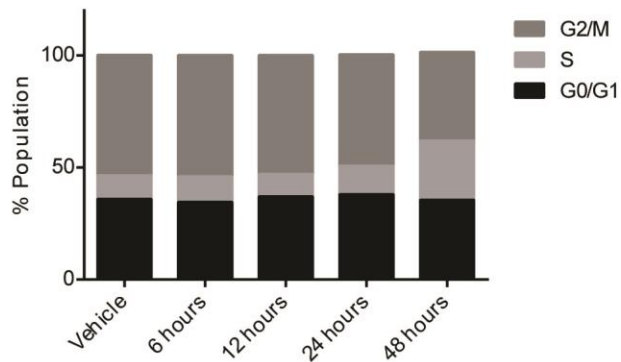
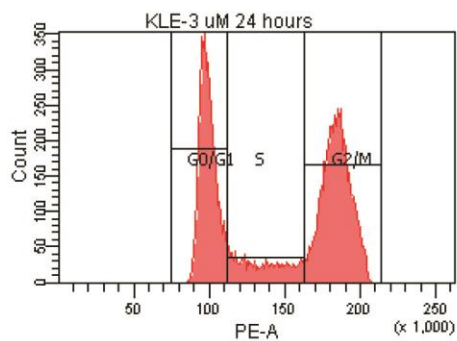
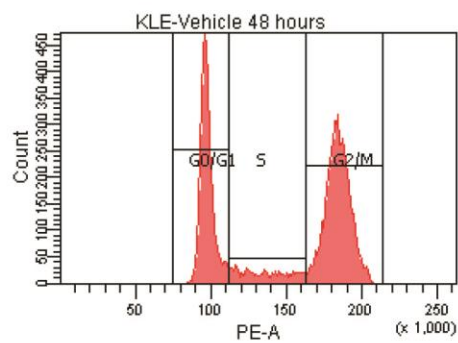
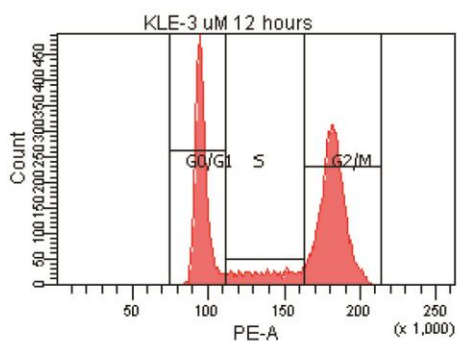
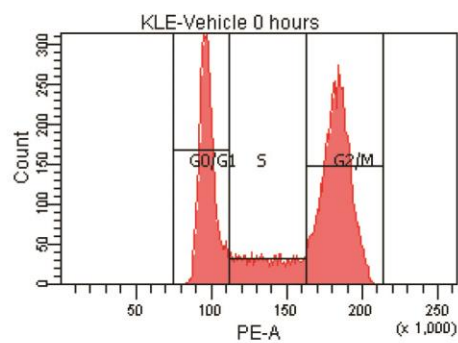
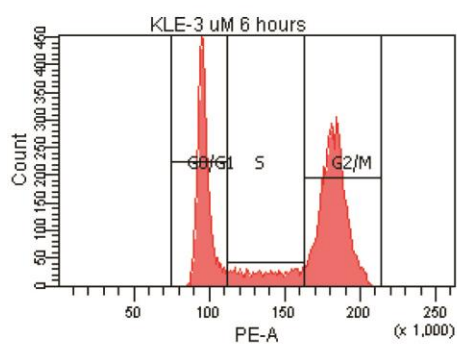


Supplementary Figure S4.1. Time course evaluation of cell cycle perturbations caused by HCI2509 treatment. (A,B) Cell cycle populations of (A) AN3CA and (B) KLE cell lines after exposure to vehicle (0 and 48 hours) or 3 μ M HCI2509 (6, 12, 24, and 48 hours). For AN3CA and KLE cells, 2×10^4 counts and 1×10^4 counts were used, respectively. Data are representative of two biological replicates.

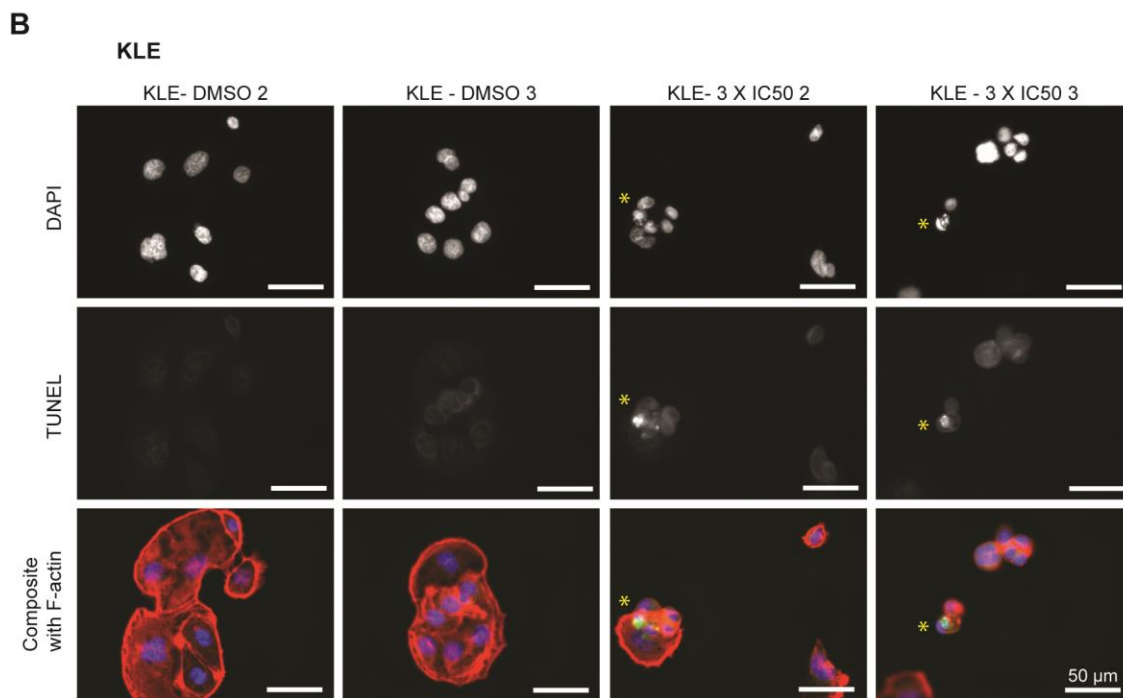
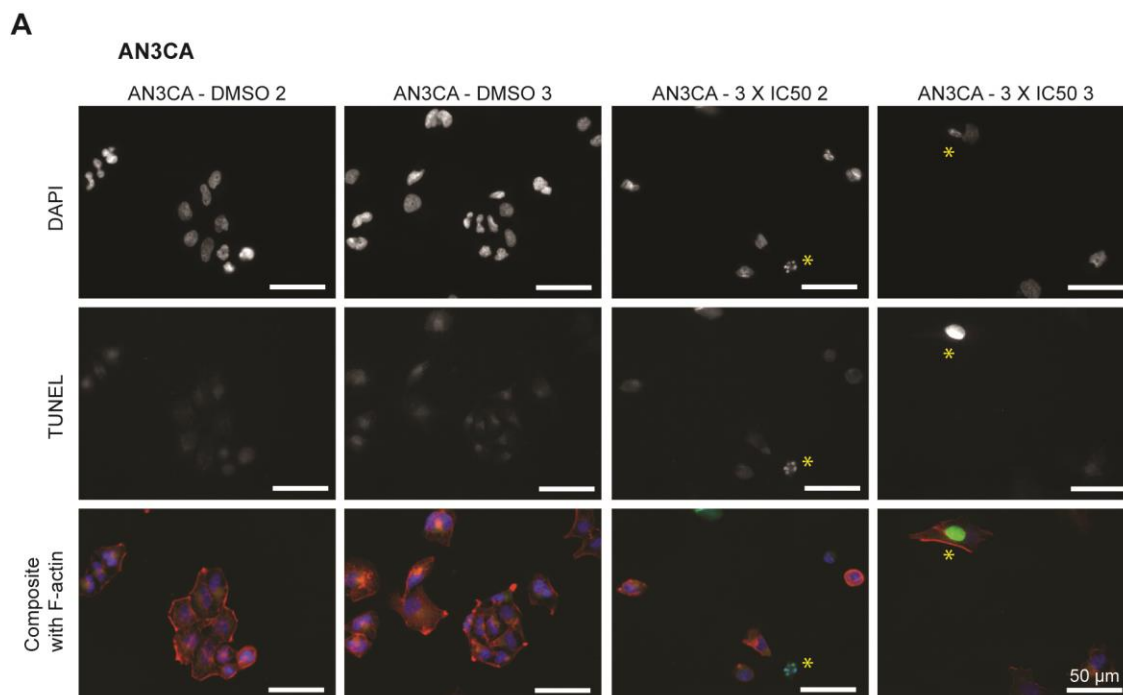
A AN3CA

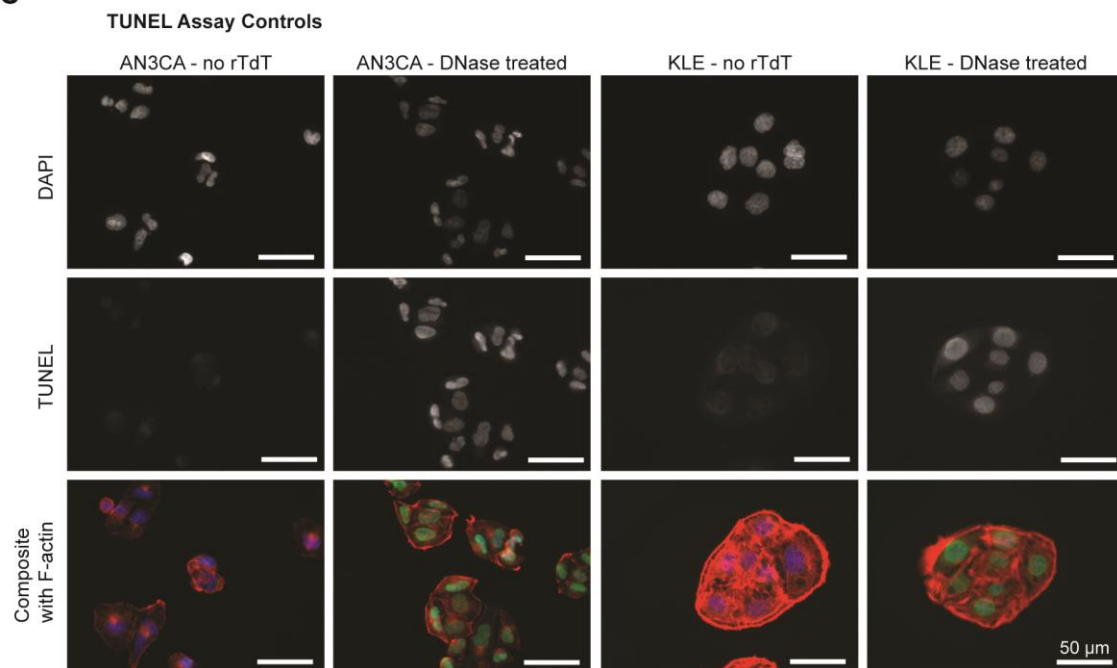


B KLE



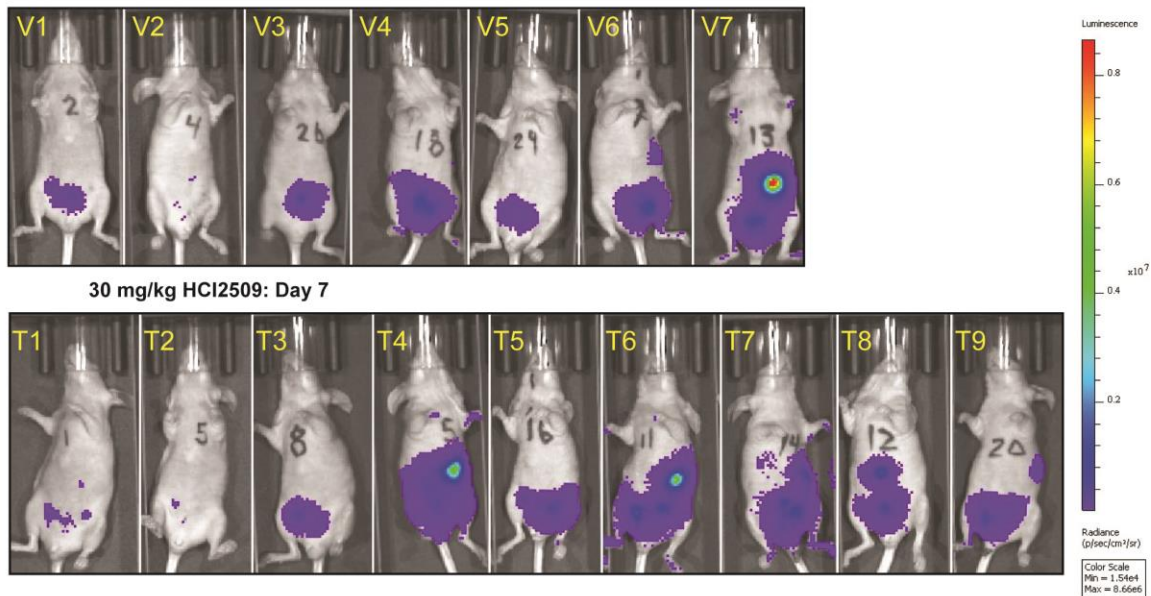
Supplementary Figure S4.2. TUNEL assay replicates and controls. (A,B) Fluorescence microscopy images of (A) AN3CA and (B) KLE cell lines after exposure to either vehicle or 3 X IC50 HCI2509 and then stained with TUNEL for apoptotic nuclei (green), DAPI for nuclei (blue), and phalloidin for actin (red). HCI2509 treatment induced apoptosis with apoptotic cells marked with (*). (C) Fluorescence microscopy images of TUNEL negative and positive controls with untreated AN3CA and KLE cells. Negative controls were generated by adding labeled nucleotide with no enzyme and positive controls were generated by pretreating DNase before TUNEL labeling. Cells are stained with TUNEL (green), DAPI (blue), and phalloidin for actin (red).



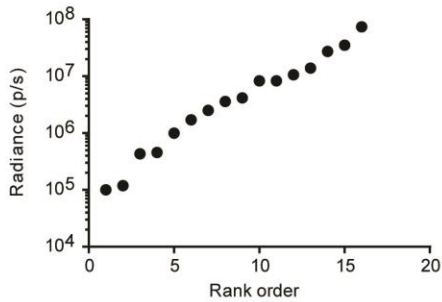
C

Supplementary Figure S4.3. In depth xenograft model analysis. (A) Individual mouse images from study day 7 (day 0 of treatment). All images are on the same luminescence scale from 1.54×10^4 p/s to 8.66×10^6 p/s. (B) Quantified bioluminescence measurements of both the vehicle and HCl2509 treatment groups pooled. Total flux (photons/second) was rank ordered and plotted on a semilog plot. The linearity of the log-transformed data supports a log-normal distribution. (C) Fisher's exact test shows significant association of HCl2509 treatment with tumor regression. Both the observed and expected contingency tables are shown with the reported p-value. (D) Tumor volume and body weight measurements including both the untreated and unimplanted control. Tumor volumes are plotted as the geometric mean of the observed luminescent signal and body weight is plotted as the average and SD.

A Vehicle: Day 7



B Tumor distribution: Day 7

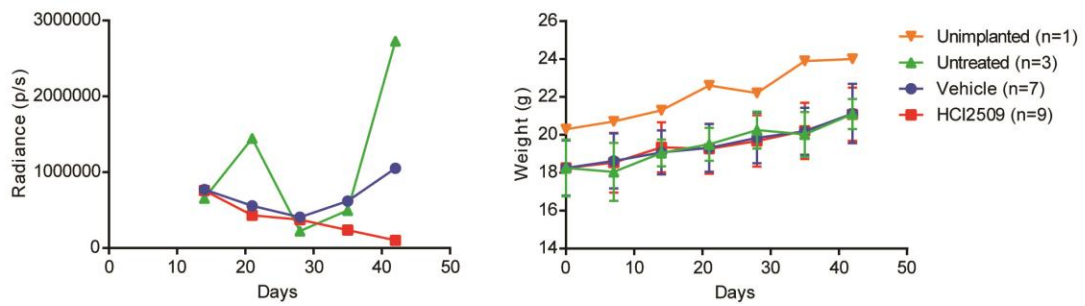


C Fisher's exact test

		Observed		Expected			
		Tumor	Regression	Tumor	Regression		
Vehicle		7	0	7	5	2	7
HCl2509		4	5	4	6	3	9
		11	5	16	11	5	16

p = 0.034

D Tumor growth and body weight with untreated and unimplanted animals group



CHAPTER 5

CONCLUSIONS AND OUTLOOK

5.1 Conclusions

This work described the discovery of a novel N¹-(1-phenylethylidene)-benzohydrazides compound series as potent, specific and reversible LSD1 inhibitors. Hit-to-lead optimization identified HCI2509 as a lead compound with nanomolar binding affinity for LSD1. HCI2509 is a noncompetitive LSD1 inhibitor with no detectable activity against either of the monoamine oxidases or other tested flavoenzymes. Treatment with HCI2509 decreased viability across numerous cancer cell lines. The overarching purpose of this work was to address the hypothesis that by targeting the key histone demethylase, potent and specific LSD1 inhibitors will exhibit single-agent efficacy in solid tumor models. We chose both Ewing sarcoma and endometrial carcinoma as model systems to test this hypothesis with HCI2509.

5.1.1 High-throughput Virtual Screening Leads to HCI2509

This work started with a high-throughput virtual screen of approximately 2 million small molecules against the crystal structure of LSD1 (PDB ID: 2Z5U). The compound library used was built with commercially available small molecules pre-filtered for favorable physicochemical properties. An initial hit, compound **1** in Chapter

2, was identified and showed LSD1 inhibition with a biochemical IC₅₀ of ~100-300 nM. Compound **1** was then optimized through iterative medicinal chemistry and biochemical testing to arrive at HCI2509 (“compound **12**” in Chapter 2) which has a K_i of ~30 nM. The hit to lead optimization process improved the specificity profile of the N’-(1-phenylethylidene)-benzohydrazides series considerably. Compound **1** showed activity against MAO B comparable to that of the MAO inhibitor tranlycypromine, while HCI2509 showed no detectable activity against either MAO A or B. HCI2509 was shown to be a noncompetitive inhibitor that perturbed LSD1 conformation in a manner distinct from tranlycypromine. The protein purification optimized to support these studies is reported in Appendix A. While the binding site of HCI2509 is predicted to fall in or near the FAD binding pocket of LSD1 based on the docking setup used, no evidence has been gathered to date which shows FAD displacement. This work showed little off-target activity against the cytochrome P450 enzymes as well as human Ether-à-go-go (hERG). Importantly and finally, HCI2509 showed activity in cell-based assays, with two additional and unpublished cell-line panels reported in Appendix B. These results informed the decision to test HCI2509 in Ewing sarcoma and endometrial carcinoma.

5.1.2 HCI2509 is Uniquely Active in Ewing Sarcoma

HCI2509 showed particularly potent activity in multiple Ewing sarcoma cell lines. LSD1 was recently discovered as critical for EWS/FLI-mediated target gene repression through recruitment as a member of the NuRD complex (1). We hypothesized that through reactivation of EWS/FLI-repressed tumor suppressors, we were inducing apoptosis and impairing transformation in Ewing sarcoma cell lines. In order to test this

we looked at the transcriptional changes induced by HCI2509 treatment by RNA-sequencing and compared them to the transcriptional changes caused by EWS/FLI knockdown in the same cell line. We found that not only was HCI2509 disrupting EWS/FLI-mediated repression globally, but that it also impaired EWS/FLI-mediated transcriptional activation of critical oncogenes. This effect was observed at both direct and indirect target genes, and contrasted with HDAC inhibition with vorinostat, which only affected the EWS/FLI-repressed targets. The effect was so striking that we next asked whether or not it was specific to EWS/FLI, or whether HCI2509 would show comparable effects in a cell line containing an alternative EWS/ETS fusion, specifically EWS/ERG. We found the same phenomena where HCI2509 treatment disrupted the global EWS/ERG transcriptional program both at activated and repressed target genes. This was also the first time that the EWS/ERG transcriptional profile was published and, while unsurprising, it was observed that both EWS/FLI and EWS/ERG regulated similar transcriptional programs.

We further hypothesized that these transcriptional changes would be consistent across cell lines. Most Ewing sarcoma cell lines tolerate EWS/FLI knockdown poorly as compared to A673 cells and RNA-sequencing experiments are costly in both time and money. We thus performed qPCR after treatment with HCI2509 in several cell lines to assess the transcriptional changes in a 9-gene panel representing characteristic EWS/FLI target genes and saw consistent downregulation of EWS/FLI activated targets and vice versa across Ewing sarcoma cell lines.

Ewing sarcoma kills patients after relapse and metastasis. The cellular morphologies associated with Ewing sarcoma metastasis have been characterized by

Chaturvedi, *et al.* (2) and show that EWS/FLI most likely promotes metastatic phenotypes through decreased cellular adhesion, though not through migration and invasiveness. This mechanism is different from epithelial cancers, and so while it does not involve the epithelial-to-mesenchymal transition that LSD1 helps to regulate (3-5), we wanted to evaluate the effects in the same *in vitro* morphology assay used in (2). HCI2509 and siRNA-mediated knockdown of LSD1 both recapitulated the EWS/FLI knockdown phenotype here and HCI2509 prevented transformation in colony forming assays, confirming that LSD1 inhibition reverses some of the cellular phenotypes driven by EWS/FLI as would be predicted by the transcriptional profiling.

This was also the first study to demonstrate target engagement in cells, though indirectly, through *HMOX1* induction. LSD1 was found associated with the *HMOX1* promoter and siRNA-mediated knockdown of LSD1 showed dose-dependent increases in *HMOX1* transcript. *HMOX1* was of interest, because not only is it repressed by EWS/FLI and activated by HCI2509, but it is also downregulated in primary patient samples (6). This suggests that LSD1 inhibition may prove relevant to the transcriptional mechanism at work in human patients. Interestingly, even with target engagement demonstrated, the changes in global methylation at LSD1 substrates H3K4 and H3K9 were more subtle than anticipated in both the A673 and TTC466 cell lines. No significant changes were observed at H3K4, though H3K9me2 and H3K9me3 both significantly increased. A mechanistic understanding is yet to be determined.

Most importantly, LSD1 inhibition with HCI2509 showed single-agent antitumor efficacy in multiple Ewing sarcoma xenograft models. These models are notoriously difficult to carry out, as tumors typically show a wide range of growth rates, and are

likely log-normal distributed in this manner. However, HCI2509 showed a clear effect in all three models tested, with two complete regressions observed, and no observed toxicity. These data are extremely promising, as few treatment options work as single agents in mouse models of Ewing sarcoma, and they suggest a therapeutic window may be wide enough in this disease.

5.1.3 Antitumor Activity of HCI2509 in Endometrial Carcinoma

Having shown both target engagement and ruled out a nonspecific cytotoxic mechanism of action, we wanted to test whether HCI2509 would also show efficacy in a second malignancy also associated with epigenetic misregulation, though perhaps through more diverse mechanisms than a single translocation. Type II endometrial carcinoma was recently shown to commonly have driver mutations in chromatin regulatory enzymes, and was also sensitive to LSD1 inhibition in our cell-line screens with HCI2509. In this model system, LSD1 inhibition showed decreased proliferation and transformation in two cell lines that were refractory to hormone treatment. LSD1 inhibition caused perturbation of the cell cycle, though the mechanisms through which this occurs remain undetermined.

However, unlike Ewing sarcoma cell lines, H3K4me3 was significantly upregulated with HCI2509 treatment, and H3K9me2 varied between cell lines. HCI2509 induced *HMOX1* and the adhesion gene *CDH1*, further supporting that the proliferation, transformation, and cell cycle effects were the result of LSD1 target engagement. Significantly, LSD1 inhibition induced apoptotic cell death. We chose to pursue the question of *in vivo* efficacy with the KLE cell line in an orthotopic model. Type II

endometrial cancer is commonly disseminated in the peritoneal cavity and subcutaneous models simply cannot recapitulate this tumor environment. Epigenetics represents the intersection of the genes with the environment and in a disease driven by genes, environment, and epigenetics, evaluation of an epigenetic therapy requires testing in the most representative system feasible. In this model system of endometrial cancer, HCI2509 treatment was significantly associated with tumor regression, demonstrating single agent efficacy.

5.1.4 Noteworthy Observations

Taken together, this body of work both supports epigenetic therapy as a powerful tool in the treatment of cancer and underscores the amount of work left to be done in order to fully understand the mechanistic basis for therapeutic efficacy. For example, the EWS/ETS-based activity seen in Ewing sarcoma suggests LSD1 may act in a manner that is Ewing sarcoma specific. While the precise mechanisms are the topic for future studies, this particular instance is proof-of-concept that in at least some malignancies, epigenomic misregulation is so central to the disease etiology that it may prove feasible to hijack the whole oncogenic program. Ewing sarcoma is unique, however, in being relatively mutationally silent at onset (7), such that malignant reprogramming happens exclusively through epigenomic mechanisms. In other malignancies, we need better tools to identify which patients might benefit from particular epigenetic therapies. While LSD1 is broadly observed to be upregulated across dedifferentiated cancers, which perhaps hints at a common role in malignancy, it should be noted that the changes to global histone methylation with HCI2509 were markedly different in Ewing sarcoma and endometrial

carcinoma. Each disease will likely have its own etiology requiring deep sequencing experiments to fully grasp. However, some progress is being made, with SOX2 overexpression suggested as a biomarker denoting sensitivity to LSD1 inhibition in lung, breast, and ovarian carcinomas (8).

Another interesting observation not fully discussed in Chapters 2-4 is the fact that while both Ewing sarcoma and endometrial carcinoma showed *in vitro* sensitivity which translated *in vivo*, this is not true for all cell lines. In fact, the PC3 cell line showed very little sensitivity in the cell line screens up to 3 μ M (Appendix B), but was exquisitely sensitive in xenograft models when the plasma concentrations were consistently 200-400 nM (9). Further, this is consistent with drug development efforts in GlaxoSmithKline's LSD1 inhibitor program. Similarly insensitive cell lines *in vitro* show delayed tumor growth in xenograft models (10). The reasons for this remain unclear, but are likely related to poor correlation between *in vitro* culture conditions and the *in vivo* tumor microenvironment and how these signals are integrated at the epigenomic level. It also underscores the importance of well-designed *in vivo* studies which recapitulate the disease state as can best be achieved before human trials as the differences between mice and men are certainly as large as that between plastic and an immunodeficient mouse.

5.2 Future Studies

While on the whole the studies reported here show significant promise for LSD1 inhibitors as they progress to and through the clinic, several lines of inquiry became apparent as a result of this work. There are important questions to be asked from both a basic and translational perspective to build an understanding of the causal relationships

by which LSD1 drives cancer and how different modes of inhibition may impair those. This will enable more precise clinical science to get the right LSD1 inhibitor to the right patient as LSD1 inhibition reaches the clinic.

5.2.1 Biophysical and Biochemical Inquiries

Several biochemical questions remain unanswered, the most obvious of which is, is there a better way to show LSD1 binding within cells, preferably direct binding? A recently reported technique utilizing an in-cell version of the thermal shift assay (CETSA) (11) for binding may provide the answer. In essence, this assay calls for drug exposure either in cell lysates or whole cells. After equilibration, the lysates or cells are incubated at temperatures varying from 40-64°C, at which point cells are lysed if necessary. Protein which has unfolded and crashed out is then removed by centrifugation and the protein of interest is detected in the supernatant by western blot. The antibody used needs to be fairly sensitive and specific for the protein of interest. Ultimately, similar to the fluorescent thermal shift assay used in Chapter 2, the readout for binding is increased amounts of protein at higher temperatures than the vehicle control, to demonstrate the stabilizing effect of ligand binding. The most immediate follow on question is whether or not the compound binds any other proteins in the cell. This would require synthesis of a biotinylated derivative and confirmation that biotinylation does not completely abolish binding affinity. Any proteins that pull down with the compound could be further confirmed with CETSA.

The real elephant in the room is the binding mode of HCI2509. Given the complexities of LSD1 regulation discussed in Chapter 1, knowing the binding pocket

would enable the generation and testing of point-mutants, which should rescue enzymatic activity in the context of drug exposure. It would also identify potential mechanisms for the development of resistance. LSD1 has been crystallized in a number of hands (12-16) and in collaboration with the Chris Hill lab; crystallography is possible, though not required for clinical translation.

5.2.2 Further Routes of Inquiry in Ewing Sarcoma

LSD1 inhibition in and the epigenomics of Ewing sarcoma are major areas of research that remain incompletely explored, but show great promise. At a basic level, the histone methylation data reported in Chapter 3 comprise a crude and preliminary evaluation of the epigenetic impacts of LSD1 inhibition in Ewing sarcoma cells. Really, the “epigenetics” of HCI2509 in Ewing sarcoma are not yet worked out in mechanistic detail and the observed changes in global histone methylation marks are quite subtle. In order to understand what changes, and whether these changes are associated with EWS/FLI or LSD1 requires a minimum of directed ChIP studies at candidate loci, but more likely ChIP-seq for the histone marks of interest, LSD1 and EWS/FLI in the absence or presence of drug or various knockdowns. The very first questions to address are the genomic co-localization patterns of EWS/FLI and LSD1, specifically at active targets, as well as the sites of histone methylation mark changes in the context of drug treatment.

Other pieces of data show different transcriptional effects with different classes of LSD1 inhibitors. The irreversible inhibitors and HCI2509 appear to both modulate *HMOX1* in a dose-dependent fashion around the cell viability IC₅₀, which supports

HMOX1 as a bonfide LSD1 target. They both leave NR0B1 unaffected. Interestingly, the EWS/FLI activated gene NKX2.2 is downregulated by HCI2509 and the EWS/FLI-repressed CTGF is upregulated by HCI2509, but not the irreversible inhibitors (Figure 5.1). This is where identification of the binding mode and relevant protein-protein interactions partners would be potentially illuminating. Given that the binding mode is unknown and that LSD1 is bound, two possibilities exist, either there is something unknown about LSD1 biology or there is an unknown off-target effect, or both, and that these unknowns are particularly impactful in Ewing sarcoma. The next step is to test other potent and reversible inhibitors for the same transcriptional activity.

While the discussion in Chapter 1 of positive controls for novel modes of LSD1 inhibition still applies, it is worth investigating whether knockdown of LSD1 by siRNA or shRNA recapitulate the transcriptional and other effects of HCI2509 in Ewing sarcoma cells by RNA-seq, morphology assessments, colony forming assays, and tumorigenic studies. Optimization of siRNA in Chapter 3 showed a 50% reduction in LSD1 protein levels as the maximum knockdown attainable. If LSD1 is as critical as the inhibition data would suggest, it may be difficult to optimize a system with 80-90% knockdown of LSD1. Moreover, if an shRNA can be optimized, to what extent do different LSD1 mutants, for example, enzymatically dead or truncated, rescue LSD1 knockdown? Answers to these questions would help map the relevant domains on LSD1 for more mechanistic biochemical studies to clarify the role of LSD1 in Ewing sarcoma.

As mentioned, metastasis and recurrent disease are the killers in Ewing sarcoma, and the xenograft studies reported in Chapter 3 address only primary subcutaneous tumors. Intratibial models were used by Chaturvedi, *et al.* (2) to investigate the metastatic

behavior of Ewing sarcoma cells. Investigation of HCI2509 treatment in intratibial models of both mice and rats may prove useful in understanding the impact of LSD1 inhibition on the development of metastatic disease. Preliminary studies in nude rats show drastic differences in the development of metastases between vehicle and HCI2509 treated animals (Figure 5.2). The lung metastases in Figure 5.2 were undetectable using bioluminescent imaging, such that optimization of a different imaging modality is required.

Both *CTGF* and *HMOX1* were observed to be downregulated in primary patient samples of Ewing sarcoma and upregulated with HCI2509 treatment. As was reported in Chapter 3, secreted proteins were significantly upregulated by HCI2509. *IL8* is another secreted protein similarly downregulated by EWS/FLI and observed to be decreased in patient samples, and upregulated by HCI2509. *TGF β R2* was validated as a tumor suppressor gene repressed by EWS/FLI, both in cell lines and the clinic, and was also induced by HCI2509 treatment (1). The continued optimization of animal models provides an opportunity to explore the pharmacodynamics of secreted proteins, such as IL8 or CTGF, which may correlate with pharmacological modulation of HMOX1 or TGF β R2 levels in tumor samples.

In addition to response biomarkers, in order to translate LSD1 inhibition to the clinic for Ewing sarcoma, the use of HCI2509 needs to be assessed in combination with the other standards of care. This is required both *in vitro* and *in vivo* to evaluate the potential for drug synergy, antagonism, or unforeseen toxicity. The most likely candidates for these studies are irinotecan and temozolomide. Preliminary data from an SK-ES-1 xenograft model suggest that HCI2509 may show synergistic effects in

combination with temozolomide and larger studies are required to validate these results in other models of the disease (Figure 5.3).

All in all, the results reported in Chapter 3 represent a major advance in our ability to target EWS/ETS-mediated oncogenic transcriptional programs. It has pushed forward in a way that raises several fundamental basic science questions to address the mechanisms by which one small molecule can flip a switch recently thought unflippable with such strategies. Moving toward the clinic will likewise require efforts to develop appropriate preclinical models to truly test in animals what we hope to test in the clinic in order maximize the predictive value of preclinical work. Ewing sarcoma is a rare disease that affects young adults, and any human trial in this population needs to be as tightly designed as possible to determine whether this could provide better therapeutic options for this aggressive malignancy.

5.2.3 Further Routes of Inquiry for Endometrial Carcinoma

Given the promising results both *in vitro* and *in vivo* in endometrial carcinoma, several follow up studies are warranted. From the perspective of basic LSD1 biology, it is interesting, though perhaps not unexpected, that the observed changes in global histone methylation are different in endometrial cancer than those shown for Ewing sarcoma. Moreover, the two cell lines tested showed slightly different global histone methylation changes in response to HCI2509 exposure, notably H3K9me2 increased in AN3CA cells while remaining unchanged in KLE cells. The biological mechanisms driving this difference may provide insight about the varying role of LSD1 in different cell lines and differentiate which phenomena are most associated with the antitumor effects of

HCI2509. Testing this pharmacodynamic marker for LSD1 inhibition across more endometrial carcinoma cell lines, both Type I and Type II, could shed further light on the impact of HCI2509 on global histone methylation in endometrial cancer, and allow analysis of whether changes in any one mark predict sensitivity to HCI2509. It would also be helpful to know how global epigenetic changes translate to transcriptional changes in endometrial carcinoma, such that RNA-seq and ChIP-seq similar to those proposed for Ewing sarcoma should be pursued. Further, validation that LSD1 inhibition phenocopies siRNA-mediated LSD1 knockdown would strengthen this work, though this approach needs to be undertaken with careful consideration due to the complexities of LSD1 biology, described in Chapter 1.

Translating this work to the clinic will required addressing whether the antitumor efficacy observed across cell lines also holds true in multiple xenograft models, including those derived from primary tumor tissue. Additionally, HCI2509 should be screened for synergy both *in vitro* and *in vivo* with the current standards of care. Pretreatment with HCI2509 for 24 hours showed no sensitization to progesterone *in vitro* for AN3CA or KLE (Figure 5.4), though this may not be true for other Type II endometrial carcinoma cell lines or models of Type I disease. Overall, the data reported for Type II endometrial cancer warrant continued preclinical evaluation of LSD1 inhibition in this aggressive gynecologic malignancy.

5.2.4 Formulation

One of the major remaining hurdles for translation of this compound series to the clinic is the optimization of a more clinically acceptable formulation. The relative

hydrophobicity ($\log P=3.96$) and high melting temperature ($>220^{\circ}\text{C}$) of HCl2509 classify the compound as “brick dust.” Moreover, the hydrazone core is amenable to a relatively planar conformation and contains several hydrogen bond donors and acceptors for inter- and intramolecular hydrogen bonding. Together, these factors contribute to drive HCl2509 to form needle-like crystals in aqueous formulations. Ideally, translation to the clinic would involve the development of an oral formulation or tablet. This would likely require the development of an amorphous form or salt, as well as inclusion of surfactants or wetting agents to promote dissolution. The hydrazone moiety also necessitates the use of enteric coating to prevent acid-catalyzed hydrolysis of the compound.

Taken together, these factors have limited the available preclinical formulation strategies. Salt formation has been attempted multiple times by Venkataswamy Sorna to no avail. Ultimately, we utilized several different cosolvent strategies for the preclinical studies reported here, with both stable solutions and suspension tested in pharmacokinetic studies. Efficacy studies utilized a stable suspension of HCl2509 crystals dosed 30 mg/kg directly into the peritoneal cavity. There are different features of Ewing sarcoma and endometrial carcinoma to consider in the design of formulations to enable future studies in these diseases. Ewing sarcoma requires systemic treatment to target metastatic and micrometastatic disease as adjuvant therapy in concert with surgical resection. Oral tablets or intravenous routes of delivery would be appropriate. However, while metastatic endometrial cancer may benefit from a similar strategy, in cases where the disease remains localized to the peritoneal cavity or uterus, delivery via intravaginal gel may offer an attractive alternative route. This type of localized delivery minimizes the risk of off-target systemic toxicities or undesirable epigenetic reprogramming. Further, a

vaginal gel might be formulated to contain varying combinations of agents which show synergistic effect, for example, progesterone therapy. Varying the formulation strategy for the same epigenetic agent could tailor the desired epigenetic reprogramming effects to the specific needs of the disease of interest.

5.3 Outlook

The overarching goal of this lab is to provide cancer patients with innovative targeted therapeutic options. This project addressed that larger goal through the identification and validation of a novel series of potent, specific, and reversible LSD1 inhibitors, both biochemically and in preclinical models of cancer. Ultimately the N'-(1-phenylethylidene)-benzohydrazides series of inhibitors have cast new light on the biology of Ewing sarcoma that may lead to improved clinical care for this rare and aggressive disease through both translational and basic research. Additionally, the compound series identified herein showed single agent efficacy in Type II endometrial cancer, suggesting epigenetic inhibition may provide therapeutic benefit in this aggressive gynecologic malignancy. Detailed mechanistic studies are still required in both disease areas to fully elucidate the biological role for LSD1 and the mechanism by which HCI2509 acts.

HCI2509 faces many hurdles on the road to the clinic. While HCI2509 is highly permeable, solubility remains a major challenge. Either analogues more amenable to salt formation or possessing more favorable solubility characteristics would be preferable for additional preclinical studies and clinical development. Candidate derivatives are currently under investigation at the Center for Investigational Therapeutics and remain a promising topic for future study. Until then, HCI2509 is a useful tool for proof-of-

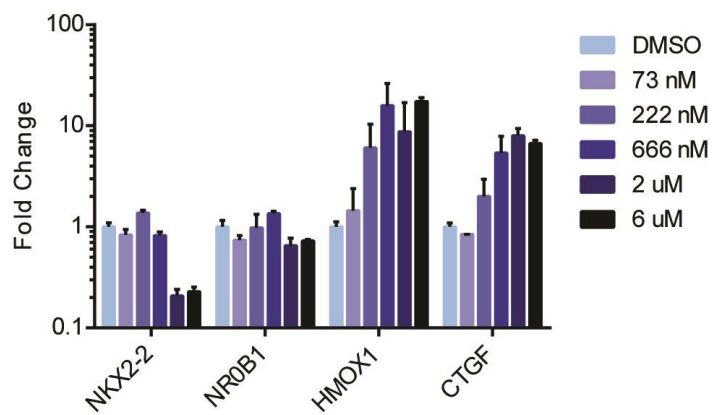
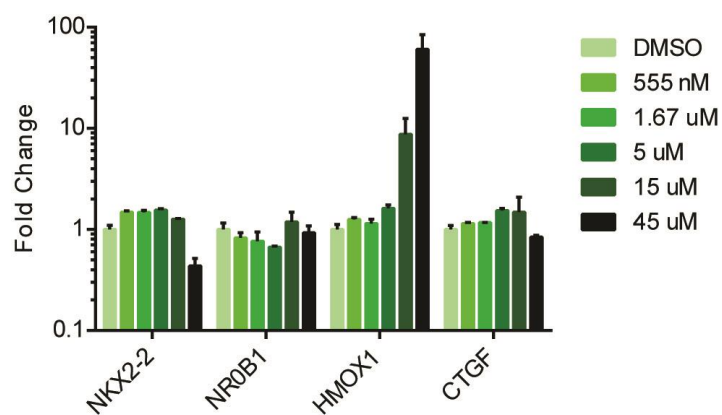
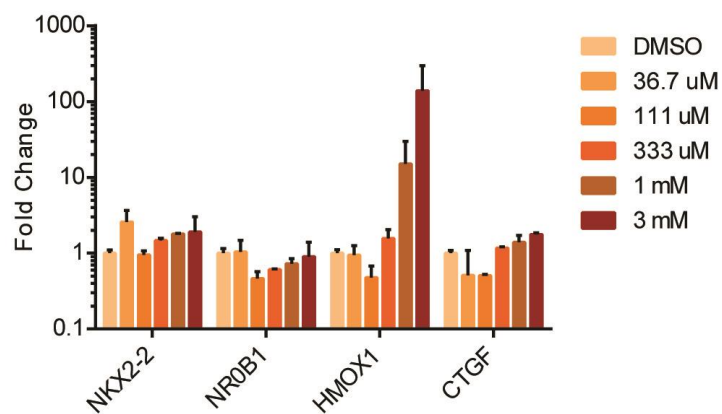
concept and mechanistic studies in both *in vitro* and *in vivo* model systems and will inform the clinical development and use of novel reversible LSD1 inhibitors for Ewing sarcoma, endometrial carcinoma, and other malignancies.

5.4 References

1. Sankar S, Bell R, Stephens B, Zhuo R, Sharma S, Bearss DJ, et al. Mechanism and relevance of EWS/FLI-mediated transcriptional repression in Ewing sarcoma. *Oncogene* 2012;32:5089-100.
2. Chaturvedi A, Hoffman LM, Welm AL, Lessnick SL, Beckerle MC. The EWS/FLI oncogene drives changes in cellular morphology, adhesion, and migration in Ewing sarcoma. *Genes Cancer* 2012;3:102-16.
3. Lin T, Ponn A, Hu X, Law BK, Lu J. Requirement of the histone demethylase LSD1 in Snail-mediated transcriptional repression during epithelial-mesenchymal transition. *Oncogene* 2010;29:4896-4904.
4. Lin Y, Wu Y, Li J, Dong C, Ye X, Chi YI, et al. The SNAG domain of Snail1 functions as a molecular hook for recruiting lysine-specific demethylase 1. *EMBO J* 2010;29:1803-16.
5. McDonald OG, Wu H, Timp W, Doi A, Feinberg AP. Genome-scale epigenetic reprogramming during epithelial-to-mesenchymal transition. *Nat Struct Mol Biol* 2011;18:867-74.
6. Kauer M, Ban J, Kofler R, Walker B, Davis S, Meltzer P, et al. A molecular function map of Ewing's sarcoma. *PLoS ONE* 2009;4:e5415.
7. Crompton B, Stewart C, Taylor-Weiner A, Alexa G, Kurek K, Calicchio M, et al. The genomic landscape of pediatric Ewing sarcoma. [abstract]. In: Proceedings of the 105th Annual Meeting of the American Association for Cancer Research; 2014 Apr 5-9; San Diego, CA. Abstract nr 999.
8. Zhang X, Lu F, Wang J, Yin F, Xu Z, Qi D, et al. Pluripotent stem cell protein Sox2 confers sensitivity to LSD1 inhibition in cancer cells. *Cell Rep* 2013;5:445-57.
9. Theisen ER, Bearss J, Sorna V, Bearss DJ, Sharma S. Targeted inhibition of LSD1 in castration-resistant prostate cancer. In: Proceedings of the American Association for Cancer Research 104th Annual Meeting 2013: 6-10 April 2013; Washington, DC.

10. Kruger R. Novel anti-tumor activity of targeted LSD1 inhibition. [Presentation]. In: Proceedings of the 105th Annual Meeting of the American Association for Cancer Research; 2014 Apr 5-9; San Diego, CA. Abstract nr SY35-03.
11. Martinez Molina D, Jafari R, Ignatushchenko M, Seki T, Larsson EA, Dan C, et al. Monitoring drug target engagement in cells and tissues using the cellular thermal shift assay. *Science*. 2013;341:84-7.
12. Yang M, Gocke CB, Luo X, Borek D, Tomchick DR, Machius M, et al. Structural basis for CoREST-dependent demethylation of nucleosomes by the human LSD1 histone demethylase. *Molecular Cell* 2006, 23:377-387.
13. Stavropoulos P, Blobel G, Hoelz A. Crystal structure and mechanism of human lysine-demethylase 1. *Nat Struct Mol Biol* 2006;13:626-32.
14. Baron R, Binda C, Tortorici M, McCammon JA, Mattevi A. Molecular mimicry and ligand recongnition in binding and catalysis by the histone demethylase LSD1-CoREST complex. *Structure* 2011;19:212-220.
15. Yang M, Culhane JC, Szewczuk LM, Gocke CB, Brautigam CA, Tomchick DR, et al. Structural basis of histone demethylation by LSD1 revealed by suicide inactivation. *Nat Struct Mol Biol* 2007;14:535-9.
16. Forneris F, Binda C, Adamo A, Battaglioli E, Mattevi A, Structural basis of LSD1-CoREST selectivity in histone H3 recognition. *J Biol Chem* 2007;282:20070-4.

Figure 5.1 The effects of different classes of LSD1 inhibitors on EWS/FLI targets. (A,B,C) The change in gene expression of EWS/FLI-activated targets *NKX2-2* and *NROB1* and EWS/FLI-repressed targets *HMOX1* and *CTGF* induced by (A) HCI2509, (B) the irreversible inhibitor OG-L002 (biochemical IC₅₀ ~ 20 nM), and (C) tranilcypromine (biochemical IC₅₀ ~ 20 uM). A673 cells were treated with varying concentrations of inhibitor for 48 hours before RNA was harvested. Doses were chosen based on the IC₅₀ of the inhibitor in a 96-hour cell viability assay such that the dose range is centered around the IC₅₀. HCI2509 results in decreased expression in *NKX2-2*, no effect on *NROB1*, and dose-dependent increases in *CTGF* and *HMOX1*, consistent with the result in Chapter 3. Interestingly, both other LSD1 inhibitors are much less potent at decreasing cell viability and only recapitulate *HMOX1* induction.

A HCl2509**B OG-L002****C Tranylcypromine**

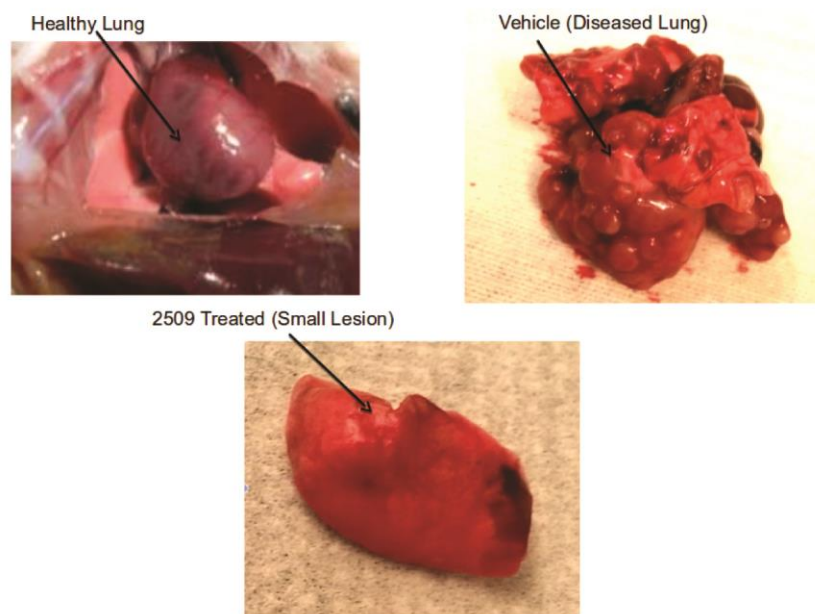


Figure 5.2 HCl2509 decreases metastasis in a nude rat model of Ewing sarcoma. A dose 5×10^6 SK-N-MC cells were implanted in the tibia of nude rats ($n=6$) and allowed to engraft for 7 days. At that time the primary tumor was imaged by bioluminescence and animals were randomized into vehicle or treatment groups. Treatment animals received daily intraperitoneal injections of 60 mg/kg of HCl2509. After 4 weeks of treatment, animals were taken off of the study and monitored. Thirty days later, rats were sacrificed and lung metastases were observed in vehicle-treated animals, while very little metastatic disease was observed in HCl2509-treated animals.

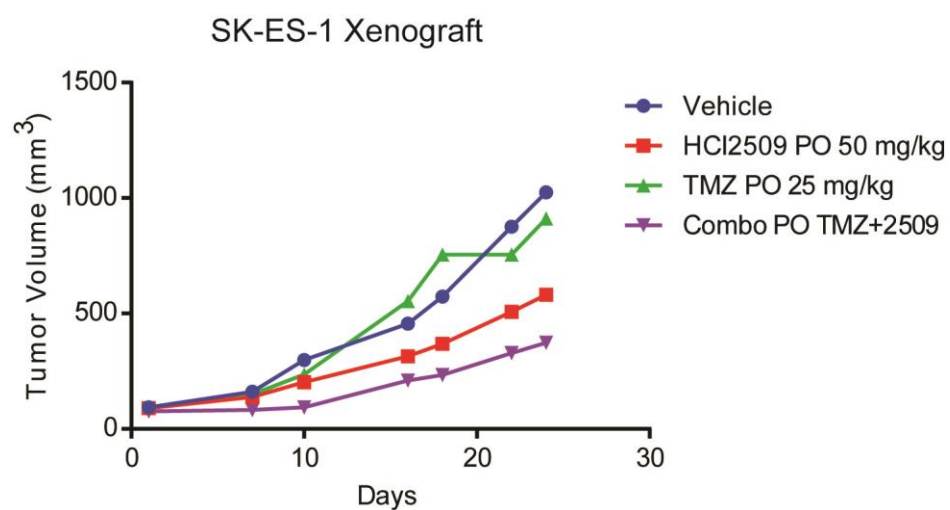


Figure 5.3 Potential synergy between HCl2509 and temozolomide *in vivo*. In a subcutaneous hindflank SK-ES-1 xenograft study of HCl2509 dosed with vehicle (n=10), 50 mg/kg HCl2509 (n=10), 25 mg/kg temozolomide (n=10), or a combination (n=10) orally showed potential synergistic activity between HCl2509 and temozolomide. The tumor model displays a fair amount of variability, such that error bars were removed for clarity. The mean for each group at their respective time point is plotted.

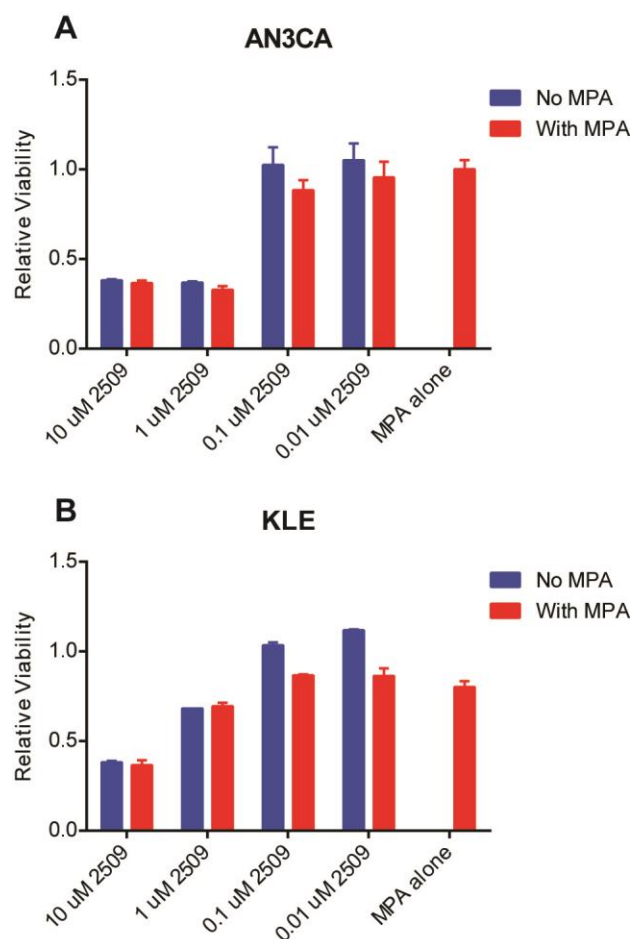


Figure 5.4 HCl2509 does not sensitize cells to treatment with medroxyprogesterone 17-acetate (MPA). (A,B) AN3CA (A) and KLE (B) cells were pretreated with varying concentrations of HCl2509 for 24 hours before being treated with either mock or 10 μ M MPA for an additional 72 hours. Controls included vehicle (0.5% DMSO) and vehicle treatment for 24 hours followed by 10 μ M MPA for an additional 72 hours (MPA alone). Overall, KLE cells were slightly affected by MPA, but no additive effects are observed in the context of HCl2509.

APPENDIX A

PURIFICATION OF LYSINE-SPECIFIC

DEMETHYLASE 1

A.1 Protein Purification Protocol: Full Length LSD1

Transform BL21*(DE3) cells with pET15b-hLSD1 (Amp resistance) and allow colonies to grow overnight at 37°C. Inoculate 5 mL of LB+Amp with one colony and allow to grow at 37°C+shaking until OD₆₀₀~0.6-1. Inoculate 50 mL of LB+Amp with desired amount of previous culture to grow at 37°C+shaking overnight. In the morning, take 6 mL for every liter of induction media to inoculate and centrifuge at 3000 rcf for 20 minutes.

Inoculate 1L of LB+Amp with desired amount of bacteria and grow until culture reaches OD₆₀₀~0.8-0.9. Induce expression with 0.5 mM IPTG and reduce temperature to 22°C and rpm to 180. Shake for 20 hours and then collect pellets.

Thaw pellet halfway in cold running water and the remaining halfway on ice. Once thawed, add 1 mg/mL lysozyme and Dnase (optional). Sonicate to lyse 7 cycles of [45 seconds on, 1 minute off]. Clean sonicator tip between tubes/beakers to improve lysis of later samples.

Ultracentrifuge lysate at 40K rcf, 4°C, for 45 minutes and discard supernatant. Resuspend pellet in His Extraction Buffer. Ultracentrifuge lysate at 40K rcf, 4°C, for 45 minutes and collect supernatant. Equilibrate column by rinsing off with His-B Buffer followed by His-A Buffer. Run supernatant over desired His column to load protein. Instead, wash with His-A Buffer until back to baseline. Elute with a 15-20 column gradient. Collect appropriate fractions.

Dialyze eluent into TGEK-50 depending on your final goal (you may need to concentrate your sample after dialysis; I would just do two size exclusion runs and combine everything). Ultracentrifuge dialyzed protein at 40K rcf, 4°C, for 45 minutes

and collect supernatant. Equilibrate S-column (S) with TGEK-1000 and -50 (1000 and 50 mM KCl, respectively). Run protein over ion exchange column and elute with a salt gradient over 15-20 columns.

Dialyze ion exchange eluent into TGEK-300. Equilibrate size exclusion column in the TGEK-300. Ultracentrifuge dialyzed protein at 40K rcf, 4°C, for 45 minutes before running size exchange. Collect appropriate fractions for use, concentrate in stirred cell if desired, aliquot, and flash freeze. Typical yield ~1 mg or less/L.

A.2 Buffers

A.2.1 His Extraction Buffer

- 25 mM Tris
- 1 M NaCl
- 0.1 mM EDTA
- 10 mM Imidazole
- +Fresh BME (7 uL per 100 mL buffer) and PMSF (0.5 mM)

A.2.2 His A Buffer

- 25 mM Tris
- 1 M NaCl
- 0.1 mM EDTA
- 10 mM Imidazole
- +Fresh BME (7 uL per 100 mL buffer) and PMSF (0.5 mM)

A.2.3 His B Buffer

- 25 mM Tris
- 1 M NaCl
- 0.1 mM EDTA
- 500 mM Imidazole
- +Fresh BME (7 uL per 100 mL buffer) and PMSF (0.5 mM)

A.2.4 T/CGEK

(For T/CEK do not add glycerol)

- T=tris (pH~7) C=citrate (pH~5.2)
- 25 mM T or C
- 10% glycerol (G)
- 1 mM EDTA (E)
- desired concentration of KCl
- +Fresh BME (7 uL per 100 mL buffer) and PMSF (0.5 mM)

A.3 Results

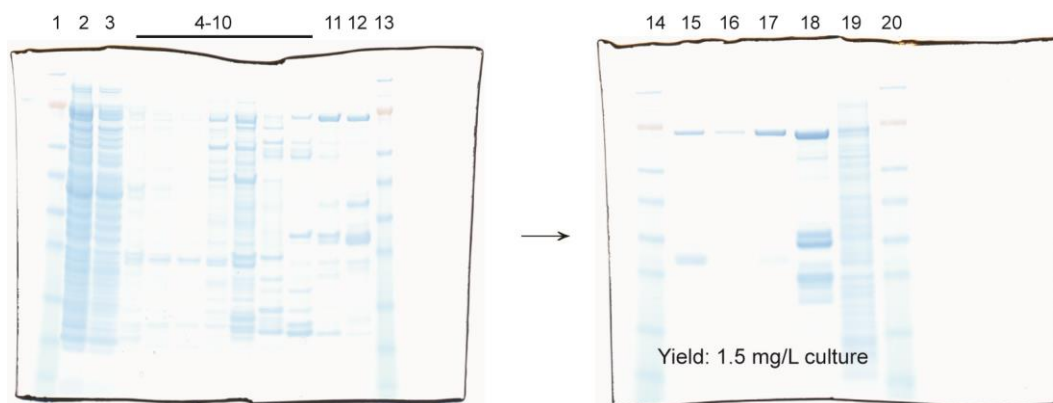


Figure A.1 Chromatography tracking LSD1 purification. The columns on the first gel are as follows: 1=ladder, 2=lysate loaded onto column, 3=flow through, 4-10=discarded elution fractions during imidazole gradient, 11-12=fractions containing LSD1 band at 96 kDa, 13=ladder. The columns on the second gel are as follows: 14=ladder, 15=loaded sample, 16=collected fractions, 17=concentrated final product, 18=positive control from Hontao Yu Lab, 19=Cayman Chemical hLSD1, 20=ladder.

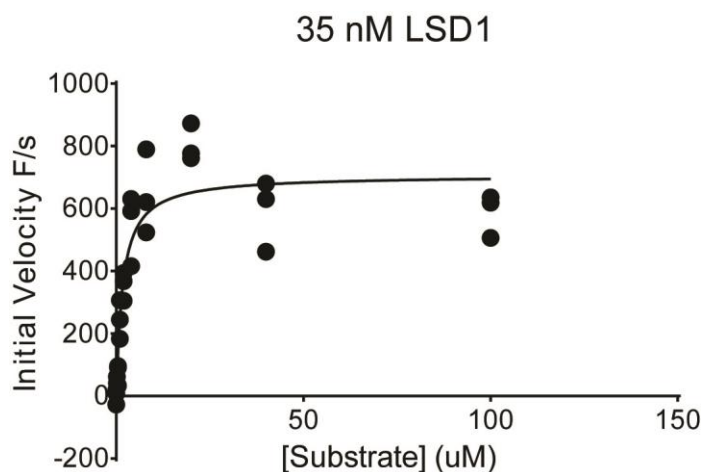


Figure A.2 Purified protein is active. Confirmation of active enzyme using the Michaelis-Menten conditions described in Chapter 1. Substrate is the H3K4me2 H3 peptide (residues 1-21).

APPENDIX B

IN-HOUSE CELL LINE SCREEN AND
XCELLIGENCE PROFILING

B.1 96-Cell Line Panel

Table B.1 A 96-cell line panel. Ninety-six cell lines were assayed for decreased cell viability by ATP-Lite after 96-hours of HCI2509 treatment.

Cell Line	IC50 (μM HCI2509)	Malignancy
SK-ES-1	0.47	Ewing's sarcoma
NCCIT	0.47	embryonal teratoma
Raji	0.49	B-Lymphocyte; Burkitt's Lymphoma
S-16		Schwann cells
Ramos	0.52	Lymphoblastoid
U-937	0.55	Macrophage; histiocytic lymphoma
H647	0.57	metastatic adenosquamous lung carcinoma
Skov-3	0.65	ovarian adenocarcinoma
MCF-7	0.66	metastatic breast adenocarcinoma
BT-20	0.77	mammary gland; carcinoma
RL-95-2	0.78	uterine endometrial carcinoma
LNCap	0.78	prostate carcinoma
AN3-CA	0.73	uterine endometrial adenocarcinoma
Her-218	0.62	breast
C-6	0.74	glioma
TC-32	0.85	Ewing's sarcoma
A673	0.93	Ewing's sarcoma
Hs-B2	0.99	Leukemic t-cell
Jurkat	0.93	T-cell
SaOS-2	0.89	osteosarcoma
LOX	0.90	malignant melanoma
BT-549	1.05	mammary gland ductal carcinoma
Hep-G2	0.94	hepatocellular carcinoma
H1666	0.97	colorectal carcinoma
F98	0.99	glioma
EWS-502	0.92	Ewing's sarcoma
Hs700-T	0.93	Pancreatic
MV4-11	0.97	biphenotypic B myelomonocytic leukemia
AGS	0.92	gastric adenocarcinoma
C-33A	1.11	cervical carcinoma
Ovcar-8	0.85	ovary

Table B.1 Continued

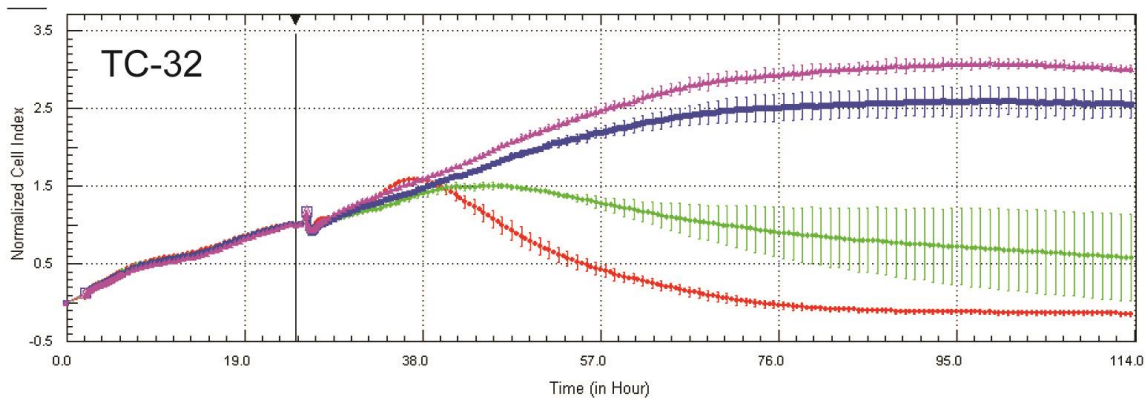
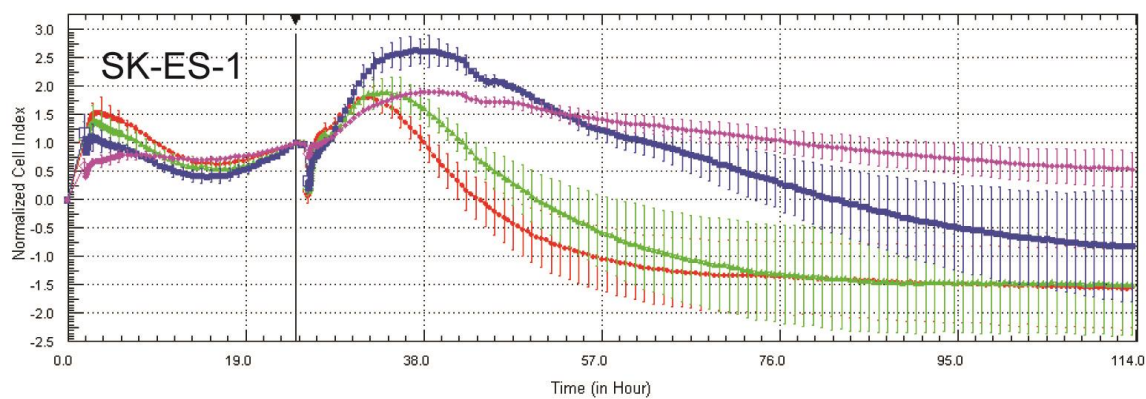
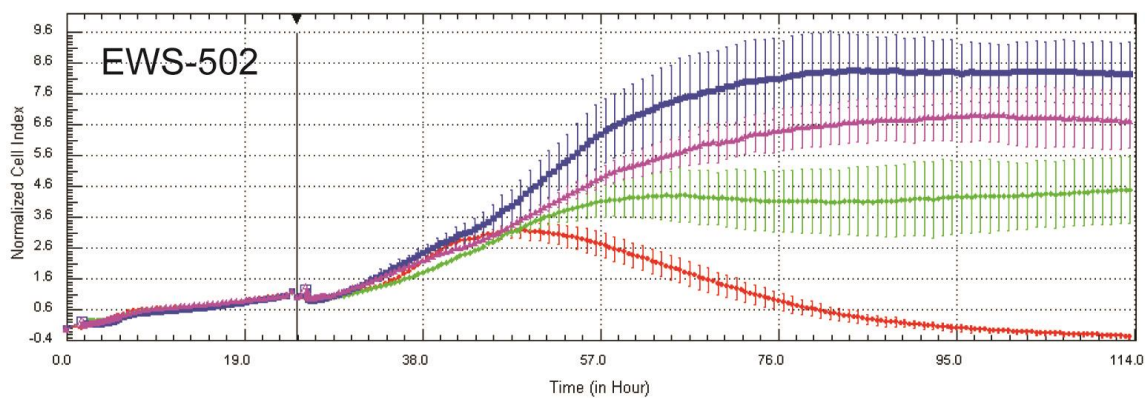
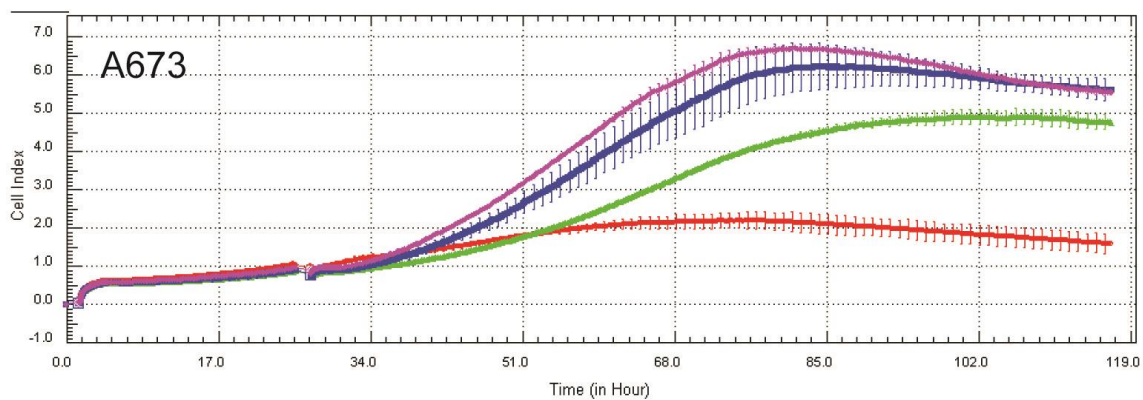
Cell Line	IC50 (μM HCl2509)	Malignancy
Hs578-T	1.15	Breast
Kato-III	1.06	gastric carcinoma
Capan-1	1.07	liver met of panc primary
U251	1.19	glioblastoma
K562	1.22	chronic myelogenous leukemia
HL-60	1.05	acute promyelocytic leukemia
MDA-MB-468	1.17	breast carcinoma
Molt-4	1.10	acute lymphoblastic leukemia
RD-ES	1.25	Ewing's sarcoma
HeLa	1.22	cervical adenocarcinoma
Hec-1-A	1.25	uterine endometrial adenocarcinoma
T98-G	1.19	glioblastoma multiforme
Colo-205	1.29	colorectal adenocarcinoma
Hs-B2	1.33	T-lymphoblastic leukemia
Su-DHL6	1.32	B-cell
HPAF-2	1.40	Pancreas
Kasumi -1	1.27	AML
KG-1	1.27	AML
A2780	1.10	Ovarian carcinoma
HCT-116	1.13	Colorectal carcinoma
HT-29	1.20	colorectal adenocarcinoma
BxPc-3	1.20	Pancreas adenocarcinoma
SK-MEL-5	1.27	melanoma
Hel	1.46	Bone-erythro leukemia
U87-MG	1.73	Glioblastoma-astrocytoma
Yugen-8	1.15	metastatic melanoma
MG-63	1.59	osteosarcoma
TC-71	1.42	Ewing's sarcoma
MDA-MB-231	1.50	Metastatic breast adenocarcinoma
AsPc-1	1.55	Metastatic pancreatic adenocarcinoma
RKO	1.74	Colorectal carcinoma
J82	1.68	bladder carcinoma
Malme-3M	1.74	malignant melanoma
H1781	1.89	NSCLC
IOMM-1	1.68	malignant meningioma
PSN-1	1.74	pancreatic adenocarcinoma
HCT-15	1.77	colorectal carcinoma

Table B.1 Continued

Cell Line	IC50 (μM HCl2509)	Malignancy
SW-480	1.60	colorectal adenocarcinoma
Hs822-T	1.96	Ewing's sarcoma
MiaPaCa-2	2.10	pancreatic carcinoma
A498	2.20	kidney carcinoma
OPM-2	2.51	myeloma
Caki-1	1.83	kidney carcinoma
HPAC	2.38	pancreatic adenocarcinoma
Wi-58	2.56	Normal Lung
786-0	2.28	renal adenocarcinoma
Du-145	2.45	brain met of prostate
SK-UT-1	2.34	uterine sarcoma
SK-MEL-2	2.62	melanoma
PC-12	2.88	adrenal phaeochromocytoma
H460	2.39	Large cell lung carcinoma
Panc-1	2.19	pancreatic carcinoma
Mut-J	2.39	pancreatic
H1975	2.89	NSCLC
H522	2.94	NSCLC
SNU-16	1.78	gastric cancer
A549	2.65	lung carcinoma
Hek-293	2.27	Embryonic kidney
Hs-766-T	2.41	Metastatic pancreatic adenocarcinoma
MDA-MB-435	2.81	Melanoma
H441	2.80	lung papillary adenocarcinoma
PC-3	2.82	Bone met of prostate
CFPAC-1	3.16	Pancreas
Hup-T4	2.67	Pancreatic adenocarcinoma
Panc-02-03	3.00	pancreatic adenocarcinoma

B.2 xCELLigence Profiling

Figure B.1 xCelligence screen of Ewing sarcoma cell lines. Real-time measurement of cellular index in four Ewing sarcoma cell lines after treatment with 0.3% DMSO (blue), 300 nM HCI2509 (purple), 1 μ M HCI2509 (green), or 3 μ M HCI2509 (red) following 24 hours of cell seeding. Measurements were taken every 2 hours. Data are presented as mean and standard deviation (n=3). These data were used to pick the appropriate dose and timing for many experiments reported in Chapter 3, specifically RNA-seq. Cellular index is a measure of electrical impedance of current passed through the media caused by the adherence of cells to gold electrode on the base of the tissue culture plate.



APPENDIX C

PHARMACOKINETIC MEASUREMENTS IN MICE

Emily R. Theisen, Jared Bearss, Adam Hollerbach

Emily R Theisen and Jared Bearss performed the animal dosing, plasma collection, extraction, and sample preparation. Adam Hollerbach of the Department of Chemistry Mass Spectrometry Core designed and optimized the mass spec detection protocol.

C.1 Mass Spectrometry Methodology

C.1.1 Quantitation of HCl-2509 in Rat and Mouse Plasma

C.1.1.1 Preparation of HCl2509 Stock Solution

Prepare stock solution of 1.25 mg/mL HCl2509 in DMSO. Add 40 μ L of stock solution to 960 μ L of plasma, to make a 50.0 μ g/mL spiking solution.

C.1.1.2 Preparation of Standard Curve

Standard (Final Conc, ng/mL)	Spiking Solution (μ g/mL)	Aliquot Volume (μ L)	Blank Plasma Volume (μ L)	Final Volume (μ L)
25,000	50.0	200	200	400
18,750	50.0	150	250	400
12,500	50.0	100	300	400
5,000	50.0	50	450	500
2500	50.0	20	380	400
1250	50.0	10	390	400
500	5.00	50	450	500
250	5.00	20	380	400
125	5.00	10	390	400
50.0	0.500	40	360	400
25.0	0.500	20	380	400
12.5	0.500	10	390	400

C.1.1.3 Preparation of HCl2528 (Compound **14** Chapter 2) Stock

Make a stock of 1.25 mg/mL HCl-2528 (internal standard) in DMSO. Add 10 μ L of stock solution to 1990 μ L of DMSO, to make a 6.25 μ g/mL spiking solution.

C.1.1.4 Sample Preparation

All samples should be kept on ice until processing. Pipette 50 μ L of blank plasma (double blank and blank), standard, or subject sample into a 1.5mL microcentrifuge tube.

Add 5 μ L of internal standard to each tube except double blank. Prepare a tube with just serum and the internal standard as a control. Add 150 μ L acetonitrile and vortex vigorously for 60 seconds. Centrifuge at top speed for 5 minutes in refrigerated centrifuge set to 4°C. Pipette 150 μ L water into a separate 1.5mL microcentrifuge tube. Add 150 μ L supernatant (top layer) from the extract and vortex vigorously for ~10 sec. Store samples and standard curve at -20°C until analysis.

C.1.1.5 Liquid Chromatography Parameters

Waters ACQUITY H-CLASS

- Column: Waters Xbridge C18 3.5 μ m, 4.6x50mm
- Solvent C Name: Formic Acid
- Solvent D Name: Acetonitrile
- Low Pressure Limit: 0 psi
- High Pressure Limit: 15000 psi
- Seal Wash Period 5.00 min
- Gradient:

Time (min)	Flow Rate (mL/min)	%C	%D	Curve
1. Initial	1.000	60.0	40.0	Initial
2. 1.00	1.000	60.0	40.0	6
3. 2.50	1.000	00.0	100.0	6
4. 4.00	1.000	60.0	40.0	6
5. 5.00	1.000	60.0	40.0	6

C.1.1.6 Mass Spec Parameters

Waters ACQUITY TQD

- Capillary (kV) 3.50

- Source Temperature (°C) 100
- Desolvation Temperature (°C) 215
- Cone Gas Flow (L/Hr) 5
- Desolvation Gas Flow (L/Hr) 550
- Collision Gas Flow (mL/Min) 0.22

C.1.1.7 MRM Parameters

Compound	Parent (m/z)	Daughter (m/z)	Dwell (s)	Cone (V)	Col (V)
HCl-2528	396.1	168	0.100	30	23
HCl-2509	468.1	168	0.100	35	25

C.2 Pharmacokinetic Measurements in Mice

C.2.1 Dosing

Mice were dosed by intravenous tail injection (IV) or by oral gavage (PO) with HCl2509. At the desired time point mice were sacrificed and blood was collected by cardiac puncture. Plasma was then stored at -80 °C until analysis. Formulations for 5mg/kg IV and 20 mg/kg PO dosing were stable solutions. Formulations for 50 mg/kg PO and 40 mg/kg IP were stable suspensions of HCl2509 crystals which were administered through a 22 ½ gauge needle.

Generally speaking, in mice, HCl2509 appears to be rapidly cleared (Cl=24.33 ml/min/kg) with a half-life of 0.87 hour. The bioavailability of HCl2509 from oral formulations varied depending on whether the form was a solution and a suspension. The solution form (F=27%) showed much greater bioavailability than the suspension (F=4.5%), consistent with high predicted permeability for HCl2509 and related

compounds. In the case of the suspension, the low bioavailability is likely due to the stability of HCl2509 crystals as they pass through the GI tract. The acid lability of the hydrazone moiety likely decreases the observed F for both oral forms. Efficacy studies utilized a suspension dosed intraperitoneally, which provided a depot for release of drug out to 4 hours.

C.2.1.1 Formulations

C.2.1.1.1 5 mg/kg IV and 20 mg/kg PO – Clear, Yellow Solution

- 15% N,N-dimethylacetamide
- 20% Propylene glycol
- 25% Water for injection
- 40% Polyethylene glycol 400 MW

C.2.1.1.2 50 mg/kg PO – Stable, Crystalline Suspension

- 10% Ethanol
- 40% Propylene glycol
- 50% Phosphate-buffered saline (pH 7.4)

C.2.1.1.3 40 mg/kg IP – Stable, Crystalline Suspension

- 50% PEG400
- 50% PBS
- Drug was completely dissolved in PEG400 using sonication and PBS added.

Table C.1 Pharmacokinetic parameters for 5 mg/kg HCl2509 dosed as solution IV.

Parameter						
Time (hr)	C_p HCl2509 (ng/ml)					
	Mice 1-8	Mice 9-16	Mice 17-24	Mean	STDEV	%CV
0.08333	7391	8228	6338	7319	947	12.9
0.25	3251	2578	3797	3209	610	19.0
0.5	1374	1768	1589	1577	197	12.5
1	655	414	891	653	239	36.5
2	119	88	235	147	77.5	52.6
4	0	24	35	19.7	17.9	91.0
8	0	17	12	9.67	8.74	90.4
24	0	0	0	0	0	
C₀ (ng/mL)	11143.85	14698.90	8188.44	11343.73	3259.83	28.7
AUC_{0-t} (ng*hr/mL)	3131.48	3389.52	3670.09	3397.03	269.39	7.9
AUC_{0-∞} (ng*hr/mL)	3203.97	3416.66	3688.64	3436.43	242.94	7.1
V_{ss} (L/kg)	0.6348	0.8337	1.001	0.8231	0.1833	22.3
Cl (mL/min/kg)	26.01	24.39	22.59	24.33	1.710	7.0
MRT (hr)	0.4067	0.5697	0.7385	0.5716	0.1659	29.0
T_{1/2} (hr)	0.4222	1.107	1.072	0.8669	0.3855	44.5

Table C.2 Pharmacokinetic parameters for 20 mg/kg HCl2509 dosed as solution PO.

Parameter						
Time (hr)	C_p HCl2509 (ng/ml)					
	Mice 1-7	Mice 8-14	Mice 15-21	Mean	STDEV	%CV
0.25	638	1162	852	884	263	29.8
0.5	851	1163	792	935	199	21.3
1	346	440	999	595	353	59.3
2	246	219	231	232	13.5	5.8
4	69	302	155	175	117	67.2
8	56	422	64	181	209	115.7
24	3	3	10	5.33	4.04	75.8
C_{max} (ng/mL)	851	1163	999	1004.33	156.07	15.5
T_{max} (hr)	0.5	0.5	1	0.6667	0.28868	43.3
AUC_{0-t} (ng*hr/mL)	1898.13	6535.13	2790.75	3741.33	2460.32	65.8
AUC_{0-∞} (ng*hr/mL)	1916.39	6546.98	2862.96	3775.44	2446.44	64.8
AUMC_{0-∞} (ng*hr²/mL)	7630.51	39569.1	12798.41	19999.3	17143.75	85.7
MRT (hr)	3.982	6.044	4.470	4.832	1.078	22.3
T_{1/2} (hr)	4.220	2.739	5.005	3.988	1.151	28.8
F_{0-t}	0.1397	0.4809	0.2054	0.2753	0.1811	65.7

Table C.3 Pharmacokinetic parameters for 50 mg/kg HCl2509 dosed as suspension PO.

Parameter						
Time (hr)	C_p HCl2509 (ng/ml)					
	Mice 1-8	Mice 9-16	Mice 17-24	Mean	STDEV	%CV
0.25	129	99	69	99	30	30.3
0.5	151	56	82	96.33	49.10	51.0
1	79	154	66	99.67	47.50	47.7
2	122	192	94	136	50.48	37.1
4	251	202	126	193	62.98	32.6
8	90	52	207	116.33	80.79	69.4
12	25	27	40	30.67	8.14	26.6
24	10	13	11	11.33	1.53	13.5
C_{max} (ng/mL)	251	202	207	220	26.96	12.3
T_{max} (hr)	4	4	8	5.33	2.309	43.3
AUC_{0-t} (ng*hr/mL)	1704.13	1557.25	1830.5	1697.29	136.75	8.1
AUC_{0-∞} (ng*hr/mL)	1768.92	1718.33	1896.80	1794.7	91.98	5.1
AUMC_{0-∞} (ng*hr²/mL)	12168.5	15122.1	15901.8	14397.5	1969.4	13.7
MRT (hr)	6.879	8.800	8.384	8.0210	1.010	12.6
T_{1/2} (hr)	4.491	8.589	4.172	5.752	2.461	42.8
F_{0-t}	0.0502	0.0458	0.0538	0.0450	0.0040	8.1

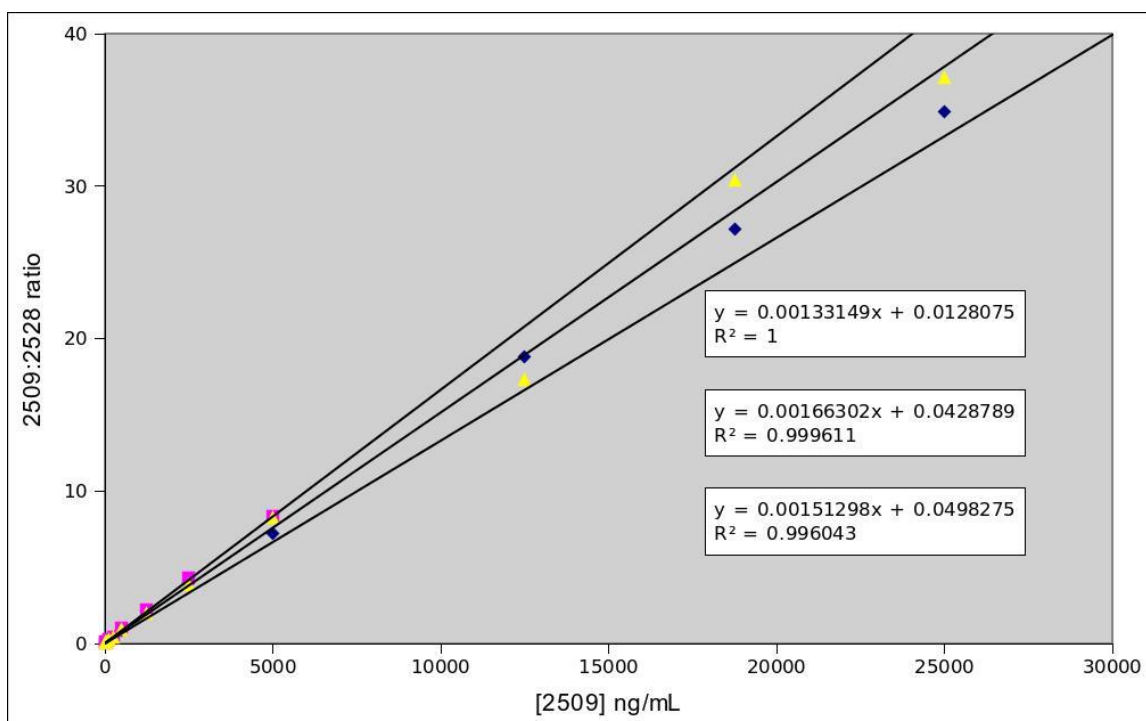


Figure C.1 Typical standard curves to quantitate HCl2509 by LC-MS/MS. Known concentrations of HCl2509 are extracted from mouse plasma, plotted as a standard curve and used to determine the concentrations of HCl2509 in mouse plasma. The limit of detection was determined using $LOD=3.3*(SD/S)$, where SD is the standard deviation in the y-intercept and S is the slope. LOD was determined to be 43 ng/mL. Linearity was observed for all tested ranges.

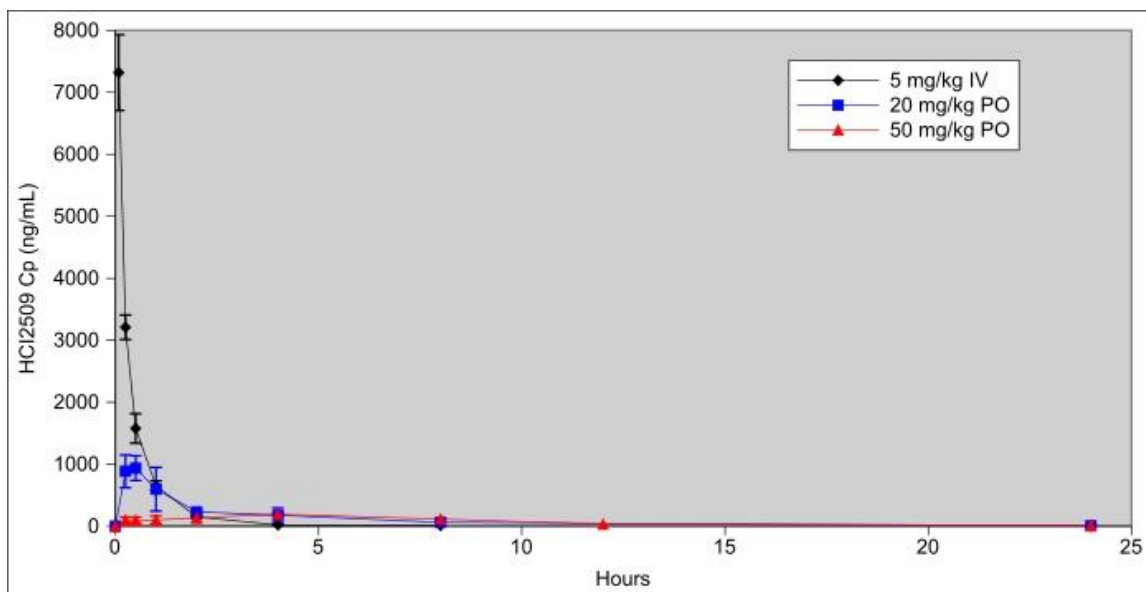


Figure C.2 Plasma concentration-time curves for HCl2509 in mice as determined by LC-MS/MS. The data in Tables C1-C3 plotted on a linear scale. Data are visualized as mean and standard deviation (n=3).

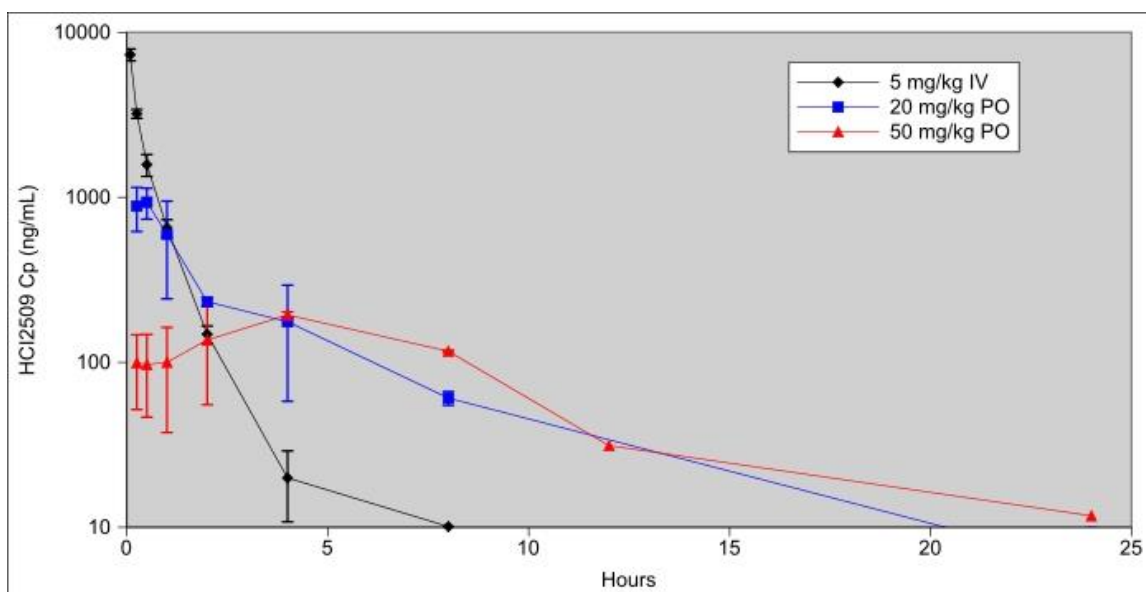


Figure C.3 Plasma concentration-time curves for HCl2509 in mice as determined by LC-MS/MS – semilog. The data in Tables C1-C3 plotted on a linear scale. Data are visualized on a semilog plot as mean and standard deviation (n=3).

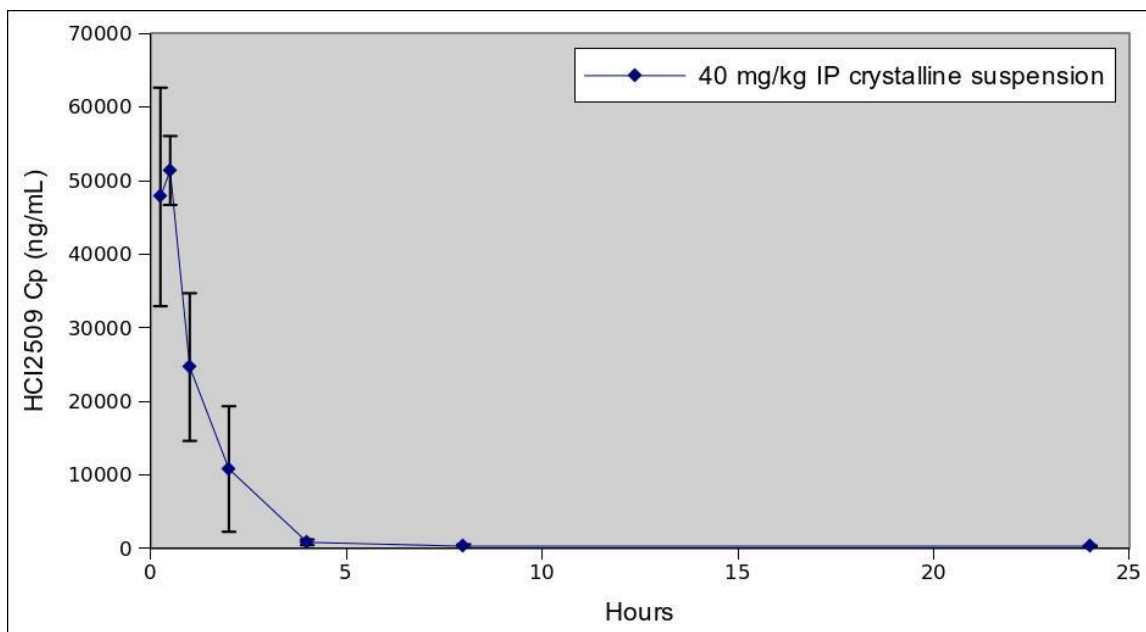


Figure C.4 Plasma concentration-time curves for 40 mg/kg HCl2509 in mice as determined by LC-MS/MS. Linear plot of 50/50 PEG400/PBS formulation used for efficacy studies. Data are visualized as mean and standard deviation (n=3).

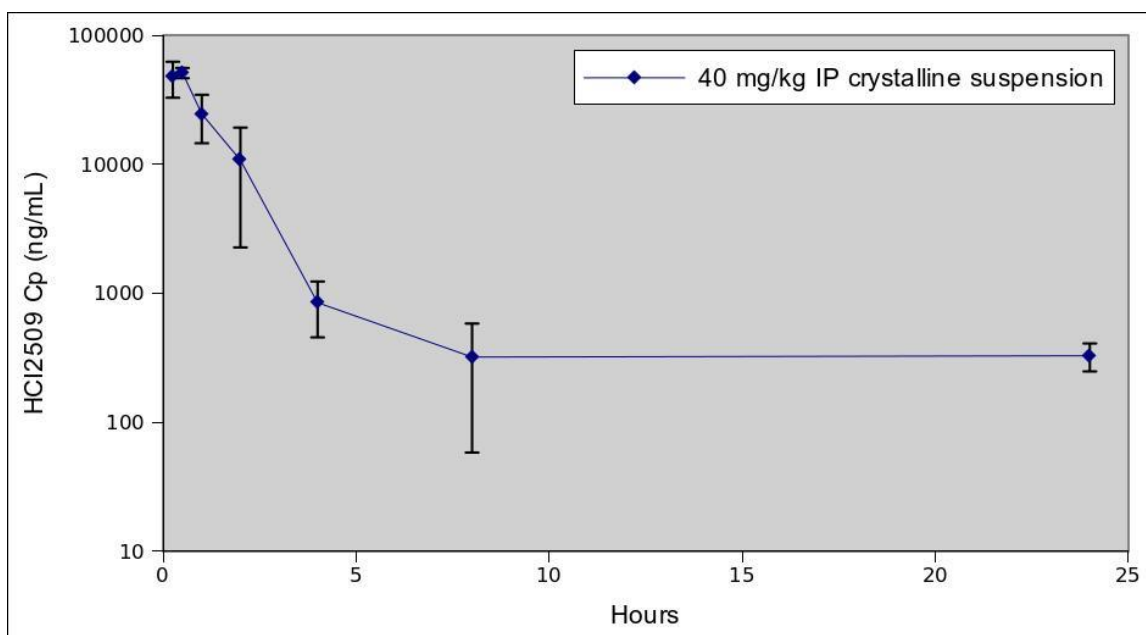


Figure C.5 Plasma concentration-time curves for 40 mg/kg HCl2509 in mice as determined by LC-MS/MS – semilog. Semilog plot of 50/50 PEG400/PBS formulation used for efficacy studies. Data are visualized as mean and standard deviation (n=3).